Structure-Function Analysis of Ebola Virus Glycoproteins

by

Darryl L. Falzarano B.Sc., M.Sc.

A Thesis submitted to the Faculty of Graduate Studies of
The University of Manitoba
in partial fulfilment of the requirements of the degree of

DOCTOR OF PHILOSOPHY

Department of Medical Microbiology
University of Manitoba
Winnipeg, MB

THE UNIVERSITY OF MANITOBA

FACULTY OF GRADUATE STUDIES
****
COPYRIGHT PERMISSION

A Thesis/Practicum submitted to the Faculty of Graduate Studies of The University of Manitoba in partial fulfillment of the requirement of the degree
of

Doctor of Philosophy

THIS THESIS HAS BEEN EXAMINED AND APPROVED.

Thesis supervisor, Dr. Heinz Feldmann, M.D., Ph.D.
Associate Professor of Medical Microbiology
Chief, Laboratory of Virology, Rocky Mountain Laboratories, DIR, NIAID, NIH

Dr. Kevin Coombs, Ph.D.
Professor of Medical Microbiology, Internal Medicine
Associate Dean (Research) Faculty of Medicine

Dr. John Wilkins, Ph.D.
Professor of Internal Medicine, Immunology, Biochemistry and Medical Genetics
Director, Manitoba Centre for Proteomics and Systems Biology

External Examiner, Dr. Anthony Sanchez, Ph.D.
Health Scientist
Centers for Disease Control and Prevention, Atlanta, GA

Date

ACKNOWLEDGEMENTS

I am grateful to the Department of Medical Microbiology and all its members for their support over the course of my graduate degrees. I would like to thank my committee members, Kevin Coombs and John Wilkins for their contributions, guidance and criticism. Hopefully it made a difference. I would also like to thank my external reviewer, Anthony Sanchez (CDC, Atlanta, GA) for accepting to review my thesis.

To all the member members of Special Pathogens program, especially the many members of the BIG lab, thanks for your inspiration, assistance and attempts to improve my "friendliness factor" (however misguided you may be). I would like to thank my supervisor, Heinz Feldmann, for providing me some exceptional opportunities to learn more about science, myself and what is right. I appreciate your open-door policy (I think I put it to good use), your candid manner (if an abstract is bad… it's bad… what else is there to say?) and how you treat everyone with a great deal of respect. Thanks to Ricki for BSL4 training… and all the $TCID_{50}$ fun.

I am indebted to Oleg Krokhin (Manitoba Centre for Proteomics and Systems Biology) for his expert mass spectrometry skills and enthusiasm to further investigate post-translational modifications that others would not even notice. I would also like to thank Ayato Takada (Hokkaido University, Sapporo, Japan) and Xiangao Qiu (Public Health Agency of Canada, Winnipeg, MB) for supplying the anti-ZEBOV monoclonal antibodies Z42/3.7 and P_{130}2H11, respectively.

I would especially like to thank: Hideki Ebihara, for sharing some of his seemingly endless knowledge of all things viral; Hans Schnittler and Jochen Seebach for the opportunity to study endothelial cells in Dresden (it was quite an experience – and yes

Canadians can handle German beer); and Ute Ströher, Allison Groseth and Thomas Hoenen for their input into these projects over the years.

I would like to thank the MHRC for graduate studentships in 2007/08 and 2008/09, in addition to the Faculty of Graduate Studies, Department of Medical Microbiology, American Society for Tropical Medicine and Hygiene and the International Congress of Virology for travel scholarships that helped support conference attendance.

To my wife, Kirsten, without whom I never would have done this (yeah… thanks a lot), for putting up with me while this was being written, our house was being renovated and right… we also had a son. To Noah, for sleeping through the night at 2 months and being good for mom – most of the time. To my parents, for everything… THANK-YOU.

TABLE OF CONTENTS

LIST OF TABLES

LIST OF FIGURES

LIST OF COPYRIGHTED MATERIALS

Figure 8 B reproduced, with permission, from MOS Technologies (Radebeul, Germany) (http://www.glpnet.de/mos-technologies/technologie/index.php).

Figure 11-14, 16 and **22** reproduced with permission from Wiley-VCH Verlag GmbH & Co. KGaA

> **Falzarano, D., Krokhin, O., Wahl-Jensen, V., Seebach, J., Wolf, K., Schnittler, H. and Feldmann, H.** 2006. Structure-function analysis of the soluble glycoprotein sGP of Ebola virus. ChemBioChem **7**(10): 1605-11.

Figure 15, 17, 19 and **23** reproduced with permission from Elsevier B.V.

> **Falzarano, D., Krokhin, O., Van Domselaar, Wolf, K., Seebach, J., Schnittler, H. and Feldmann, H.** 2007. Ebola sGP – the first viral glycoprotein shown to be C-mannosylated. Virology 368(1): 83-90.

LIST OF ABBREVIATIONS

A	adenine
AG	chicken β-actin/rabbit β-globin hybrid promoter
Ala (A)	alanine
Amp	ampere
Arg (R)	arginine
Asn (N)	asparagine
Asp (D)	aspartic acid
BEBOV	*Bundibugyo ebolavirus*
BSA	bovine serum albumin
BSL	biosafety level
C	cytosine
°C	degrees Celsius
cAMP	cyclic adenosine monophosphate
CD (e.g. CD4)	cluster of differentiation
CDC	Centers for Disease Control and Prevention
cDNA	complementary deoxyribonucleic acid
CID	collision-induced dissociation
CIEBOV	*Cote d'Ivoire ebolavirus*
CMV-IE	human cytomegalovirus immediate early promoter enhancer
cm	centimetre (10^{-2} metre)
CO_2	carbon dioxide
CPE	cytopathic effect
CRISP2	cysteine-rich secretory protein 2
C-terminus	carboxyl-terminus
Cys (C)	cysteine
Da	Daltons
DAPI	4',6-diamidino-2-phenylindole
DC-SIGN	dendritic cell-specific ICAM-3-grabbing non-integrin
DC-SIGNR	dendritic cell-specific ICAM-3-grabbing non-integrin receptor
DC-SIGN/R	DC/SIGN and DC-SIGNR
DHB	2,5-dihydroxybenzoic acid
DIC	disseminated intravascular coagulation
DMEM	Dulbeco's modified Eagle medium
DNA	deoxyribonucleic acid
dol-P	dolichol-phosphate
DRC	Democratic Republic of Congo
dsDNA	double-stranded deoxyribonucleic acid
dsRNA	double-stranded ribonucleic acid
DTT	dithiothreitol
dyn	dyne (1 dyn = 10μN)
EBOV	Ebola viruses
ECGM	endothelial cell growth media
EHF	Ebola hemorrhagic fever
ePCR	endothelial cell protein C receptor

ER	endoplasmic reticulum
FBS	fetal bovine serum
FITC	fluorescein isothiocyanate
FIV	feline immunodeficiency virus
FFU	focus-forming units
FR-α	folate receptor-α
FWHM	full-width half-maximum
G	guanine
GalNac	N-acetyl galactosamine
GDP	guanidine diphosphate
GGN1	gametogenetin-1
GlcNAc	N-acetyl glucosamine
Gln (Q)	glutamine
Glu (E)	glutamic acid
Gly (G)	glycine
GP	glycoprotein
$GP_{1,2}$	spike glycoprotein
$GP_{1,2\Delta TM}$	spike glycoprotein without the transmembrane domain up to the TACE cleavage site
GPA	guinea pig-adapted
GPI	glycosylphosphatidylinositol
H_2O_2	hydrogen peroxide
HA	hemagglutinin
HIV	human immunodeficiency virus
His (H)	histidine
HmGB1	high-mobility group box 1
hMGL	human macrophage galactose- and acetylgalactosaime-specific C-type lectin
HMM	hidden Markov model
HPLC	high pressure liquid chromatography
HR	heptad repeat
HRP	horseradish peroxidase
HSV-1	herpes simplex virus-1
HUVEC	human umbilical vein endothelial cells
Hz	Hertz (cycles per second)
ICTV	International Committee on Taxonomy of Viruses
IFN	interferon
IgG	immunoglobulin G
IκK epsilon	IκB kinase epsilon
IL (e.g. IL-2)	interleukin
Ile (I)	isoleucine
IP-10	interferon-inducible protein 10
IRF	interferon regulatory factor
ITO	indium tin oxide
iVLP	infectious virus-like particle
kb	kilobases (10^3 bases)

kDa	kiloDaltons (10^3 Daltons)
L	polymerase protein
Leu (L)	leucine
LSECtin	lymph node sinusoidal endothelial cell C-type lectin
Lys (K)	lysine
M	molar (mol/litre)
MA	mouse-adapted
MALDI	matrix-assisted laser desorption ionization
Man	mannose
MARV	*Lake Victoria marburgvirus*
MCP-1	monocyte chemoattractant protein 1
Met (M)	methionine
mF	milliFarads (10^{-3} Farads)
μg	microgram (10^{-6} gram)
MHz	megaHertz (10^6 Hertz)
MIP-1 β	macrophage inflammatory protein-1 β
μl	microlitre (10^{-6} litre)
ml	millilitre (10^{-3} litre)
MLV	murine leukemia virus
μm	micrometre (10^{-6} metre)
MOI	multiplicity of infection
MPER	membrane proximal external region
MRad	megaRad (10^6 Rad)
mRNA	messenger ribonucleic acid
MS	mass spectrometry
MS/MS	tandem mass spectrometry
MW	molecular weight
MWCO	molecular weight cut-off
m/z	mass divided by charge
ng	nanogram (10^{-9} gram)
NHP	nonhuman primate
nm	nanometre (10^{-9} m)
NMR	nuclear magnetic resonance
NN	neural network
NO	nitric oxide
NP	nucleoprotein
NS	non-structural
N-terminal	amino-terminal
OD	optical density
ORF	open reading frame
P	phosphate
PAGE	polyacrylamide gel electrophoresis
PBS	phosphate-buffered saline
Phe (F)	phenylalanine
PI3K	phosphoinositide 3-kinase
PMF	peptide mass fingerprint

ppm	parts per million
Pro (P)	proline
PVDF	polyvinylidene difluoride
PVP	polyvinyl-pyrrolidone
QqTOF	quadrupole quadrupole time-of-flight
RANTES	regulated on activation, normal T-cell expressed and secreted
RBS	receptor binding site
RC	Republic of Congo
REBOV	*Reston ebolavirus*
RNA	ribonucleic acid
rNAPc2	recombinant nematode anticoagulant protein C2
RNP	ribonucleoprotein complex
RO	reverse osmosis
RPM	revolutions per minute
SDS	sodium dodecyl sulphate
SEBOV	*Sudan ebolavirus*
Ser (S)	serine
sGP	secreted glycoprotein
SNP	single nucleotide polymorphism
ssGP	small secreted glycoprotein
STAT-1	signal transducers and activators of transcription-1
T	thymine
TACE	TNF-α converting enzyme
TER	transendothelial resistance
Thr (T)	threonine
TF	tissue factor
TFA	trifluoroacetic acid
TFPI	tissue factor pathway inhibitor
Thr (T)	threonine
TNF-α	tumour necrosis factor-α
TOF	time of flight
Trp (W)	tryptophan
Tyr (Y)	tyrosine
U	units
U	uracil
Val (V)	valine
VLP	virus-like particle
VP	virion protein
VSV	vesicular stomatitis virus
WT	wild-type
w/v	weight per volume
X	any amino acid
xg	x gravity (9.81 m/s^2)
$\|Z\|$	impedance magnitude
ZEBOV	*Zaire ebolavirus*

ABSTRACT

STRUCTURE-FUNCTION ANALYSIS OF EBOLA VIRUS GLYCOPROTEINS

Darryl L. Falzarano, B.Sc., M.Sc.
University of Manitoba, 2010

As a result of transcriptional editing, Ebola virus (EBOV) produces multiple soluble products from its glycoprotein gene, the primary product of which is the secreted glycoprotein (sGP), in addition to the membrane-bound viral spike protein $GP_{1,2}$. A lack of leukocyte infiltration is observed during EBOV infection, which is thought to allow virus replication to proceed unchecked and thus represents a significant role in the immunopathology of the disease. Currently the only know function of sGP is that it has an anti-inflammatory effect on endothelial cells treated with TNF-α, an effect that has been hypothesized to interfere with recruitment or extravasation of leukocytes. To better characterize this anti-inflammatory function, a link between sGP structure and function was sought. Mass spectrometry (MS) analysis of recombinant sGP demonstrated that it is a parallel-orientated disulphide-linked homodimer that contains Cys53-C53' and Cys306-C306' intermolecular disulphide bonds. In addition to being glycosylated with complex N-glycans, sGP also contained a novel post-translation modification, termed C-mannosylation. C-mannosylation was not required for the anti-inflammatory function of sGP; however, glycine mutations at amino acids 53 and 306 resulted in the complete loss of the anti-inflammatory effect on TNF-α treated endothelial cells. Thus, a specific structure mediated by intermolecular disulphide bonds is required for the proposed anti-inflammatory function of sGP, suggesting that this effect is the result of a specific interaction. The spike protein $GP_{1,2}$, also contains C-mannosylation motifs. MS analysis

of $GP_{1,2}$ indicated that GP_1 was C-mannosylated, while two adjacent motifs in the membrane proximal region (MPER) of GP_2 were not. The infectious virus-like particle (iVLP) assay, a system for investigating virus particle assembly and entry, was utilized to determine the functional importance of these conserved tryptophans. Elimination of the C-mannosylation motif, which resides in an external loop region of GP_1, increased reporter activity, suggesting that particle entry is enhanced and this region may interact with the cell surface despite being outside of the receptor binding site. Decreased reporter activity was observed for all MPER mutants, with multiple MPER tryptophan mutations resulting in decreased $GP_{1,2}$ incorporation. These data place the MPER tryptophan residues in an important role for glycoprotein incorporation and particle entry. Given the tryptophan content and location is similar to the MPER of HIV gp41, where these residues are required for glycoprotein incorporation and fusion, the MPER of EBOV GP_2 may function similarly.

1. INTRODUCTION

1.1 Virus Taxonomy and Particle Structure

Ebola viruses (EBOV) belong to the family *Filoviridae* (filamentous viruses) in the order *Mononegavirales* (Feldmann et al., 2005), which comprises the non-segmented negative-sense RNA genome enveloped viruses. This family is separated into two genera: *Ebolavirus* and *Marburgvirus*, with the former being further subdivided into the following 5 species based on geographic origin, serological cross-reactivity and genetic analysis (Figure 1): *Zaire ebolavirus* (ZEBOV), *Sudan ebolavirus* (SEBOV), *Cote d'Ivoire ebolavirus* (CIEBOV), *Reston ebolavirus* (REBOV) and *Bundibugyo ebolavirus* (BEBOV) - a recently identified, proposed separate species, isolated in Uganda in 2007 (Towner et al., 2008). The most widely investigated isolate is *Zaire ebolavirus* strain Mayinga, which is the basis for all of the studies described herein unless otherwise noted.

EBOV cause a severe hemorrhagic fever, termed Ebola hemorrhagic fever (EHF) in humans and non-human primates (NHPs), with case-fatality rates in humans as high as 90% (Feldmann et al., 2003; Sanchez et al., 2001). EHF is characterized by systemic viral replication, high levels of inflammatory cytokines, generalized immunosuppression, coagulation abnormalities and fluid distribution problems (Bray and Mahanty, 2003; Geisbert and Jahrling, 2004; Geisbert et al., 2003c; Geisbert et al., 2003d; Hensley et al., 2002). The end result of these processes is haemorrhage and vascular leakage, finally culminating in shock and multi-organ failure (Feldmann et al., 2003; Geisbert and Jahrling, 2004). An absence of a vigorous immune response and lymphopenia are characteristics of individuals who do not survive infection (Baize et al., 1999; Geisbert et

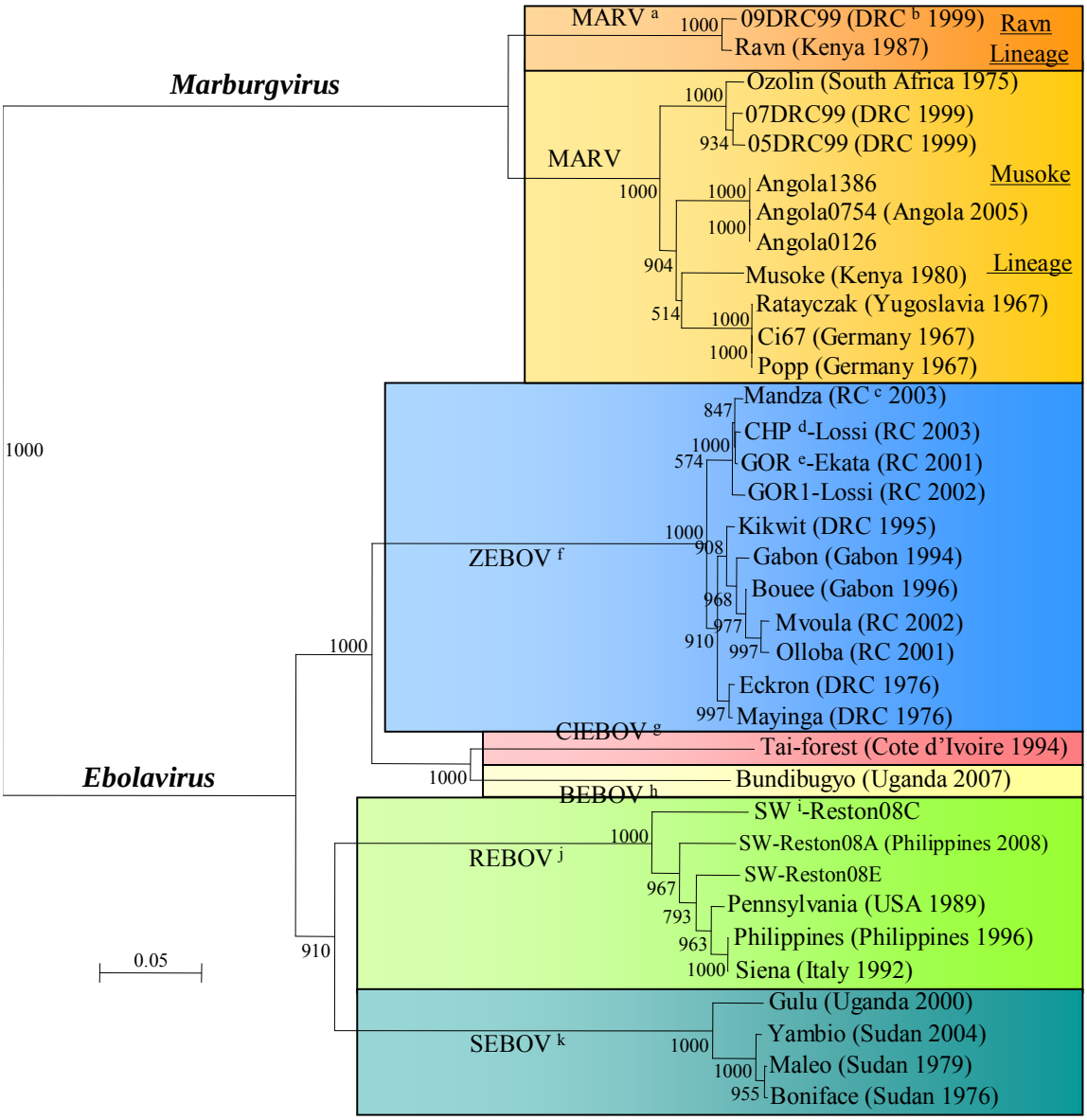

Figure 1**. Phylogenetic tree of the family *Filoviridae*.** Neighbour-Joining analysis of the amino acid sequence of the GP gene of Marburg and Ebola virus isolates, indicating the two lineages of Marburg virus and the different species of Ebola. Sequences were obtained from GenBank. Confidence values at branch point were obtained from 1000 bootstraps. The bar length equals 5% amino acid difference. [a] *Lake Victoria marburgvirus*, [b] Democratic Republic of the Congo, [c] Republic of the Congo, [d] chimpanzee, [e] gorilla, [f] *Zaire ebolavirus*, [g] *Cote d'Ivoire ebolavirus*, [h] *Bundibugyo ebolavirus*, [i] swine, [j] *Reston ebolavirus*, [k] *Sudan ebolavirus*.

al., 2000; Ksiazek et al., 1999; Mohamadzadeh, 2009; Mohamadzadeh et al., 2006; Mohamadzadeh, Chen, and Schmaljohn, 2007; Sanchez et al., 2004).

Recently, viral RNA and antibodies (IgG) against EBOV have been detected in three species of fruit bats suggesting these species may be a natural reservoir (Leroy et al., 2005). Two of these species (*Hypsignathus monstrosus* and *Epomops franqueti*) were noted to be present during a massive bat migration where contact with these bats was strongly associated with the start of an outbreak of Ebola virus in Luebo, Democratic Republic of the Congo (DRC) in 2007 (Leroy et al., 2009). Due to the high case-fatality rates observed during EBOV outbreaks, the potential of person-to-person transmission and the lack of an approved vaccine or effective therapy, these viruses are classified as biosafety level (BSL) 4 pathogens (Sanchez, Geisbert, and Feldmann, 2007), which require maximum containment facilities that operate under specific regulations when infectious work is performed.

The negative-sense single-stranded RNA genome (Regnery, Johnson, and Kiley, 1980; Sanchez and Kiley, 1987) is 18.9-kb in length and non-infectious with the following gene order: 3' leader, nucleoprotein (NP), virion protein (VP) 35, VP40, glycoprotein (GP), VP30, VP24, polymerase protein (L) and the 5' trailer (Figure 4 A) (Elliott et al., 1993; Feldmann, Klenk, and Sanchez, 1993; Sanchez et al., 1993). The genome contains a 3' leader and 5' trailer region as well as intergenic regions between NP/VP35, VP40/GP and VP30/VP24. There are also gene overlaps between VP35/VP40, GP/VP30 and VP24/L (Figure 4 A) (Sanchez et al., 1993). Virus particles are filamentous and can appear as U-shaped, 6-shaped, circular or branched. While they are uniformly 80 nm in diameter, they can vary in length from 800 to 14 000 nm, with peak infectivity

ranging between 970 nm and 1200 nm (Geisbert and Jahrling, 1995; Kiley et al., 1982). Virus particles possess a helical central core, known as the ribonucleoprotein complex (RNP), which is approximately 50 nm in diameter with a central axial space approximately 20 nm in diameter (Sanchez, Geisbert, and Feldmann, 2007). The RNP is composed of NP, VP35, VP30, L and the viral RNA (Elliott, Kiley, and McCormick, 1985). Genome replication can be driven by NP, VP35 and L; however, transcription requires VP30 (Muhlberger et al., 1999; Volchkov et al., 2001). The surface consists a of cell-derived lipid envelope containing the membrane-anchored glycoprotein ($GP_{1,2}$) (Elliott, Kiley, and McCormick, 1985), which projects approximately 10 nm from the surface (Geisbert and Jahrling, 1995; Sanchez, Geisbert, and Feldmann, 2007). The matrix proteins VP40 and VP24 underlie the membrane and it appears that VP40 is the driving force behind virus particle formation (Noda et al., 2002).

1.2 Transmission and Clinical Symptoms

To date, all outbreaks of Ebola hemorrhagic fever (EHF) in humans have originated in tropical Africa between 5^{o} North and 5^{o} South (Hoenen et al., 2006a) (Figure 2). Transmission is typically due to direct contact with blood (Ndambi et al., 1999), secretions or tissues from infected patients or animals (e.g. gorillas and chimpanzees) (Feldmann et al., 2003). Analysis of clinical specimens found evidence of virus in saliva, stool, semen, breast milk, tears and blood as well as nasal and skin swabs (Bausch et al., 2007), thereby presenting additional sources for potential transmission. Mucosal exposure has also been demonstrated as a route of infection in experimentally-exposed NHPs (Jaax et al., 1995; Johnson et al., 1995) and there are unconfirmed data

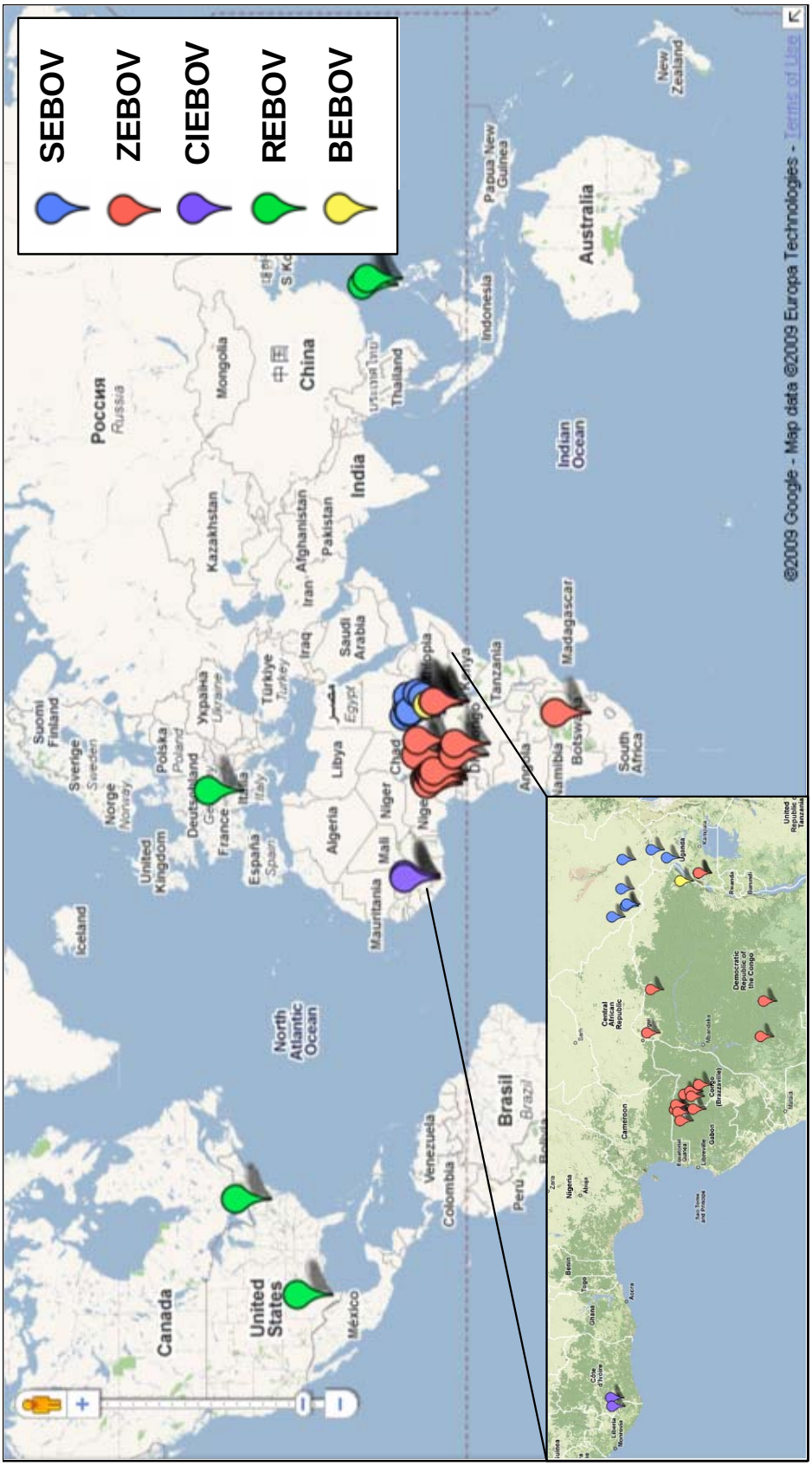

Figure 2. **Worldwide occurrences of Ebola virus.** Marker indicates the location of confirmed occurrences of Ebola virus and may represent multiple occurrences. (Inset) A higher magnification of the location of Ebola virus occurrences in equatorial Africa. Locations not found by the search engine are approximated based on descriptions in reports.

that suggest an airborne route as the mode of transmission in a limited number of human cases (Roels et al., 1999).

The incubation period is 4 to10 days, followed by abrupt onset of fever (>38.3°C) and other non-specific symptoms including chills, muscle pain, sore throat, nausea, vomiting, abdominal pain and diarrhoea (Bwaka et al., 1999; Formenty et al., 1999; Isaacson et al., 1978; Piot et al., 1978; Smith, Francis, and Simpson, 1978; Sureau, 1989). Evidence of coagulation abnormalities may be observed and can manifest as conjunctival haemorrhages, bruising, bleeding ulcerations on the mouth and lips, gingival bleeding, failure of clotting at venipuncture sites and the presence of blood in the urine or feces. Observations from Kikwit, DRC noted clinical manifestations of coagulation disorders in less than 45% of the cases (Bwaka et al., 1999), while increased D-dimers (highly suggestive of coagulation abnormalities) were observed in nearly all of the samples analyzed during an outbreak of SEBOV in Uganda in 2000 (Rollin, Bausch, and Sanchez, 2007). Approximately 50% of infected individuals develop a maculopapular rash (Sanchez, Geisbert, and Feldmann, 2007). Profuse bleeding is rare and if present is restricted to the gastrointestinal tract. The later stages of the disease are characterized by severe nausea, obtundation, tachypnea, vomiting, prostration, increased respiratory rate, anuria, and decreased body temperature indicative of the onset of shock (Bwaka et al., 1999; Isaacson et al., 1978; Piot et al., 1978). An elevation of liver enzymes has also been noted (Formenty et al., 1999). Individuals who survive frequently have prolonged arthralgia, headache, lethargy and ocular disorders (Bwaka et al., 1999; Kibadi et al., 1999; Smith, Francis, and Simpson, 1978).

1.3 Outbreaks of Ebola Virus

The first identified cases of what would become known as EHF occurred in 1976 simultaneously in Sudan (284 cases, 53% case-fatality rate) and the DRC (formerly Zaire) (318 cases, 88% case-fatality rate) (Bowen et al., 1977; CDC, 1976; WHO, 1978a; WHO, 1978b). Subsequently it was noted that these outbreaks were actually caused by two separate species of Ebola virus, which would later be named SEBOV and ZEBOV (Figure 1) (Johnson et al., 1977) (for a global map of reported occurrences of Ebola see Figure 2). In 1977, there was a single fatal case of ZEBOV in DRC (Heymann et al., 1980) and in 1979 there were 34 cases of SEBOV in Sudan (65% case-fatality rate) (Baron, McCormick, and Zubeir, 1983; CDC, 1979; WHO, 1979). Following these occurrences, there was a 14 year period with no reported cases of EHF.

In 1994, two cases of what would be called CIEBOV were noted (one in Cote d'Ivoire and one in Liberia), with both persons surviving (Formenty et al., 1999; Le Guenno et al., 1995; WHO, 1995a). Since 1994, there have been sporadic occurrences of ZEBOV in the central African rainforest region along the border of Gabon and the Republic of Congo (RC) with at least 463 cases (79% case-fatality) (Figure 2 inset) (Amblard et al., 1997; Georges et al., 1999; Pourrut et al., 2005; WHO, 1997). It now appears that EHF is endemic in this region, with varying numbers of cases annually. In 1995, ZEBOV re-emerged in DRC (315 cases, 81% case-fatality rate) (CDC, 1995a; CDC, 1995b; CDC, 1995c; CDC, 1995d; Muyembe and Kipasa, 1995; WHO, 1995b). Then in 2000/2001, the largest SEBOV outbreak to date occurred in Uganda (425 cases, 53% case-fatality rate) (CDC, 2001; Okware et al., 2002; WHO, 2000; WHO, 2001). This was followed by another smaller occurrence of SEBOV in Sudan (17 cases, 41%

case-fatality), in 2004 (WHO, 2005). In 2007, Uganda had another occurrence of hemorrhagic fever (149 cases, 25% case-fatality rate), which was identified as a proposed new species, BEBOV (Towner et al., 2008; WHO, 2008). Sequence analysis has indicated that this virus is most closely related to CIEBOV (Figure 1), providing a possible explanation for the comparably low case-fatality rate.

Four known high-risk laboratory exposures to EBOV have been reported, with the first occurring in the United Kingdom in 1976 (SEBOV). Following treatment with human interferon (IFN) and human convalescent plasma, the patient survived (CDC, 1976; Emond et al., 1977; WHO, 1977). In two separate incidents in 2004, accidental needle sticks occurred while working with animals; one in the United States (mouse-adapted ZEBOV), where the person did not appear to be infected (Kortepeter et al., 2008) and one in Russia (guinea-pig-adapted ZEBOV), where the infected individual did not survive (IJID, 2004). Most recently (2009), a needle stick occurred while infecting animals with ZEBOV in Germany. It is uncertain whether this individual was actually infected; however, following post-exposure vaccination with a live attenuated vesicular stomatitis virus (VSV)-based vaccine expressing ZEBOV GP (Feldmann et al., 2007; Jones et al., 2005), the individual did not exhibit any signs of illness (Tuffs, 2009).

The only species of Ebola that has not appeared in tropical Africa is REBOV, which was identified in imported cynomolgus macaques in 1989 at a quarantine facility in Virginia, USA (Figure 2) (Dalgard et al., 1992; Jahrling et al., 1990). This scenario has occurred multiple times, with infected macaques at quarantine facilities also being identified in 1990 and 1996 in the United States (Rollin et al., 1999) and in Italy in 1992 (WHO, 1992). All REBOV-infected primates were traced back to one holding facility in

the Philippines, but a source of infection was not identified. In 2008, during an investigation regarding high swine mortality at multiple farms in the Philippines, a number of pigs that had died tested positive for REBOV (Barrette et al., 2009; Cyranoski, 2009; Normile, 2009; WHO, 2009); however, it is unclear if REBOV infection was the cause of death. While REBOV is virulent in monkeys, to date there has been no apparent pathogenicity in humans despite at least 25 infections (0% case-fatality rate) (Hayes et al., 1992; Miranda et al., 1999).

Different species of EBOV appear to have varying apparent pathogenicities, with ZEBOV and SEBOV typically resulting in high (>50%) case-fatality rates. Thus far, BEBOV appears somewhat less severe with an approximately 25% case-fatality rate, despite a large number of infected individuals. There have only been 2 reported cases of CIEBOV to date (with no fatalities) and no apparent fatalities or illness in humans exposed to REBOV, despite a number of seropositive individuals from the Philippines, United States and Italy. Differences in virulence among NHPs is also observed; however, a large scale direct comparison between and within species and isolates has not been carried out. Limited data suggest that differences in the glycoprotein (GP) may be the most important factor affecting virulence (Yang et al., 2000). The expression of REBOV GP did not disrupt the vasculature of human blood vessels, while ZEBOV GP clearly had a negative effect. It has been speculated that EBOV may control GP cytotoxicity (which possibly varies between species) by regulating its expression through RNA editing (Alazard-Dany et al., 2006; Volchkov et al., 2001), although data supporting this hypothesis is currently limited.

1.4 Ebola Virus Life Cycle

The life cycle of EBOV can be summarized into a number of major steps which include: 1) glycoprotein-mediated attachment of the virus to the cell surface with subsequent entry into the cell; 2) pH-dependent membrane fusion with release of the viral RNP complex into the cytoplasm where transcription and replication occurs; 3) accumulation of viral proteins and genomes with subsequent assembly of RNP complexes and transport of building blocks to sites of assembly; and 4) budding of the virion at the plasma membrane with subsequent release. These steps are summarized in Figure 3 and explained in greater detail below.

1.4.1 Attachment

The amino acids responsible for cell surface attachment of EBOV have been mapped to a region in GP_1 that includes residues 54–201 (Figure 5 B) (Kuhn et al., 2006). Despite this information, a receptor has yet to be described, although a number of distinct and functionally unrelated cell surface proteins have been identified as enhancing EBOV entry. These proteins come from functionally and structurally unrelated groups, making the interactions between EBOV and cell surface proteins a complex process that is not yet fully understood. Lymphoid cells (and cell lines) do not appear to be susceptible to infection by either infectious virus or pseudotyped particles (Chan et al., 2000; Geisbert et al., 2000; Geisbert et al., 1992; Wool-Lewis and Bates, 1998). Data from pseudotyped viruses has indicated that reporter activity was decreased when cells were pre-treated with either tunicamycin (an inhibitor of intracellular N-glycosylation) or endoglycosidase H (which cleaves high mannose type N-glycosylated carbohydrates), indicating that the cell surface interacting partner may be N-glycosylated and that this is important for the

Figure 3. **Ebola virus life cycle.** Following GP-mediated interaction with cellular attachment factor(s) and/or receptor(s) on the cell surface (1), the EBOV particle enters the cell via receptor-mediated endocytosis (2). The virus is transported by endosomes on microtubules (3), where a decrease in pH and processing of GP by cellular cathepsins and additional proteolytic factors (4) leads to membrane fusion (5). This releases the viral ribonucleoprotein complex (RNP) into the cytosol where transcription and genome replication occur (6). Capped, polyadenylated mRNA are generated by the viral polymerase complex and translated by the host cell machinery (7). It is thought that accumulation of NP leads to a switch from transcription to replication of the genome, which requires the generation of complementary RNA (cRNA) that is then used as a template to generate the viral RNA (vRNA) genome (8). The glycoprotein is processed through the endoplasmic reticulum (ER) and Golgi complex (9) and then transported to the cell surface (10). VP40 is actively transported to the cell surface where it drives virus assembly (11), in addition to facilitating transport of newly formed RNP complexes to virus assembly sites (12). At these sites the RNP complex is incorporated into virus particles that bud from cell and are released as an enveloped progeny virion (13).

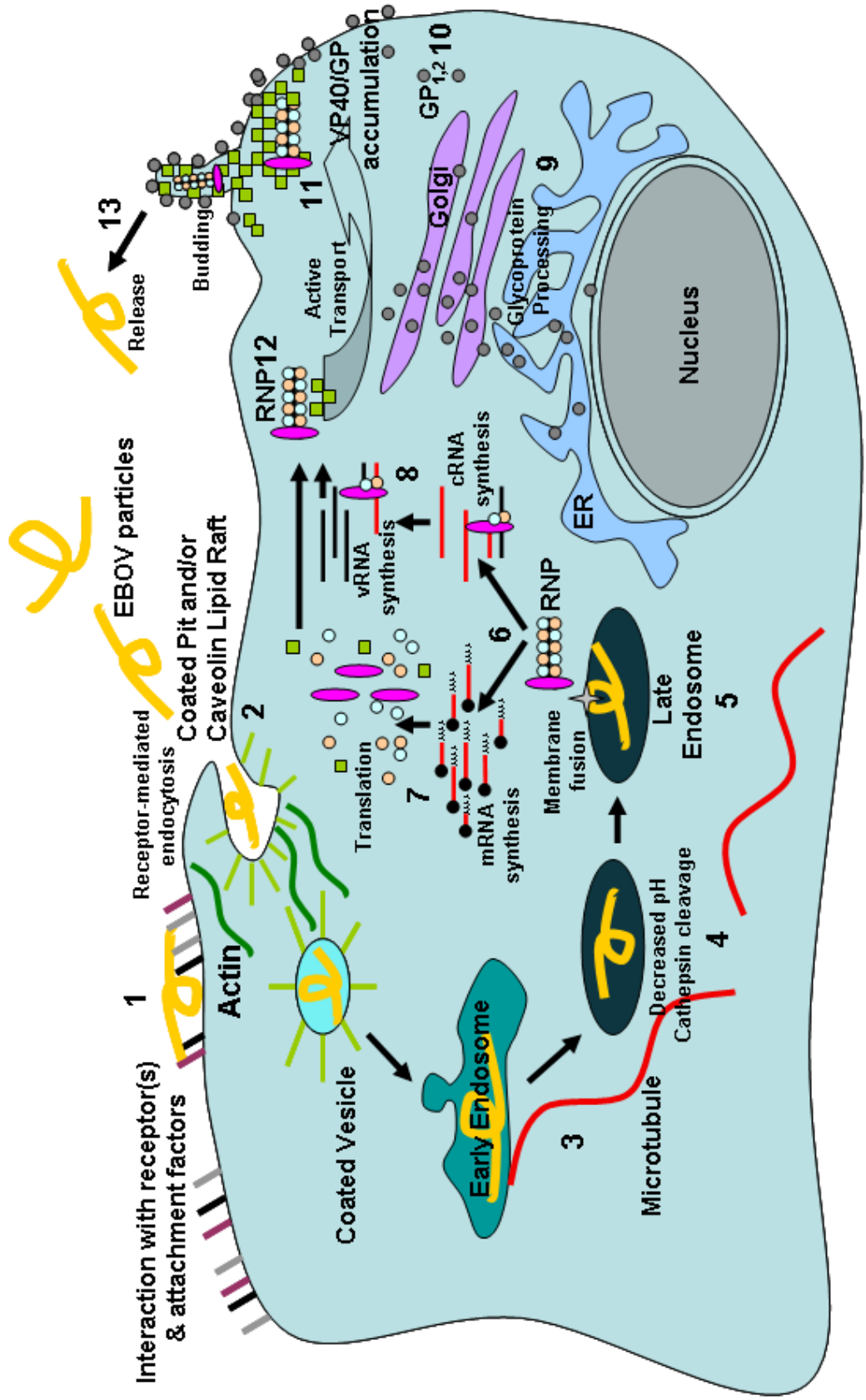
Interaction with receptor(s) & attachment factors
1
Actin
Receptor-mediated endocytosis
Coated Pit and/or Caveolin Lipid Raft
EBOV particles
2
Coated Vesicle
Early Endosome
3
Microtubule
Decreased pH
Cathepsin cleavage
4
Late Endosome
5
Membrane fusion
RNP
6
Translation
7
mRNA synthesis
vRNA synthesis
8
cRNA synthesis
ER
Glycoprotein Processing
9
Golgi
$GP_{1,2}$ 10
VP40/GP accumulation
11
Active Transport
RNP12
Budding
13
Release
Nucleus

interaction (Chan et al., 2000). Subsequent screening of libraries in the non-permissive Jurkat cell line indicated that folate receptor-α (FR-α) was a significant cofactor for EBOV entry (Chan et al., 2001). This protein is highly conserved in many mammalian species and expressed in a wide variety of cell types, thus it appeared to be a good candidate for a receptor. However, certain cell types that are permissive to EBOV infection do not express FR-α, thus entry was not solely dependent on this factor (Chan et al., 2001; Simmons et al., 2003; Sinn et al., 2003).

Members of the calcium-dependent (C-type) lectins have also been suggested as potential receptors for EBOV. These proteins contain carbohydrate recognition domains that recognize high-mannose carbohydrates such as those found on the EBOV glycoprotein. Dendritic cell-specific ICAM-3-grabbing non-integrin (DC-SIGN), its homologue DC-SIGNR (collectively referred to as DC-SIGN/R) and lymph node sinusoidal endothelial cell C-type lectin (LSECtin) were shown to bind EBOV-pseudotyped lentiviruses and enhance infection of non-permissive Jurkat cells (Alvarez et al., 2002; Gramberg et al., 2005; Lin et al., 2003). Furthermore, these molecules are also present on the surface of cells that are targets of infection, such as macrophages, dendritic cells and endothelial cells in the liver and lymph nodes (Bashirova et al., 2001; Pohlmann et al., 2001).

Remarkably, DC-SIGN/R has been shown to recognize the high-mannose carbohydrate moieties of a wide array of viruses, bacteria, parasites and yeast. This includes human immunodeficiency virus-1 (HIV-1) , human T-cell lymphotropic virus-1, hepatitis C virus, herpes simplex virus-1 and 2, human herpes virus-8, measles virus, West Nile virus, *Mycobacterium sp.*, *Leishmania sp.* and *Candida albicans* (Cambi,

Koopman, and Figdor, 2005), suggesting that DC-SIGN/R functions more as a universal pathogen receptor (Geijtenbeek and van Kooyk, 2003) that may help mediate attachment to the cell surface (Cambi, Koopman, and Figdor, 2005), instead of acting as a distinct receptor for a plethora of pathogens. Studies with HIV have suggested that DC-SIGN/R captures and concentrates HIV particles on the cell surface, permitting interaction with other host cell factors that are actually required for entry and infection (Arrighi et al., 2004; Snyder et al., 2005). This interaction is also thought to protect HIV from degradation by dendritic cells (Geijtenbeek et al., 2000; Halary et al., 2002) and may increase the efficiency of endocytosis, as DC-SIGN contains internalization motifs (Engering et al., 2002). For EBOV attachment, DC-SIGN/R certainly enhances infection in poorly permissive cell lines (Marzi et al., 2006); however, its expression alone was not sufficient to render all refractory cell lines permissive (Marzi et al., 2007). Thus C-type lectins serve to concentrate the virus on the cell surface of primary target cells, providing an opportunity for interaction(s) with other receptor(s) that are possibly expressed at a relatively low-level (Marzi et al., 2007). Human macrophage galactose- and acetylgalactosaime-specific C-type lectin (hMGL) has also been described as an attachment factor for EBOV (Takada et al., 2004). hMGL specifically recognizes galactosyl residues and is expressed on immature dendritic cells and macrophages; however, this also does not appear to be a definitive receptor as entry can proceed independent of this molecule.

A third group of cell surface molecules involved in interaction with EBOV GP is the β1 integrin adhesion receptors. To date, there is no evidence of direct involvement with these molecules; however, anti-β1 integrin antibodies and the soluble α5β1 integrin

complex have been demonstrated to inhibit entry of EBOV-GP pseudotyped VSV (Takada et al., 2000). Finally, the most recent candidate receptors: Axl, Dtk and Mer, belong to the Tyro3 family of receptor tyrosine kinases (Shimojima et al., 2006). These proteins are highly conserved between species and are expressed on a wide variety of cell types, with the exception of lymphocytes and granulocytes. Recently, it has been proposed that Axl may enhance endocytosis following attachment of EBOV to the cell surface (Shimojima, Ikeda, and Kawaoka, 2007); however, Vero E6 cells were shown to undergo Tyro3 independent entry of EBOV GP murine leukemia virus (MLV)-pseudotyped particles (Shimojima et al., 2006).

While it seems to be accepted that lectins, integrins and the Tyro3 family members have a role to play during the process of EBOV attachment and entry, their specific roles remain to be clarified. EBOV appears to be capable of interacting with multiple factors in order to attach to the cell surface and certain molecules (e.g. DC-SIGN/R) can further enhance this interaction. It remains unclear whether interaction with a specific receptor is required to initiate entry once the virus has attached to the cell surface or whether multiple interactions with different cell surface proteins is sufficient to uptake into the cell.

1.4.2 Entry

The spike glycoprotein, $GP_{1,2}$, is the sole protein on the surface of the virion and mediates entry into target cells (Takada et al., 1997; Wool-Lewis and Bates, 1998; Yang et al., 1998). GP_1 interacts with attachment factor(s) and/or the virus receptor(s) (described above) to initiate entry, while the GP_2 subunit modulates membrane fusion. Following binding of the virus to the cell surface, EBOV enters the cell via the endocytic

pathway (Figure 3) (Dolnik, Kolesnikova, and Becker, 2008). Indirect evidence suggests that EBOV enters via caveolin-mediated or clathrin- and caveolin-independent endocytosis, as caveolin-1 has been shown to localize with HIV particles pseudotyped with EBOV GP (Empig and Goldsmith, 2002). EBOV has been observed to be associated with lipid rafts (Bavari et al., 2002; Yonezawa, Cavrois, and Greene, 2005), which are required for both these mechanisms of endocytosis (Parton and Richards, 2003; Simons and Ikonen, 1997). The use of caveolae is surprising, as the size of EBOV (80 x 650-1000 nm) would tend to rule out a caveolin-mediated entry mechanism (Dolnik, Kolesnikova, and Becker, 2008); however, these pseudotyped particles are significantly smaller than EBOV particles suggesting that this system may not reflect what actually happens during EBOV entry. Recent data using live cell imaging has found no evidence that EBOV virus-like particles (VLPs) co-localize with caveolin-1, making it quite unlikely that EBOV uses caveolae for entry (Aleksandrowicz et al., 2008). This also supports earlier data, which shows that expression of caveolin-1 does not rescue infectivity in cells that are refractory to infection (Simmons et al., 2003).

Only recently has infectious ZEBOV been used to determine whether information based on pseudotyped viruses reflects that of the actual virus. In Vero cells, EBOV appears to enter via receptor-mediated endocytosis by way of clathrin-coated pits and caveolae, while also requiring actin filaments and microtubules (Sanchez, 2007). While the mechanism of endocytosis has still not been clearly defined, a possible trigger mechanism for endocytosis has been described. ZEBOV particles cause the phosphorylation of Akt, which results in the induction of class 1A phosphoinositide 3-kinases (PI3Ks) (Saeed et al., 2008). Furthermore, it has been proposed that ZEBOV

interaction with Tyro3 family receptor tyrosine kinases, an interaction that has been observed (e.g. with Axl, Dtk and Mer (Shimojima et al., 2006)) leads to the direct or indirect activation of PI3Ks (Jiang and Liu, 2008) and downstream effectors resulting in virus endocytosis (Saeed et al., 2008). Currently, there is substantial evidence that EBOV enters cells via endocytosis; however, the exact mechanism of endocytosis remains to be determined and while a possible signalling mechanism that triggers endocytosis has been described, it is probably not the complete story, as entry of EBOV can occur independent of Tyro3 receptor tyrosine kinases.

Following endocytosis the viral genome must be able to escape the endosome in order for replication to occur. This requires fusion of the virus membrane with the membrane of the endosome (Figure 3). It is thought that a structural rearrangement of the metastable, pre-fusion GP occurs whereby the GP_1 clamp on GP_2 is released (Lee et al., 2008); however, the mechanism by which this occurs is not well understood. Decreased endosomal pH is a requirement for fusion (Takada et al., 1997; Wool-Lewis and Bates, 1998) and experiments using ammonium chloride (which prevents acidification of endosomes) exhibited a dose-dependent effect on pseudotype particle entry (Chan et al., 2000). Additional factors are thought to be required for the induction of fusion, as syncytia formation has not been observed in GP-expressing cells exposed to a low pH environment (Takada et al., 1997). However, cell-cell fusion has been indirectly observed using a reporter system that detects cytoplasmic exchanges (Bar et al., 2006). Initially it was thought that furin cleavage during processing in the secretory pathway was a requirement for fusion, but it has since been shown to be dispensable for infection of both cell lines and Rhesus macaques (Neumann et al., 2002; Neumann et al., 2007). The

second requirement for fusion is additional proteolytic processing in the endosome by cellular cysteine proteases, namely cathepsin B and cathepsin L (Figure 3) (Chandran et al., 2005). This generates a 19 kDa GP_1 intermediate, which primes the glycoprotein for fusion, while a third endosomal/lysosomal factor (suggested to be a lysosomal thiol reductase) triggers fusion (Schornberg et al., 2006). It is currently unclear whether low pH is actually required for triggering fusion or if it is required for the optimal functioning of endosomal proteases (Schornberg et al., 2006).

The current model for GP-induced fusion indicates that prior to proteolysis, GP_1 interferes with a conformational change in the GP_2 trimer that allows it to form an extended structure, resulting in fusion of the virion and endosomal membrane (Weissenhorn et al., 1998b). Once the structural constraints of GP_1 are released, the heptad repeat (HR) regions of GP_2 (Figure 5 B) can undergo the necessary conformational alteration. Comparison of pre- and post-fusion GP_2 fragments revealed that the heptad repeats unfold to form a single 44-residue helix encompassing all of HR1 (Lee et al., 2008; Malashkevich et al., 1999; Weissenhorn et al., 1998a). Following the conformational shift, the residues of the hydrophobic fusion peptide most likely insert into the host membrane (Ito et al., 1999; Watanabe et al., 2000) where they adopt a 3_{10} helix conformation (Freitas et al., 2007). HR2 then swings from the viral membrane-proximal surface towards the host membrane-proximal surface resulting in the close packing of HR1 to form the post-fusion GP_2 six-helix bundle (Lee et al., 2008). This results in juxtaposition of the internal fusion loop and the transmembrane domain facilitating fusion of the host and viral membranes (Lee et al., 2008) and releasing the RNP into the cytoplasm. While certain steps of the entry process have been resolved, the

mechanism of endocytosis remains to be determined, as well as what additional proteolytic processing steps are required, in what cellular compartment fusion occurs and what cellular factors are involved in the trafficking and sorting of EBOV-containing endosomes.

1.4.3 Genome Replication

Following EBOV particle entry, membrane fusion and subsequent RNP release into the cytoplasm, transcription is the first event to occur. Due to the similar genome organization among all members of the *Mononegavirales*, transcription and replication are assumed to follow common mechanisms (Weik et al., 2005). Transcription requires NP, VP35, L and VP30, while genome replication can proceed in the absence of VP30 (Muhlberger et al., 1999; Volchkov et al., 2001). The viral polymerase complex (which consists of L and VP35) produces polyadenylated, monocistronic mRNAs that are likely capped at the 5′ end for each viral gene in a 3′ to 5′ direction (Figure 3) (Ferron et al., 2002; Volchkov et al., 1995; Weik et al., 2002). These transcripts contain stem-loop structures at their 5’ ends which may play a role in transcript stability, ribosome binding and/or translation (Sanchez and Kiley, 1987; Sanchez et al., 1993). It is thought that the polymerase complex undergoes starting and stopping as it encounters conserved start (initiation) and stop (termination/polyadenylation) sites along the genome. The glycoprotein gene of EBOV is transcribed in a unique manner that makes it distinct from MARV. This is the only example of an edited glycoprotein; however, this phenomenon is also observed in the phosphoprotein gene from members of the *Paramyxovirinae* subfamily (Thomas, Lamb, and Paterson, 1988). EBOV GP is transcribed in at least three open reading frames (see biosynthesis of glycoprotein products and Figure 4 B) allowing

the production of 3 different glycoprotein products (Sanchez et al., 1996; Volchkov et al., 1995). The ability of the polymerase to stutter on a poly(U) template (thus allowing synthesis of poly A tails on the mRNA) is thought to be the possible mechanism behind transcriptional editing (Sanchez, Geisbert, and Feldmann, 2007). It has also been suggested that this occurs in combination with RNA secondary structures, although this has not been demonstrated experimentally. This may also explain the presence of the minor product ssGP, which is produced as a result of an additional frame shift, indicating a possible lack of precision.

Similar to other negative sense RNA viruses, the genome ends have a high degree of sequence complementarity (Crary et al., 2003; Feldmann and Kiley, 1999; Sanchez and Rollin, 2005) making it likely that they form stem-loop structures at the 3' and 5' ends of genomic and antigenomic RNAs. These structures are thought to be important for replication. Initial transcription leads to an accumulation of viral proteins, especially NP. It is hypothesized that accumulation of NP triggers a switch from transcription to replication (Whelan, Barr, and Wertz, 2004); however, this has not been demonstrated experimentally for EBOV. Replication proceeds from the *cis*-acting promoter at the 3' end of the genomic RNA, resulting in the synthesis and encapsidation of antigenomic RNA molecules. These in turn serve as templates for the genomic RNA that are also encapsidated (Figure 3) (Weik et al., 2005). Once high levels of NP are depleted, it is believed that transcription resumes until NP starts to accumulate again. This is thought to be a dynamic process, which eventually reaches equilibrium where transcription and replication occur simultaneously. As genome replication proceeds, RNPs containing the

genomic RNA accumulate and are directed to the plasma membrane, possibly through an interaction with VP40, for virion assembly.

1.4.4 Virus assembly and release

VP40, the major matrix protein, is an essential factor for virus assembly and budding (Jasenosky et al., 2001; Noda et al., 2006; Noda et al., 2002; Timmins et al., 2001). When expressed alone, it is capable of forming VLPs that resemble authentic particles. During the production of viral proteins, NP induces the formation of inclusion bodies, which also accumulate other viral proteins that form the RNP complex (Huang et al., 2002). RNPs are likely assembled in these inclusions when sufficient levels of viral proteins and negative-sense genomes are reached. An interaction between RNPs and VP40 directs the transport of RNPs to the plasma membrane (Noda et al., 2006), where VP40 most likely initiates the assembly process (Jasenosky and Kawaoka, 2004) (Figure 3). VP40 is also thought to be transported to the plasma membrane independent of RNPs, most likely via the vacuole sorting pathway (Timmins et al., 2003; Yasuda et al., 2003), after which it is recruited to lipid rafts (Aman et al., 2003; Bavari et al., 2002). GP trimers are transported to the cell surface membrane where they also have an affinity for lipid rafts, likely due to the palmitoylation of its transmembrane domain (Bavari et al., 2002; Feldmann et al., 1999). At the plasma membrane, dimers of VP40 associate to form octameric rings that have a central pore and bind RNA (Gomis-Ruth et al., 2003). While this octamerization is not essential for particle formation, it does appear to be essential for virus replication (Hoenen et al., 2005). VP24 also associates with the plasma membrane and may play a role in particle formation (Han et al., 2003). Once all the virus structural components are together in one location, the VP40 octamers (which encompass

the RNP via interactions with viral RNA) are also tightly associated with GP lipid rafts, allowing the entire complex to be enveloped and extruded from the host cell as infectious virions (Figure 3) (Jasenosky and Kawaoka, 2004; Licata et al., 2004).

1.5 Biosynthesis and Structure of the Glycoprotein Products

The fourth gene of the EBOV genome encodes the precursors of a soluble non-structural glycoprotein (pre-sGP), a second small soluble non-structural glycoprotein (ssGP) and the structural transmembrane glycoprotein (pre-GP) (Figure 4 B) (Sanchez et al., 1996; Volchkov et al., 1995). The ratio of the different transcripts in Vero cells is approximately 16:4:1 for sGP, GP and ssGP, respectively (Mehedi et al., 2008). The primary product is the 364-residue pre-sGP, which undergoes processing that includes: the removal of the signal peptide (Sanchez et al., 1998), N-glycosylation (Volchkov et al., 1995) and oligomerization (Sanchez et al., 1998) in the endoplasmic reticulum (ER). It is also cleaved in the trans-Golgi network at the multi-basic site (R-X-R/K-R) by the ubiquitous pro-protein convertase furin (Figure 5 A) (Volchkov et al., 1998a; Volchkova, Klenk, and Volchkov, 1999), into sGP and Δ-peptide, both of which are secreted from infected cells (Volchkova et al., 1998; Volchkova, Klenk, and Volchkov, 1999). Significant quantities of sGP have been detected in the serum of infected individuals (Sanchez et al., 1996; Volchkova et al., 1998) and a number of different functions during infection have been proposed (described in further detail below).

The transcript that codes for the 676-residue GP is only generated following a transcriptional editing event, whereby an additional adenosine residue is inserted at the editing site, consisting of 7 uridine residues on the genomic RNA template (Sanchez et

Figure 4. **A schematic representation of the organization of the *Zaire ebolavirus* genome (A) and production of products of the glycoprotein gene (B).** (A) The genome is negative-stranded single-sense RNA and contains a leader, trailer and the following seven genes: nucleoprotein (NP), virion protein (VP35), VP40, glycoprotein (GP), VP30, VP24 and polymerase (L). Also indicated are the location of intergenic regions (IR) and the regions of gene overlap (indicated by overlapping ascending genome). (B) As a result of transcriptional editing, whereby adenosine residues are either added or deleted to the transcript, the glycoprotein gene produces multiple products. Pre-sGP (far left) is cleaved by furin into the secreted glycoprotein (sGP), which forms homodimers, and Δ-peptide. These products are secreted from infected cells. Pre-GP is cleaved by furin into GP_1 and GP_2 (centre), which are disulphide-linked, forming the full-length surface spike glycoprotein ($GP_{1,2}$) that mediates attachment and entry. Disulphide bond instability with GP_2 possibly results in secretion of GP_1 (centre left). Cleavage of $GP_{1,2}$ on the cell surface by TNF-α converting enzyme (TACE) leads to a transmembrane-deleted protein ($GP_{1,2\Delta TM}$) that is shed from infected cells (centre right). The small secreted glycoprotein (ssGP) is a proposed product that if produced would also be expected to be secreted from infected cells (far right).

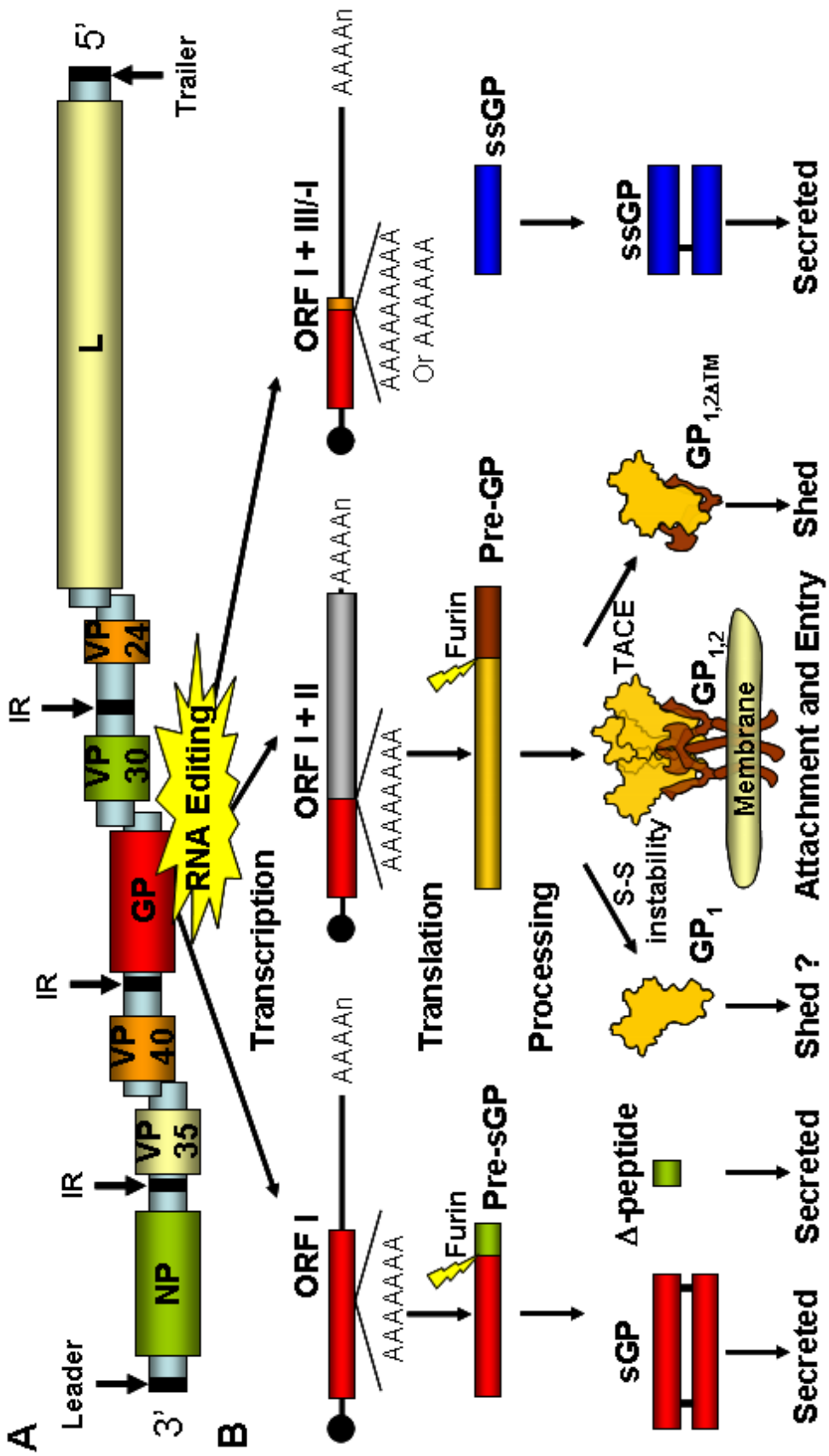
A
Leader
3'
NP
VP 35
VP 40
GP
VP 30
VP 24
L
5'
Trailer
IR
IR
IR
RNA Editing
B
Transcription
ORF I
AAAAn
AAAAAAA
Furin
Pre-sGP
sGP
Secreted
Δ-peptide
Secreted
ORF I + II
AAAAn
AAAAAAAA
Translation
Furin
Pre-GP
Processing
S-S instability
GP1
Shed ?
TACE
GP1,2
Membrane
GP1,2ΔTM
Shed
Attachment and Entry
ORF I + III/-I
AAAAn
AAAAAAAAA
Or AAAAAA
ssGP
ssGP
Secreted

al., 1996; Sanchez et al., 1998). This results in a -1 shift in the open reading frame (ORF) at the editing site generating the full-length glycoprotein $GP_{1,2}$ (Figure 4 B). Pre-GP also undergoes signal peptide removal, N-glycosylation and furin cleavage (Sanchez et al., 1998; Volchkov et al., 1998a). In addition, $GP_{1,2}$ is also acetylated in a pre-Golgi compartment (Ito et al., 2001) and undergoes O-glycosylation and N-glycan maturation in the Golgi (Figure 5 B) (Feldmann et al., 1994; Volchkov et al., 1995). The mature protein, $GP_{1,2}$, is linked via a disulphide bond between cysteine (Cys) 53 of GP_1 and Cys609 of GP_2 and is transported to the cell surface via the classical pathway where it remains anchored in the cell membrane by a hydrophobic domain in the carboxy-terminus of GP_2 (Figure 5 B) (Sanchez et al., 1998; Volchkov et al., 1998b).

An additional transcriptional product, which is the result of either the deletion of one (+1 ORF) or the addition of two (-2 ORF) uracil residues at the editing site results in an additional non-structural protein termed ssGP (Figure 4B) (Volchkov et al., 2000; Volchkova et al., 1998). It is presumably processed by signalase, but is not known to undergo any further proteolytic processing. Due to the location of the editing site, sGP shares the 295 amino- (N) terminal amino acids with GP_1 and ssGP (Sanchez et al., 1996; Volchkov et al., 1995). The carboxyl- (C) terminus of sGP has 28 unique amino acids, while ssGP has two or three (dependant of the ORF shift) unique amino acids and is essentially a truncated version of sGP. The sequence of Δ-peptide, GP_2 and the remainder of GP_1 are unique.

sGP is known to form dimers via two intermolecular disulphide bonds, however, there is some controversy as to whether these are arranged in a parallel (Cys53-Cys53'/Cys306-cys306') (Barrientos et al., 2004) or an anti-parallel (Cys53-

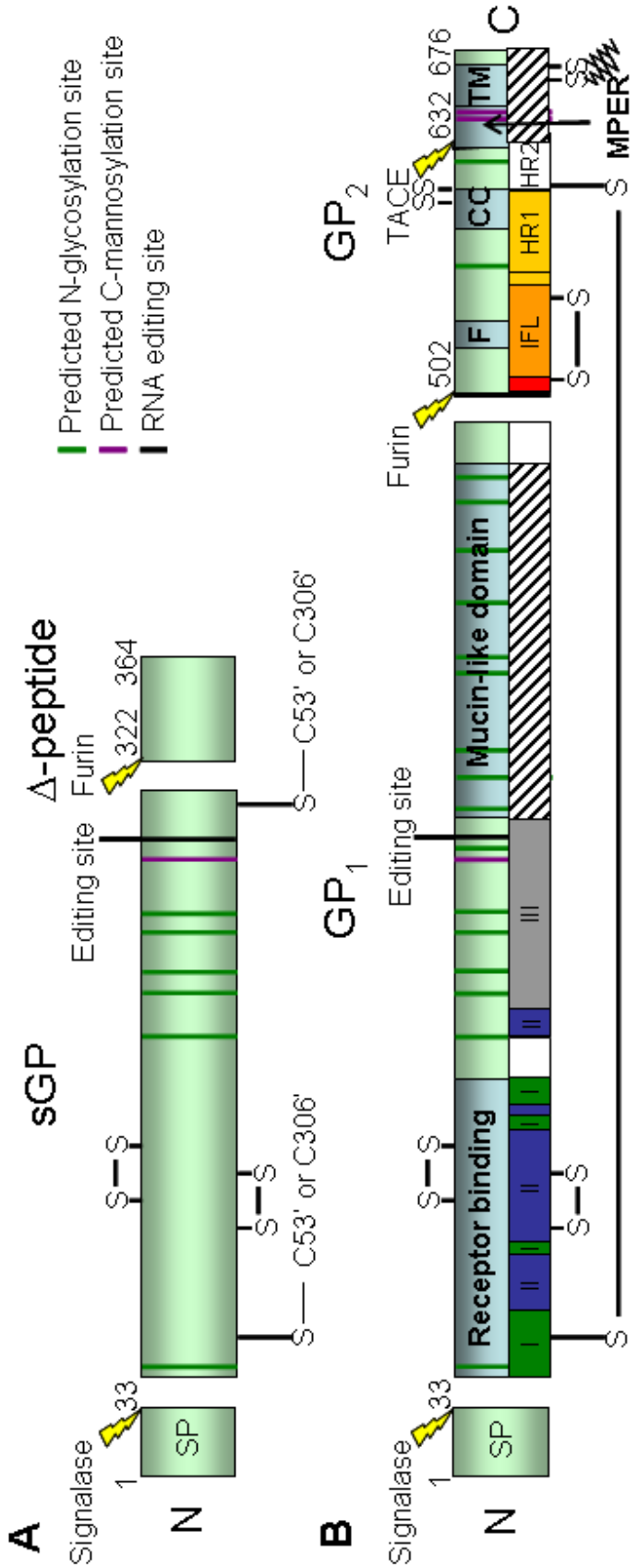

Figure 5. **Schematic diagram of sGP (A) and GP (B).** (A) Pre-sGP undergoes proteolysis by signalase to remove the signal peptide (SP) and by furin to separate sGP from Δ-peptide. Intramolecular disulphide bonds (-S-S-) are indicated while intermolecular disulphide bonds exist between either C53' or C306' of another sGP molecule. Green bars indicate predicted N-linked glycosylation sites. Purple bars indicated potential C-mannosylation sites. Black bars indicate the RNA editing site. B) Pre-GP is also processed by signalase to remove the signal peptide and furin, which cleaves GP_1 from GP_2. A disulphide bond then links GP_1 and GP_2 forming a heterodimer which associates with other heterodimers to form trimers (see Figure 4). The receptor binding domain, mucin-like domain, fusion peptide (F), coiled-coil domain (CC), membrane proximal external region (MPER) and the transmembrane domain (TM) are indicated. $GP_{1,2}$ can be cleaved from the cell surface by TNF-α converting enzyme (TACE) as indicated. The domains as described by the crystal structure (Lee et al., 2008) are indicated in the lower portion of the figure: white regions were structurally disordered, hash-marked regions were deleted from the construct, GP_1 base (I), GP_1 head (II) , GP_1 glycan cap (III), internal fusion loop (IFL), heptad repeat (HR1/2). Palmitic acid is indicated by the zigzag line.

Cys306'/Cys306-Cys53') orientation (Volchkova et al., 1998). The predicted mass of sGP is 36 kDa; however, its actual mass is approximately 50 kDa due to N-glycosylation and possible O-glycosylation. sGP has 6 potential N-glycosylation sites (Asn-X-Thr/Ser) but it is unknown which sites are occupied. Further experimental structural data for sGP is lacking; however, the residues included between Cys108 and Cys147 have been described to be similar to an F2-like module, as the disulphide bond topology is similar to that of fibronectin type II domains (F2 modules) (Barrientos et al., 2004). sGP still remains to have a definitive function assigned to it despite a number of suggested functions (see function of the secreted glycoproteins, below).

The sequence of Δ-peptide varies in length between different EBOV species (from 40 to 48 amino acids) (Volchkova, Klenk, and Volchkov, 1999). Its apparent molecular mass of 10-14 kDa is much larger than its predicted mass of 4.7 kDa, but it does not appear to form any sort of multimer. Instead its mass is thought to be due to extensive O-glycosylation (Volchkova, Klenk, and Volchkov, 1999). This peptide has not been studied extensively and currently has no known function but presumably is secreted in levels comparable to sGP. As ssGP has only recently been characterized, its structure is not well defined. It appears to be a dimer, likely as a result of an intermolecular disulphide bond between Cys53 residues, as Cys306 is not included in ssGP (Mehedi et al., 2008).

$GP_{1,2}$ is a type I transmembrane protein, which forms metastable non-covalently attached trimers of heterodimers on the cell surface (Figure 4 B) (Lee et al., 2008; Sanchez et al., 1998; Volchkov et al., 1998a; Volchkova et al., 1998). A crystal structure for $GP_{1,2}$ has been resolved, based on a modified version of the protein in a complex with

monoclonal antibody F_{ab} KZ52. How accurately this reflects the actual structure is not known, as multiple modifications including the deletion of the mucin-like domain, membrane proximal external region (MPER) and transmembrane domain were required for crystallization, in addition to the mutation of two N-linked glycosylation sites (Thr42Val/Thr230Val) (Figure 5 B). Trimerization is mediated through multiple GP_1–GP_2 and GP_2–GP_2 contacts with no major contacts noted between neighbouring GP_1 molecules (Lee et al., 2008). The three GP_1 ectodomains form a chalice or bowl-like structure, which is encircled by helices of the three GP_2 subunits. The structure of each GP_1 molecule consists of a single domain that includes a base, head and glycan cap region (Lee et al., 2008). The base region clamps the internal fusion loop and a helix of GP_2 via hydrophobic interactions. This region also contains Cys53, which is thought to form an intermolecular disulphide bridge to Cys609 of GP_2 (Jeffers, Sanders, and Sanchez, 2002); however, this was not confirmed in the structure, as the region containing Cys609 was disordered. The head region is located between the base and glycan cap towards the host membrane surface. Two intramolecular disulphide bonds (Cys108–Cys135 and Cys121–Cys147) were observed in this region (Lee et al., 2008), confirming previous biochemical data (Jeffers, Sanders, and Sanchez, 2002). The glycan cap region contains four predicted N-linked glycans (Asn228, Asn238, Asn257 and Asn268) and forms a dome over the GP_1 head region. It is predicted that if the mucin-like domain was included in the structure, it would further encompass the region, resulting in the majority of the protein being shielded by extensive glycosylation. The only predicted exposed region would include the KZ52 binding site, the flexible regions of HR2 and the membrane-proximal external region (Figure 5 B) (Lee et al., 2008). In addition to the

large ectodomain described above, there is a lipid-membrane spanning domain (which is predicted to consist of approximately 30 amino acids) and a short cytoplasmic tail of four amino acids (Feldmann et al., 2001). A putative receptor binding site (RBS) has been mapped to residues 54–201 (Figure 5 B) (Kuhn et al., 2006), which includes part of the base and head regions of GP_1 (Lee et al., 2008). Additional studies have identified at least 19 GP_1 residues from this region that are important for attachment and entry (Brindley et al., 2007; Manicassamy et al., 2005; Mpanju et al., 2006). These residues tend to be highly conserved among the EBOV species. Many of these residues are apolar or aromatic and are predicted to be involved in maintaining the structural integrity of GP_1 for receptor binding or fusion. One of the difficulties with relating the crystal structure to current data concerns the putative receptor binding site, which is completely buried in the structure and covered by the extensive glycan shield. This suggests that it would not be accessible for receptor binding.

GP_2 is responsible for fusion of viral and host cell membranes and contains the internal fusion loop and the heptad repeat regions, HR1 and HR2 (Figure 5 B). The structure of the GP_2 ectodomain consists of a long, triple-stranded, coiled-coil, followed by a disulphide-bonded loop, which reverses the direction of the chain and connects to an α-helix that is packed anti-parallel to the core helixes (Malashkevich et al., 1999; Weissenhorn et al., 1998a; Weissenhorn et al., 1998b). The internal fusion loop (residues 511–556) is packed into a region on the GP_1 head of a neighbouring subunit in the trimer (Lee et al., 2008). The pre-fusion GP_2 adopts a novel conformation, intimately curled around GP_1; however, based on the structure of GP_2 alone, it has striking similarities to

influenza H2 and HIV-gp41, suggesting that these diverse viruses may have a common membrane fusion mechanism (Weissenhorn et al., 1998b).

ssGP is essentially a truncated version of sGP with only a few (minimum two – dependant upon editing) unique (i.e. not included in sGP or GP_1) amino acids at the carboxy-terminus. It lacks Cys306, thus potentially altering its tertiary structure compared to sGP. Transcripts that code for ssGP have been identified both *in vitro* and *in vivo* during ZEBOV infection; however, production of this protein during virus infection has only been confirmed *in vitro* (Mehedi et al., 2008).

1.6 Pathogenesis of Ebola Virus Infection

The initial targets of EBOV infection are monocytes/macrophages and dendritic cells (Geisbert et al., 2003b). EBOV infection results in the activation of monocytes/macrophages, leading to the systemic release of cytokines, chemokines and other mediators such as tissue factor (TF) (Figure 6) (Feldmann et al., 1996; Geisbert et al., 2003c; Schnittler and Feldmann, 1999; Schnittler and Feldmann, 2003; Stroher et al., 2001; Wahl-Jensen et al., 2005a). Conversely, infection of dendritic cells by EBOV leads to impaired functioning, including a decreased ability to secrete pro-inflammatory cytokines, a lack of up-regulation of co-stimulatory molecules, a decreased ability to stimulate T cells (Mahanty et al., 2003) and a decreased ability to produce type I IFN (Figure 6) (Chang et al., 2009). Dissemination of the virus is thought to be aided by these initial target cells as these cells are trafficked to regional lymph nodes, the liver and the spleen, where resident macrophages and dendritic cells are subsequently infected. The activation of monocytes/macrophages, with the subsequent release of cytokines and other

Figure 6. **Pathogenesis of Ebola virus infection.** The initial targets of EBOV infection are monocytes/macrophages and dendritic cells. Infection of monocytes/macrophages inhibits the production of IFN resulting in an impaired innate immune response. In addition, EBOV infection of monocytes/macrophages has multiple other consequences including: the up-regulation of tissue factor, which activates the coagulation cascade leading to disseminated intravascular coagulation; production of inflammatory cytokines/chemokines that can result in endothelial cell (EC) activation and increased permeability, interference with normal T-lymphocyte functioning resulting in bystander apoptosis and immunosuppression. Virus is spread to regional lymph nodes, liver and spleen by the trafficking of infected target cells to these tissues. This results in the subsequent infection of parenchymal cells causing apoptosis and/or necrosis. Direct infection of endothelial cell occurs late in infection and may result in altered EC barrier function and vascular leakage. Infection of dendritic cells leads to disregulation of dendritic cell function and the inhibition of innate immunity. It may also initiate signalling that results in the inhibition of proper T-lymphocyte functioning. Adapted from Ebihara et al. 2005

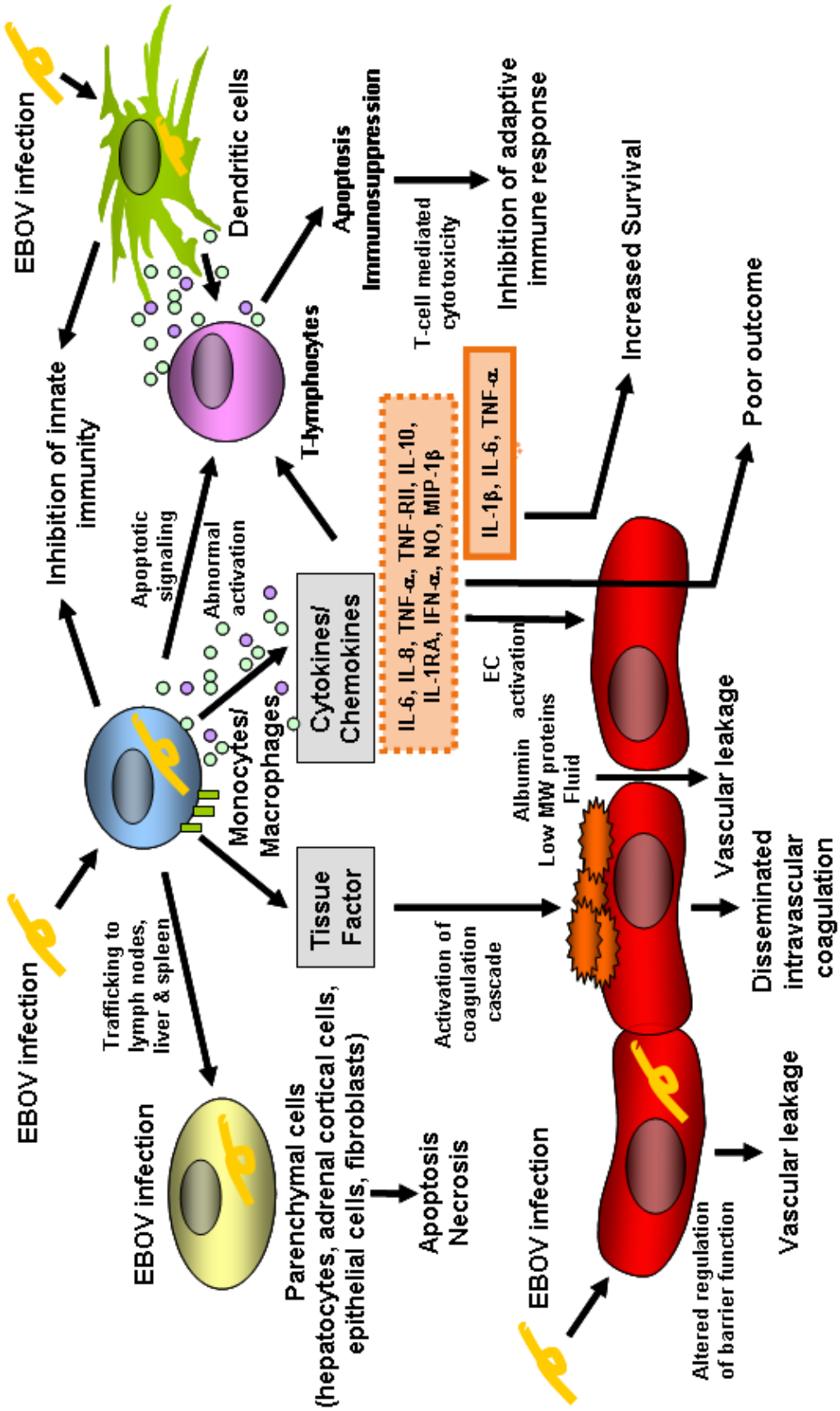
EBOV infection
Dendritic cells
Inhibition of innate immunity
Apoptotic signaling
Abnormal activation
Monocytes/ Macrophages
T-lymphocytes
Apoptosis
Immunosuppression
T-cell mediated cytotoxicity
Inhibition of adaptive immune response
Cytokines/ Chemokines
IL-6, IL-8, TNF-α, TNF-RII, IL-10, IL-1RA, IFN-α, NO, MIP-1β
IL-1β, IL-6, TNF-α
Increased Survival
Poor outcome
EBOV infection
Trafficking to lymph nodes, liver & spleen
Tissue Factor
Activation of coagulation cascade
EC activation
Albumin
Low MW proteins
Fluid
Vascular leakage
Disseminated intravascular coagulation
EBOV infection
Parenchymal cells (hepatocytes, adrenal cortical cells, epithelial cells, fibroblasts)
Apoptosis
Necrosis
EBOV infection
Altered regulation of barrier function
Vascular leakage

mediators, most likely recruits additional target cells to areas of infection thus providing a greater number of targets for replication. EBOV also infects a wide variety of other cell types, including endothelial cells, fibroblasts, hepatocytes, adrenal cortical cells and several types of epithelial cells, as observed in samples obtained from either human or NHP infections (Baskerville et al., 1985; Davis et al., 1997; Geisbert et al., 1992; Geisbert et al., 2003d; Jaax et al., 1996; Ryabchikova, Kolesnikova, and Luchko, 1999; Zaki and Goldsmith, 1999; Zaki et al., 1999). *In vivo* data indicates that lymphocytes are not infected by EBOV and it is generally accepted that lymphocytes are not a significant site of replication; however, a very low level of infection has been noted in certain lymphoid cell culture systems (Marzi et al., 2007).

The liver and adrenal cortex are also considered to be important targets of virus replication, with high virus titres being recovered from these organs. Following infection, both the liver and the adrenal cortex show evidence of extensive virus replication and necrosis (Geisbert et al., 2003a; Geisbert et al., 2003b; Jaax et al., 1996; Ryabchikova, Kolesnikova, and Luchko, 1999; Zaki and Goldsmith, 1999). Clinical observations in humans and NHPs correlate well with pathological findings, as an elevation of liver enzymes is consistently observed (Geisbert et al., 2003a; Geisbert et al., 2003b; Jaax et al., 1996; Ryabchikova, Kolesnikova, and Luchko, 1999). While the extent of liver impairment is not considered to be significant enough to be the sole cause of death, it likely contributes to overall pathogenesis. Coagulation abnormalities are thought to be exacerbated by a decreased synthesis of coagulation factors and other plasma proteins as a result of liver damage. It is also probable that impairment of the adrenal cortex

contributes to hypotension and sodium loss with hypovolemia that is observed during infection (Sanchez, Geisbert, and Feldmann, 2007).

In the late stages of infection, extensive necrosis is observed in parenchymal cells of many organs, including the liver, spleen, kidney and gonads with little infiltration of immune cells into infected tissues (Zaki and Goldsmith, 1999). This highlights the large range of cell types that EBOV infects and also suggests that the immune response to infection is inhibited (Figure 6). Direct viral damage is thought to be one of the major elements of EBOV pathogenesis as tissue damage typically correlates with the presence of viral antigens and nucleic acid (Sanchez, Geisbert, and Feldmann, 2007). Cytotoxic effects on the cell are though to be primarily caused by the expression of the glycoprotein (see GP cytotoxicity); however, this has not been experimentally demonstrated.

Multiple studies have noted that, despite escaping infection, lymphocytes are depleted during infection and necrosis is observed in the spleen, thymus, and lymph nodes of fatal human cases as well as in experimentally-infected NHPs (Fisher-Hoch et al., 1983; Geisbert et al., 2003b; Jaax et al., 1995; Ryabchikova, Kolesnikova, and Luchko, 1999; Zaki and Goldsmith, 1999). In some cases large numbers of apoptotic lymphocytes were observed in both humans and NHPs (Baize et al., 1999; Baize et al., 2000; Geisbert et al., 2000; Reed et al., 2004). While this may explain the loss of lymphocytes, the mechanism of induction of apoptosis remains unknown and large numbers of apoptotic lymphocytes have not been observed in all studies. GP_2 contains an retrovirus-like immunosuppressive motif in its C-terminal region (Volchkov, Blinov, and Netesov, 1992) that has been implicated in lymphocyte depletion (Chepurnov et al., 1999) and decreased activation of CD4+ and CD8+ T cells (Yaddanapudi et al., 2006). It

is not clear whether this occurs in the context of the virus particle or as soluble protein shed from infected cells (e.g.$GP_{1,2\Delta TM}$).

Despite the depletion of lymphocytes, there is still a substantial innate immune response to EBOV infection. It is thought that this highly inflammatory immune response contributes to pathogenesis. Infection typically elicits a severe inflammatory response with increases in the expression of interleukin (IL)-6, IL-8, IL-10, IL-12, IFN-inducible protein (IP)-10, monocyte chemoattractant protein-1 (MCP-1), regulated on activation, normal T-cell expressed and secreted (RANTES), TNF-α and reactive oxygen (e.g. H_2O_2) and nitrogen species (e.g. NO) (Figure 6) (Baize et al., 1999; Baize et al., 2002; Geisbert et al., 2003a; Geisbert et al., 2003b; Hensley et al., 2002; Hutchinson and Rollin, 2007; Hutchinson et al., 2001; Ignatiev et al., 2000; Sanchez et al., 2004; Villinger et al., 1999). Data indicate that early detection of the inflammatory cytokines IL-1RA, IL-6, IL-8, IL-10 as well as macrophage inflammatory protein-1 β (MIP-1β) correlate with a fatal outcome, further supporting the idea that this response is detrimental to the host (Figure 6) (Baize et al., 2002; Hutchinson and Rollin, 2007). Infection of the initial target cells is suspected to be the cause of this pro-inflammatory response, as *in vitro* experiments indicate that a variety of primary human cells (such as monocytes and macrophages) release these cytokines as a result of EBOV infection (Feldmann et al., 1996; Hensley et al., 2002; Stroher et al., 2001; Wahl-Jensen et al., 2005a).

Increased levels of NO have been observed in the blood of humans and NHPs (Baize et al., 2002; Geisbert et al., 2003d; Hensley et al., 2002; Sanchez et al., 2004) and these increases have been associated with mortality (Figure 6) (Sanchez et al., 2004). NO is primarily produced by monocytes/macrophages and mediates hypotension as well as

being a component of the innate immune response (Culotta and Koshland, 1992). However, overproduction can have deleterious effects on the host including direct tissue damage, induction of apoptosis of bystander lymphocytes, and decreases in vascular integrity (Figure 6) (Hou, Janczuk, and Wang, 1999). As monocytes/macrophages are infected by EBOV early in the disease process it is possible that infection of these cells results in the production of large amounts of NO, which is harmful to the host instead of controlling the infection.

Limited data suggests that an effective IFN response may be the most useful mechanism to control EBOV replication (Ebihara et al., 2006; Kash et al., 2006) and early IFN-α production has been associated with survival (Hutchinson and Rollin, 2007). Unfortunately for the host, the IFN response is usually suppressed (Basler and Amarasinghe, 2009), resulting in the inability to control infection (Figure 6). While the complete mechanism of IFN suppression has yet to be determined, VP35 has been characterized as blocking the phosphorylation of IFN-regulatory factor-3 (IRF-3), a factor necessary for the transcription of IFN genes (Basler et al., 2003; Basler et al., 2000). VP35 also interferes with interactions between the kinases IκB kinase epsilon (IκK epsilon), TBK-1 and their normal partners, which include IRF-3 and IRF-7, resulting in reduced INF-β promoter activity (Chang et al., 2009; Prins, Cardenas, and Basler, 2009). It was also shown that the C-terminal region of VP35 has a double-stranded RNA (dsRNA)-binding motif, similar to influenza A virus NS1 protein, which also functions as an IFN antagonist (Hartman, Towner, and Nichol, 2004). Furthermore, VP24 has been demonstrated to inhibit IFN-α/β and -γ signalling by inhibiting the interactions between STAT-1 and its nuclear localization signal receptors karyopherin

α1, 5 and 6, thus limiting nuclear accumulation of phosphorylated STAT-1 (Reid et al., 2006; Reid et al., 2007).

1.6.1 Role of the endothelium in Ebola hemorrhagic fever

Poorly maintained fluid distribution and uncontrolled coagulation are hallmarks of EBOV infection, suggesting that alterations to the endothelium play an important role in EBOV pathogenesis (Hensley and Geisbert, 2005; Mahanty and Bray, 2004). During infection this is manifested as systemic oedema and disseminated intravascular coagulation (DIC), respectively. Since expression of the glycoprotein resulted in cytotoxicity *in vitro*, it was assumed that direct infection of endothelial cells was the primary determinant of vascular cell injury (Figure 6) (Yang et al., 2000), which resulted in activation of coagulation and inflammation as well as altering fluid distribution. Observations that endothelial cells from a variety of tissues appear to be infected in samples from deceased human patients (Zaki and Goldsmith, 1999), NHPs (Geisbert et al., 2003d; Ryabchikova, Kolesnikova, and Luchko, 1999), mice (Bray et al., 1998; Gibb et al., 2001) and guinea pigs (Connolly et al., 1999) further supported this idea.

While endothelial cells are undoubtedly infected with EBOV (Geisbert et al., 2003d; Harcourt, Sanchez, and Offermann, 1998; Schnittler and Feldmann, 2003) and *in vitro* this causes cytopathic effects, serial sampling of NHPs has provided no evidence of direct cytopathic effects to endothelial cells, despite virus replication being detected (Geisbert et al., 2003d). Infection of endothelial cells was not observed until at least one day following the onset of DIC and perivascular oedema (Geisbert et al., 2003d). Moreover, the only time point where significant infection of endothelial cells was observed was in the terminal stages of the disease (Geisbert et al., 2003d) and even then

the endothelium was morphologically intact despite some indications of increased vascular permeability. Historically, there is no account of vascular lesions as a result of EBOV infection from pathological analysis of either human (Murphy, 1978) or NHP tissues (Baskerville et al., 1978; Baskerville et al., 1985; Davis et al., 1997; Geisbert et al., 2003d; Jaax et al., 1996; Ryabchikova, Kolesnikova, and Luchko, 1999). The finding that serum albumin levels were decreased while total serum protein levels remained constant further supports a lack of total disruption of the endothelium (Figure 6) (Geisbert et al., 2003c). The loss of the low molecular weight proteins (Figure 6) suggests that their endothelial barrier function is decreased but that the endothelium does not undergo severe necrosis, as this would result in a drop in total serum protein levels (Sanchez, Geisbert, and Feldmann, 2007). Finally, it was demonstrated that ZEBOV infection actually resulted in the up-regulation of anti-apoptotic genes in primary human endothelial cells (Geisbert et al., 2003d), suggesting that it is unlikely these cells undergo substantial apoptosis. Thus, current data suggests that it is unlikely that direct infection of endothelial cells is the primary cause of disregulated coagulation and fluid distribution.

Despite the lack of evidence of direct infection, vascular function is still disrupted during EBOV infection and is considered a major factor that contributes to fatal outcomes (Figure 6) (Schnittler et al., 2004). Presumably decreased vascular function occurs due to the loss of endothelial barrier function; however, it is unclear whether activation of the endothelium occurs as a result of host factors (such as TNF-α), viral factors (such as GP) or a combination (Schnittler and Feldmann, 2003). Levels of TNF-α are frequently elevated during EBOV infection and an increase in TNF-α has been associated with fatal outcomes (Villinger et al., 1999). TNF-α is known to increase the

permeability of endothelial cells, although its effect in the context of the multiple cytokines, chemokines and other factors is unknown (Falzarano et al., 2006; Ferrero, 2004; Wahl-Jensen et al., 2005b). Limited i*n vitro* data suggests that EBOV-induced cytokine release (i.e. TNF-α) results in the activation of the endothelium causing a breakdown in the barrier function (Wahl-Jensen et al., 2005b); however, this was investigated under static conditions while endothelial cells *in vivo* are subjected to constant shear stress. Furthermore, GP contained in VLPs has been shown to cause activation of endothelial cells resulting in the breakdown of the barrier function (Wahl-Jensen et al., 2005b).

These data support the idea that the disruption of the endothelium indirectly results from a mediator-induced inflammatory response of primary target cells (i.e. monocytes/ macrophages) rather than by direct EBOV replication-induced cytopathology (Sanchez, Geisbert, and Feldmann, 2007). This hypothesis suggests that an EBOV-induced elevation of TNF-α causes vascular dysfunction; however, the *in vivo* levels of TNF-α are probably not sufficient to result in major changes to the endothelium alone. In combination with other factors such as NO, TNF-α can have a priming effect on endothelial barrier function and NO levels have been noted to be substantially increased during infection (Geisbert et al., 2003c; Hensley et al., 2002). Increased levels of NO have also been found in infected humans and high levels correlate with fatal outcome (Baize et al., 2002; Sanchez et al., 2004). NO is a potent endogenous vasodilator and is involved in the development of vasodilatory shock (Landry and Oliver, 2001). In the presence of NO, lower amounts of TNF-α are capable of resulting in systemic vascular barrier dysfunction in a NO-dependant mechanism (Worrall et al., 1997). Therefore,

current data would suggest that a combination of EBOV-induced inflammatory mediators is either wholly or partially responsible for the disruption of vascular function.

Coagulation and fibrinolysis are also severely disrupted during EBOV infection and can be observed as thrombocytopenia, consumption of clotting factors and increased levels of fibrin degradation products (Figure 6). This pro-coagulant state enhances inflammation, which subsequently induces further coagulation (Hensley et al., 2005; Levi, 2004). TNF-α can also induce the expression of TF on endothelial cells (Szotowski et al., 2005) and can impair the function of the anticoagulant-protein-C pathway by down regulating thrombomodulin (Levi, 2004). DIC is a routine finding in NHPs and there is clinical laboratory evidence to suggest that it occurs in human infection as well (Fisher-Hoch et al., 1983; Fisher-Hoch et al., 1985; Geisbert et al., 2003a; Geisbert et al., 2003c; Geisbert et al., 2003d; Hensley and Geisbert, 2005; Hensley et al., 2007; Rollin, Bausch, and Sanchez, 2007). Despite the consumptive coagulopathy, massive loss of blood is not frequently observed. When present, it is usually restricted to the gastrointestinal tract and is not considered sufficient to account for death (Sanchez, Geisbert, and Feldmann, 2007).

1.6.2 Disseminated intravascular coagulation

DIC appears to be consistently observed during EBOV infection in both humans (Rollin, Bausch, and Sanchez, 2007) and NHPs (Baskerville et al., 1978; Bray et al., 2001; Davis et al., 1997; Fisher-Hoch et al., 1992; Fisher-Hoch et al., 1983; Geisbert et al., 2003a; Geisbert et al., 2003b; Geisbert et al., 2003c; Jaax et al., 1996; Ryabchikova, Kolesnikova, and Luchko, 1999). DIC is a syndrome that results from systemic activation of the blood coagulation system (Vincent and De Backer, 2005). During this process the

normal regulatory mechanisms that control clotting (i.e. protein C pathway, anti-thrombin) are quickly overwhelmed leading to fibrin generation and deposition (Levi, 2004). Fibrin deposition results in the development of microvascular thrombi in various organs leading to ischemia and impaired organ perfusion, which contributes to multi-organ failure (Vincent and De Backer, 2005). The processes that lead to the generation of fibrin consume factors that are involved in coagulation in addition to platelets, which ultimately results in a decreased clotting ability.

A critical mediator of DIC is the transmembrane glycoprotein, TF. Normally, TF is present in the vascular adventitia (the connective tissue surrounding most organs), the epithelium of the skin and mucosa as well as a number of other sites that are likely not relevant to EBOV infection (Drake, Morrissey, and Edgington, 1989; Faulk, Labarrere, and Carson, 1990; Fleck et al., 1990; Flossel et al., 1994). In monocytes, macrophages and endothelial cells, TF is not expressed unless induced (Camerer, Kolsto, and Prydz, 1996). The up-regulation of TF in vascular endothelial cells and monocytes/macrophages has been characterized as resulting from inflammatory cytokines (IL-1 and TNF-α), various mitogens, IFN, endotoxins, virus infection, thrombin, immune complexes, phorbol ester and occupancy of cell adhesion molecules (Camerer, Kolsto, and Prydz, 1996).

The mechanism(s) responsible for triggering DIC during EBOV infection is not completely understood; however, it seems to be an early event, as a serial sampling study noted elevated D-dimers levels (one of the indicators of DIC) as early as one day post-infection - two full days before viremia was detected (Geisbert et al., 2003b). While the induction of coagulopathy is likely to be multimodal, the early up-regulation and release

of TF from infected monocytes/macrophages is suspected to be a critical factor as it is a potent initiator of the serine protease cascade of coagulation (Esmon, 2008). *In vivo* data supporting this hypothesis is based on increased TF mRNA; however, this is not noted until two days following the increase in D-dimers (Geisbert et al., 2003c). To date, most studies have focused on the up-regulation of TF mRNA at early time points following the stimulus. *In vivo* studies typically lack confirmation of up-regulation of TF at the protein level (this is also true for the EBOV infection model). It is thought the increase in TF at the protein level does occur but that it is quickly negatively regulated by endogenous factors such as cAMP, IL-4, IL-10, IL-13 and retinoic acid (Barstad et al., 1995; Herbert et al., 1993; Ishii et al., 1992; Lyberg, 1983; Martin, Jamieson, and Tuffin, 1993; Ramani et al., 1994; Ramani et al., 1993a; Ramani et al., 1993b) as well as tissue factor pathway inhibitor-1 (TFPI-1) (McGee, Foster, and Wang, 1994).

In vitro, EBOV can directly induce the expression of TF on the surface of macrophages (Geisbert et al., 2003c). While it is not clear if increased levels of TF are induced by TNF-α and/or other inflammatory cytokines or by direct infection of macrophages, it is likely that substantially increased levels of TF would contribute to the activation of the clotting cascade, eventually leading to the development of DIC. The difficulties in detecting an up-regulation of TF at the protein level is not atypical as demonstrating this on the endothelium or on monocytes *in vivo* during studies of both sepsis and hemorrhagic fever have been difficult (Faust, Heyderman, and Levin, 2001; Geisbert et al., 2003a; Geisbert et al., 2003d). Liver impairment as a result of virus replication is also a contributing factor to coagulopathy as many of the components consumed during DIC (e.g. protein C, all factors except VIII) are generated by the liver.

During EBOV infection, the level of protein C in the plasma has been observed to dramatically drop as early as two days post-infection (Geisbert et al., 2003c).

Further supporting TF as the driving force behind DIC, or at least an important pathogenesis mediator, is the observation that inhibitors of TF decrease the levels of the inflammatory cytokines IL-6 and MCP-1 and increase the time-to-death of NHPs (Geisbert et al., 2003a). The importance of coagulation in EBOV infection is also highlighted by the findings that treatment of ZEBOV-infected Rhesus macaques with recombinant nematode anticoagulant protein C2 (rNAPc2) (an inhibitor of factor VIIa and TF), increased survival to 33% and extended mean survival by three days (Geisbert et al., 2003a). Additionally, ZEBOV-challenged macaques treated with activated protein C (Xigris) achieved 18% survival and increased mean survival by 4 days, while infection was fatal in 100% of untreated animals (Hensley et al., 2007). It has also been suggested that soluble glycoproteins, such as sGP and Δ-peptide, may also effect the coagulation cascade (Kuhn, 2008; Volchkova et al., 1999) but this has not been thoroughly investigated.

1.7 Functions of the Soluble Glycoproteins

1.7.1 Direct functions of the soluble glycoproteins

EBOV is unique among the filoviruses in that it produces multiple transcripts from its glycoprotein gene resulting in the production of at least 6 distinct protein products (sGP, Δ-peptide, $GP_{1,2}$, $GP_{1,2\Delta TM}$, GP_1 and ssGP). Apart from $GP_{1,2,}$ which is the surface spike glycoprotein, the other products are secreted or shed from infected cells. It is suspected that these secreted and/or shed products must somehow modulate the host

response or play some role in pathogenesis. sGP is produced in large amounts and high levels have been observed in the plasma of infected individuals (Sanchez et al., 1996). It is assumed that a substantial amount of Δ-peptide is also secreted from infected cells; however, this has not been confirmed. The first proposed function for sGP stated that it bound $F_c\gamma$RIIIB (CD16b) on neutrophils, inhibiting L-selectin down-regulation, thus blocking neutrophil migration into tissues (Yang et al., 1998). Further work suggested a mechanism whereby the CD16b and CR3 interaction was disrupted by sGP, which resulted in the inhibition of neutrophil migration (Kindzelskii et al., 2000). Unfortunately, other groups have not been able to demonstrate direct binding of sGP to neutrophils by CD16b (Maruyama et al., 1998b; Sui and Marasco, 2002); therefore, this role has been discounted.

It has been suggested that sGP, GP_1 and/or $GP1_{1,2\Delta TM}$ could act as decoys for virus-neutralizing antibodies (Dolnik et al., 2004; Ito et al., 2001), although the role of sGP as a decoy is controversial as its quaternary structure is expected to be markedly different. Nonetheless, the neutralizing effect of antiserum against $GP_{1,2}$ and sGP is markedly reduced in the presence of sGP (Ito et al., 2001). Providing support for this theory is the observation that shed $GP_{1,2\Delta TM}$ binds neutralizing antibodies and significant levels of this protein were detected in infected guinea pigs (Dolnik et al., 2004). Furthermore, up-regulation of TNF-α converting enzyme (TACE) has been noted during infection and detection of shed $GP_{1,2\Delta TM}$ has also been described in NHP EBOV infections (Rubins et al., 2007). While the disease course is quite rapid, it is possible that neutralizing antibodies are generated before individuals succumb and that these secreted and shed products play an immune evasion role. ssGP is also secreted from infected cells

and thus may also play a decoy role. It is also possible that it could alter the host response; however, based on the quantity of transcripts, only small amount would be expected to be produced as compared to sGP.

As numerous cell types are activated during EBOV infection, studies were undertaken to determine if the secreted glycoproteins play a role in the activation of macrophages or endothelial cells. Macrophages and endothelial were treated with sGP, Δ-peptide, GP_1 or $GP_{1,2\Delta TM}$ but there was no indication that these soluble factors activate these cells; however, $GP_{1,2}$ in the context of a membrane-bound form (i.e. together with VP40 as a VLP) has been shown to result in activation of both these cell types (Wahl-Jensen et al., 2005a; Wahl-Jensen et al., 2005b). During these investigations, a novel role was described for sGP whereby it rescued endothelial cell barrier function following treatment with TNF-α, while the other secreted glycoproteins did not show this effect (Wahl-Jensen et al., 2005b). Whether this effect may counteract the barrier decrease that is caused during EBOV infection is unknown and it has been suggested that this anti-inflammatory effect may interfere with either rolling, attachment or extravasation of immune cells to sites of infection, thus further preventing an effective immune response.

The development of DIC is noted during EBOV infection in both humans and NHPs during infection. While it is likely that a transient up-regulation of TF is responsible for the initiation of coagulation, it has been suggested that the secreted glycoprotein products could interfere with normal haemostasis; however, experimental data supporting this idea is currently lacking. This is further supported by the observation that DIC in EBOV infection is severe, while pathological findings relating to DIC were less prominent in MARV infection and these animals were not protected by rNAPc2

(Geisbert et al., 2007). One of the major differences between these two viruses is the process of transcriptional editing that occurs in the EBOV glycoprotein, which is absent in MARV. Therefore, pathological differences may be the result of the additional glycoprotein products.

1.7.2 sGP indirectly limits $GP_{1,2}$ expression and cytotoxicity

$GP_{1,2}$ is thought to be an important viral determinant of cytotoxicity and cellular injury. When expressed in cell culture, $GP_{1,2}$, results in cytotoxic effects such as cell rounding, detachment and increased permeability in vessel explants (Yang et al., 2000); however, the cells generally remain viable (Chan, Ma, and Goldsmith, 2000; Simmons et al., 2002). The down-regulation of the cell surface molecules β-integrin (which is involved in attachment of cells to the extracellular matrix and signal transduction), αV-integrin, epidermal growth factor receptor, transferrin receptor and MHC-1 appear to be the cause of rounding and detachment (Simmons et al., 2002; Takada et al., 2000). Cytotoxicity has been linked to the highly O-glycosylated mucin-like domain and deletion of this region is sufficient to cease cell rounding and detachment (Simmons et al., 2002; Sullivan et al., 2005; Yang et al., 2000; Zampieri et al., 2007). Others have associated the C-terminal region of GP_2 with cytotoxicity and observed that cytotoxicity could be blocked by the serine/threonine kinase inhibitor 2-aminopurine, suggesting that this process is dependent on phosphorylation signalling (Chan, Ma, and Goldsmith, 2000). It has also been shown that the proposed ectodomain and its anchorage in the membrane is required for cytotoxicity (Takada et al., 2000).

In the context of the actual EBOV infection, reverse genetics has been used to demonstrate that over expression of $GP_{1,2}$ results in cytotoxicity (Volchkov et al., 2001).

Typically only 20% of transcripts from the glycoprotein gene code for $GP_{1,2}$, resulting in lower expression of this protein compared to the recombinant systems described above. To study the effect of $GP_{1,2}$ over expression, a mutant virus was generated that replaced the editing site AAAAAAA with the following sequence AAGAAGAA, allowing production of exclusively $GP_{1,2}$ transcripts. This virus was extremely cytotoxic *in vitro* but had a lower pathogenicity in the guinea pig model, supporting the idea that $GP_{1,2}$ expression via editing is an optimized process. If sGP is added back into the system as a gene inserted between VP35 and VP40 in the editing mutant background, this virus behaves similarly to the editing mutant indicating that sGP itself does not play a direct role in limiting GP-induced cytotoxicity (Volchkova et al., 2008).

1.8 Role of Glycosylation in Protein Structure and Function

Glycosylation is the most common of all the known protein post-translational modifications. These carbohydrates can modulate the biological functions of a glycoprotein, affect their folding, protect a protein against hydrolysis, change their cellular location and reduce or prevent aggregation of a protein (Maeda and Kinoshita, 2008; Morelle et al., 2009). Many cellular secreted and cell surface proteins are modified with one or more forms of glycosylation by being directed through the ER-Golgi network during processing. Each glycosylation site on a protein can contain different glycan structures but the importance of this micro-heterogeneity is not known. Furthermore, resolving how different glycan structures influence protein function remains poorly studied. This is in part due to the difficulty in determining exact carbohydrate structures and in part due to micro-heterogeneity (Morelle et al., 2009). Certain viral proteins,

typically those that are on the surface of the virus, can also be glycosylated. Glycosylation of viral proteins has been demonstrated to affect protein folding, trafficking, receptor binding, infectivity, release and neurovirulence (Vigerust and Shepherd, 2007).

The most widely known form of protein glycosylation is N-linked, where the sugar moiety is covalently attached to the nitrogen atom of asparagine, in the tripeptide consensus sequence Asn-X-Thr/Ser (where X can be any amino acid except Pro) (Figure 7) (Hart, 1992; Kornfeld and Kornfeld, 1985). The precursors for both N-linked glycosylation and C-mannosylation are dolichol (dol)-phosphate (P)-sugars, which are generated exclusively on the luminal side of the ER (Figure 7) (Abeijon and Hirschberg, 1992; Clarke, Naylor, and Lennarz, 1989; Herscovics and Orlean, 1993). N-linked glycosylation is initiated by the transfer of a glycan chain from the lipid carrier, dol-P, to the polypeptide chain during synthesis in the ER (Figure 7). The glycan chain consists of a trimannosyl-chitobiose core [N-acetyl glucosamine (GlcNAc)]$_2$ [mannose]$_3$ to which chains of mannose residues are attached (Figure 7) (Sugrue, 2007). Glucose residues can be attached to the mannose residues by oligotransferases at this time; however, these glucose residues will eventually be removed by glucosidases. At this point, the glycan chain has a relatively high amount of mannose residues and is thus termed high mannose or simple glycans (Figure 7). Following these modifications in the ER, the high mannose glycosylated protein is transported to the Golgi. If these simple glycans are inaccessible to glycosidases in the Golgi due to protein folding they will remain as high mannose sugar moieties. Otherwise these mannose residues are selectively trimmed in the Golgi by mannosidases, leaving the trimannosyl-chitobiose core attached to the protein. This can

Figure 7. **Highlights of the glycosylation pathways used by EBOV.** N-glycosylation is the most common form of glycosylation. It starts with the transfer of GDP-mannose to a dolichol-phosphate (dol-P) moiety that contains two N-acetyl glucosamine (GlcNAc) residues on the cytoplasmic face of the endoplasmic reticulum (ER). This structure is then flipped inside where addition of multiple mannose and glucose residues can occur. This glycan can then be transferred from the dol-P to an asparagine in the consensus sequence Asn-X-Ser/Thr. Following trimming whereby the glucose residues are removed if the glycan is not further modified it is classified as a high mannose sugar. As it passes through the Golgi complex further processing can result in the addition of GlcNAc as well as galactose, fucose and terminal sialic acids. Depending on its composition the sugar can be either hybrid (containing at least one chain that possesses only mannose residues) or complex with no exclusive mannose chains. Multiple branching and the variety of sugars leads to a large variation in potential sugar composition. O-glycosylation is also a common post-translational modifications. It occurs strictly in the Golgi where N-acetyl galactosamine (GalNAc) is transferred to a Ser or Thr residue. This structure is added to by different enzymes resulting in many possible sugar structures that are terminated with sialic acid. C-mannosylation is a rarely described modification that occurs as the result of the transfer of a mannose residue from a dol-P-mannose in the ER. The mannose is then transferred to the first Trp in the consensus sequence Trp-X-X-Trp.

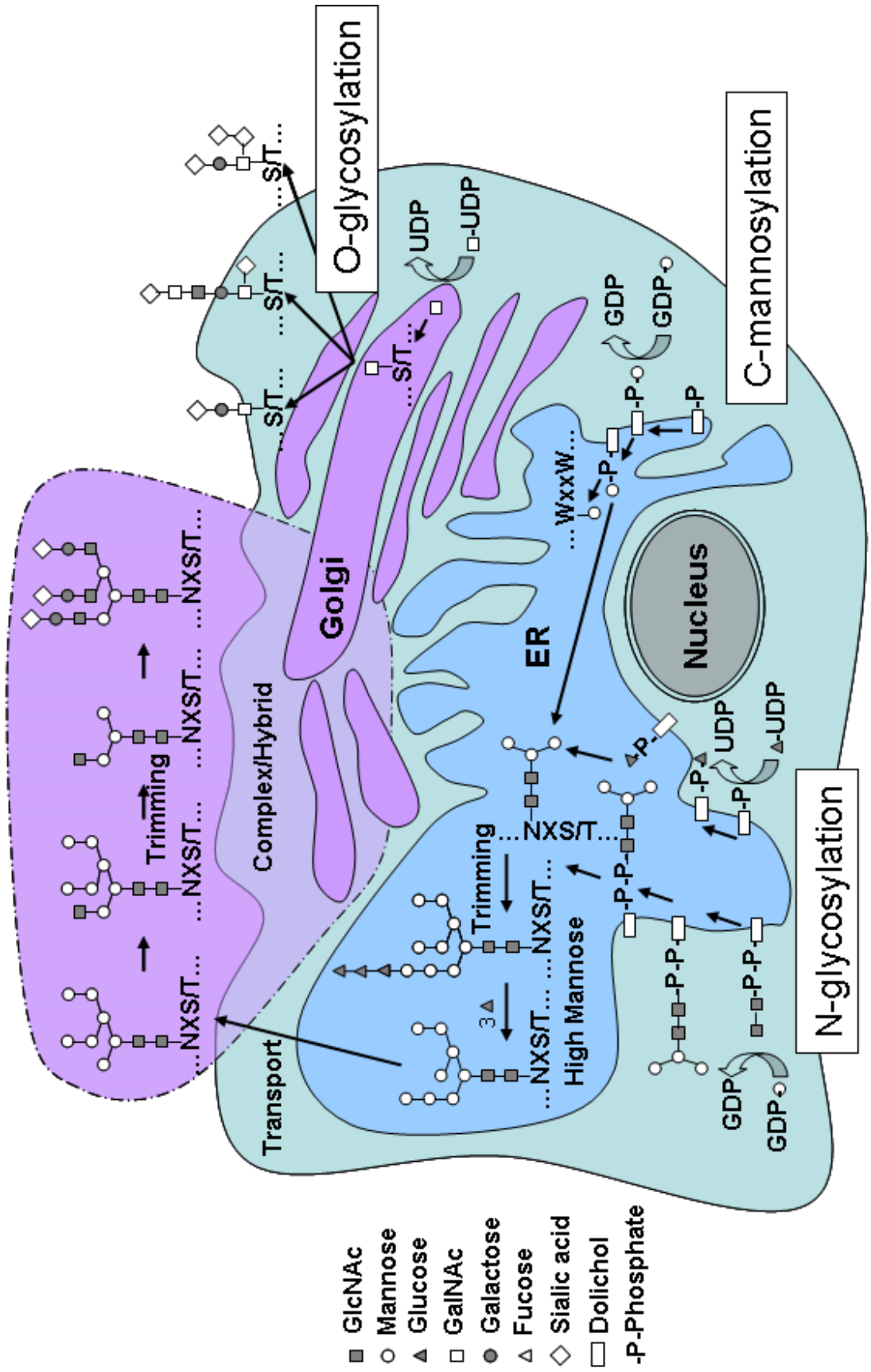
O-glycosylation
C-mannosylation
N-glycosylation
Golgi
ER
Nucleus
Complex/Hybrid
High Mannose
Transport
Trimming
...NXS/T...
...WxxW...
UDP
GDP
-P
-P-P-P
GlcNAc
Mannose
Glucose
GalNAc
Galactose
Fucose
Sialic acid
Dolichol
-P-Phosphate

then serve as the base for other terminal monosaccharides such as galactose, fucose and N-acetyl glucosamine (Vigerust and Shepherd, 2007). Fucose can also be attached to the GlcNAc involved in the linkage to the protein. This addition of multiple types of sugars leads to a high variety of structures and as such are referred to as complex glycans (Figure 7). It is also possible to generate intermediate structures that contain a high mannose content and complex structure. These are referred to as hybrid glycans. While the terminal sugars can differ, even greater heterogeneity of structure is generated by multiple branching of glycan chains (Sugrue, 2007). Complex glycans can exist as bi-antennary, tri-antennary and tetra-antennary chains.

Mucin type O-glycosylation is also a frequently observed form of glycosylation, which consists of a glycan chain linked via the oxygen atom of a Ser or Thr residue (Hart, 1992). This type of glycosylation does not require a consensus sequence. In contrast to N-linked glycosylation, mucin type O-glycosylation occurs exclusively in the Golgi and starts with the addition an N-acetyl galactosamine (GalNAc) and does not require a lipid carrier (Figure 7) (Roth et al., 1994). While GalNAc is typically the monosaccharide that forms the initial attachment of the glycan to the protein, other monosaccharides such as glucosamine and mannose can be used. The sugar chain is elongated by multiple glycosyltransferases which add specific monosaccharide such as GlcNAc, GalNAc and sialic acid to the growing chain (Figure 7) (Sugrue, 2007). Proteins that contain O-linked glycosylation typically have multiple sites that are glycosylated (e.g. EBOV GP mucin-like domain); therefore, significant additional mass is added (Sugrue, 2007).

C-mannosylation involves the covalent attachment of an α-mannopyranosyl residue to the indole C2 carbon atom of tryptophan via a C–C link (de Beer et al., 1995;

Hofsteenge et al., 1994). The linear recognition sequence consists of W-x-x-W/F, in which the first Trp residue becomes mannosylated (Figure 7) (Doucey et al., 1998). The C-mannosylation synthesis pathway appears to share the same source of mannose as that of the N-linked glycosylation pathway with GDP-Man being transferred to Dol-P-Man, which is then used as the precursor for (C^2-Man-)Trp (Figure 7). The transfer of the mannose to the Trp is assumed to be enzymatically catalyzed (Doucey et al., 1999; Doucey et al., 1998) by proteins present in liver microsomes (Krieg et al., 1998) but the enzyme(s) that perform this reaction have not been identified. Other forms of glycosylation, such as O-linked mannosylation and glycosylphosphatidylinositol (GPI)-anchor, are also possible; however, O-linked mannosylation and GPI-glycosylation are not known to be relevant to EBOV proteins and are not discussed further.

In general, the role of many glycans remains undefined; however, it is thought that they fit into one of two broad categories: structural/modulatory or specific recognition. N-glycans tend to be associated with protein folding and trafficking, while O-glycans possibly confer stickiness to proteins, which may aid in the attachment to the cell surface. Both forms of glycosylation may shield proteins from degradation, proteolytic cleavage and play a role in immune evasion. In the case of the EBOV glycoprotein products, the role(s) of the glycans are not specifically defined but are thought to play both a structural (N-glycans of GP_1 and sGP, O-glycans of Δ-peptide) and recognition role (mucin domain of GP_1). While C-mannosylation has not been assigned a clear function, there is some evidence that it affects protein structure (Furmanek and Hofsteenge, 2000; Li et al., 2009).

1.9 Objectives and Hypothesis

1.9.1 Significance

EBOV causes a severe hemorrhagic fever that typically results in high case-fatality rates and is considered to be a high-priority (category A) agent due to its potential use in bioterrorism. A lack of effective treatment or an approved vaccine leaves no options other than supportive care to individuals who become infected. The glycoprotein gene of EBOV is unique in that it produces multiple products as a result of transcriptional editing; however, most of these products do not have a well defined role in the virus life cycle or pathogenesis. Substantial amounts of sGP are produced during EBOV infection but a clearly defined function remains elusive. One proposed function is that sGP acts as an anti-inflammatory molecule (Wahl-Jensen et al., 2005b), which reverses or attenuates cytokine-induced increases in endothelial barrier function. It is thought that its effect on endothelial cells may interfere with extravasation of immune cells to sites of virus replication, which would make sGP an important mediator of immune suppression and pathogenesis. Demonstrating that the anti-inflammatory effect of sGP is structure dependent, as well as determining under what conditions (e.g. shear stress) this effect is exerted, would provide evidence that barrier function rescue is a specific effect that occurs under different physiological conditions. This would support further investigation into the effect of sGP on endothelial cells, such as determining the mechanism of this anti-inflammatory effect or whether sGP actually blocks extravisation of immune cells. This information could lead to a better understanding of viral pathogenesis, the absence of a vigorous immune response in infected tissues and could potentially provide a target for future therapeutic interventions.

As C-mannosylation has yet to have a well-described function, the potential role of this modification in sGP and $GP_{1,2}$ functions was pursued. Determining a function for specific post-translational modifications could lead to the identification of novel roles for glycosylation that result in a paradigm shift of how cell functions. For example, the recent description of the role that specific O-glycans play in intracellular signalling has been suggested to have the potential to be of comparable importance to phosphorylation (Luther and Haltiwanger, 2009). Furthermore, as this modification has not yet proven to have a definitive role in cellular proteins, it is possible it plays a role in viral protein function. If C-mannosylation were to prove important for EBOV protein function then it is possible that it could represent a unique target for anti-viral interventions.

1.9.2 Hypothesis

The function of the Ebola virus glycoproteins, sGP and $GP_{1,2}$, is dependent on their structure, in particular proper oligomerization and co- and post-translational processing, and alteration of specific amino acid residues involved in these processes will lead to loss of or decreased function of these proteins.

1.9.3 Objectives

1.) Structurally characterize the Ebola virus secreted glycoprotein, sGP, focusing on disulphide bond assignment and the identification of co- and post-translational modifications (i.e. glycosylation).

2.) Determine the effect sGP has on the endothelial cell barrier function under inflammatory (TNF-α), static and shear stress conditions as well as endogenous sGP expression and whether these effects are dependent on sGP structure (i.e. disulphide bonding, C-mannosylation).

3.) Determine whether potential C-mannosylation motifs in GP_1 and GP_2 are modified and whether these motifs affect GP biosynthesis, transport, particle incorporation and entry function.

2. MATERIALS AND METHODS

2.1 Isolation and Maintenance of Cells

2.1.1 Maintenance of cell lines

293T (human embryonic kidney) cells (obtained from Hans Schnittler, TU-Dresden, Dresden, Germany) were maintained in Dulbeco's modified Eagle medium (DMEM) (Invitrogen, Burlington, ON) with 10% heat-inactivated (30 minutes, 56ºC) γ-irradiated fetal bovine serum (FBS) (Wisent, St Bruno, QC) and 2mM L-glutamine (Invitrogen). Vero E6 (African green monkey kidney cells) (obtained from CDC, Atlanta, GA) and Huh7 cells (human hepatoma) (obtained from Michael Carpenter, National Microbiology Laboratory, Winnipeg, MB) were maintained in DMEM with 10% FBS, 2 mM L-glutamine, 100 U/ml penicillin and 100 μg/ml streptomycin. All cells were maintained in a humidified incubator at 37°C in 5% CO_2.

2.1.2 Isolation and culture of human umbilical vein endothelial cells

Human umbilical vein endothelial cells (HUVECs) were obtained from umbilical cords donated from local hospitals in Dresden, Germany. They were isolated and cultured as previously described (Schnittler et al., 1990). Briefly, umbilical cords were clamped inside the knots made at the hospital near the ends of the cord and the cord was immersed in 70% ethanol for 1 minute. Fresh cuts were made at both ends of the cord just inside the knots. A blunt needle was inserted into the vein and all blood was rinsed out with phosphate buffered saline (PBS). One end of the cord was clamped with a haemostat and collagenase solution containing 0.5 mg/ml collagenase II (Sigma, Munich, Germany) in PBS was added through the needle until the vein was full. Following this, both ends of the cord were clamped and the cord was incubated for 12 minutes in PBS at 37°C. The

cord was washed in 70% ethanol for 20-30 seconds and then shaken on a sterile towel to remove residual ethanol and to provide some mechanical disruption to the cells. At one end, the cord was cut inside of the haemostat and the second clamp was released. The collagenase solution and cells were collected into 25 ml of complete M199 medium (M199 with 10% FBS, 1% penicillin/streptomycin, 1% bovine lens growth factor) (Invitrogen, Karlsruhe, Germany). The cells were centrifuged for 5 minutes at 230 xg, the supernatant removed and cells resuspended in 5ml (for a cord less than 30 cm) or 10 ml (cord longer than 40 cm) of complete M199 and seeded onto pre-coated (0.5% gelatine in PBS for 1 hour at room temperature) T25 flasks. HUVECs were incubated for 24 hours in a humidified incubator at 37°C in 5% CO_2 and then the media was removed, the cells were washed with PBS to removed any erythrocytes and replaced with fresh complete M199. Flasks that were not confluent within 2 to 3 days were discarded. When splitting cells into chambers for impedance spectroscopy, cells were split into Endothelial cell growth media with growth factors (PromoCell, Heidelberg, Germany), 100 U/ml penicillin and 100 μg/ml streptomycin (ECGM+/+).

2.2 Virus Infection

2.2.1 Virus strains

All infectious EBOV work was performed in the BSL4 facilities at the Public Health Agency of Canada according to standard operating procedures. *Zaire ebolavirus*, strain Mayinga, was used for all experiments where indicated. The titre of the virus stock was obtained by immunoplaque (see below). All virus stocks were stored in liquid

nitrogen and were used immediately upon thawing; any remaining stock was discarded according to standard operating procedures.

2.2.2 Determination of virus titre by immunoplaque

Vero E6 cells were split 1:3 the day prior to starting the assay so that cells would be approximately 100% confluent. 10-fold dilutions of the virus stock were prepared in DMEM. Media was removed from the plate and virus dilutions were added (100 µl – 24 well plate). Virus was allowed to adsorb for 1 hr at 37°C. Virus was removed and cells were overlaid with 500 µl of 2x EMEM, 5% FBS, 2 mM l-glutamine, 100 U/ml penicillin and 100 µg/ml streptomycin mixed 1:1 with sterile 3% carboxymethyl cellulose (medium viscosity) in water. Cells were incubated for 4 days at 37°C in 5% CO_2, then the media was removed and cells were washed three times with PBS. Cells were then fixed with 10% PBS-buffered formalin for 10 minutes, the formalin removed and then washed with PBS. PBS+0.1% TritionX100 was added to the wells and incubated for 30 minutes at room temperature. This was removed and the cells were blocked with PBS with 1% bovine serum albumin (BSA) for 30 minutes at room temperature. The wells were subsequently washed three times with PBS. The primary antibody (rabbit anti-VP40) was added at a 1/500 dilution in PBS with 1% BSA (200 µl/well). This was incubated for 1 hour at room temperature and then washed three times with PBS. The secondary antibody (anti rabbit FITC (Sigma F-0382)) was diluted in PBS with 0.1% BSA and incubated for 1 hour at room temperature. This was then washed three times. Cells were then imaged inside BSL4 on a Zeiss Axiovert 40 CFL fluorescent microscope and positive cells counted.

2.3 Cloning and Site-Directed Mutagenesis

2.3.1 Preparation of chemically competent cells

All bacterial cloning procedures were performed in chemically competent TOP10 [genotype: F- *mcrA* Δ(*mrr-hsdRMS-mcr*BC) ϕ80*lacZ*ΔM15 Δ*lac*X74 *rec*A1 *ara*D139 Δ(*ara-leu*) 7697 *gal*U *gal*K *rsp*L (Str^R) *end*A1 *nup*G λ-] cells that were produced in-house or obtained commercially (One Shot, Invitrogen). In-house chemically competent cells were produced as previously described (Chung, Niemela, and Miller, 1989). Briefly, freshly thawed commercial TOP10 cells were grown overnight at 37°C in LB-Lennox broth with 0.5% NaCl (hereafter designated LB) and diluted 1:100 into fresh LB the next day. These cells were then grown at 37°C until an optical density at 600 nm (OD_{600}) of 0.5-0.8 was reached. Cells were incubated on ice for 20 minutes and then centrifuged at 3000 xg for 10 minutes at 4°C. The supernatant was discarded and the pellet was resuspended in 10% of the original culture volume of TSS buffer (85% LB broth, 10% polyethylene glycol 8000, 5% dimethyl sulfoxide and 50 mM $MgCl_2$). The resuspended cells were then dispensed into 100 µl aliquots and rapidly frozen in a dry ice/methanol bath, then transferred to -80°C.

2.3.2 Transformation of chemically competent cells

To introduce plasmid DNA into chemically competent TOP10 cells a standard heat shock method was used. Briefly, cells stored at -80°C were thawed on ice and 10 ng of DNA or 1 µl of a ligation reaction (diluted 1:5) were added to the cells and gently mixed. The mixture was placed on ice for 30 minutes, heat shocked for 45 seconds in a 42°C water bath and returned to the ice for an additional 2 minutes. 250 µl of room temperature SOC (Invitrogen) was added to the tube and it was incubated with shaking

for 1 hour at 37°C. Following incubation, 100 µl of the culture was plated on to an LB agar plate with the appropriate selective antibiotic (100 µg/ml ampicillin or 30 µg/ml Zeocin). Inverted plates were incubated overnight at 37°C. Individual colonies were picked and grown overnight in 5 ml of LB broth with the appropriate antibiotic. The following day, plasmid DNA was extracted with the QiaPrep Spin Miniprep kit (Qiagen, Mississauga, ON) according to the manufacturer's instructions. Purified DNA was digested with the appropriate enzymes and run on 1% agarose gel. Preparations that appeared correct were sent for sequencing to confirm the introduction of mutations and verified clones were then maxi-prepped according to the manufacture's instructions using the QiaFilter Plasmid Maxi kit (Qiagen).

2.3.3 Cloning and site-directed mutagenesis. The regions of the GP gene corresponding to the ZEBOV strain Mayinga sGP, GP_1, $GP_{1,2\Delta TM}$ and Δ- peptide open reading frames (ORF) but lacking the signal peptide were cloned into the pDisplay vector (Invitrogen, Burlington, ON), which contains an endogenous signal peptide and an N-terminal HA-tag, as previously described (Wahl-Jensen et al., 2005a). For the introduction of point mutations, site-directed mutagenesis was performed with the QuickChangeII site-directed mutagenesis kit (Stratagene) according to the manufacturer's instructions with specifically altered oligonucleotides resulting in the desired mutations (see Appendix A for primer sequences). The full-length glycoprotein $GP_{1,2}$ from ZEBOV strain Mayinga was cloned into the mammalian expression vector pCAGGS (Niwa, Yamamura, and Miyazaki, 1991), which contains a chicken β-actin/rabbit β-globin hybrid promoter (AG) and a human cytomegalovirus immediate early promoter (CMV-IEE) enhancer (see Appendix B – Figure 31 for a vector map of pCAGGS). For the introduction of point

mutations into pCAGGS-$GP_{1,2}$, the glycoprotein cassette was first sub-cloned into pDisplay (as pCAGGS contains structural elements that make it refractory to site-directed mutagenesis) using restriction enzymes *Eco*RI and *Xho*I (New England Biolabs, Pickering, ON), where site directed mutagenesis was performed as above. Following sequence confirmation, the mutated GP cassette was digested with the same enzymes and ligated overnight with T4 DNA ligase (New England Biolabs) back into pCAGGS. The presence of the mutations was verified by sequencing after purification of plasmid DNA using the QIAfilter Plasmid Maxi kit (Qiagen) according to the manufacture's instructions.

2.3.4 Determination of DNA concentration

The concentration of plasmid preparations was determined on a Nanodrop ND-1000 UV-Vis spectrophotometer (Nanodrop Technologies, Wilmington, DE) according to the manufacturer's instructions based on the adsorption spectra using 1μl of the plasmid preparation.

2.4 Protein Expression and Purification

2.4.1 Transfection and purification of glycoproteins

Prior to the addition of cells, flasks were incubated with 0.1 mg/ml poly-D lysine (Sigma, Oakville, ON) in PBS for 30 minutes at 37°C. Following this, the poly-D lysine solution was removed and stored at -20°C (for up to 5 uses) and the flasks were washed extensively with PBS. Low passage 293T cells (less than 40) were split 1:3 into pre-coated 500 cm^2 triple flasks (Nunc) 24 hours prior to transfection. Cells were washed with plain DMEM and then 40 ml of OptiMEM was added to the cells. The desired

plasmid (e.g. pDisplay-sGP) was mixed with FuGene6 (Roche Diagnostics) (3 μl per 1 μg DNA; 0.22 μg DNA/cm^2 cells) in 0.02 ml/cm^2 OptiMEM (Invitrogen), incubated at room temperature for 30 minutes then added to the cells. 72 hours post-transfection the supernatant was collected and centrifuged at 5000 xg for 15 minutes to remove cell debris. The cell-free supernatant was concentrated with a Centricon PL-70 (30000 MWCO) (Millipore, Cambridge, ON) and added to anti-HA affinity matrix (Roche Diagnostics) as per the manufacturer's instructions and rotated overnight at 4°C. The supernatant plus the matrix was added to gravity flow columns and washed extensively with TNE buffer (20mM Tris-HCl, 100mM NaCl, 0.1 mM EDTA) containing 0.05% Tween20. The HA-tagged glycoproteins were eluted with excess HA peptide (1 mg/ml) (American Peptide Company, Sunnyvale, CA) and the HA peptide used for elution was eliminated by multiple washes through an Amicon Ultra 4 (30000 MWCO) (Millipore). The matrix was regenerated with 0.1 M glycine (pH 2) and then stored in TNE with 0.09% sodium azide.

Virus-like particles (VLPs) were generated by transfection of pCAGGS-$GP_{1,2}$ and pCAGGS-VP40 together into 293T cells, essentially as described above; however, 0.11 μg of each plasmid was used per cm^2 of cells. The supernatant was collected 72 hours post-transfection and centrifuged at 800 xg for 5 minutes. The supernatant was removed and centrifuged again for an additional 5 minutes. The supernatant was then layered on top of 3 ml of 20% sucrose in PBS and centrifuged at 21000 RPM for 2.5 hours in an SW41 rotor at 4°C. Following centrifugation, the supernatant was decanted and the pellet was resuspended in TNE buffer. The presence of the recombinant protein was confirmed by western blot using two monoclonal antibodies directed against ZEBOV GP (Z42/3.7

and P_{130}2H11, courtesy of A. Takada, Hokkaido University, Japan, and M. Suresh, University of Alberta). These monoclonal antibodies were generated against $GP_{1,2}$ and detect both GP_1 and sGP by western blot. The purity of the proteins was assayed by SDS-PAGE and silver stain (GE Healthcare, Baie d'Urfe, QC) and the protein concentration was determined using the DC Protein Assay (BioRad, Hercules, CA). Purified proteins used for endothelial cell experiments were assayed for endotoxin levels by the chromogenic Limulus Amebocyte Lysate QCL-1000 (Cambrex, East Rutherford, NJ) assay according to the manufacture's instructions.

2.4.2 SDS-PAGE and western blot

Sodium dodecyl sulphate (SDS) polyacrylamide gels were prepared using the Protean III gel system (BioRad). For all experiments, 10% polyacrylamide resolving and 4% stacking gels (prepared as described in Appendix C) were used. Gels were either subjected to Coomassie stain (Appendix C), silver stain (see 2.6.4) or western blot.

For western blots, polyvinylidene difluoride (PVDF) (GE Healthcare) was soaked in methanol for 5 minutes. Transfer filter pads were soaked in anode and cathode buffer respectively. The anode of the Semi-Dry transblot apparatus (BioRad) was wet with water and the filter pad soaked in anode buffer was placed on it. The membrane was immersed in anode buffer then placed on top of the filter pad. The gel was briefly placed in anode buffer and then placed on top of the membrane. The filter pad in the cathode buffer was added on top and a roller was used to remove any air bubbles. The cathode was wet with water and then placed on top of the stack. Finally the top of the apparatus was put in place. The proteins were transferred to the membrane at 0.8Amp/cm2 (60mA per minigel) for 90 minutes. Following transfer, the membrane was incubated in blocking

solution (5% skim milk in PBS with 0.01% Tween20) for 1 hour at room temperature or overnight at 4°C.

The primary antibody was diluted in blocking solution and incubated with the membrane in a heat-sealed bag for 1 hour at room temperature. Following this, the membrane was washed three times in PBS with 0.05% Tween20 for 10 minutes each. The secondary antibody was diluted in blocking solution and incubated with the membrane in a heat-sealed bag for 1 hour at room temperature. Following this, the membrane was washed three times in PBS with 0.05% Tween20 for 10 minutes each and then washed once more in PBS.

Western blots against sGP, GP_1 and $GP_{1,2\Delta TM}$ used mouse monoclonal antibody Z42/3.1 unless otherwise noted at a dilution of 1/4000 and anti-mouse IgG-HRP (KPL, Gaithersburg, MD) as a secondary at 1/10,000 dilution. Rabbit anti-HA antibody (Roche Diagnostics) was used to detect HA-tagged Δ-peptide at a dilution of 1/2000 with anti-rabbit IgG-HRP at a dilution of 1/2000 (Sigma). For characterization of C-mannosylation mutants of sGP monoclonal antibody P_{130}2H11 (from Xiangao Qui, Public Health Agency of Canada) was used at 1/100 dilution. The same secondary conditions were used as for Z42/3.7. β-actin was used as a loading control for the quantification of GP_1 expression. For this anti-β-actin monoclonal (Cell Signalling Technology, Danvers, MA) was used at a 1/1000 dilution. For the characterization of GP incorporation into VLPs guinea pig anti-VP40 was used with anti-guinea pig IgG-HRP (Sigma).

ECL Plus substrate (GE Healthcare) was added as per the manufacturer's instructions and then the membrane was exposed to Hyperfilm ECL (GE Healthcare) for the appropriate amount of time and developed with an automated X-ray film developer

(Konica Minolta, Mississauga, ON). For blots that were stripped and re-probed membranes were incubated with western stripping buffer for 45 minutes at 50°C. Subsequently, the membrane was washed extensive with water (at least 1 hour), followed by PBS with 0.05% Tween20 (30 minutes) and then blocked overnight at 4°C with blocking solution.

2.4.3 Determination of protein concentration

Protein concentration was determined using the DC protein assay (BioRad) microplate assay protocol according to the manufacturer's instructions. Briefly, 20 µl of reagent S was added per 1 ml of reagent A. Five dilutions of a known quantity of BSA were used as a standard in TNE buffer (5 to 0.3 mg/ml). 5 µl of standard or sample were pipetted into a microtitre plate and 25 µl of reagent A+S was added to each well. Subsequently, 200µl of reagent B was added to each well and the contents of each well were mixed. The plate was incubated at room temperature for 15 minutes and the absorbance read on a plate reader at 750 nm. A standard curve was generated from BSA dilutions and used to calculate the concentration of the purified protein solution.

2.4.4 Silver Stain of SDS-PAGE gels

Following electrophoresis, the gel was silver stained using the Plus One silver stain kit (GE Healthcare) using a modified protocol. The gel was fixed in 40% ethanol, 10% acetic acid for 1 hour, with a solution change after 30 minutes. Then the gel was sensitized for at least 30 minutes in 30% ethanol, 0.2% sodium thiosulphate (w/v), 0.8 M sodium acetate. The gel was washed in dH_2O three times for 5 minutes, then stained for 20 minutes in 0.25% silver nitrate (w/v) and washed twice in dH_2O for 1 minute. The gel was developed in 0.2 M sodium carbonate with 0.0074% formaldehyde (w/v) until the

desired darkness was reached. The developer was stopped with 0.4 M EDTA for 10 minutes. The gel was then washed in dH_2O twice for 10 minutes. Developed gels were either mounted or the desired bands excised with a scalpel and prepared for mass spectrometry.

2.4.5 Partial purification of sGP from ZEBOV-infected supernatant

Vero E6 cells (approximately 90% confluent) were infected with *Zaire ebolavirus* (strain Mayinga) in the BSL4 laboratory at the National Microbiology Laboratory at an MOI of approximately 0.5 per cell. When cytopathic effect (CPE) was evident (three days post-infection) the supernatant was removed and centrifuged at 5000 x g for 15 minutes. To remove most of the virus, the supernatant was centrifuged at 21000 rpm in a SW-41 rotor for 30 minutes. The supernatant was then poured off and passed through a 0.22 μm filter, while the pellet was inactivated and discarded. SDS was added to the supernatant to 0.5% and the sample was irradiated (2 MRad). The supernatant was dialyzed extensively against 20 mM Tris-HCl, 500 mM NaCl, pH 7.4 (TN buffer) and then added to a concanavalin A column (GE Healthcare). Unbound protein was washed through with TN buffer. Bound protein was eluted with 0.75 mM methyl-α-D-glucopyranoside in TN buffer. The fractions were concentrated with an Amicon (Millipore) and subjected to western blot. The appropriate fraction was then prepared for mass spectrometry.

2.5 Analysis of Intracellular and Surface Expression of $GP_{1,2}$.

293T cells were grown on poly-D-lysine coated cover slips (BD Biosciences) in 12-well plates. Cells were transfected with pCAGGS-$GP_{1,2}$ wild-type (WT) or various

point mutants (W291A, W648A, W651A, W648/651A, W644/645/648/651A) as described above. At 2, 6, 12, 24 and 48 hours post-transfection media was removed from the wells and cells were stained with the monoclonal mouse anti-GP antibody P_{130} 2H11 for 10 minutes at 37°C. Following this, cells were quickly washed 3 times with PBS and then fixed with fresh 2% paraformaldehyde (Sigma) in PBS. Cells were washed 3 times with PBS and incubated with goat anti-mouse AlexaFluor488 (Molecular Probes, Burlington, ON) for 1 hour at room temperature. Cells were washed 3 times with PBS and permeabilized with 0.1% Triton X100 for 15 minutes at room temperature. Cells were washed 3 times with PBS and stained with mouse monoclonal antibody P_{130} 2H11 for 1 hour at room temperature. Cells were washed 3 times and then stained with goat anti-mouse AlexaFluor657 (Molecular Probes) for 1 hour at room temperature. Cells were washed 3 times with PBS and 1 time with sterile dH_2O. Appropriate controls (i.e. isotype control (mouse anti-MARV GP) and no permeabilization were also carried out). The cover slips were mounted on slides in ProLong Gold AntiFade with DAPI (Molecular Probes) and allowed to dry overnight. The next day they were sealed with clear nail polish. Slides were imaged on a Zeiss LSM 700 at the Laboratory of Virology (Rocky Mountain Laboratories, NIH, Hamilton, MT).

2.6 Mass Spectrometry

Mass spectrometry is a useful tool for the study of certain structural elements of proteins. While many different aspects can be studied here we focused on mapping of disulphide bonds and identification of post-translational modifications. Matrix-assisted laser desorption ionization (MALDI) - time of flight (TOF) mass spectrometry (MS),

described in detail elsewhere (Loboda et al., 2000), was utilized because it simplifies the analysis as typically only +1 charge peptides are detected making it suitable for disulphide bond mapping and identification of post-translational modifications (Krokhin et al., 2003; Krokhin, Ens, and Standing, 2005). In some cases high pressure liquid chromatography (HPLC) chromatography was utilized prior to MS to fractionate the sample allowing for greater sensitivity and additional information, such as peptide hydrophobicity, to be collected. For confirmation, certain peptides were subjected to tandem MS (MS/MS), which allows partial to complete sequencing of the peptide.

2.6.1 Peptide mapping and disulphide bond assignment

Sample preparation for peptide mapping of HA-tag purified sGP by MALDI-MS and HPLC-MALDI MS involved in-solution protein reduction (10 mM dithiothreitol (DTT), 65^{o}C, 30 min), alkylation with iodoacetamide (50 mM, room temperature, 45 min), dialysis (7,500 MWCO, against 100 mM ammonium bicarbonate) and tryptic digestion (ProMega, Madison, WI) with a 1:50 enzyme/substrate ratio (with or without prior deglycosylation with 0.5U of PNGaseF) (New England Biolabs). Resultant digests were spotted directly on MALDI target at a 1:1 ratio with 2,5-dihydroxybenzoic acid (DHB) matrix solution (0.5 M in 50% acetonitrile) or directly injected (5 μl) into the micro HPLC system. The HPLC-MALDI MS (MS/MS) analysis setup is described in detail elsewhere (Krokhin, Ens, and Standing, 2005). Briefly, peptide mixtures were fractionated on micro C18 columns using a linear water/acetonitrile gradient containing trifluoroacetic acid (0.01%) as an ion-pairing modifier. Column effluent was mixed on-line with DHB matrix solution and fractions were deposited directly on MALDI target. Both non-separated samples and chromatographic fractions were analysed by MS and by

tandem mass spectrometry (low-energy CID, MS/MS) in the Manitoba/Sciex prototype MALDI quadrupole/TOF (QqTOF) mass spectrometer (Loboda et al., 2000). This instrument provides resolving power of 10,000 FWHM (full width half maximum) and mass accuracy ~10 ppm in both MS and MS/MS modes.

Sample preparation for disulphide bond assignment of sGP involved the same steps, excluding reduction/alkylation. Disulphide patterns were assigned based on results of MS/MS analysis of the fragments carrying non-reduced Cys-Cys bonds (Krokhin et al., 2003). The candidates for MS/MS were chosen following reduction (5 mM DTT, 65°C, 30 min) of non-reduced digests (see discussion). For analysis of $GP_{1,2}$, VLPs were generated as described above (see 2.4.1). Prior to reduction/alkylation VLPs were heated to 100°C for 10 minutes, with and without 0.1% NP40, to break apart the virus-like particles and dissociate GP_2 from the membrane.

2.6.2 In gel digestion of SDS-PAGE purified sGP to confirm disulphide bond assignment

Gel slice destaining was performed as described previously (Sumner et al., 2002). Briefly, gel slices were washed twice with sterile water (Sigma) followed by two washes in 25 mM ammonium bicarbonate (Sigma). The silver stain was removed with 1% hydrogen peroxide (Fisher, Ottawa, ON) in 25 mM ammonium bicarbonate and then washed with water. The pH of the gel plug was then lowered with 1% formic acid (Sigma). The gel slices were then cut into approximately 1mm pieces and covered with acetonitrile (Sigma):100 mM ammonium bicarbonate (1:1, v/v). The liquid was removed and the gel pieces were covered with acetonitrile. All of the preceding steps were incubated at room temperature for 5 minutes. The liquid was removed and the gel pieces

were dried in a SpeedVac vacuum centrifuge (Savant, Ramsey, MN) for 5 minutes without heat. The gel pieces were rehydrated in digestion buffer (50 mM ammonium bicarbonate with 5 mM calcium chloride and 5 ng/µl sequencing grade trypsin (Sigma) on ice for 45 minutes. The liquid was removed, replaced with digestion buffer without enzyme and the gel pieces were incubated at 37^{o}C overnight. Following digestion the tube was spun briefly and the liquid transferred to a new tube. Digested peptides were sequentially extracted in 2-3 gel volumes 0.01% trifluroacetic acid (TFA) (Sigma) followed by 0.01% TFA: acetonitrile (1:1, v/v) and placed in a sonicating water bath for 10 minutes. The liquid was removed to the new tube after each step. The extraction was repeated for a total of three times. The gel was further extracted with 2-3 gel volumes acetonitrile followed by extraction with 5% formic acid in 50% acetonitrile. This was repeated for a total of two times. The pooled extracts were then dried with a SpeedVac without heat and stored at -20^{o}C. Prior to MALDI-TOF MS analysis the sample was reconstituted in 10 µl of 0.1% TFA. A ZipTip (Millipore) was used to clean-up the sample which was eluted in 2 µl of 50% acetonitrile in water. An equal volume of 0.2% TFA was then added to the sample.

2.6.3 Data analysis

Spectra analysis and peak assignment was performed using the in-house software time-of-flight mass analysis (TOFMA). Subsequently, this data was submitted for peptide mass fingerprinting to ProFound (http://prowl.rockefeller.edu/prowl-cgi/profound.exe). Manual selection of glycosylated peaks was performed in TOFMA and submitted to GlycoMod (http://www.expasy.ch/tools/glycomod/) in order to determine the predicted composition of N-glycan sites. Samples run on LC-MALDI MS were analyzed with the

in-house software search using mass and retention time (SMART) and submitted to ProFound. Both manual and automated searches for C-mannosylated peptides were performed during the analysis of $GP_{1,2}$.

2.7 Barrier Function Analysis of Endothelial Cells

Impedance spectroscopy is a highly sensitive biophysical assay that provides a unique possibility to study the endothelial barrier function under resting (Lo, Keese, and Giaever, 1995) and shear stress conditions with high time resolution (DePaola et al., 2001; Seebach et al., 2000; Seebach et al., 2005). This technique determines the transendothelial electrical resistance (TER) of a cultured endothelial cell monolayer and predominantly reflects the changes in paracellular permeability (Figure 8 A) (Claude, 1978; Powell, 1981). Endothelial cell barrier function is frequently studied in transwell filter systems by analysing the passage of tracer substances (Dejana, Spagnuolo, and Bazzoni, 2001; Esser et al., 1998; Feldmann et al., 1996). In contrast to impedance spectroscopy, which reliably detects changes in barrier function of about 2%, (Seebach et al., 2000) tracer systems are limited in time resolution and sensitivity and thus allow for the detection of strong effects only. Thus this assay is suited to determine the effect of alterations to the structure of sGP. TER is measured by three small, independent ITO electrodes and one large counter electrode. Shear stress can be generated by a rotating cone and plate multi-channel rheological *in vitro* system (Figure 8 B) (MOS Technologies, Dresden, Germany) that is described in detail elsewhere (Dieterich et al., 2000; Schnittler et al., 1993) that uses a rotating cone to produce a defined laminar shear stress level between 0 and 200 dyn/cm^2.

Figure 8. **Schematic of (A) the model used to measure transendothelial resistance (TER) and (B) the cone and plate rheological chamber used to measure TER under shear stress.** (A) The TER was calculated by measuring the impedance magnitude at multiple frequencies from 10 Hz to 1 MHz between the electrode area of the ITO slide and a counter electrode. The cell membrane acts as a capacitor with a near constant value while at certain frequencies the paracellular path behaves as an ohmic resistor (i.e. TER) that can be used to determine the tightness of cell-to-cell contacts. (B) The cone and plate rheological system used to monitor TER under shear stress conditions. The cone rotates at a set speed supplying a calibrated shear force evenly across the cells in a chamber that contains three ITO electrodes that measure TER using the above model. Adapted from MOS Technologies (http://www.glpnet.de/mos-technologies/technologie/index.php) with permission.

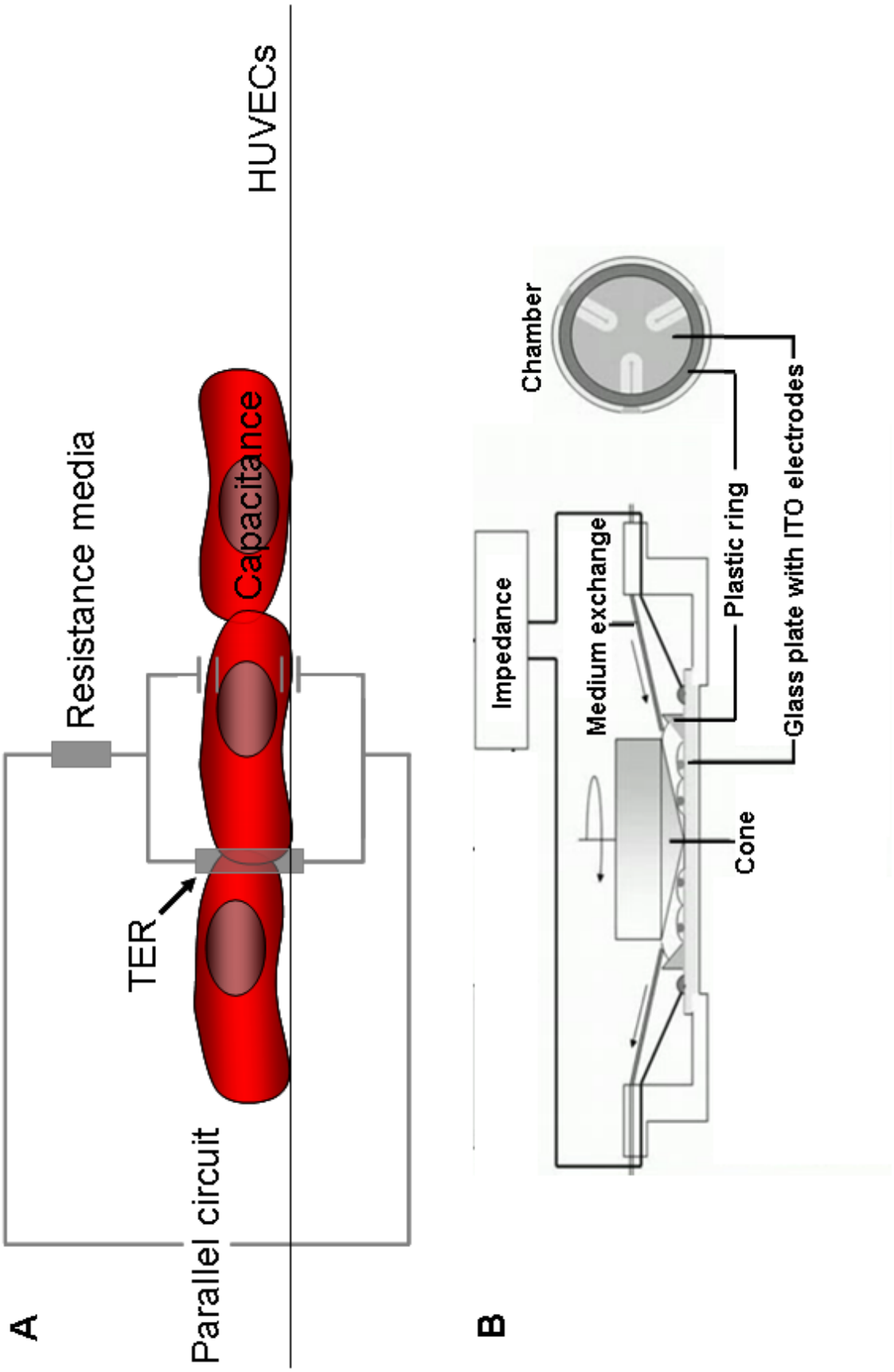
A
Resistance media
HUVECs
Capacitance
TER
Parallel circuit
B
Chamber
Impedance
Medium exchange
Plastic ring
Glass plate with ITO electrodes
Cone

2.7.1 Preparation of chambers for impedance spectroscopy

Chambers (both round and multi-well chamber slides were sonicated for 15 minutes at 40°C in reverse osmosis (RO) water. The chambers were washed with liquid soap and sonicated again. They were rinsed extensively with RO water and sonicated again for 15 minutes. Next, the chambers were treated with 1% trypsin for 1 hour at 37°C then extensively washed with RO water. Sterile gelatine (0.5% in PBS) was added to the chambers and incubated at 37°C for 30 minutes. The gelatine was removed and fixed with 2% glutaraldehyde in water for 5 minutes at room temperature. The glutaraldehyde was removed and chambers were rinsed with 70% ethanol. Then the chambers were filled to the top with 70% ethanol and incubated for 15 minutes at room temperature. Ethanol was aspirated off and the chambers were washed 5 times for 5 minutes with sterile water. PBS with 22.2mM glycine was then added to the chamber and left overnight at room temperature. The following day the PBS/glycine was removed and chambers were washed 5 times for 5 minutes with sterile water. ECGM+/+ was added to the chamber and incubated at room temperature for 5 minutes, then removed and HUVECs were seeded. Media was refreshed 24 hours later and cells had to be confluent within three days, otherwise they were discarded.

2.7.2 Shear stress and impedance spectroscopy

Impedance spectroscopy of HUVECs was performed as previous described (Schnittler et al., 1993; Seebach et al., 2000; Seebach et al., 2005). Briefly, an alternating voltage was applied and the impedance magnitude (|Z|), which equals the ratio between the amplitude of an alternating voltage applied to the system and the amplitude of the associated alternating current, was measured at frequencies from 10 Hz to 1 MHz

between the electrode area of the indium tin oxide (ITO) slide and a counter electrode. In the absence of a cell monolayer the impedance of the system is essentially a series connection of an ohmic resistor representing the resistance of the medium and a constant phase element represented by the electrode (Figure 8 A). At the measured frequencies, the overall impedance of the system is determined by the frequency-independent ohmic resistor (Wegener et al., 1999). The presence of a cell monolayer completely covering the electrodes significantly increases the impedance in the range between 10^3 Hz and $3x10^5$ Hz (Seebach et al., 2000). Depending on the applied frequency, the alternating current may flow through the intercellular junctions and/or may traverse the monolayer transcellularly via the plasma membranes. The paracellular path has properties of an ohmic resistor (i.e. TER) and is used to determine the tightness of cell-to-cell contacts, while the transcellular path is characterized by the membrane capacitance which is fairly constant and if both the apical and the basolateral membranes are included, the theoretical value for a confluent cell monolayer is approximately 0.5 mF/cm2 (Wegener et al., 1999). For all impedance spectroscopy experiments, the TER, representing the tightness of cell-to-cell contacts, was calculated from the resultant spectra as previously described (Seebach et al., 2000) based on the model of (Wegener et al., 1999). For this model to be valid the cell layer must be confluent. Sub-confluent cultures still influence the impedance spectra (Janshoff et al., 1996) but they show distinct differences between the form of the measured and the calculated impedance spectra that can be quickly identified so sub-confluent chambers can be excluded from the experiment. Data acquisition and analysis was performed by custom software based on the visual programming language LabVIEW (National Instruments, Munich, Germany).

For shear stress studies, HUVECs were seeded onto gelatine-coated 16cm^2 round glass slides with three small, independent ITO electrodes (0.05 cm^2 each) and one large (6 cm^2) counter electrode. Confluent cultures (verified by phase-contrast microscopy) were inserted into the sample mounting support of cone and plate multi-channel rheological *in vitro* system (Figure 8 B) (MOS Technologies, Dresden, Germany) that is described in detail elsewhere (Dieterich et al., 2000; Schnittler et al., 1993). The rotating cone is capable of producing a defined laminar shear stress levels between 0 and 200 dyn/cm^2. This novel setup allows concomitant phase-contrast microscopy observation and impedance analysis of the cell monolayer under laminar shear stress. For shear stress experiments, the media was replaced with ECGM+/+ with 3% polyvinyl-pyrrolidone (PVP) (MW 360 kDa) added to it to increase the dynamic viscosity. Cells were allowed to equilibrate at 2 rpm (0.2 dyn/cm^2) for 1-3 hours until a consistent baseline was achieved. Chambers that did not establish a consistent barrier function were excluded. After a consistent baseline was recorded for 1 hour, recombinant sGP (10 μg/ml) or an equivalent volume of TNE buffer was added to the chamber and shear stress exposed chambers were increased to 80 rpm (12 dyn/cm^2).

For static studies, HUVECs were seeded onto gelatine-coated indium 1.8 cm^2 chamber glass slides with an ITO electrode and one larger counter electrode. Cultures were checked by phase-contrast microscopy to ensure that they were confluent. Slides were placed in a 37°C incubator and connected to the impedance spectrometer. Prior to addition of TNF-α (1 ng/ml) (R&D Systems, Minneapolis, MN) and sGP or cysteine mutant (10μg/ml) cells were equilibrated for 1-2 hours to establish a baseline TER. All electrical resistance data are presented as normalized to baseline resistance values

(TER/TER0). TER data are shown as mean +/- standard error. Data were compared by unpaired t-test. Values were considered to be statistically significant when *P* was <0.05.

2.7.3 Infection of HUVECs with Lentivirus vector expressing sGP

HUVECs cultured in 16cm^2 round glass chambers were washed with ECGM without growth factors or penicillin/streptomycin (ECGM-/-). Virus stocks of either replication-deficient Lentivirus expressing sGP or enhanced green fluorescent protein (eGFP) were diluted in ECGM-/- resulting in an MOI of approximately 10. The diluted virus was added to the cells and incubated at 37°C for 1 hour. Subsequently, the virus was removed and replaced with pre-warmed ECGM+/+ with 3% PVP and the chambers were placed in the cone and plate multi-channel rheological *in vitro* system as described above, while the barrier function was monitored by impedance spectroscopy. Cells were equilibrated for 1 hour at 2 rpm (0.2 dyn/cm^2) then shear stress exposed chambers were increased to 80 rpm (12 dyn/cm^2).

2.8 Viral Protein Database Search for C-mannosylation Motifs

Using scripts written in PEARL (with the assistance of Gary Van Domselaar, Bioinformatics Core, National Microbiology Laboratory), protein sequences from the non-redundant NCBI RefSeq viral protein database (ftp://ftp.ncbi.nih.gov/refseq/release/viral/viral1.protein.faa.gz) were scanned for the recognition sequence W-X-X-W. These sequences were then truncated to the N-terminal 90 amino acid residues and run through the SignalP 3.0 Server (http://www.cbs.dtu.dk/services/SignalP/) in both Neural Net (NN) and Hidden Markov Model (HMM) modes. These algorithms predict whether a protein is likely to contain a signal peptide. Proteins that answered “yes” in NN (to

containing a signal peptide) and/or "signal peptide" or "signal anchor" in HMM were selected and categorised. For sGP and $GP_{1,2}$ the amino acid sequences were submitted to NetCGlyc 1.0 (www.cbs.dtu.dk/services/NetCGlyc/), a neural network analysis that predicts C-mannosylation (Julenius, 2007). This prediction takes into account factors in addition to the W-X-X-W consensus motif, such as the preference for small and/or polar residues, such as Ser, Ala, Gly and Thr, in position +1 and discriminates against Phe and Leu in this position.

2.9 Infectious Virus-Like Particle (iVLP) Assay

The study of EBOV assembly, budding and entry is hampered by the need for biological containment; therefore, to study these events in BSL2 conditions an infectious virus-like particle (iVLP) system was developed (Watanabe et al., 2004). The system is based on the original minigenome systems (Boehmann et al., 2005; Groseth et al., 2005; Muhlberger et al., 1999) but in addition to RNP-complex proteins it also includes the remainder of the structural proteins (VP24, VP40 and GP) allowing production of particles that resemble actual virus particles but contain a minigenome with a reporter in place of the full-length genome (Figure 9). In place of earlier reporters (e.g. chloramphenicol acetyltransferase or green fluorescent protein) this next generation iVLP system uses *Renilla* luciferase, greatly increasing the sensitivity of the assay, and allowing the infection of naïve target cells (Vero E6) instead of pre-transfected or helper virus infected cells (Hoenen et al., 2006b).

iVLP assays were performed as previously described (Hoenen et al., 2006b). Briefly, Vero E6 cells (p0) in 6-well plates were transfected in 2ml DMEM with 5% FBS

Figure 9. **Schematic of the infectious virus-like particle (iVLP) reporter system.** The mini-genome system includes plasmids that encode for the proteins required for transcription of the virus genome (NP, VP30, VP35 and L) in addition to the mini-genome that contains only the leader and trailer regions from the ZEBOV genome in between which a reporter is inserted (in this case *Renilla* luciferase – indicated by the green particles). The iVLP system includes all the components of the mini-genome in addition to plasmids that encode the remainder of the structural proteins (GP, VP24 and VP40). The allows the formation of virus-like particles that are capable of infecting target cells where the reporter activity can be assayed to determine the efficiency of particle formation and entry.

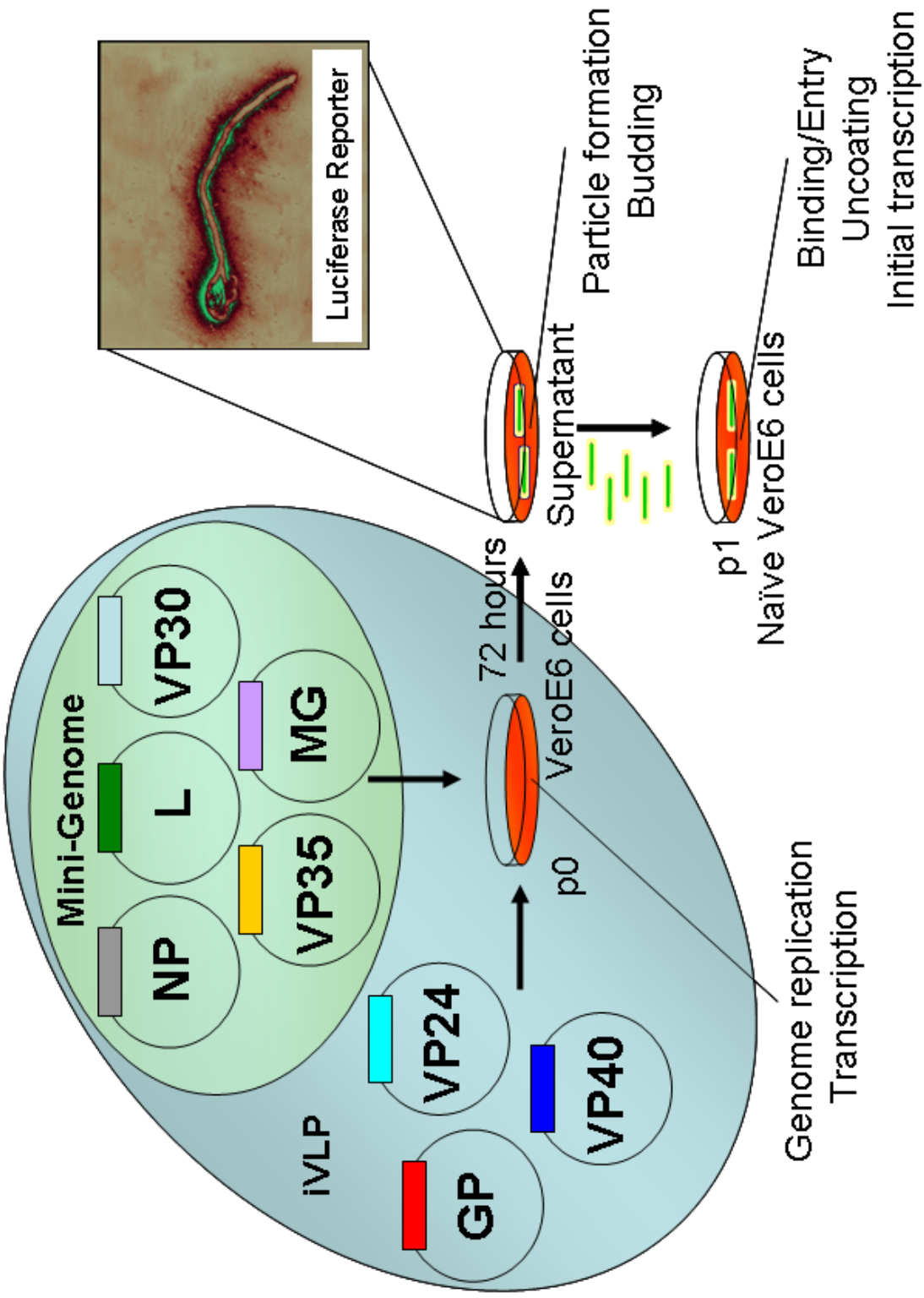
Luciferase Reporter
Particle formation
Budding
Supernatant
Binding/Entry
Uncoating
Initial transcription
p1
Naïve VeroE6 cells
72 hours
VeroE6 cells
p0
Mini-Genome
NP
L
VP30
VP35
MG
iVLP
GP
VP24
VP40
Genome replication
Transcription

using FuGENE6 with plasmids encoding each ZEBOV structural protein (125 ng pCAGGS-NP, 125 ng pCAGGS-VP35, 75 ng pCAGGS-VP30, 1000 ng pCAGGS-L, 250 ng pCAGGS-GP, 250 ng pCAGGS-VP40, and 60 ng pCAGGS-VP24), a T7-driven minigenome encoding a Renilla luciferase reporter (250 ng) and 250 ng of pCAGGS-T7. 24 hours post-transfection cells were washed once with 2 ml of DMEM and then medium was exchanged against 4 ml DMEM with 5% FBS, 100 U/ml penicillin and 100 µg/ml streptomycin. Supernatant containing released iVLPs was collected 3 days post-transfection, centrifuged twice at 800 xg for 5 minutes to clear cellular debris and then subsequently used to infect naïve target Vero E6 cells. Cell from p0 were lysed in 1000 µl passive lysis buffer and reporter activity in p0 was determined by dual-luciferase assay (Promega). Two days post-infection p1 cells were lysed in 100 µl passive lysis buffer and reporter activity was assayed by the dual-luciferase assay. To ensure that activity in p1 was not due to unspecific reporter protein transfer, a plasmid encoding firefly luciferase under the control of an SV40 promoter (250 ng pGL2-Control; Promega) was co-transfected with the other plasmids in p0. The ratio of firefly luciferase activity (control) to minigenome-encoded Renilla luciferase activity was then determined in p0 and in p1.

3. RESULTS

3.1 Structural Analysis of sGP

3.1.1 Construction, production and biochemical characterization of sGP and cysteine mutants

As protein structure is considered important for protein function, it was necessary to define the arrangement (parallel or anti-parallel) of the sGP homodimer, as conflicting evidence has been presented in the literature (Barrientos et al., 2004; Volchkova et al., 1998). A combination of site-directed mutagenesis and disulphide bond mapping with off-line high pressure liquid chromatography (HPLC) matrix-assisted laser desorption ionization-time of flight mass spectroscopy (MALDI-TOF MS) tandem MS (MS/MS) was performed to determine the native structure of EBOV sGP and its glycosylation status. sGP was produced in a mammalian cell-based recombinant expression system using the pDisplay vector and 293T cells. This vector includes an N-terminal HA tag, which was used to purify sGP by affinity chromatography from the supernatant of transfected cells. The presence of the correct protein was verified by SDS-PAGE and western blot using monoclonal mouse anti-sGP/GP_1 Z4.2/37 (Figure 10 A). This setup was capable of producing up to 5 mg of purified sGP from 3000 cm^2 of cells with a purity of >95% (as approximated by silver stain of SDS-PAGE). Cysteine to glycine mutations were introduced at cysteine residues C53 and C306, which have been shown to be involved in the formation of intermolecular disulphide bonds (Barrientos et al., 2004; Volchkova et al., 1998). The following three mutants were generated: C53G, C306G and C53/306G (with the cysteines replaced with glycine residues at positions 53 and 306). Following sequencing, these mutants were produced and purified under the same

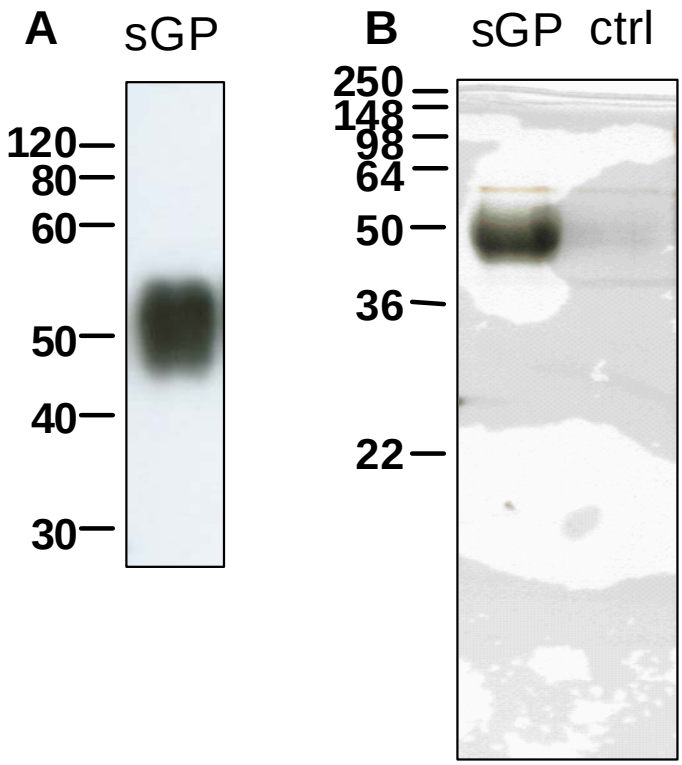

Figure 10. **Analysis of HA- purified sGP.** (A) Western blot analysis of purified sGP using anti-GP/sGP monoclonal antibody Z42/3.1 (1/4000 dilution). The numbers at the left indicate molecular mass in kDa. (B) Silver stain of 1µg of sGP indicating that this purification procedure yields highly purified sGP.

conditions as the sGP. The protein concentration of all preparations was quantified using the DC-protein assay.

Biochemical characterization using SDS-PAGE demonstrated that sGP migrated at a different apparent molecular weight under reducing and non-reducing SDS-PAGE, which corresponds to the monomer (approx. 50 kDa) and dimer (approx. 100 kDa), respectively (Figure 11 A). To determine whether the cysteine mutants possessed the same properties as the wild-type sGP, equivalent amounts of the mutants were run on SDS-PAGE under reducing and non-reducing conditions. The double mutant C53/306G, was unable to form dimers (Figure 11 A, right panel). The two single cysteine mutants (C53G and C306G) were mainly expressed as dimers under non-reducing conditions, although a small amount of monomeric protein was present. The dimers formed by the C53G and C306G mutants displayed a faster migration on non-reducing SDS-PAGE compared to sGP dimers (Figure 11 A, right panel); however, under reducing conditions, all sGP and cysteine mutants migrated at nearly identical molecular weights and at comparable signal strengths (Figure 11 A, left panel).

3.1.2 Confirmation of primary structure and disulphide bond assignment in sGP

Investigating disulphide bond patterns requires that near complete peptide mapping of the target protein (Krokhin et al., 2003) can be performed, where the identification of all cysteine-containing fragments is the primary goal. This is necessary to confidently assign all disulphide bonds. During this process, additional information can be simultaneously extracted, such as amino acid mutations and post-translational modifications. Here we performed peptide mapping of both native and deglycosylated (PNGaseF) sGP using an off-line HPLC-MALDI MS combination similar to that

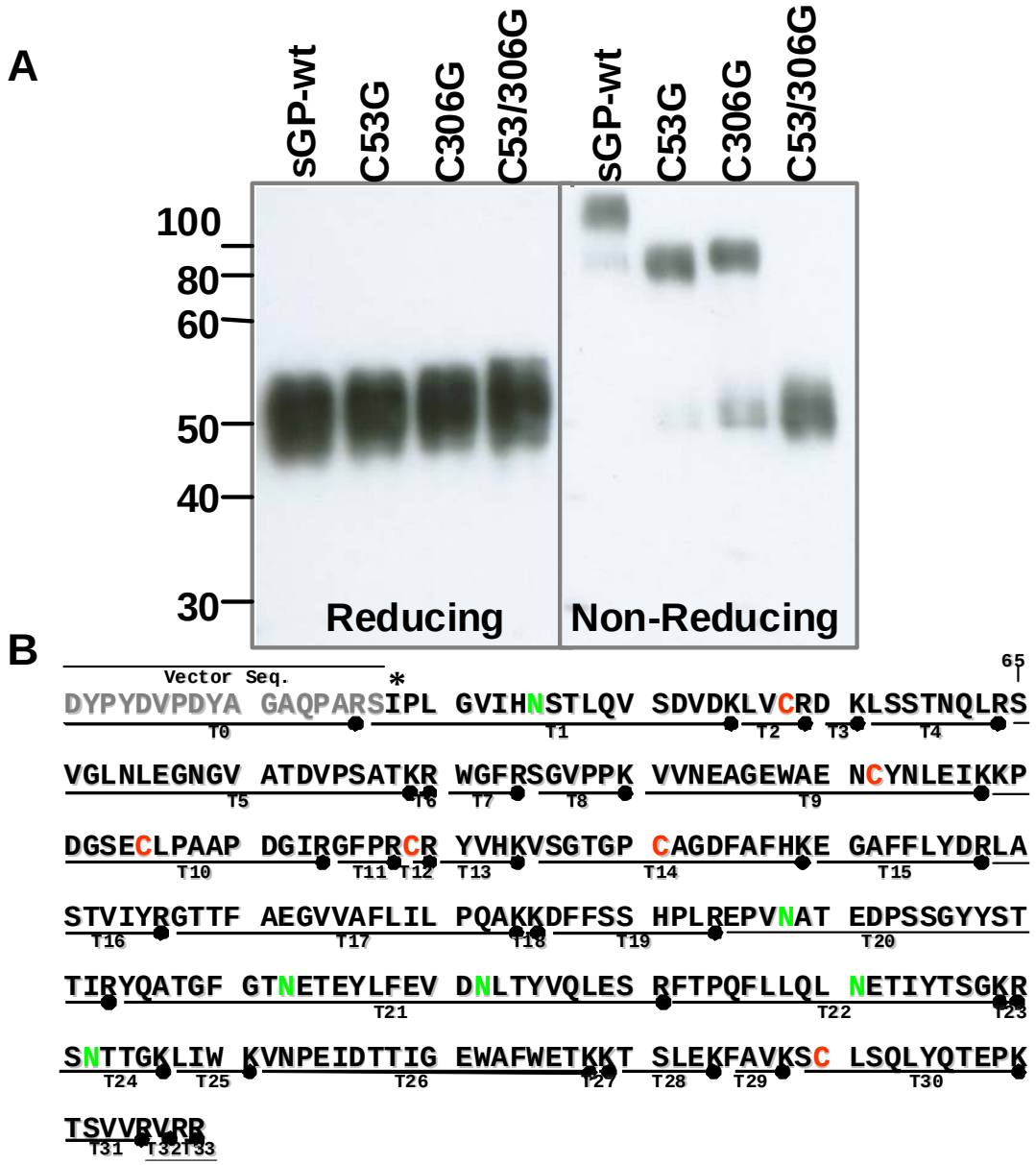

Figure 11. **Biochemical analysis (A) and tryptic map of sGP (B).** (A) Western blot analysis of sGP and cysteine mutants under reducing and non-reducing conditions with monoclonal antibody Z42/3.1 (1/4000 dilution). Molecular mass (kDa) is indicated on the left. (B) Amino acid sequence and tryptic digest fragments of recombinant HA-tagged ZEBOV sGP (A). Tryptic fragments (T0-T33) are indicated (black line and closed circle below text) as are potential N-glycosylation sites (green N), cysteine residues (red C) and fragments not identified (underline). The vector sequence encoding the HA tag is indicated in grey letters. The asterisk (*) marks amino acid 33 of sGP which is proposed to be the authentic amino-terminus following signal peptide cleavage. The numbers on the right indicate the corresponding amino acid position in the sGP open reading frame. (Modified from Falzarano et al. 2006. Copyright Wiley-VCH Verlag GmbH & Co. KGaA. Reproduced with permission.)

previously described (Krokhin et al., 2003). N-linked glycan removal by PNGaseF converts glycosylated Asn-X-Thr/Ser sequences into Asp-X-Thr/Ser, with a resultant +0.984 Da mass shift. For samples prepared under reducing conditions, cysteines were converted to S-carboxymethylcysteine by iodoacetamide, resulting in a +57.5 Da mass increase. From in-solution digests, 37 tryptic sGP fragments (including partially digested products) were recovered from the deglycosylated sGP digest (Table 1). This resulted in 98.9% sequence coverage, including all cysteine-containing peptides and all peptides with potential N-glycosylation sites (Figure 11 B). This was sufficient to attempt to carry out disulphide bond mapping.

MS assignment of disulphide bonds is generally achieved by comparing the masses of non-reduced digests containing intact disulphide bonds, with those of reduced digests (Gorman, Wallis, and Pitt, 2002). Under non-reducing conditions, a higher molecular weight product results from the two tryptic peptides which are linked together by a disulphide bond. Correct disulphide-carrying candidates should disappear following reduction and new fragments should appear corresponding to the peptides with free cysteine. All peaks in the non-reduced sGP digest were submitted to the search algorithm for disulphide bond assignment (Craig et al., 2003). A summary of experimental masses for disulphide-linked tryptic fragments is shown in Table 2. Figure 12 shows a region of the spectra with the intact (Figure 12 A) and reduced (Figure 12 B) disulphide 53-53' linked fragment (two identical peptides 51-54 LVCR (T2), calculated m/z 977.538). Tryptic fragments 165-172 LASTVIYR (T16) and 57-64 LSSTNQLR (T4), are also shown and appear to be nearly identical in both panels (Figure 12 A, B).

Table 1. Experimental masses for tryptic fragments of *Zaire ebolavirus* sGP (* indicates deglycosylated peptides).

Experimental mass (Da)	Calculated mass (Da)	Error (ppm)	Residue number	Missed cleavages	Sequence
334.139	334.142	9	135-136	0	CR
463.281	463.279	4	301-304	0	FAVK
475.256	475.254	4	131-134	0	GFPR
545.298	545.296	4	137-140	0	YVHK
546.297	546.295	4	51-54	0	LVCR
558.353	558.353	0	273-276	0	LIWK
560.330	560.328	3	317-321	0	TSVVR
564.278	564.281	-4	86-89	0	WGFR
576.311	576.312	-1	296-300	0	TSLEK
583.334	583.333	2	90-95	0	SGVPPK
607.283*	607.281	3	267-272	0	SDTTGK
704.407	704.407	0	295-300	1	KTSLEK
720.382	720.382	0	85-89	1	RWGFR
763.388*	763.382	7	266-272	1	RSDTTGK
917.492	917.493	0	57-64	0	LSSTNQLR
921.523	921.528	-5	165-172	0	LASTVIYR
1104.536	1104.535	0	192-200	0	DFFSSHPLR
1116.518	1116.524	-5	156-164	0	EGAFFLYDR
1160.613	1160.615	-1	55-64	1	DKLSSTNQLR
1232.630	1232.630	0	191-200	1	KDFFSSHPLR
1452.690	1452.692	-1	305-316	0	SCLSQLYQTEPK
1549.703	1549.698	3	141-155	0	VSGTGPCAGDFAFHK
1681.810	1681.809	0	115-130	0	KPDGSECLPAAPDGIR
1861.018	1861.035	-9	173-190	0	GTTFAEGVVAFLILPQAK
1927.994	1927.985	4	65-84	0	SVGLNLEGNGVATDVPSATK
2022.061*	2022.063	-1	32-50	0	SIPLGVIHDSTLQVSDVDK
2084.087	2084.086	0	65-85	1	SVGLNLEGNGVATDVPSATKR
2086.932*	2086.933	0	201-219	0	EPVDATEDPSSGYYSTTIR
2100.063*	2100.078	-7	248-265	0	FTPQFLLQLDETIYTSGK
2135.022	2135.021	0	277-294	0	VNPEIDTTIGEWAFWETK
2256.187*	2256.179	3	248-266	1	FTPQFLLQLDETIYTSGKR
2263.117	2263.116	0	277-295	1	VNPEIDTTIGEWAFWETKK
2300.042	2300.042	0	96-114	0	VVNYEAGEWAENCYNLEIK
2550.338*	2550.343	-2	32-54	1	SIPLGVIHDSTLQVSDVDKLVCR
3173.462*	3173.458	1	192-219	1	DFFSSHPLREPVDATEDPSSGYYSTTIR
3301.551*	3301.553	-1	191-219	2	KDFFSSHPLREPVDATEDPSSGYYSTTIR
3287.526*	3287.515	3	220-247	0	YQATGFGTDETEYLFEVDNLTYVQLESR

Table 2. Experimental masses for dominant tryptic fragments involved in disulphide bonds of *Zaire ebolavirus* sGP.

Experimental Mass (Da)	Calculated Mass (Da) of disulphide-linked fragment	Error (ppm)	Residue Number	Missed Cleavages	Sequence	Disulphide Bond
976.533	976.530	3	51-54	0	LVCR	53-53’
			51-54	0	LVCR	
2518.125	2518.156	0	135-136	0	CR	108-135
			96-114	0	VVNYEAGEWAENCYNLEIK	
3115.456	3115.451	2	115-130	0	KPDGSECLPAAPDGIR	121-147
			141-155	0	VSGTGPCAGDFAFHK	
2789.323	2789.324	0	305-316	0	SCLSQLYQTEPK	306-306’
			305-316	0	SCLSQLYQTEPK	

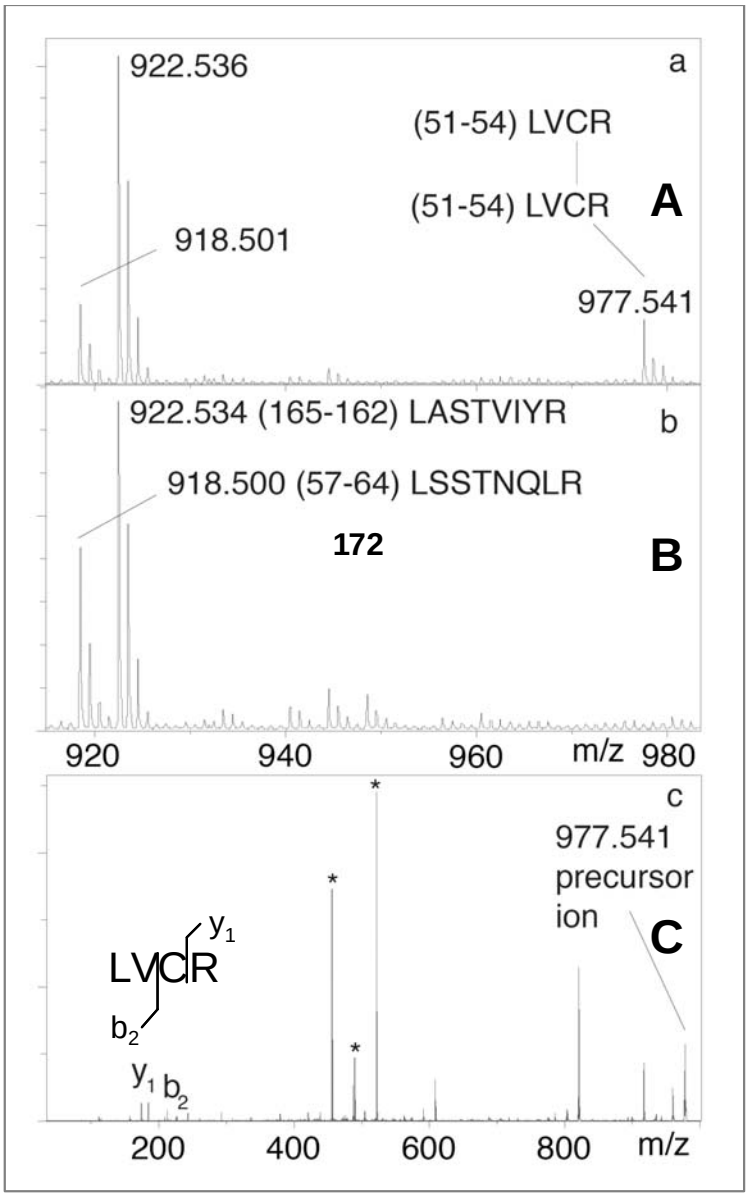

Figure 12. **Disulphide bond assignment of C53 using reduction (A, B) with MS/MS confirmation (C).** Disulphide bonds can be assigned by observing the disappearance of peaks that do not correspond to the predicted masses of tryptic peptides following reduction. MS/MS analysis of the non-reduced peaks can then be used to confirm that they contain the predicted disulphide-linked peptide. (A) A portion of the spectra of a non-reduced digest carrying disulphide-linked fragment m/z 977.541 and normal tryptic peptides m/z 918.501 and 922.536. (B) Following reduction the m/z 977.541 fragment disappears, while the 918.501 and 922.536 fragments remain intact. (C) MS/MS spectra of the disulphide-linked m/z 977.541 fragment: y1 and b2 ions from fragmentation of the 51-54 LVCR peptide are shown as well as a characteristic triplet (*) due to breakage of -S-S- bond. (Modified from Falzarano et al. 2006. Copyright Wiley-VCH Verlag GmbH & Co. KGaA. Reproduced with permission.)

This indicates that under non-reducing (A) and reducing (B) conditions, the samples are comparable and the loss of 977.541 in (B) is likely due to a reduction of the disulphide bond. The identities of disulphide-carrying peptides were confirmed by MS/MS (Figure 12 C). For peak 977.541, y1 (corresponding to R) and b2 ions (corresponding to LV) were detected, confirming the identity of 977.541 as containing 51-54 LVCR. A characteristic triplet was also noted, which occurs due to the breakage of the disulphide bond (Figure 12 C).

The tryptic peptide containing the other cysteine thought to be involved in intermolecular bonding (C306) was found as intact (Figure 13 A) disulphide 306-306' linked fragment (two identical peptides 305-316 SCLSQLYQTEPK (T30), calculated mass 2790.324). Following reduction (Figure 13 B), this peak disappears, while two other identified peaks remain. This indicates that conditions in (A) and (B) are comparable and demonstrates that reduction of a disulphide bond results in loss of 2790.331. The identity of the predicted disulphide-carrying peptide was confirmed by MS/MS (Figure 13 C). For peak 2790.331, a y ion series (2, 4, 5, 6, 7, 9) corresponding to PK, TEPK, QTEPK, YQTEPK, LYQTEPK and SQLYQTEPK was detected, confirming the identity of 2790.331 as containing 305-316 SCLSQLYQTEPK. The characteristic triplet was also noted (Figure 13 C). These data allow the assignment of major intermolecular disulphide bonds between C53-C53' and C306-C306' (Figure 17). In addition, intramolecular disulphide bonds were identified between C108-C135 and C121-C147 (Table 2), as previously described (Jeffers, Sanders, and Sanchez, 2002). Although several low abundance fragments corresponding to alternative disulphide bonds, such as C108-C147, C108-C121 and C108-C306 were noted, there was no evidence of 53-306' linkage. This

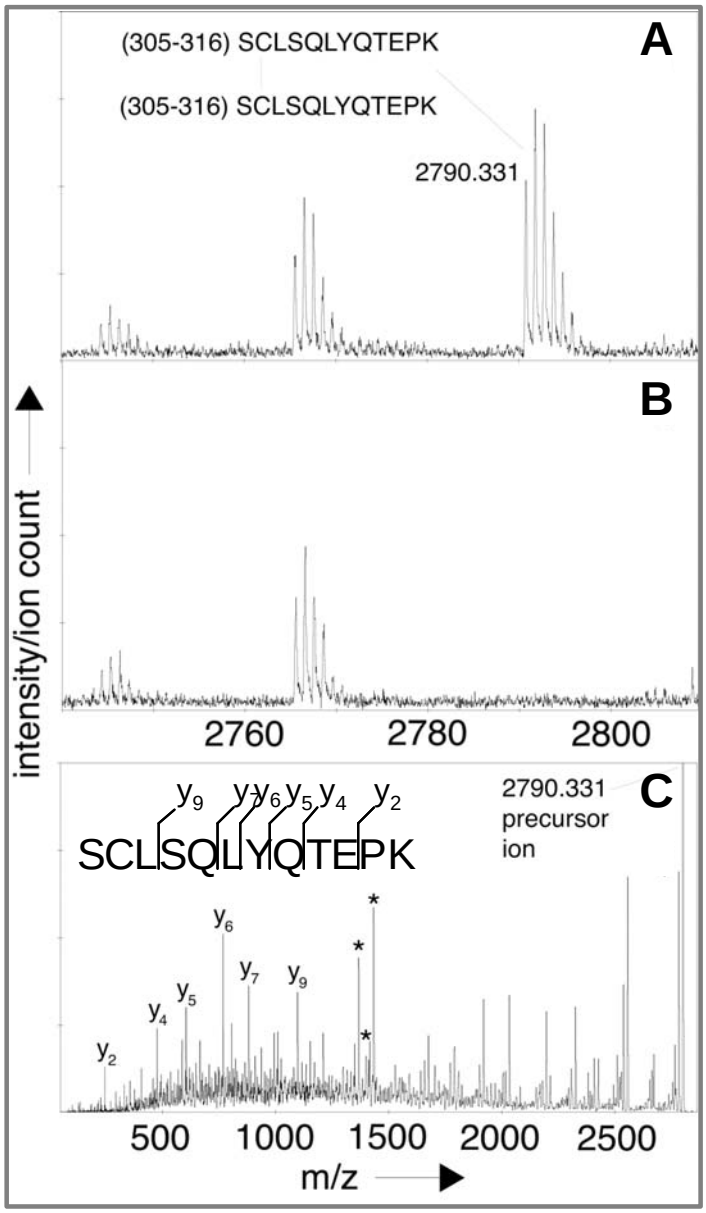

Figure 13. **Disulphide bond assignment of C306 using reduction (A, B) with MS/MS confirmation (C).** (A) A portion of the spectra of a non-reduced digest carrying disulphide-linked fragment m/z 2790.331 and normal tryptic peptides. (B) Following reduction the m/z 2790.331 fragment disappears. (C) MS/MS spectra of the disulphide-linked m/z 2790.331 fragment: y ions from fragmentation of the 305-316 SCLSQLYQTEPK peptide are shown as well as a characteristic triplet (*) due to breakage of -S-S- bond. (Modified from Falzarano et al. 2006. Copyright Wiley-VCH Verlag GmbH & Co. KGaA. Reproduced with permission.)

allowed unequivocal assignment of a parallel orientation to the sGP dimer (Figure 17). This was confirmed by repeating disulphide bond mapping on gel-fractionated samples under non-reduced conditions. This resulted in the identification of three disulphide-linked fragments (C108-C135, C121-C147, and C306-C306) confirming data from the in-solution digests.

3.1.3 Determination of site-specific N-glycosylation of sGP

HPLC-MALDI MS analysis of native sGP tryptic digests provided information on masses and the possible composition of sugar moieties. Glycopeptide-containing fractions were identified by their specific m/z spacing patterns (162, 203, 291 Da) between glycoforms and then analysed by MS/MS (Table 6 – see Appendix D) (Krokhin et al., 2004). Figure 14 shows MS spectra from both native (A) and deglycosylated (B) sGP HPLC-MS runs as well as a typical MS/MS analysis of sGP. Glycopeptides of increasing mass, corresponding to the addition of sugars (i.e. 291 corresponding to additional sialic acids) were observed (Figure 14 A). Following treatment with PNGaseF (which removes N-linked glycans), these glycopeptides disappear (Figure 14 B) and peak 2101.071 corresponding to the deglycosylated 248-264 FTPQFLLQLDETIYTSGK (T22) was observed. Such analysis permits confirmation of the peptide identity and extracts information related to sugar composition. Submission of resultant sugar masses (Table 6) to GlycoMod (www.expasy.org) indicated that all N-glycosylated sites on sGP contained complex N-glycans. To further confirm the presence of glycosylation, glycosylated peptide 3868.742 was selected for MS/MS (Figure 14 C). Physical removal of sugar moieties during MS/MS revealed unglycosylated peptide 2100.113, in addition to fragmented peptides, intact peptides with fragmented sugar moieties and the parent

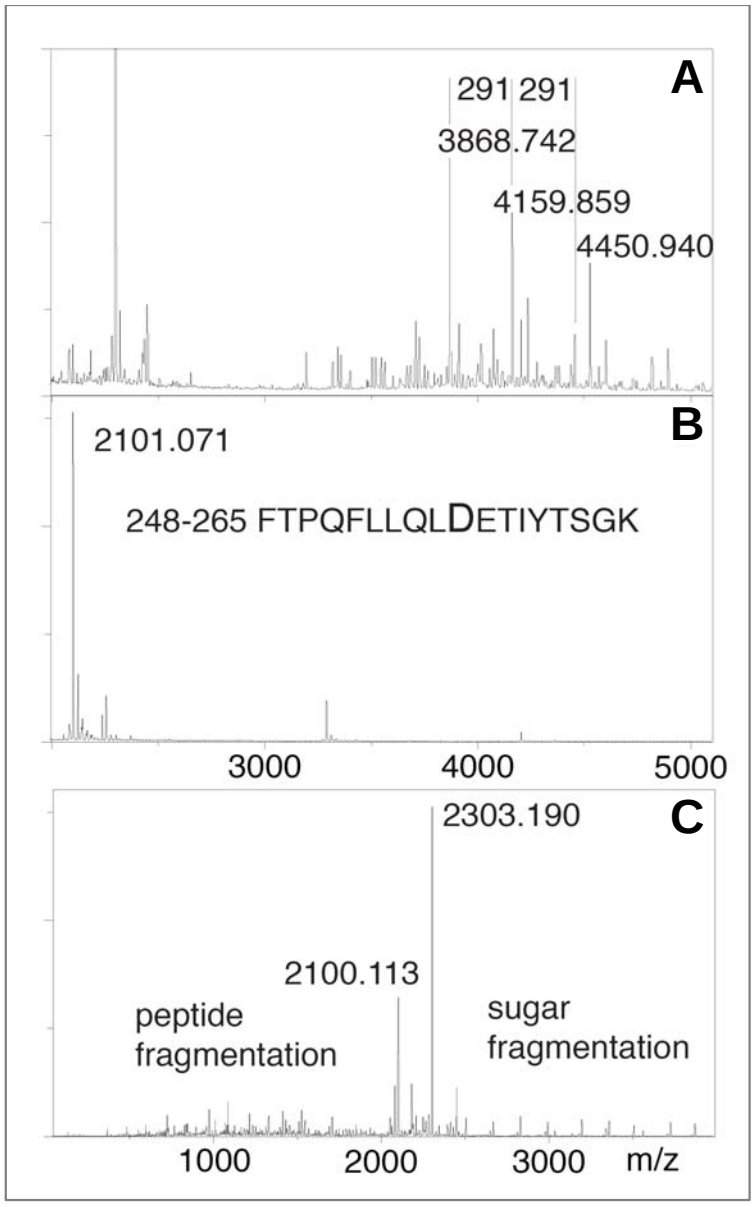

Figure 14. **Peptide mass fingerprint of native and deglycosylated sGP.** (A) Fraction #24 from a non-deglycosylated digest showing a typical glycopeptide pattern of T22 (248-265 fragment) with a characteristic +291 Da spacing. (B) Deglycosylated T22 (248-265) FTPQFLLQLDETIYTSGK peptide 2101.086 calculated m/z in fraction #27 of a deglycosylated digest. (C) MS/MS confirmation of identity for the 3868.742 peptide. A typical parent peptide + 203 Da doublet is shown. (From Falzarano et al. 2006. Copyright Wiley-VCH Verlag GmbH & Co. KGaA. Reproduced with permission.)

peptide with a +203 Da doublet representing the base N-acetylglucosamine (Figure 14 C). MS/MS of deglycosylated peptides allowed unequivocal assignment of all glycosylation sites. While there are six predicted N-glycosylation sites in sGP, only five were consistently glycosylated (N40, N204, N228, N257 and N268) (Figure 17). A general lack of conversion of N238 to D238 following PNGaseF treatment, suggests N238 is glycosylated infrequently (Table 6). While MS/MS data that could be used to predict the exact composition of the sugar moieties on each peptide was collected and analyzed, the large number of possible sugar combinations (e.g. typically >20) made it unfeasible to suggest an exact molecular composition for each N-linked sugar.

To more completely characterize glycosylation, sGP was also analyzed to determine if it contains O-linked glycans. However, as all peptide fragments were represented after treatment with PNGaseF (Table 2), it is unlikely that any of the predicted O-glycosylation sites are modified. In addition, all non-assigned peaks of high intensity or those from clusters containing characteristic glycopeptide spacing from the original HPLC-MS peptide mass fingerprints (PMF) of native sGP digests were subjected to MS/MS analysis to search for O-glycosylated species. Negative outcomes from these attempts further suggest that sGP does not contain any O-glycans.

3.1.4 Identification of C-mannosylation, a novel post-translational modification, on sGP

During sGP peptide mapping by MALDI MS and HPLC-MALDI MS, two unmodified tryptic peptides containing amino acids 288-291 WAFW were found: 2136.028 Da 277-294 VNPEIDTTIGEWAFWETK (T26) and 2264.112 Da 277-295 VNPEIDTTIGEWAFWETKK (T26+T27) (Figure 15 A, Figure 11 B, Table 1). The

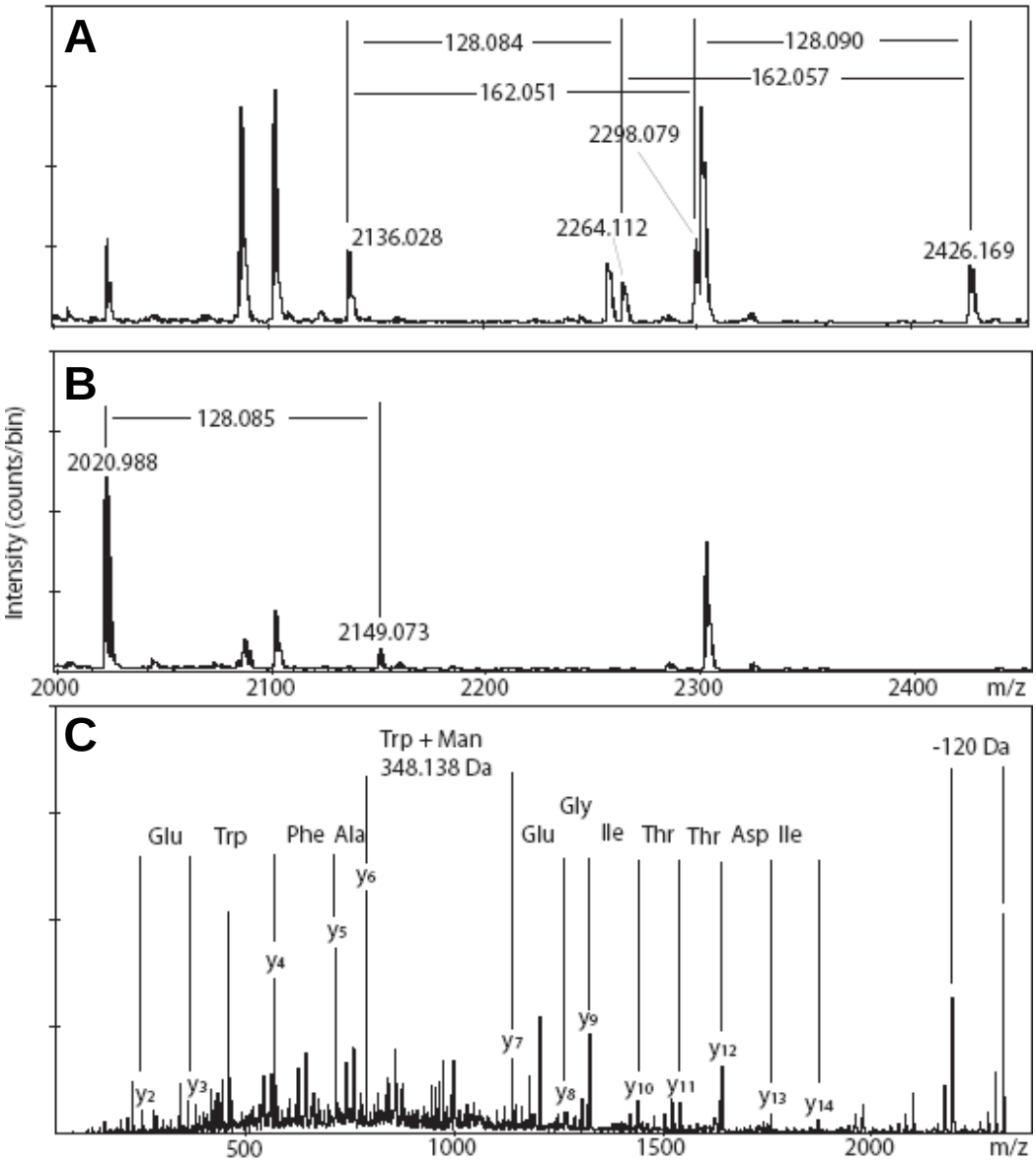

Figure 15. **Identification of C-mannosylation on sGP by mass spectrometry.** (A) A portion of MALDI/TOF MS (MS/MS) spectra of tryptic digests of purified sGP containing C-mannosylated fragment m/z 2298.079 VNPEIDTTIGEWAFWETK (T26) and 2426.169 VNPEIDTTIGEWAFWETKK (T26+T27), the +162 Da shift resulting from the addition of the mannose is indicated. The mass of the extra lysine is indicated by the 128 Da difference. (B) Spectra demonstrating that fragment of sGP-WXXA mutated to prevent C-mannosylation does not contain a peak shift of +162 Da. The fragment with the additional lysine is indicated (+128 Da). (C) MS/MS spectra of C-mannosylated peptide m/z 2298.079 fragment. y ions from the fragmentation of the (277-294) VNPEIDTTIGEWAFWETK peptide are shown as well as the characteristic 120 Da loss from the parent peptide due to the stability of the C-bond and the y7 ion with a mass of 348.138 indicative of a tryptophan residue with a mannose attached. (From Falzarano et al. 2007, with permission)

presence of a peptide with a missed cleavage is typical when there are two adjacent cut sites (KK). In this case, the result is two peaks separated by ~128.095 Da (Figure 15 A), corresponding to the extra lysine (K) residue. Both peptides showed +162 Da adducts (2298.079 and 2426.169) (Figure 15 A), consistent with the mass of a hexose residue (162.053 Da, Delta Mass – a database of protein post-translational modifications, http://www.abrf.org/index.cfm/dm.home). Comparison of the relative intensities of the non-modified peptides and their respective +162 Da adducts suggested that approximately 60% of the peptides were modified. MALDI MS analysis allowed all four of the fragments to be observed simultaneously, while HPLC-MALDI MS analysis introduced an additional retention time shift for the +162 Da modified species. Specifically, they elute approximately 1 minute earlier under the chromatographic conditions used. This finding is consistent with the addition of a hydrophilic sugar moiety to a hydrophobic tryptophan (W) residue. The identification of this post-translational modification was further supported by the presence of the recognition sequence W-x-x-W, for C-mannosylation at amino acid position 288 to 291 (W-A-F-W) of sGP, which was part of both peptides. C-mannosylation consists of a single aldohexopyranosyl residue (mannose) that is linked to the C2 atom of the indole ring of a tryptophan via a carbon-carbon bond (Figure 16 C).

Confirmation of W_{288} C-mannosylation was obtained during low-energy collision-induced dissociation (CID) MS/MS analysis of the modified peptides. Figure 15 C shows MS/MS spectrum of the +162 Da adducts of the 2298.079 peptide (T26). A complete series of y ions (y_2 to y_6) confirms that W_{291} is unmodified, while all y ions starting at y_7 have a mass increase of 162 Da. This is a strong indication that a mannose residue is

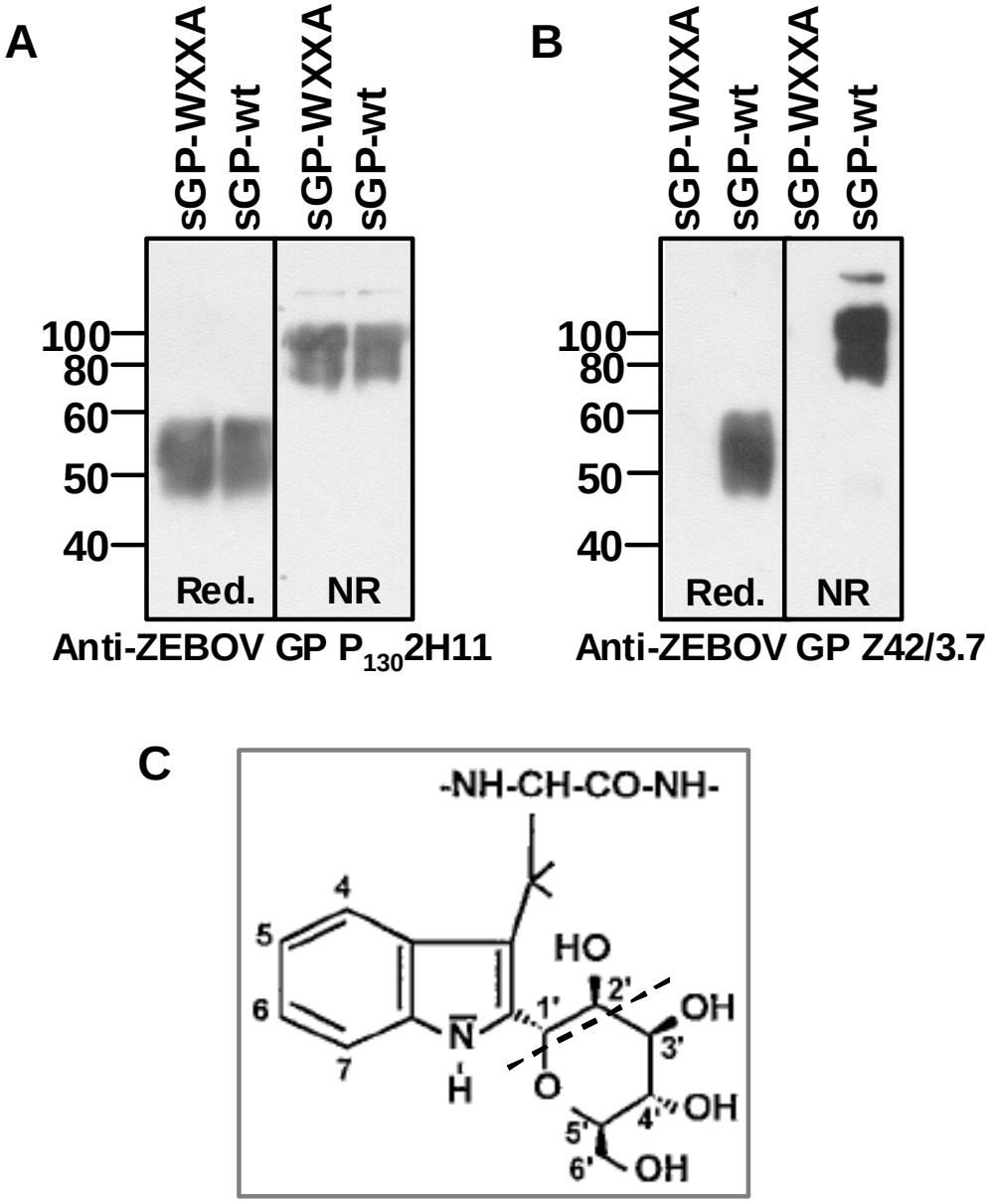

Figure 16. **Characterization of sGP and sGP-WXXA biosynthesis and structure.** SDS-PAGE (10%) analysis of sGP and sGP-WXXA under reducing (Red.) and non-reducing (NR) conditions using monoclonal antibodies (A) P_{130}2H11 (1/100 dilution) and (B) Z42/3.7 (1/4000 dilution). The numbers on the left indicate molecular mass in kDa. (C) A schematic of the structure of C-mannose tryptophan with the location of the CID breakage point (dashed line). (Modified from Falzarano et al. 2007, with permission)

attached to W_{288}. Furthermore, the characteristic 120 Da loss (Furmanek and Hofsteenge, 2000) that occurs during CID of mannosylated peptides was also observed (Figure 15 C). MS/MS analysis of the second mannosylated peptide 2426.169 (T26+T27) showed similar results. Following the identification of C-mannosylation on sGP, a neural network predictor of C-mannosylation was published (Julenius, 2007). To test the accuracy of this model, the amino acid sequence of sGP was analyzed (NetCGlyc 1.0) and found to have a predictive score of 0.455 (cut-off of 0.5), suggesting that sGP would not be modified.

3.1.5 Alteration of the WXXW motif prevents C-mannosylation of Ebola virus sGP

To confirm C-mannosylation of W_{288}, the motif for this modification was altered by site-directed mutagenesis of pDisplay-sGP such that W_{291} was replaced with alanine to generate sGP-WXXA. This mutation has been demonstrated to eliminate C-mannosylation (Krieg et al., 1998). sGP-WXXA was expressed at similar levels to sGP and was secreted from the cell as a homodimer with the same molecular mass as sGP (Figure 16 A), indicating that biosynthesis, processing and transport of the mutant was not significantly affected. Interestingly, the mutation abrogated one of the immunogenic epitopes on sGP, since monoclonal antibody Z42/3.7 was not able to detect sGP-WXXA by western blot (Figure 16 B). A comparable peptide mapping of sGP-WXXA by MALDI MS and HPLC-MALDI MS resulted in the elimination of the +162 Da mass shift observed for peptides T26 and T26+T27 derived from wild-type sGP (Figure 15 B). All identified post-translational modifications and disulphides bonds for sGP are summarized in Figure 17.

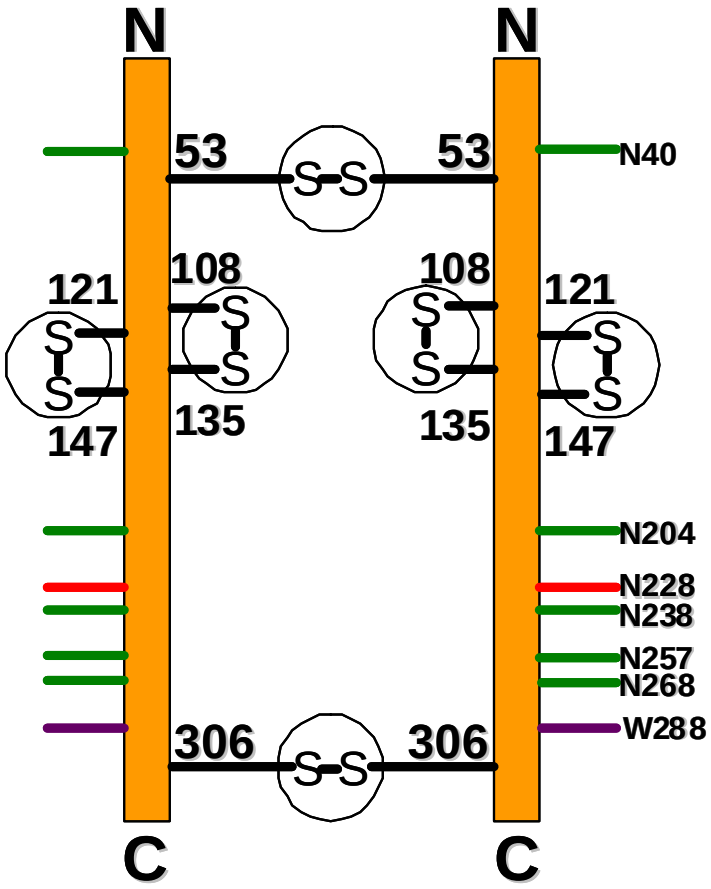

Figure 17**. Schematic of the structure of the sGP homodimer.** Intermolecular disulphide bonds between cysteine residues 53 and 306, as well as intramolecular disulphide bonds between cysteine residues 108-135 and 121-147, are indicated. N-glycosylation sites that contain complex N-glycans are indicated in green (N40, N204, N228, N257, N268). The N-glycosylation site that is only partially glycosylated (N238) is indicated in red. The C-mannosylation site (W288) is indicated in purple. (Modified from Falzarano et al. 2006. Copyright Wiley-VCH Verlag GmbH & Co. KGaA. Reproduced with permission.)

3.1.6 C-mannosylation of sGP occurs in multiple cells lines and during ZEBOV infection

To ensure that C-mannosylation was not a unique feature of a specific cell line (293T), sGP was also purified from transfected Huh7 and Vero E6 cell lines (Figure 18 A). MALDI MS revealed similar spectra to that of the 293T cell-derived sGP, with peaks at 2298 and 2426. This indicates the presence of a mannose residue and unmodified peptides at 2136 and 2264 (Figure 19 A, B). To determine if sGP was also C-mannosylated during EBOV infection, Vero E6 cells were infected with ZEBOV (strain Mayinga) at an MOI of 0.5. The appropriate time point for collection of the supernatant was optimized to maximize the amount of sGP, while keeping GP_1 and additional contaminating cellular protein (as a result of CPE) to a minimum. Day three post-infection was determined as the appropriate time point to harvest the supernatant, as there was considerable sGP signal, minimal GP_1 signal (Figure 18 B) and CPE was approximately +2 (rounded cells, with a limited number of cells detached from the monolayer). Virus was removed from the supernatant by ultracentrifugation and sGP was partially purified by differential filtration and lectin-binding chromatography. Digests of partially purified sGP from ZEBOV-infected Vero cells contained the C-mannosylated peptide 277-294 VNPEIDTTIGEWAFWETK (T26) as determined by HPLC-MALDI MS (Figure 19 C), but in contrast to the transfected cell lines, only C-mannosylated peptides were detected. To confirm this result, 2298.082 (corresponding to C-mannosylated T26) was selected for MS/MS which yielded results identical to Figure 15 C.

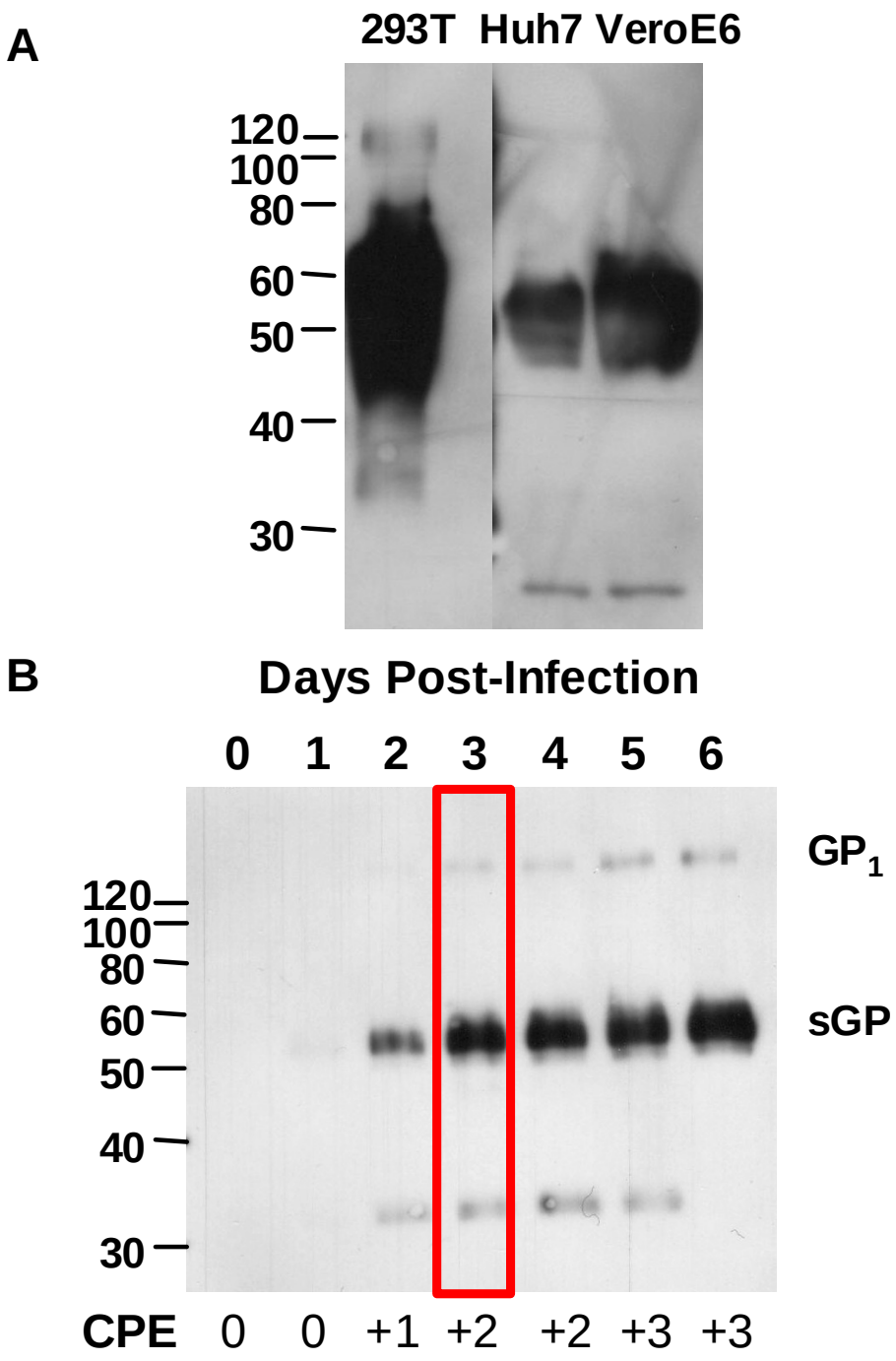

Figure 18. **Expression of sGP in multiple cell lines and during virus infection.** (A) Western blot of sGP produced following transfection of 293T, Huh7 and VeroE6 cells with monoclonal antibody Z42/3.1 (1/4000 dilution). Equivalent amounts of protein were added to each lane demonstrating the differences in expression/transfection efficiency between the different cell lines. (B) Western blot of supernatant from ZEBOV-infected VeroE6 cells. For MS analysis of sGP a time point where sGP production was high but cytopathic effect (CPE) and $GP_{1,2}$ production was low had to be determined. Based on this data supernatant was harvested on day 3.

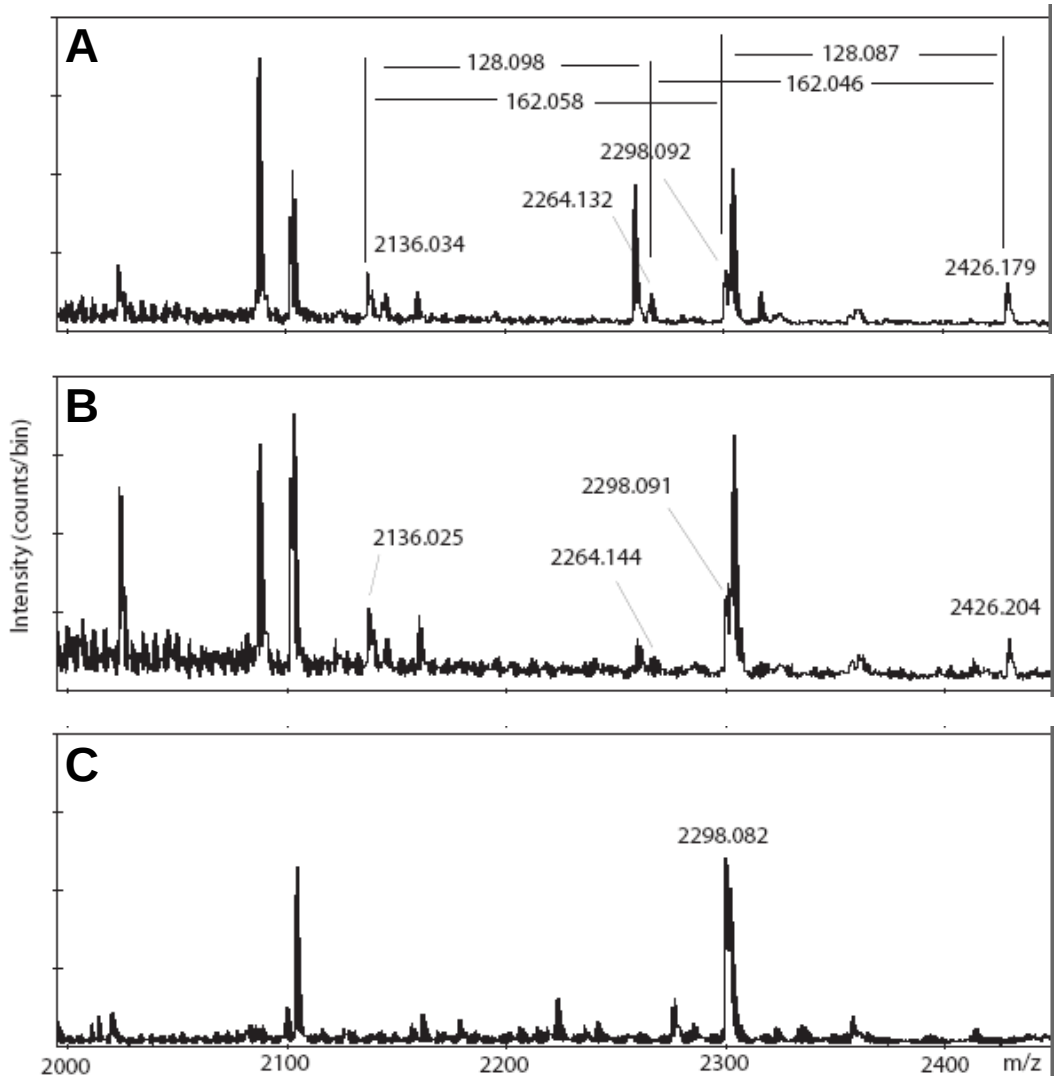

Figure 19. **C-mannosylation of sGP occurs in multiple cell lines and during EBOV infection.** (A) MALDI/TOF MS spectrum of tryptic digests of purified sGP from Huh7 and (B) Vero E6 cell lines showing non-modified m/z 2136 (VNPEIDTTIGEWAFWETK), 2264 (VNPEIDTTIGEWAFWETKK) and C-mannosylated fragments m/z 2298 and 2426, respectively. The addition of the mannose (+162 Da) is indicated. (C) Spectrum of fraction 28 from purified supernatant of *Zaire ebolavirus* infected Vero E6 cells indicating C-mannosylated peptide m/z 2298.082. (From Falzarano et al. 2007, with permission)

3.2 Effect of sGP on Endothelial Barrier Function

3.2.1 sGP treatment of endothelial cells exposed to shear stress does not affect shear stress-induced changes to barrier function

Previous data has indicated that sGP does not affect the barrier function of endothelial cell under static conditions (Wahl-Jensen et al., 2005b); however, endothelial cells are constantly subjected to shear stress i*n vivo*, resulting in morphologies, protein expression and signalling that differs from that of endothelial cells cultured under static conditions. To determine if sGP had an effect on endothelial barrier function, HUVECs were subjected to either moderate (12 dyn/cm^2) shear stress or no shear stress (0.2 dyn/cm^2), 30 minutes following the addition of 10 μg/ml sGP or the cysteine mutants C53G, C306G, C53/306G. Subsequently, the trans-endothelial resistance (TER), which reflects the endothelial barrier function, was monitored by impedance spectroscopy. Purified proteins used in all endothelial cell experiments were assayed to determine the level of endotoxin. Endotoxin levels were consistently <0.5 U of endotoxin per ml, which is sufficiently low to not alter endothelial barrier function alone (data not shown).

Neither sGP, as previously described (Wahl-Jensen et al., 2005b), nor the cysteine mutants altered the barrier function (as measured by TER) of HUVECs under static conditions (Figure 20). These cells underwent an initial small gradual decrease in barrier function for the first 200 minutes after which they underwent a continuous gradual increase in TER until the experiment was terminated (Figure 20). Cells exposed to shear stress underwent a characteristic rapid sharp increase in TER, which quickly decreased at approximately the same rate. This was followed by a very small gradual increase until approximately 250 minutes, after which there was a continuous drop in the TER over

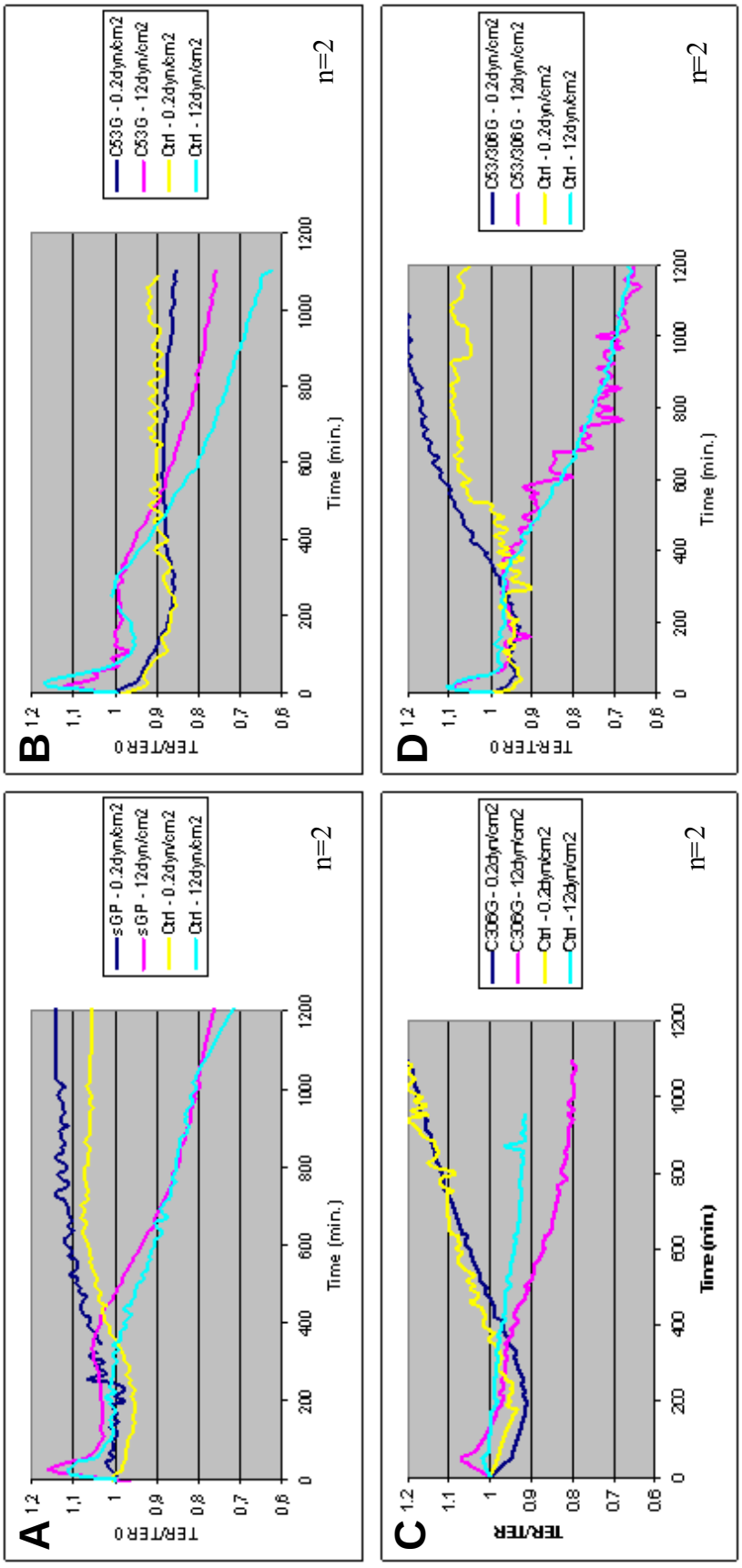

Figure 20. **Effect of exogenous sGP on barrier function of endothelial cells under shear stress and static conditions.** HUVECs were equilibrated at 2 rpm for 1-2 hours to generate a baseline TER. sGP (10 µg/ml) (A) or the cysteine mutants C53G (B), C306G (C) or C53/306G (D) were added to the medium as indicated, while an equivalent volume of TNE buffer was added to control chambers. Following treatment, static chambers were maintained at 2 rpm for the duration of the experiment (0.2dyn/cm^2), while shear stress exposed chambers were maintained at 2 rpm for 30 minutes and then increased to 80 rpm (12dyn/cm^2) for the duration of the experiment.

time (Figure 20). Under shear stress, both control and sGP- (or cysteine mutant) treated cells essentially exhibited the same TER pattern.

3.2.2 Endogenous expression of sGP in endothelial cells exposed to shear stress does not alter shear stress-induced changes to barrier function

While exogenous exposure to sGP does not appear to affect barrier function under static and shear-stress conditions, it is unknown if endogenous expression of sGP in endothelial cells would have an effect. It is expected that endothelial cells would express significant quantities of sGP when infected late in the course of the disease. Therefore, HUVECs were infected with a high MOI of replication incompetent Lentiviruses that express sGP or eGFP (as a control), to determine if endogenous expression affects TER. Following infection, cells were either exposed to no shear stress (0.2 dyn/cm^2) or moderate shear stress (12 dyn/cm^2) and barrier function was monitored by impedance spectroscopy. Small differences in the pattern of TER alterations were observed at very early time points (i.e. within the first 60 minutes) (Figure 21 A). In cells infected with Lentiviruses expressing sGP, the characteristic rapid increase and decrease in TER (following application of shear stress (12 dyn/cm^2)) was not observed and the TER did not undergo the small decrease normally seen in cells that are not subjected to shear stress (0.2 dyn/cm^2). However, at time points beyond 60 minutes, the TERs were comparable for both cells exposed to shear stress and those that were not, regardless of infection with sGP or eGFP expressing Lentivirus (Figure 21 A).

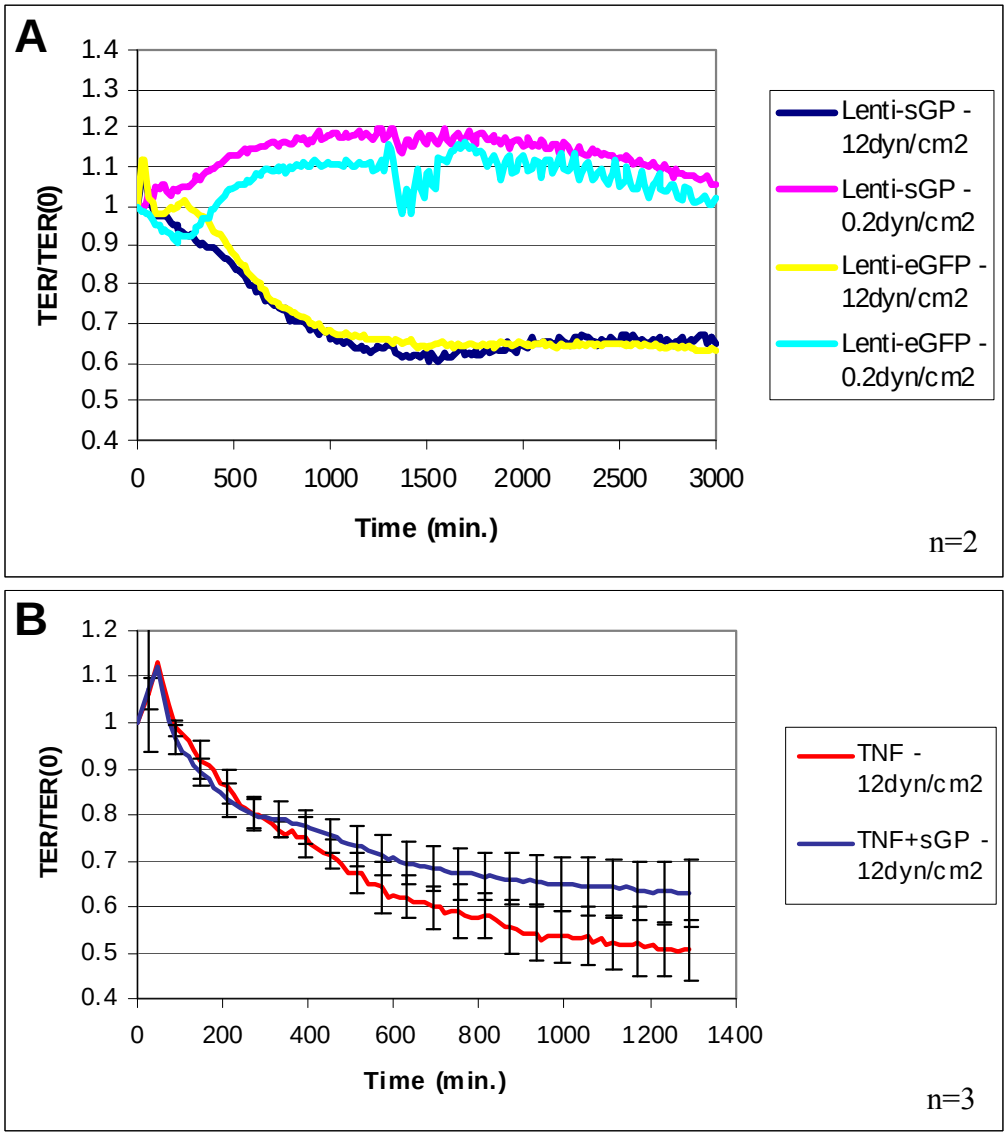

Figure 21. **Endothelial barrier function following endogenous expression of sGP (A) and exogenous treatment with TNF-α (B) with and without sGP under shear stress and static conditions.** (A) HUVECs were infected with Lentiviruses expressing either sGP or eGFP (as a control) 1 hour prior to monitoring of TER. Following infection, cells were equilibrated at 2 rpm for 1 hour to establish a baseline TER. Static chambers were maintained at 2 rpm for the duration of the experiment (0.2dyn/cm^2), while shear stress exposed chambers were increased to 80 rpm (12dyn/cm^2) for the duration of the experiment. The endogenous expression of either sGP or eGFP did not significantly alter TER. (B) HUVECs were treated with TNF-α (1ng/ml) with and without sGP (10μg/ml) and then immediately subjected to shear stress (12dyn/cm^2) while monitoring the TER. The application of shear stress has a significant effect on the TER, causing a permanent decrease in barrier function after a rapid transitory increase (A, B). Treatment of HUVECs with sGP and TNF-α resulted in TER values that were higher than TNF-α alone indicating that sGP may protect barrier function under shear stress conditions.

3.2.3 sGP provides limited rescue of TER following TNF-α treatment of endothelial cells exposed to shear stress

To determine if sGP causes alteration to endothelial cells that are treated with TNF-α and shear stress, the TER of HUVECs treated with TNF-α or TNF-α with sGP under shear stress (12 dyn/cm^2) was monitored (Figure 21 B). The application of shear stress causes the most significant alterations in TER; however, cells treated with TNF-α alone had a consistently lower TER past the 300 minute mark than cells treated with TNF-α and sGP together. This suggests that sGP also provides a protective effect under shear stress conditions following TNF-α treatment; however, this effect was not statistically significant (p=0.052).

3.2.4 sGP cysteine mutants have significantly reduced abilities to rescue endothelial barrier function following TNF-α treatment under static conditions

It has been previously reported that sGP mediates an accelerated recovery of the TER following treatment of endothelial cells with TNF-α under static conditions (Wahl-Jensen et al., 2005b). As protein function should be structure-dependent, we investigated whether the cysteine mutants (Figure 11 A) would demonstrate the same protective effect using impedance spectroscopy. HUVECs were equilibrated for 1 hour to generate a baseline TER, then TNF-α, with and without sGP (or the indicated cysteine mutant), was added to the medium and cells were monitored by impedance spectroscopy for 24 hours. It was previously determined that 1 ng/ml of TNF-α produced a moderate, but reliable decrease in endothelial cell barrier function (Wahl-Jensen et al., 2005b); therefore, this quantity was used in all experiments. Neither sGP, nor the cysteine mutants alone (10μg/ml) affected the TER of the endothelial cell monolayer within 24 hours of

addition. Approximately 5 hours post-treatment with TNF-α, the TER decreased continuously, reaching a steady state of 60% at 16 hours post-treatment (Figure 22). As previously described (Wahl-Jensen et al., 2005b), the simultaneous administration of sGP and TNF-α resulted in an accelerated recovery of the TER (Figure 22). In contrast, all mutants (C53G homodimer, C306G homodimer and C53/306G monomer) were impaired in their ability to reverse the TNF-α-mediated TER decrease of endothelial cell monolayer (Figure 22). C53G and C306G provided no accelerated recovery, while C53/306G provided an intermediate rescue effect that was notably less than that of sGP. At approximately 420 minutes, the TER was significantly different ($p<0.05$) between endothelial cells treated with TNF-α alone and TNF-α with sGP. At 840 minutes, the difference between TNF-α with sGP and TNF-α with the indicated mutants was significantly different. This data clearly demonstrates that a correctly folded parallel homodimer is essential for full functioning of sGP in this assay.

3.2.5 Elimination of C-mannosylation on sGP does not affect its ability to rescue endothelial barrier function following TNF-α treatment

sGP is able to restore the decrease in barrier function of endothelial cells, which can be provoked through TNF-α treatment (Wahl-Jensen et al., 2005). Furthermore, this potential anti-inflammatory role of sGP is structure-dependent. It has been suggested that C-mannosylation may play a role in protein folding, especially involving folding around disulphide bonds. The location of the C-mannosylated W_{288} is in close proximity to the cysteine residue involved in one of the intermolecular disulphide bonds (C_{306}), which is important for the formation of sGP homodimers (Barrientos et al., 2004; Falzarano et al., 2006); therefore, the effect of eliminating the C-mannose on sGP function was

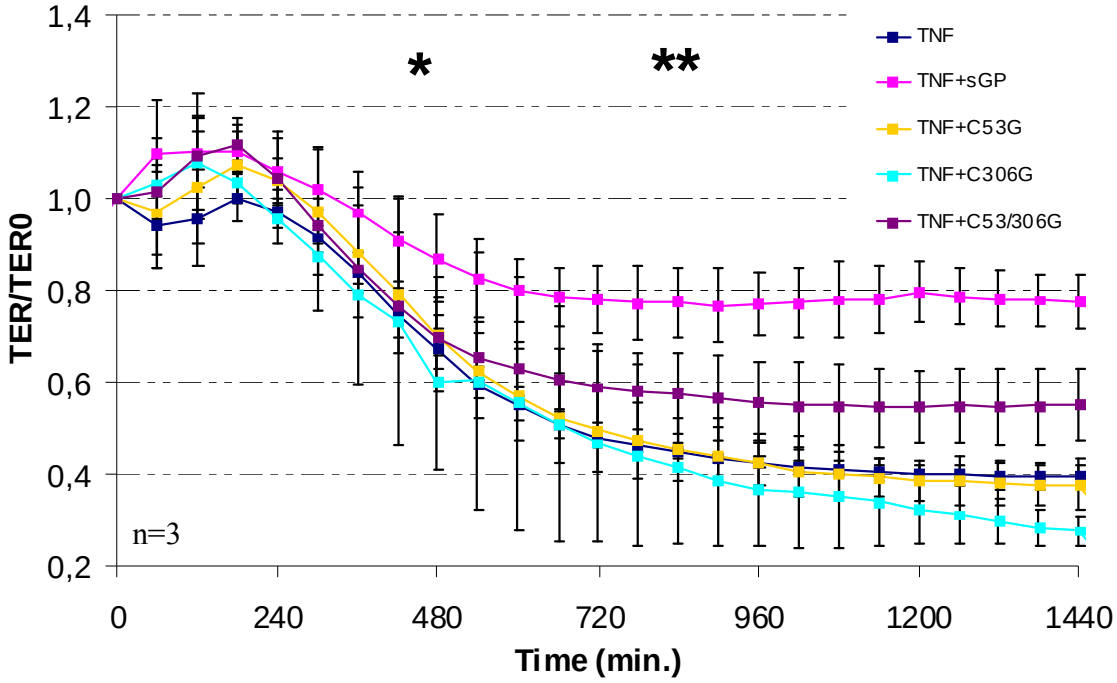

Figure 22. **Effect of sGP and cysteine mutants on TNF-α treated endothelial cells under static conditions.** HUVECs were equilibrated for 1 hour to generate a baseline TER. TNF-α (1ng/ml) with and without sGP or cysteine mutants (10μg/ml) were added to the medium, as indicated. Following treatment, the chambers were monitored by impedance spectroscopy. The difference in TER was significant ($p<0.05$) between endothelial cells treated with TNF-α alone and TNF-α with sGP (*) and between TNF-α with sGP and TNF-α with the indicated mutants (**). (Modified from Falzarano et al. 2006. Copyright Wiley-VCH Verlag GmbH & Co. KGaA. Reproduced with permission.)

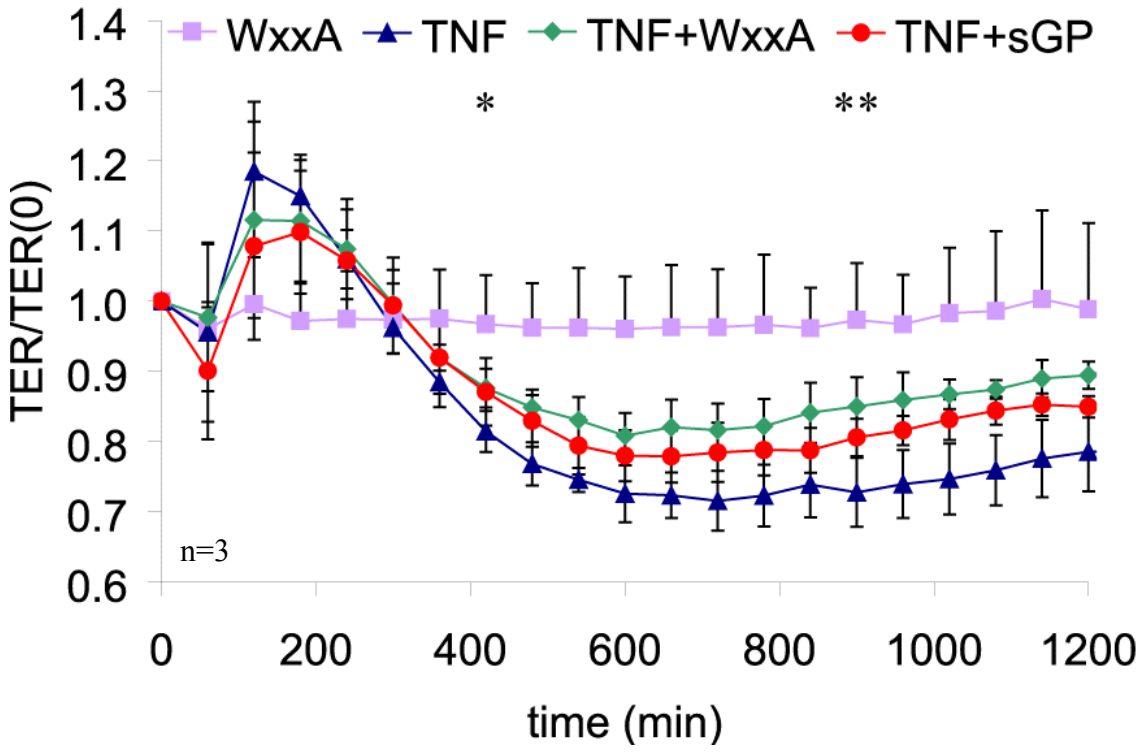

Figure 23. **Effect of C-mannosylation on sGP rescue of TNF-α-treated endothelial cells under static conditions.** Human endothelial cells (HUVEC) were equilibrated for 1 hour to generate a baseline TER. TNF-α (1ng/ml) with and without sGP or sGP-WXXA (10μg/ml) were added to the medium as indicated. Following treatment the chambers were monitored by impedance spectroscopy. There was a significant difference ($p<0.05$) between the TER of cells treated with TNF-α alone and cells treated with TNF-α and sGP or sGP-WXXA at 900 min. for sGP and 420 min. for sGP-WXXA. (Modified from Falzarano et al. 2007, with permission)

determined. As previously demonstrated (Wahl-Jensen et al., 2005), treatment of endothelial cells with TNF-α lead to a decrease in TER, which can be partially reversed by sGP (Figure 23). The same rescue effect was also observed when endothelial cells were treated simultaneously with TNF-α and sGP-WXXA (Figure 23). A significant difference ($P<0.05$) between the TER of cells treated with TNF-α alone and cells treated with TNF-α and sGP or sGP-WXXA was noted at 900 min. for sGP and 420 min. for sGP-WXXA. This demonstrates that C-mannosylation of W_{288} does not alter this biological function of sGP, albeit this modification may be relevant for another, as of yet unidentified function.

3.3 The Potential for C-mannosylation of Other Viral Proteins

3.3.1 Search for WXXW motifs in viral proteins that contain signal peptides

A search of the non-redundant NCBI RefSeq viral protein database revealed 2323 proteins that contain the recognition sequence WXXW for C-mannosylation. As only proteins that are processed through the ER are considered to have the potential to be C-mannosylated, all protein sequences containing WXXW were run through the SignalP 3.0 server in both neural network (NN) and hidden Markov model (HMM) modes to predict whether the protein contains a signal peptide. This predictive modeling gives a yes/no (NN) or a predicted signal peptide/non-secretory protein/anchor signal prediction (HMM). From this analysis, 373 viral proteins were predicted to have signal peptides, indicating that they may have the potential to be C-mannosylated (for a complete list of proteins, see Appendix E). Candidate proteins from potential human and animal viruses are listed in Table 3, which includes the EBOV spike glycoprotein $GP_{1,2}$ (discussed in

Table 3. Proteins from selected human and animal viruses that contain the C-mannosylation recognition sequence WXXW and are predicted to have the potential to cross the ER membrane as determined by SignalP 3.0 in both Neural Net (NN) and Hidden Markov Model (HMM) modes. NN predicts the presence/absence of a signal peptide (yes/no). HMM predicts the presence of a signal peptide/signal anchor or the lack thereof (non-secretory). The viruses are grouped according to the guidelines of the International Committee on Taxonomy of Viruses (ICTV). [1] double-stranded DNA, [2] reverse transcribed, [3] double-stranded RNA, [4] negative-sense single-stranded RNA, [5] positive-sense single-stranded RNA, [6]signal peptide, [7]signal anchor, [8] non-secretory (modified from Falzarano et al., 2007).

	Family	**Virus**	**Protein**	**NN**	**HMM**
dsDNA[1]	*Poxviridae*	Myxoma virus	m4.1	Yes	SP[6]
		Molluscum contagiosum virus	MC011L	Yes	SP
	Herpesviridae	Human herpesvirus 1	virion glycoprotein M	No	SA[7]
		Human herpesvirus 2	virion glycoprotein M	No	SA
			tegument protein	No	SP
	Hepadnaviridae	Hepatitis B virus	S protein	Yes	SP
RT[2]	*Retroviridae*	Friend murine leukemia virus	envelope protein	Yes	SP
		Human immunodeficiency virus 1/2	gp41	Yes	SP
			gp160	Yes	SP
		Simian immunodeficiency virus	env	Yes	SP
dsRNA[3]	*Reoviridae*	Human rotavirus	VP7	Yes	SA
(-)ssRNA[4]	*Bornaviridae*	Borna disease virus	glycoprotein	Yes	SP
	Rhabdoviridae	Vesicular stomatitis virus	glycoprotein	Yes	SP
		Mokola virus	transmembrane glycoprotein	Yes	SP
	Filoviridae	Bundibugyo ebolavirus	secreted glycoprotein	Yes	SP
			structural glycoprotein	Yes	SP
		Cote d'Ivoire ebolavirus	secreted glycoprotein	Yes	SP
			structural glycoprotein	Yes	SP
		Reston ebolavirus	secreted glycoprotein	Yes	SP
			structural glycoprotein	Yes	SP
		Sudan ebolavirus	secreted glycoprotein	Yes	SP
			structural glycoprotein	Yes	SP
		Zaire ebolavirus	sGP	Yes	SP
			ssGP	Yes	SP
			spike glycoprotein precursor	Yes	SP
	Orthomyxoviridae	Influenza A virus (A/New York/392/2004(H3N2))]	hemagglutinin	Yes	SP
		Influenza C virus	CM2 protein	Yes	SP
	Bunyaviridae	Crimean-Congo hemorrhagic fever virus	glycoprotein precursor	Yes	SP
(+)ssRNA[5]	*Coronaviridae*	Human coronavirus 229E	surface glycoprotein	Yes	SP
			4a protein	Yes	SP
			membrane protein	Yes	NS[8]
		Murine hepatitis virus	E1 glycoprotein	No	SA
			E2 glycoprotein precursor	Yes	SP
			spike glycoprotein S	Yes	SP
			membrane protein M	Yes	SA
		SARS coronavirus	E2 glycoprotein precursor	Yes	SP
			matrix protein	Yes	SA
	Flaviviradae	Dengue virus type 1	non-structural protein 2B	Yes	SA
		West Nile virus	polyprotein precursor	No	SP
		Hepatitis C virus	NS2 protein	Yes	SA
	Togaviridae	Ross River virus	6K protein	No	SA
		Rubella virus	glycoprotein E1	No	SP
	Parvoviridae	Canine parvovirus	polyprotein	No	SP

further detail below). Additional candidate proteins for C- mannosylation are found among RNA viruses and include the single transmembrane proteins Vesicular Stomatitis virus (VSV) G, Borna disease virus (BDV) G and Crimean-Congo hemorrhagic fever virus (CCHF) G_C, the hemagglutinin and M2 proteins of influenza virus, the E2 protein of SARS-coronavirus, the spike proteins of other human coronaviruses and the envelope proteins of Human Immunodeficiency Virus (HIV)-1 and 2 (Table 3). This modification may also be present in glycoproteins of DNA viruses including Hepatitis B virus, Myxoma virus and Herpesviruses.

3.3.2 C-mannosylation motifs are present in GP_1 and GP_2

EBOV $GP_{1,2}$ is included in the list of proteins with the potential to be C-mannosylated. The surface glycoprotein possesses 3 potential C-mannosylation sites that are conserved in all 5 EBOV species (Figure 24); therefore, this modification or these residues may be important for the function of $GP_{1,2}$. The first potential C-mannosylation site on W_{288} of GP_1, is identical to that of sGP as it occurs prior to the editing site (see introduction and Feldmann et al., 2001). This site is also present in ssGP; however, this was not investigated further as the production of this protein during virus infection has only recently been confirmed. The second and third C-mannosylation motifs are located adjacent to each other in GP_2, just outside of the predicted transmembrane region (Figure 24), in a region termed the membrane proximal external region (MPER) (Lee et al., 2008).

3.3.3 Analysis of potential C-mannosylation sites on $GP_{1,2}$

To determine if the motifs for C-mannosylation were actually modified in GP_1 and GP_2, it was necessary to generate partially purified GP_1 and/or GP_2 for mass

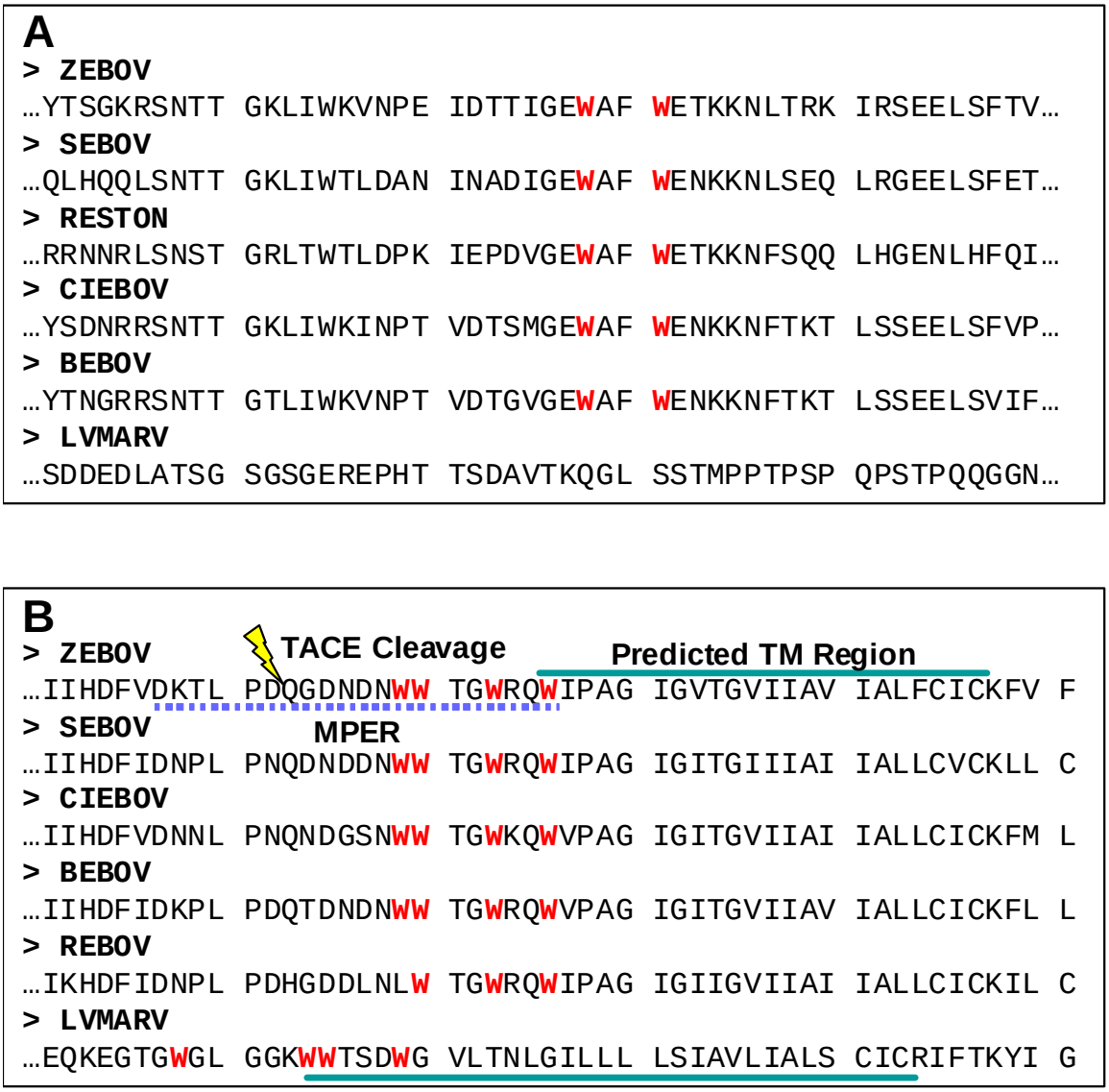

Figure 24. **Alignment of regions containing C-mannosylation motifs in GP_1 (A) and GP_2 (B) of the different filovirus species.** (A) Alignment the region in GP_1 that contains a C-mannosylation motif (highlighted in red) indicating that this motif is conserved in all EBOV species and absent in MARV. (B) Alignment of the region in GP_2 that contains two adjacent C-mannosylation motifs (highlighted in red) just outside of the predicted transmembrane domain region (green line) in the membrane-proximal external region (MPER) (blue dashed line). While C-mannosylation motifs are not conserved in MARV an unusually high number of tryptophan residues are present in a similar region (adjacent to or part of the transmembrane domain region. The location of the TACE cleavage site is also indicated (lightening bolt).

spectrometry. It would have been possible to perform mass spectrometry analysis on affinity purified GP_1 using the same method as for sGP (i.e. transient expression from the pDisplay vector); however, this would not have included GP_2. Likewise, the pDisplay vector containing $GP_{1,2\Delta TM}$, did not contain the sequence of GP_2 that includes the C-mannosylation motifs, as the TACE cleavage site is at D_{637} (Figure 24). As the full-length $GP_{1,2}$ contains a transmembrane anchor, this protein is not secreted; therefore, solubilisation of the membrane and subsequent purification would have been necessary. To simplify this process, $GP_{1,2}$ was co-expressed with VP40 (both in the pCAGGS vector) to generate virus-like particles (VLPs). These particles can be subjected to centrifugation through a sucrose cushion, thereby partially purifying the sample prior to mass spectrometry analysis. Partially purified VLPs were processed for mass spectrometry as described for sGP. While both unmodified and C-mannosylated peptides bearing 288-291 WAFW from GP_1 were detected by HPLC MALDI-TOF MS, the peptide containing the two adjacent C-mannosylation motifs in GP_2 634-649 TLPDQGDNDNWWTGWR was not detected (data not shown). This peptide is either immediately adjacent to or partially embedded in the membrane; therefore, it was suspected that it was necessary to disrupt the membrane to access this protein. To address this issue, prior to reduction and alkylation, VLPs were treated with either heat (95°C, 10 minutes) or 0.1% NP40 to dissociate the VLP membrane. Samples were then processed as described above. Spectra from samples treated with NP40 were significantly suppressed by the detergent (data not shown), while sufficient data was obtained from the heat-treated VLPs.

HPLC-MALDI MS analysis of heat-treated VLPs revealed two unmodified tryptic peptides containing amino acids 288-291 WAFW in fraction #26: 2136.049 Da 277-294 VNPEIDTTIGEWAFWETK and 2264.136 Da 277-295 VNPEIDTTIGEWAFWETKK (Figure 25 A). Similar to sGP, two peptides were observed as a result of a missed cleavage at two adjacent cut sites (KK), with a separation of 128.087 Da (Figure 25 A), corresponding to the extra lysine (K) residue. In fraction #24, both peptides showed +162 Da adducts (2298.114 and 2426.221) (Figure 25 B), consistent with the mass of a hexose residue (162.053 Da, Delta Mass – a database of protein post-translational modifications, http://www.abrf.org/index.cfm/dm.home). As observed with sGP, the C-mannosylated peptides eluted in an earlier fraction, consistent with the addition of a hydrophilic sugar moiety to a hydrophobic tryptophan (W) residue. Tryptic peptide 634-649 TLPDQGDNDNWWTGWR, containing the two adjacent C-mannosylation sites in GP_2, was observed in fraction #23 containing non-modified fragment 1960.866 (Figure 25 C). Both automated and manual searches of all fractions failed to detect any peaks corresponding to +162.053 or +324.106 Da (2122.919 or 2284.972).

Following the analysis of C-mannosylation by mass spectrometry, a predictive modeling program for C-mannosylation became available. Based on cellular proteins that have been identified as C-mannosylated, this model takes into account other parameters in addition to the consensus sequence WXXW (Julenius, 2007). Analysis of the C-mannosylation sites of GP_1 and GP_2 by NetCGlyc 1.0 indicates that W288 of GP_1 has a predictive score of 0.455 (similar to sGP), and W645 and W648 of GP_2 have predictive scores of 0.305 and 0.517, respectively. With a cut-off value of 0.5, this indicates that

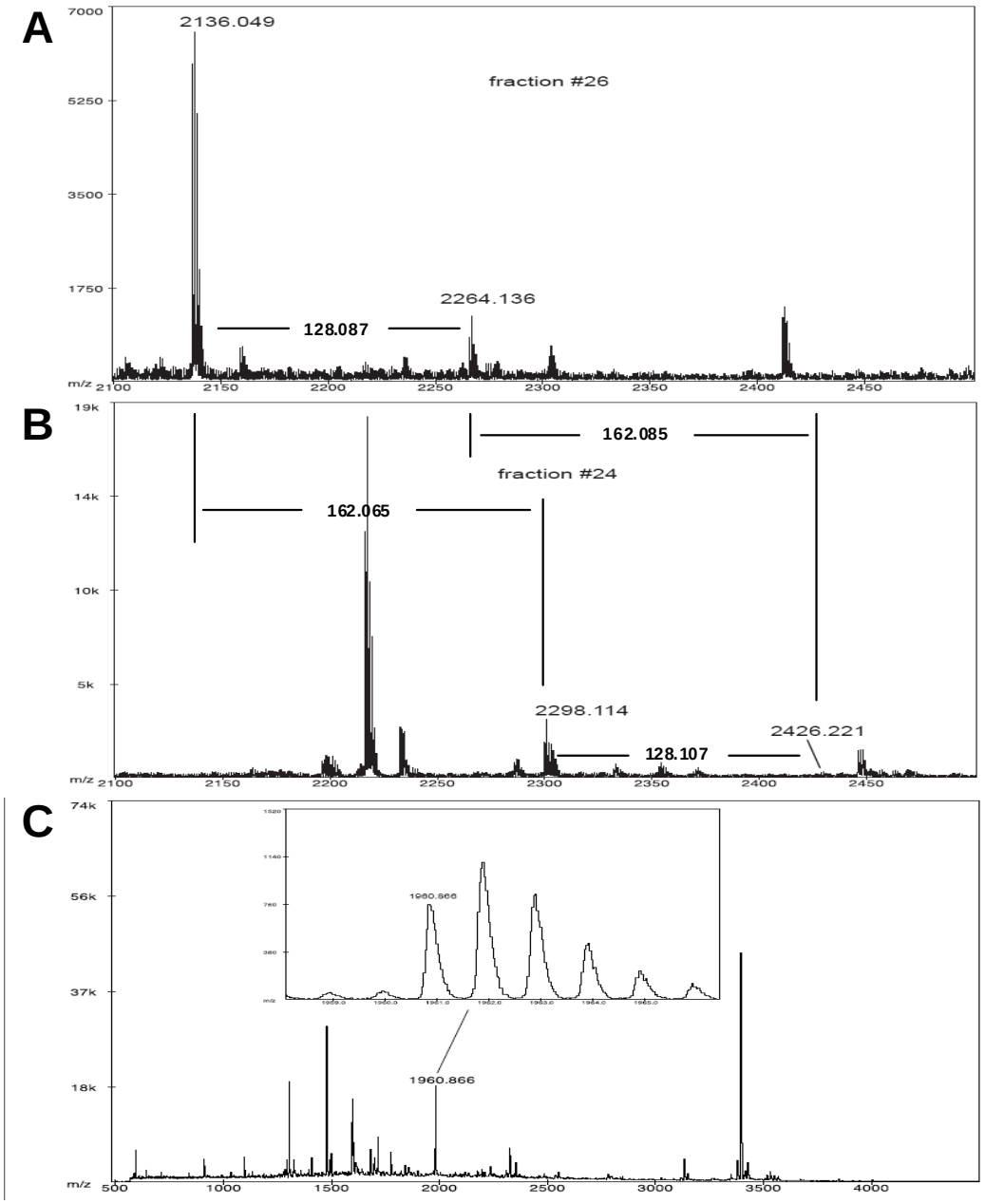

Figure 25. **Analysis of C-mannosylation on $GP_{1,2}$ by mass spectrometry.** (A) A portion of MALDI/TOF MS spectra of HPLC-separated tryptic digests of partially purified VLPs showing fraction #26 containing non-modified fragments m/z 2136.049VNPEIDTTIGEWAFWETK and 2264.136 VNPEIDTTIGEWAFWETKK. The mass of the extra lysine is indicated by the 128 Da difference. (B) Spectra from fraction #24 demonstrating C-mannosylated peptides 2298.114 VNPEIDTTIGEWAFWETK and 2426.221 VNPEIDTTIGEWAFWETKK. The +162 Da peak shift as a result of the addition of a mannose residue is indicated. (C) Spectra from fraction #23 containing non-modified fragment 1960.866 TLPDQGDNDNWWTGWR. The isotopic series is shown (inset).

W648 should be C-mannosylated, while the other sites should not. However, W288 is modified, while W645 and W648 are not, suggesting that this model is not accurate for the prediction of C-mannosylation on EBOV glycoproteins.

3.4 Functional Analysis of C-mannosylation Motifs in $GP_{1,2}$

Analysis of the consequences of altering the tryptophans involved in the C-mannosylation motifs of $GP_{1,2}$ was carried out concomitantly with mass spectrometry investigations. To determine the functional significance of these motifs, point mutants were generated by site-directed mutagenesis of the $GP_{1,2}$ sequence in the pDisplay vector and the glycoprotein cassette was subsequently sub cloned into the pCAGGS expression vector. The following constructs were used: wild-type (WT), W291A (tryptophan $(W)_{291}$ replaced with alanine), W648A, W651A, W648/651A and W644/645/648/651A. The constructs were used in a functional assay; specifically, the infectious virus-like particle (iVLP) assay, which allows the study of particle formation, budding, binding, entry and initial transcription (Figure 9). In addition, these constructs were also used to look for differences in expression, intracellular transport and incorporation of the glycoprotein into virus-like particles.

3.4.1 Expression of $GP_{1,2}$ mutants was not significantly different

To determine if expression of the glycoprotein was significantly affected by the introduction of point mutations at C-mannosylation sites, the various constructs were transfected into 293T cells and cell lysate was subjected to western blot (Figure 26). Expression levels were not identical; however, all constructs (WT, W291A, W648A, W651A, W648/651A, and W644/645/648/651A) were expressed at comparable levels.

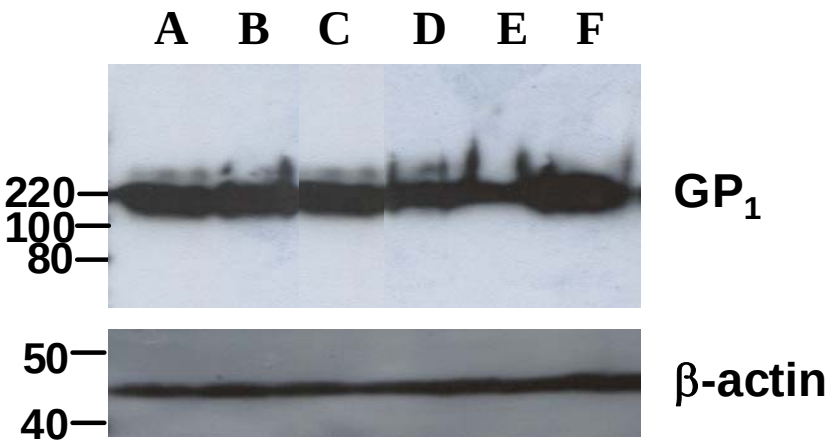

Figure 26. **Point mutations at C-mannosylation motifs do not significantly affect GP production.** Western blot of cell lysate using monoclonal antibody P_{130}2H11 (1/100 dilution) harvested at 72 hours post-transfection from 293T cells transfected with pCAGGS-$GP_{1,2}$ wild-type (A) or the following point mutants W291A (B), W648A (C), W651A (D), W648/651A (E) and W644/645/648/651A (F). The blot was stripped and subsequently probed for β-actin as a loading control with an anti-β-actin monoclonal antibody (1/1000 dilution).

3.4.2 Mutation of tryptophans in $GP_{1,2}$ alters reporter activity in an infectious virus-like particle assay

The infectious virus-like particle (iVLP) assay is a sensitive method to study various steps in the EBOV life cycle under BSL2 conditions. It makes use of a mini-genome containing a reporter gene (*Renilla* luciferase) in place of the full-length genome and in contrast to the mini-genome reporter systems (Boehmann et al., 2005; Groseth et al., 2005; Muhlberger et al., 1999) includes all structural EBOV proteins. This allows the formation of particles (iVLPs) that resemble EBOV virus particles but in place of the full-length infectious genome only contain the mini-genome (Hoenen et al., 2006b). These iVLPs can be used to infect naïve target cells, resulting in transcription of the reporter in these cells, reflecting the efficiency of assembly, binding, entry and initial transcription. Reporter activity is measured at two separate stages: p0, which is the cell lysate from the initial transfection of all components of the iVLP system and represents transcription and replication of the minigenome; and p1, which is the cell lysate from target cells infected with iVLPs and represents transcription of the reporter gene following entry. Values represent normalized reporter activity $^{+}/_{-}$ standard deviation with WT set to 100% activity. The data from all constructs was analyzed by one-way ANOVA and subsequently all constructs were compared to WT by two sample difference of means t test assuming unequal variance.

Reporter activity in p0 reflects minigenome replication and transcription. Single mutants W291A (112%), W648A (98%) and W651A (98%) had comparable levels of reporter activity to WT. Constructs with multiple mutations, W648/651A (74%) and W644/645/648/651A (63%), as well as the absence of GP (-GP) (46%) show a

statistically significant ($p<0.05$) decrease in reporter activity in p0 (Figure 27 A). The reporter activity in p1 reflects iVLP entry, delivery and initial transcription of the minigenome solely by the viral proteins transported in the iVLPs. In the absence of GP (-GP), there is essentially no reporter activity (0.30%) owing to a lack of the glycoprotein to facilitate entry into target cells. Surprisingly, W291A showed an increase in reporter activity (162%), which was statistically significant ($p = 0.0158$) and suggests either enhanced particle formation or entry. The single mutants of GP_2, W648A (78%) showed significantly decreased ($p = 0.0286$) reporter activity, while W651A (86%) was not statistically significant ($p = 0.0808$). The multiple mutants W648/651A (30%) and W644/645/648/651A (0.36%) had significantly decreased reporter activity ($p = 3.36e-6$ and 3.15e-5 respectively) (Figure 27 B). The activity of W644/645/648/651A is essentially comparable to that of the samples lacking GP (-GP).

3.4.3 Transport of mutant $GP_{1,2}$ to the surface is not affected

The iVLP assay indicated that there were differences in reporter activity for some of the $GP_{1,2}$ mutants; therefore, we sought to determine where this effect was occurring. To determine if expression and/or transport of the glycoprotein was affect by the indicated point mutations, cells transfected with the various point mutants were subjected to surface and internal glycoprotein immunofluorescence staining at various time points following transfection. These were analyzed by laser scanning confocal microscopy. Cells stained as early as 2 hours post-transfection were observed to have detectable intracellular staining; however, this was not detectable using the standardized laser intensity selected for analysis of the other time points (data not shown). The surface of the cells were live stained with anti-GP_1, fixed and then stained with AlexaFluor488

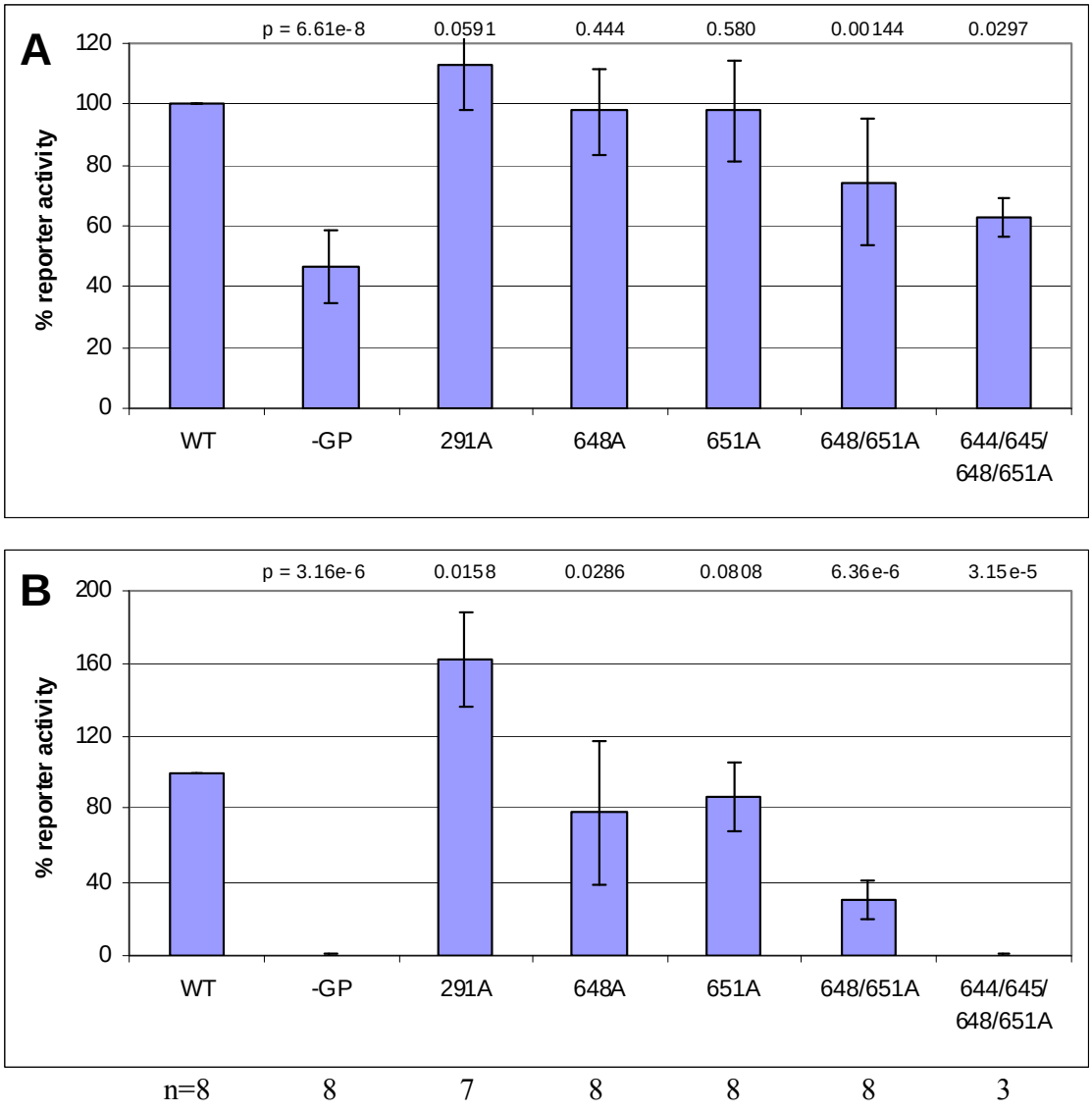

Figure 27. **Infectious virus-like particle assay with GP mutants.** Percent reporter (Luciferase) activity in p0 (A), reflects the initial replication and transcription of the minigenome following transfection. Transfer of the supernatant from p0 to naïve cells (B) results in reporter activity in p1 that reflects iVLP particle assembly, budding, binding, entry, uncoating and initial transcription events. Samples are normalized to WT (100%) for p0 and p1, respectively. Data was analyzed by one way ANOVA, which indicated significant difference between groups in p0 (5.03e-16) and in p1 (1.35e-17). The corresponding p values calculated from two sample difference of means t test are shown above the graph.

(green). Following permeabilization, the cells were stained again with anti-GP_1 followed by AlexaFluor594 (red). Cover slips were then mounted in AntiFade with DAPI (blue). This procedure stains the cell surface of GP-expressing cells green (with no evidence of uptake into the cell), intracellular GP red (red may also be present on the surface of the cell) and the nucleus blue.

At six hours post-transfection, intracellular accumulation of GP was evident throughout the cytoplasm, with some localized regions of higher signal (Figure 28 A). The level of GP expression and the localization in the cytoplasm was essentially equivalent between mutants. For all constructs, a range of expression was observed at this time point, with cells that showed lower intracellular levels and surface expression of GP. There were also a few cells that showed higher levels of expression both intracellularly and on the surface. The data shown here is representative of cells expressing intermediate levels of staining (the most frequently observed) from randomized fields of view. Mutant W219A appears to show the highest level of GP on its cell surface (Figure 28 A, upper middle). GP is clearly evident on the surface for all constructs; however, surface staining is mainly discontinuous with bright points indicating that the levels of GP on the surface are lower than at the 24 hour time point.

At 24 hours post-transfection, most cells expressing GP exhibit continuous green staining on the surface, indicating higher levels of GP on the cell surface than at 6 hours and comparable levels of intracellular GP (Figure 28 B). Again, there was cell-to-cell variation within a sample but there was no significant difference between the surface expression and the intracellular expression or localization between the different constructs. Isotype controls using an anti-MARV GP antibody show an absence of non-

Figure 28. **Analysis of the expression and localization of GP by laser scanning microscopy.** 293T cells transfected with pCAGGS-GP (or the indicated mutants) were live-stained either (A) 6 hours or (B) 24 hours post-transfection with anti-GP antibody, fixed and stained with anti-mouse IgG AlexaFluor488 (green). Following permeabilization, cells were stained again with anti-GP antibody and anti-mouse IgG AlexaFluor568 (red). Cover slips were then mounted in AntiFade gold with DAPI (blue) and imaged by laser scanning microscopy on a Zeiss LSM700 at 63x under oil-immersion. Imaged regions were randomly chosen and are representative of other fields of view. Standardized laser intensities and exposures were used for all samples (C) Antibody and permeabilization controls were performed on pCAGGS-GP wild-type transfected cells at 24 hours post-transfection.

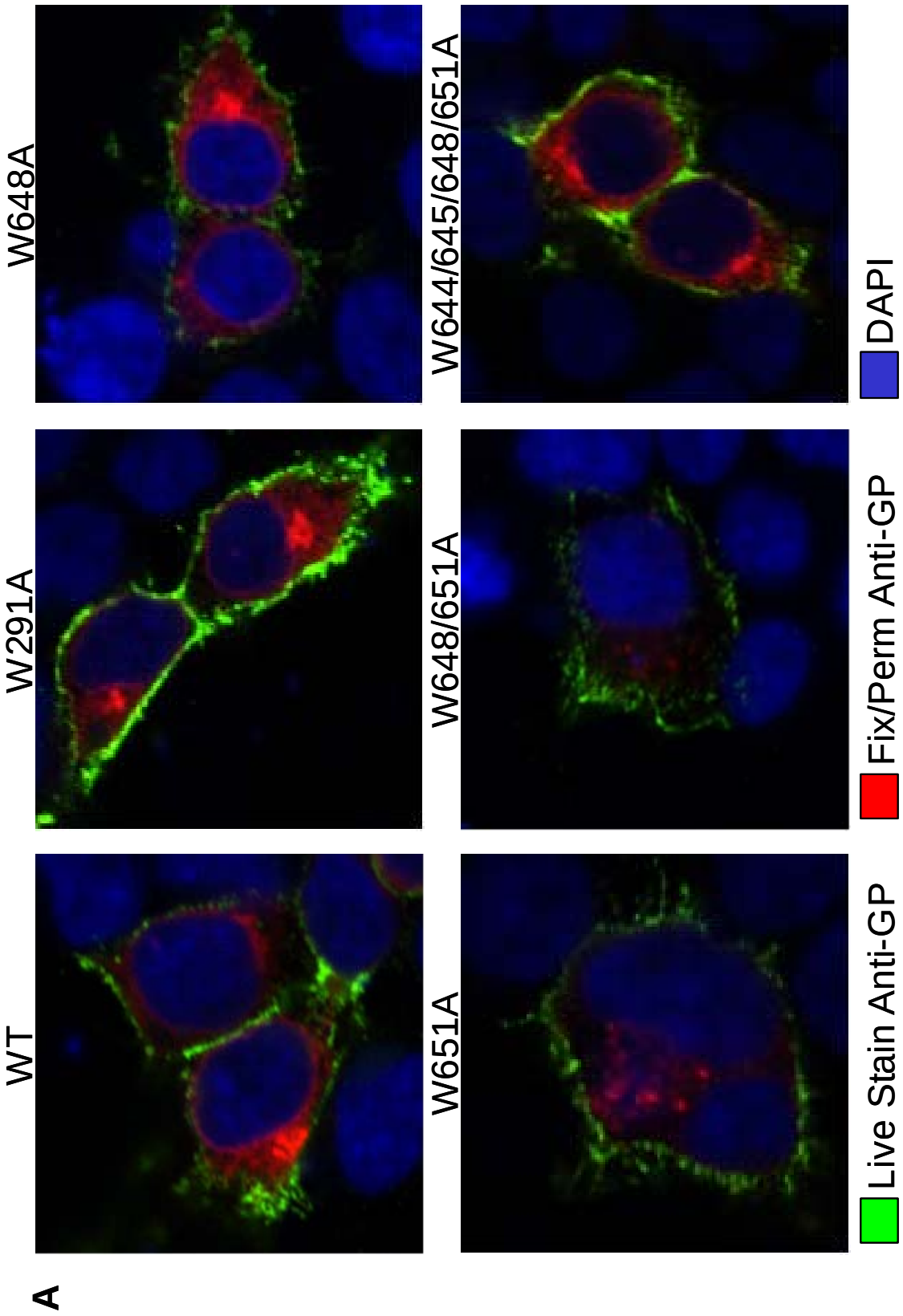
A
WT
W291A
W648A
W651A
W648/651A
W644/645/648/651A
Live Stain Anti-GP
Fix/Perm Anti-GP
DAPI

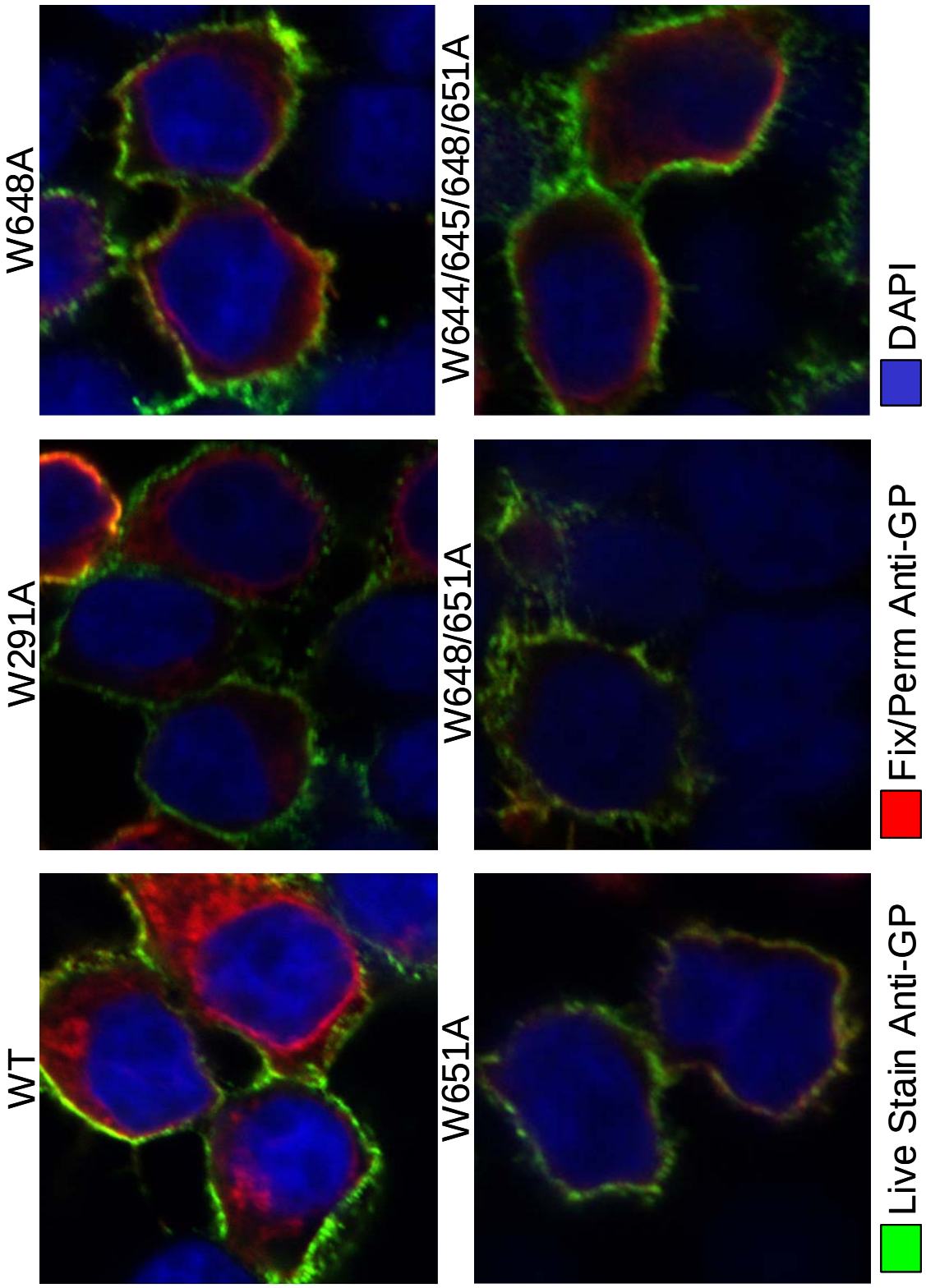
W648A
W644/645/648/651A
DAPI
W291A
W648/651A
Fix/Perm Anti-GP
WT
W651A
Live Stain Anti-GP
B

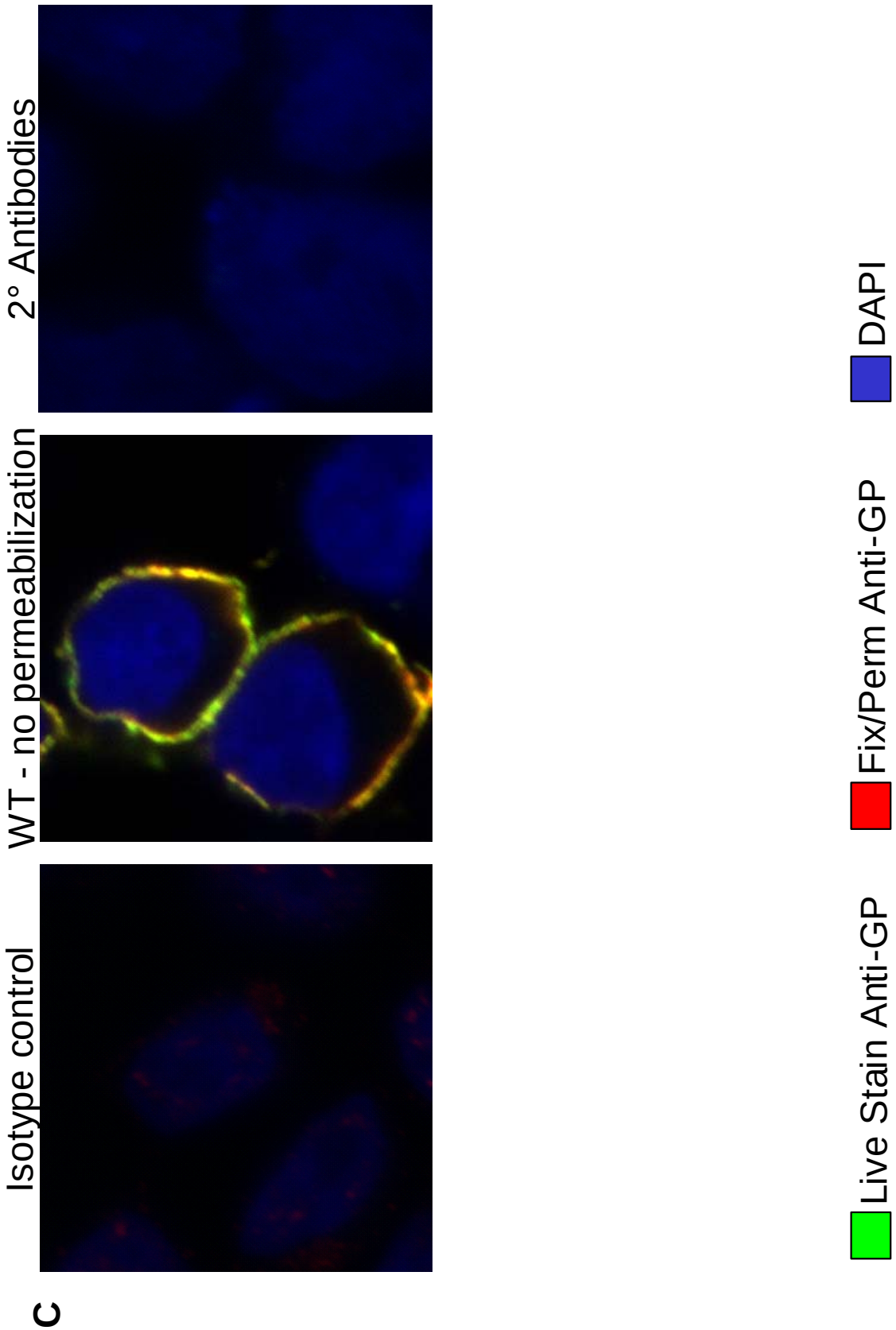
c
Isotype control
WT - no permeabilization
2° Antibodies
Live Stain Anti-GP
Fix/Perm Anti-GP
DAPI

specific background staining at the settings used for imaging (Figure 28 C). Cells that were not permeabilized do not show evidence of intracellular staining. Instead they show yellow staining on the cell surface as a result of co-localization of the red and green secondary antibodies.

3.4.4 Incorporation of tryptophan mutant $GP_{1,2}$ constructs

As differences in reporter activity in the iVLP assay could be due to alteration of GP incorporation during particle assembly and budding or from attachment and entry, iVLPs from the supernatant of p0 were analyzed for GP content in relation to VP40 (which is expected to be released from the cell at a consistent rate). In addition, the cell lysate from p0 was analyzed for GP content to determine the amount of intracellular GP present. iVLPs containing different mutant GPs purified from p0 supernatant showed similar levels of VP40 (Figure 29 C) by western blot between samples. Therefore, this protein was acceptable to use as a standard of comparison for GP incorporation into iVLPs. In contrast, the levels of incorporated GP were decreased for W291A and W648/651A, while almost absent for W644/645/648/651A (Figure 29 A). These blots were analyzed by densitometry to determine the ratio of GP:VP40. For WT, the ratio was 1.46, which is relatively similar to the values of W648A and W651A at 1.87 and 1.93, respectively (Figure 29 B). W291A and W648/651A have a decreased amount of GP relative to WT, with ratios of 0.76 and 1.07, respectively. W644/645/648/651A (with a ratio of 0.067), essentially does not incorporate GP into iVLPs. These two mutants also showed much higher levels of intracellular GP in the cell lysate of p0 (Figure 29 D) than the other constructs. This is in agreement with previous data (Figure 26), suggesting that expression of the constructs is not hampered by the mutations. In the cell lysate WT,

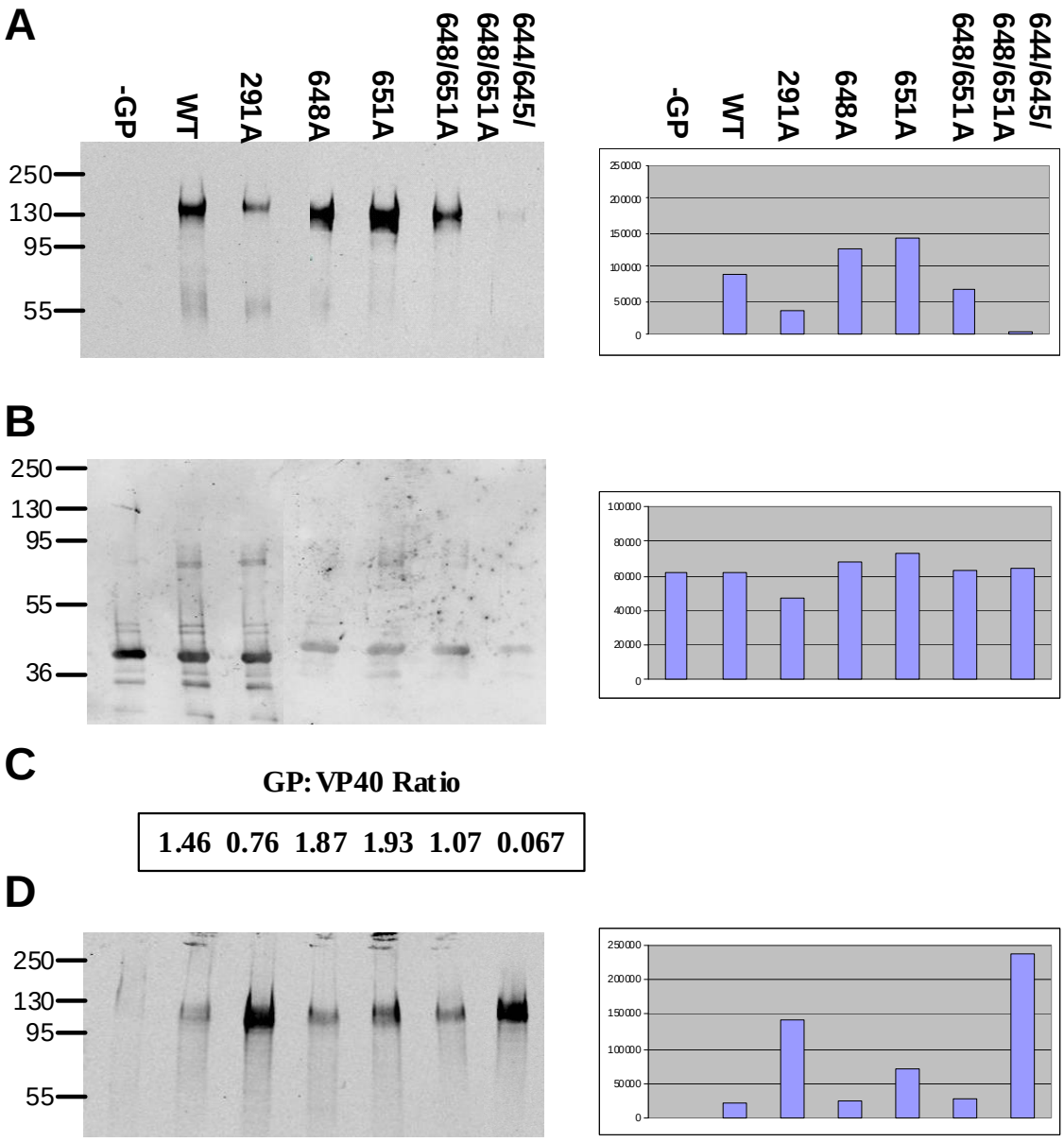

Figure 29. **Incorporation of GP into iVLPs is altered by specific tryptophan mutations.** To determine the relative amount of $GP_{1,2}$ incorporated into virus particles, purified iVLPs (from p0) were subjected to western blot with (A) anti-GP_1 monoclonal antibody 1G12 (1/5000 dilution) and (B) guinea pig anti-VP40 (1/1000 dilution). Densitometry (right column) was used to determine (C) the ratio of GP:VP40. Lysates from the cells used to produce the iVLPs were also collected to determine the intracellular quantity of $GP_{1,2}$.

W648A, W648/651A have essentially the same level of intracellular GP, while W651A is somewhat increased but not nearly to the extent of the other mutants, which show considerable accumulation.

4. DISCUSSION

4.1 Structural Analysis of sGP

4.1.1 Orientation of the sGP homodimer

Prior to this study, it was accepted that sGP is secreted as a homodimer; however, the actual orientation of the two molecules within the homodimer was not clearly established. Therefore, the first step was to conclusively determine the orientation of the sGP homodimer, either parallel or anti-parallel, to resolve inconsistent data presented in the literature (Barrientos et al., 2004; Volchkova et al., 1998). sGP has been observed to have an anti-inflammatory effect on endothelial cells (Wahl-Jensen et al., 2005b). This effect has been proposed to inhibit leukocyte recruitment to infected parenchymal cells, a lack of which is noted during EBOV infection *in vivo*. One of the proposed mechanisms by which this would occur is by interfering with extravisation. This would place sGP in an important role as a contributor to EBOV immunopathology. In the absence of a mechanism for sGP function and the technical difficulties in demonstrating interference with leukocyte recruitment, determining the structure of sGP and linking the importance of this structure to endothelial barrier function rescue was sought to further progress the hypothesis that sGP modulates endothelial barrier function under inflammatory conditions through interactions that are structure specific. To determine sGP structure, a combination of site-directed mutagenesis and disulphide bond mapping with off-line HPLC-MALDI-TOF MS (MS/MS) was performed to determine the native structure of ZEBOV sGP, its glycosylation status and the presence of any additional post-translational modifications.

For these studies, sGP was produced in a mammalian cell-based recombinant expression system and constructs with cysteine to glycine mutations at C53 and C306 were generated. Under reducing and non-reducing SDS-PAGE, sGP migrated at different apparent molecular weights, corresponding to the monomer (approx. 50 kDa) and dimer (approx. 100 kDa), respectively (Figure 11 A). In contrast to previous data where only C53G was observed to form dimers (Volchkova et al., 1998), the two single cysteine mutants (C53G and C306G) were expressed mainly as dimers under non-reducing conditions (Figure 11 A). This alone suggests a parallel orientation, as single mutations in an anti-parallel orientated dimer should be sufficient to negate dimer formations. It may also suggest that alternative disulphide linkages are possible in the absence of the natural linkages. Only the double mutant C53/306G (lacking both cysteine residues at positions 53 and 306) was unable to form dimers (Figure 11 A, right panel), thereby confirming that these two positions are the only cysteines involved in intermolecular disulphide bonds. The difference in the ratio of monomer to dimer between C53G and C306G (Figure 11 A, right panel) suggests that the cysteine residue at position 306 is more important in the initial dimerization process, as indicated previously (Volchkova et al., 1998). Compared to sGP dimers, the faster migration of C53G and C306G on non-reducing SDS-PAGE, was unexpected (Figure 11 A, right panel). It is possible that the remaining intermolecular disulphide bond in either mutant mediated a different quaternary structure in these proteins, resulting in differential migration through the gel. A small difference in MW is also noticeable between the single mutants, which may also be attributed to a difference in quaternary structure. Supporting this hypothesis is the observation that under reducing conditions, all sGP and cysteine mutants migrate at near

identical apparent MWs (Figure 11 A, left panel), indicating the shift is not the result of some confounding factor caused by alteration of the amino acid residues at these sites.

To carry out disulphide bond mapping and post-translation modification analysis by mass spectrometry, it was necessary to identify nearly all tryptic peptides; or as a minimum, at least all peptides involved in disulphide bonding and all peptides that were potentially glycosylated. By HPLC-MALDI-TOF MS, with and without PNGaseF treatment, peptides covering 98.9% of the protein sequence were identified (Figure 11 B, Table 1). All cysteine-containing peptides were included, as well as those with potential glycosylation sites. Only peptides T32 and T33 (Figure 11 B, Table 1) were not identified. These make up the three C-terminal amino acids, consisting of VR and R, respectively and as a result of their low mass, they cannot be detected by this analysis. As they are not involved in disulphide bonding or predicted to contain any co- or post-translational modifications, the sequence coverage was considered to be sufficient for further analysis using the experimental setup tested.

To assign disulphide bonds, the masses of non-reduced digests (containing intact disulphide bonds) were compared to those of reduced digests as previously described (Gorman, Wallis, and Pitt, 2002). Peaks in the non-reduced sGP digest were submitted to the search algorithm for disulphide bond assignment (Craig et al., 2003). To confirm these linkages, higher mass disulphide-carrying candidates must disappear following reduction, while new lower mass fragments should appear, corresponding to the peptides with free cysteine. MS/MS of the non-reduced sample was also used to further confirm the presence of the expected amino acid sequence as well as the characteristic triplet from the breakage of the disulphide bond. The triplet is the result of 0, 1 or 2 sulphide residues

remaining on the peptide following breakage of the disulphide bond during CID. Figure 12 shows a region of the spectra with the intact (Figure 12 A) and reduced (Figure 12 B) disulphide 53-53' linked fragment (two identical peptides 51-54 LVCR, calculated m/z 977.538). In the non-reduced sample, a peak is present at m/z 977.541, which disappears following reduction. Other sGP peptides not involved in disulphide bonding remain present (m/z 918.500 and 922.534). The presence of 51-54 LVCR was further confirmed by MS/MS, where y1 and b2 ions (corresponding to the correct sequence) were identified as well as the characteristic triplet, which is indicative of disulphide bond breakage (Figure 12 C). This indicates that C53 binds to the C53 (designated C53') of another sGP molecule. Combined with the SDS-PAGE, this data supports a parallel orientation; however, additional data confirming a C306-C306' disulphide bond is also present. Figure 13 shows a region of the spectra with the intact (Figure 13 A) and reduced (Figure 13 B) disulphide 306-306' linked fragment (two identical peptides 305-316 SCLSQLYQTEPK, calculated m/z 2789.324). In the non-reduced sample, a peak is present at m/z 2790.331, which disappears following reduction; other peaks on the spectra remain present. The presence of 305-316 SCLSQLYQTEPK is further confirmed by MS/MS, where a y ion series was identified (corresponding to the correct sequence) as well as the characteristic triplet, which is indicative of disulphide bond breakage (Figure 13 C). This indicates that C306 is disulphide linked to C306 of another sGP molecule.

Data from the cysteine mutants and disulphide bond mapping provide conclusive evidence the sGP homodimer consists of two parallel-oriented sGP molecules bound by disulphide bonds between C53-C53' and C306-C306' (Figure 17) (Falzarano et al., 2006). In addition, intramolecular disulphide bonds 108-135 and 121-147 were identified

as previously described (Table 2) (Jeffers, Sanders, and Sanchez, 2002). Several low abundance, alternative disulphide bonds were also identified corresponding to 108-147, 108-121, 108-306; however, there was no evidence of 53-306' linkage (data not shown). This most likely corresponds to sGP molecules that are improperly folded and were not targeted for degradation during their maturation process. The data presented above was also confirmed by disulphide bond mapping on gel-fractionated samples under non-reducing conditions, where three disulphide-linked fragments (108-135, 121-147, 306-306') were recovered. Taken together, this data supports the unequivocal assignment of a parallel orientation to the sGP dimer (Figure 17).

4.1.2 Identification of co- and post-translational modifications

In addition to the data on disulphide linkages, HPLC-MALDI MS analysis of native sGP tryptic digests provided information on masses as well as the composition of sugar moieties. Glycopeptides were identified by their specific m/z spacing patterns (i.e. 162, 203, 291 Da corresponding to the mass of hexose (mannose/galactose), HexNAc (GlcNAc/GalNAc) or sialic acid respectively) between glycoforms and then analysed by MS/MS, as previously described (Krokhin et al., 2004). Analysis of the resultant sugar masses to GlycoMod (www.expasy.org) indicated that all N-glycosylated sites on sGP contained complex N-glycans. MS/MS of deglycosylated peptides allowed for the unequivocal assignment of all glycosylation sites. There are 6 predicted N-glycosylation sites in sGP; however, only 5 were consistently glycosylated (N40, N204, N228, N257, N268) with the remaining site (N238) being glycosylated infrequently (Figure 17). MS/MS data was also collected and analyzed to determine sugar composition. Unfortunately, a large number of possible compositions and branching patterns were

predicted (data not shown) making it difficult to determine the sugar structures. Subsequently, the predicted sugar structures were described using sGP that was produced during ZEBOV infection, with considerable micro-heterogeneity being noted (Barrientos et al., 2007). In contrast to our results, this data indicates that N238 is fully glycosylated. This minor difference is likely attributed to the expression and/or the cell systems used, suggesting that recombinant over-expression leads to incomplete N-glycosylation, presumably due to unfavourable conditions (i.e. decreased access) at the N238 site.

sGP was also analyzed to determine whether it contained O-linked glycans. However, since all peptides were represented after treatment with PNGaseF (which does not remove O-linked glycans) it is unlikely that any of the predicted O-glycosylation sites are modified. Furthermore, all non-assigned peaks of high intensity or those from clusters containing characteristic glycopeptide spacing from original HPLC-MS peptide mass fingerprints (PMF) of native sGP digests were subjected to MS/MS analysis to find any O-glycosylated species. Negative outcomes from these attempts suggest that sGP does not contain any O-glycans, a finding supported by others using recombinant sGP (Volchkova, Klenk, and Volchkov, 1999) and sGP purified from infected cells (Barrientos et al., 2007). This is surprising, as the other glycoprotein products (Δ-peptide, $GP_{1,2}$, GP_1 and $GP_{1,2\Delta TM}$) all contain O-linked glycans (Feldmann et al., 1994; Feldmann et al., 2001; Volchkov et al., 1998a; Volchkova, Klenk, and Volchkov, 1999).

This analysis also noted that C-mannosylation, a novel type of glycosylation, appeared to be present. Prior to this finding, this modification has not been described for any viral protein. C-mannosylation involves the covalent attachment of an α-mannopyranosyl residue to the indole C2 carbon atom of a tryptophan via a C–C link

(Figure 16 C) (de Beer et al., 1995; Hofsteenge et al., 1994). This post-translation modification is observed infrequently and its function is not well-described; however, it has been implicated in playing a role in protein folding and/or trafficking (Furmanek and Hofsteenge, 2000). sGP was found to possess a C-mannose on tryptophan (Trp) residue 288 (W_{288}) during complete peptide mapping. While the expected masses were observed for T26 and T26T27 (2136.028 and 2264.112, respectively), these peptides produced relatively low signal compared to two peaks that were shifted by 162.05 Da (Figure 15 A). A search of the post-translation modification database indicated that a +162 Da mass shift was indicative of C-mannosylation and that this modification occurs at the motif W-X-X-W, which was present on these peptides. This shift occurred on both peptides; therefore, it appeared that these peptides are actually modified even though this modification has not been described for viral proteins. Data from MS/MS analysis was consistent with C-mannosylation. The y ion series included a mass shift at y7 (W_{288}) of +162 Da, with all subsequent y ions also shifted (Figure 15 C). A -120 Da loss from the parent peptide, which occurs as the result of the stability of the C-C bond (Figure 16 C), and the absence of a -162 Da loss that is characteristic of N- and O-linked sugars (Furmanek and Hofsteenge, 2000), also provides evidence for C-mannosylation during MS/MS.

4.1.3 Confirmation of C-mannosylation of sGP

As this was the first identification of C-mannosylation on a viral protein we sought to provide additional evidence that this modification occurred in multiple cell lines and during ZEBOV infection. The second tryptophan in the C-mannosylation motif of sGP was mutated to alanine by site-directed mutagenesis, which has been previously

described to prevent this modification (Krieg et al., 1998). MS analysis of this mutant (sGP-WXXA) did not reveal a +162Da mass shift in the peptides (Figure 15 B) that would contain the C-mannose residue. This suggests that the wild-type sequence of sGP is C-mannosylated, confirming that this is not an artefact generated during purification and processing of the protein for MS.

Purified sGP expressed by transient transfection of Huh7 and Vero E6 cells was also observed to be C-mannosylated by MS (Figure 19 A, B), which yielded similar spectra to that of 293T cells (Figure 15 A). This was not unexpected, as others have reported that C-mannosylation occurs in multiple tissue types (Doucey et al., 1998; Furmanek and Hofsteenge, 2000; Krieg et al., 1997). sGP purified from the supernatant of ZEBOV-infected Vero E6 cells was also observed to be C-mannosylated (Figure 19 C); however, in contrast to recombinant expressed sGP, it appeared that all peptides were modified. The presence of unmodified peptides from transfected cells is likely a result of high levels of protein expression, which saturates the components that are responsible for this modification. This is also likely to be the basis for incomplete N-glycosylation of N228 in recombinant-expressed sGP (Falzarano et al., 2006), whereas sGP produced during virus infection was fully glycosylated (Barrientos et al., 2007). Incomplete, or altered glycosylation, has been identified during recombinant MARV GP expression (Becker, Klenk, and Muhlberger, 1996), where increased expression results in decreased glycosylation.

The discovery of C-mannosylation in a viral protein is of considerable interest as many post-translational modifications are essential for the function and/or regulation of a given protein. Taken together, the data described above provide substantial evidence for

the presence of this infrequently described modification on ZEBOV sGP, which also occurs during virus infection. Moreover, this modification has been described infrequently and a clear functional role has yet to be determined. C-mannosylation of tryptophan residues was first described for Trp_7 of human RNase2 from human urine (de Beer et al., 1995; Hofsteenge et al., 1994). Using mass spectrometry, a specific tryptophan-bearing peptide showed a molecular mass that was 162 Da higher than expected, which was subsequently confirmed with ^{1}H and ^{13}C NMR (Loffler et al., 1996). This was a novel finding, as all previously observed carbohydrates were attached to the amino acid side chain of asparagine, serine or threonine, via either an N- or an O-glycosidic bond. Since then, C-mannosylation has been shown to be part of the normal biosynthetic pathway in *Caenorhabditis elegans*, insects, amphibians, birds and mammals; however, it does not appear to occur in plant, yeast or bacterial cells (Doucey et al., 1998; Krieg et al., 1997; Munte et al., 2008). At least 69 occurrences of C-mannosylation have been experimentally confirmed on cellular proteins (Julenius, 2007), with a number of these proteins having multiple C-mannosylated tryptophan residues (Table 4). This modification tends to occur predominantly on either secreted or membrane proteins (Perez-Vilar, Randell, and Boucher, 2004) that serve a wide variety of functions, including extracellular matrix proteins, axonal guidance proteins, proteins involved in angiogenesis, metalloproteases and immune modulators.

Table 4. Cellular proteins characterized as containing C-mannosylated tryptophans. The number of confirmed C-mannosylation sites is indicated as well as the potential function of this modification.

Protein	(C^2-Man)Trp sites	Proposed role for (C^2-Man)Trp	Reference
Carausius morosus hypertrehalosaemic factor ii	1	unknown	(Gade et al., 1992; Munte et al., 2008)
RNase2	1	protein folding (presumed)	(Hofsteenge et al., 1994)
ribonuclease-2	1	unknown	(Hofsteenge et al., 1994)
IL-12	1		(Doucey et al., 1999)
C6	6		(Hofsteenge et al., 1999)
C7	4		
C8α	4		
C8β	4		
C9	2		
properdin	14		(Hartmann and Hofsteenge, 2000)
thrombospondin-1	4		(Hofsteenge et al., 2001)
F-spondin	8		(Gonzalez de Peredo et al., 2002)
erythropoietin receptor	1		(Furmanek et al., 2003)
MUC5AC	1	- protein folding (presumed)	(Perez-Vilar, Randell, and Boucher, 2004)
MUC5B	1		
ADAMTS-like 1/punctin-1	2	- deletion leads to ER accumulation and decreased secretion	(Wang et al., 2009)
ADAMTS5	1		
MP20	2	- interaction with galactin-3 - deletion leads to ER accumulation and decreased secretion	(Ervin et al., 2005)
mindin	1	interaction with LPS	(Li et al., 2009)

4.2 Functional Analysis of sGP on Endothelial Barrier Function

4.2.1 Effect of sGP on endothelial barrier function

Previous data has indicated that sGP mediates an accelerated recovery of the trans-endothelial resistance (TER) following treatment of endothelial cells with TNF-α. By itself, sGP does not appear to affect barrier function or activation of endothelial cells (Wahl-Jensen et al., 2005b). These data were collected on endothelial cells under static (i.e. no shear stress) conditions; however, endothelial cells are typically subjected to shear stress as well as tensile hoop strain (as a result of cyclic stretching and contraction of vessel walls) *in vivo*, effectively altering their adhesion molecule expression and morphology (Breen, McHugh, and Murphy, 2009). sGP (or cysteine mutants) treatment of endothelial cells exposed to shear stress 30 minutes following treatment, did not alter the shear stress-induced changes in TER, nor did it alter the TER of cells that were not exposed to shear stress (Figure 20). Following the application of shear stress, a typical pattern of TER alterations initiates between 2 and 4 minutes following the onset of shear stress (between 2 and 50 dyn/cm^2) and reaches a transient maximum at approximately 10 minutes (Seebach et al., 2000). This is followed by a slow decrease in the TER which eventually stabilizes some hours later. Cells that are exposed to 0.5 dyn/cm^2 of force or less have no significant alterations in TER (Seebach et al., 2000). Therefore, the morphological and physiological alterations to endothelial cells during the establishment of barrier function are unaffected by sGP (or the cysteine mutants).

Endothelial cells are believed to be a late site of virus replication (Geisbert et al., 2003d). While it is likely that sGP is produced in these cells, this has not been proven experimentally. Endogenous expression of sGP from a non-replicating Lentivirus vector

did not significantly affect the establishment of barrier function (Figure 21 A). Therefore, under both static and shear stress conditions, long-term endothelial barrier function establishment and maintenance is not affected by either endogenous or exogenous sGP. While the characteristic rapid increase and decrease in TER, was notably absent in sGP-expressing cells, the mechanism behind these rapid changes during the initial exposure to shear stress has yet to be investigated as technical limitations currently prevent further study. It is expected that signalling events (i.e. phosphorylation) and changes in protein-protein interactions are responsible for these rapid alterations in barrier function. The removal of shear stress almost immediately results in the reversion of these TER alterations at these early time points, such that sample collection will be difficult to achieve.

sGP had been observed to rescue endothelial barrier function following treatment with TNF-α under static conditions (Wahl-Jensen et al., 2005b); therefore, the significance of this effect under shear stress conditions was also investigated. The combination of sGP and TNF-α treatment of endothelial cells subjected to shear stress is similar to that of cells subjected to shear stress alone, while that of cells subjected to TNF-α treatment and shear stress (but not sGP) leads to a lower mean TER by approximately 300 minutes. This suggests that sGP still provides a protective effect from TNF-α treatment under shear stress as well as static conditions. It is likely that the decreased protective effect of sGP under shear stress is actually the result of the endothelial cells (under shear stress) being less responsive to TNF-α than endothelial cells under static conditions (Bergh et al., 2009; Cicha et al., 2009).

Taken together, this data suggests that sGP could directly interact with TNF-α or its receptors (TNFR1 and TNFR2) to attenuate the decrease in barrier function on endothelial cells. Alternatively, sGP may activate signalling pathways that are relevant during exposure to TNF-α but not under non-inflammatory conditions (see Figure 30 for a proposed model for the anti-inflammatory effect of sGP). Attempts to show a direct interaction with either TNF-α or its receptors by co-immunoprecipitation were hampered by poor reactivity of commercial antibodies with purified recombinant TNF-α and its receptors. In addition, previous work failed to show a direct interaction between sGP and TNF-α (Schnittler, H., personal communication). While sGP appears to attenuate the effect of the pro-inflammatory cytokine TNF-α *in vitro* under static and shear stress conditions, the relevance of this finding *in vivo* remains unknown. In order to elucidate the breadth of the protective effect of sGP and whether this anti-inflammatory effect is likely to occur *in vivo* it would be useful to determine if other pro-inflammatory cytokines (e.g. IL-1α/β, IL-6, IL-8, IL-12, IP-10, MCP-1, and RANTES), alone or in combination, could also induce changes in TER that can be attenuated by sGP or whether this is specific to TNF-α. It would also be important to determine the effect of sGP on endothelial cells that have fully adapted to shear stress and established a stable TER, as this would more accurately reflect conditions *in vivo*. At the time this was not possible, as this experimental setup requires extended monitoring of TER (up to 72 hours) with continuous media exchange. While technically possible, this was not available at the time experiments were carried out.

During EBOV infection, there are numerous factors present in the bloodstream, such as those produced by activated monocytes/macrophages (Feldmann et al., 2003).

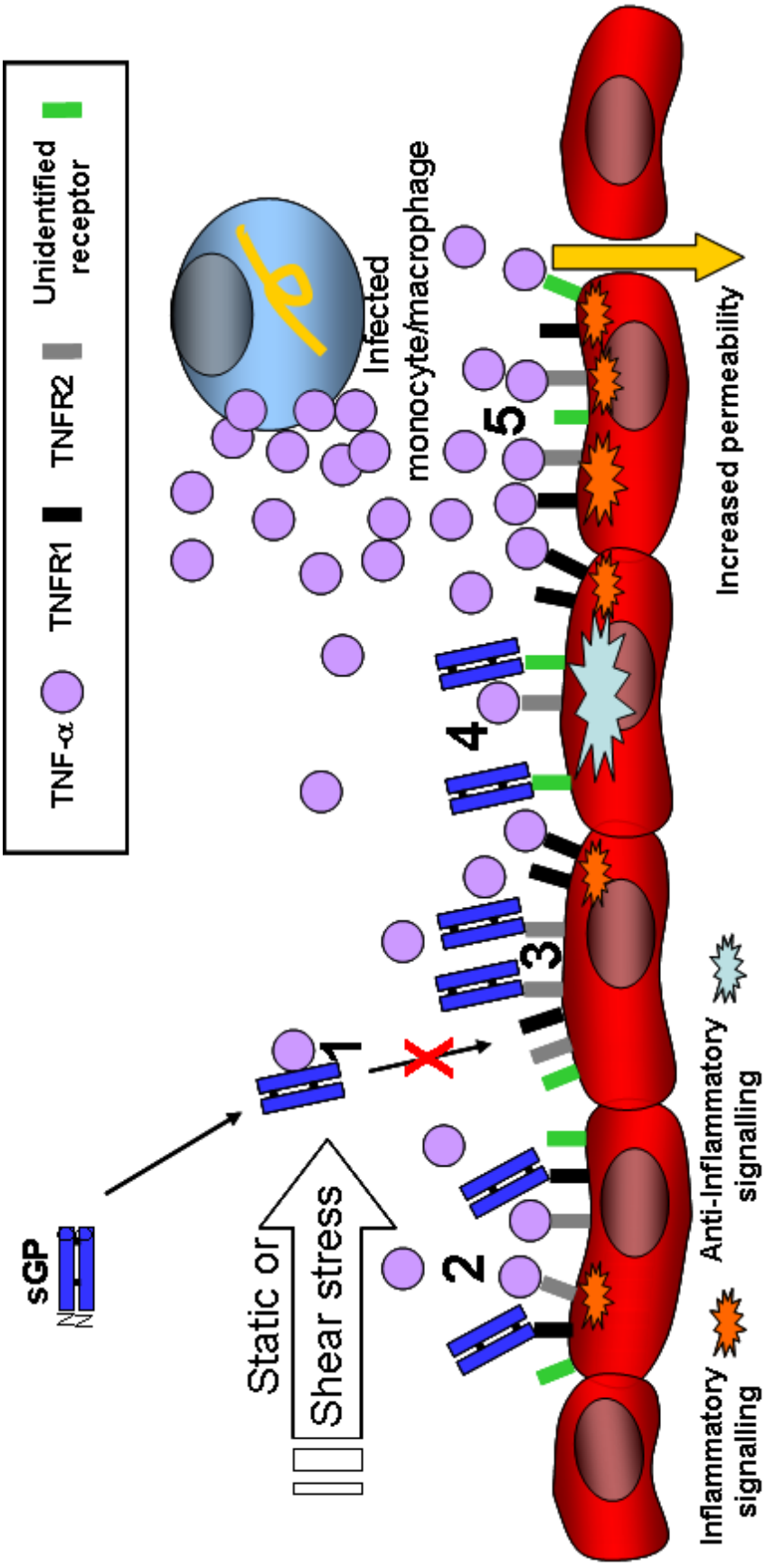

Figure 30. **Proposed model for the anti-inflammatory effect of sGP on endothelial cells.** During EBOV infection, infected cells (e.g. monocytes/macrophages) secrete inflammatory cytokines, such as TNF-α. sGP rescues endothelial barrier function, in a structure-dependent manner, under static and shear stress conditions following TNF-α treatment by interacting either with: TNF-α to prevent or decrease its interaction with its receptors (1); TNFR1 (2) or TNFR2 (3) to prevent their interaction with TNF-α; or an unidentified receptor that results in signalling that reverses the effect of TNF-α (4). Treatment of endothelial cells with TNF-α alone results in a permanent decrease in barrier function with a subsequent increase in paracellular permeability (5).

These factors likely play a key role in the alterations of the endothelium observed during infection; therefore, it would be valuable to determine the effect of plasma or serum from infected animals, which contain a mix of pro-inflammatory cytokines. It have also been hypothesized that the anti-inflammatory effect of sGP could prevent extravisation of immune cells to sites of infection (Wahl-Jensen et al., 2005b), a theory that has yet to be experimentally tested, but is supported by a lack of infiltration of immune cells to necrotic areas of infection (Ryabchikova, Kolesnikova, and Luchko, 1999; Ryabchikova, Kolesnikova, and Netesov, 1999; Zaki and Goldsmith, 1999).

Table 5. Summary of the effect of sGP on TER in the presence or absence of TNF-α and static or shear stress conditions. [1]steady state – absence of rapid changes in TER over time, [2]rescue effect – a reversal of the TNF-α-induced decrease in TER, [3]normal shear effect – includes the immediate-early rapid changes in TER and a continuous decrease in TER over time

Treatment		**Shear stress**	**Effect on TER**
-	TNF-α	Static (0 or 0.2 dyn/cm^2)	Long-term decrease
sGP	-		Steady state[1]
sGP	TNF-α		Rescue effect[2]
sGP - endogenous	-		Steady state
-	TNF-α	Shear stress (12 dyn/cm^2)	Attenuated long-term decrease
sGP	-		Normal shear effect[3]
sGP	TNF-α		Attenuated rescue effect
sGP - endogenous	-		Altered immediate-early effect

4.2.2 sGP intermolecular disulphide bonds are important for its anti-inflammatory effect

While a definitive function for sGP is still lacking, it has been proposed that it acts as an anti-inflammatory mediator of endothelial cells. An assay has been established for this anti-inflammatory role; therefore, to provide further evidence that this is a specific effect, it was necessary to determine whether the structure of sGP was related to its function in this assay. As a mechanism for the anti-inflammatory effect of sGP has yet to be established, demonstrating the importance of sGP structure allows the assumption that specific interactions lead to this effect, providing further validation that sGP specifically rescues endothelial barrier function. Protein function should be structure-dependent; therefore, impedance spectroscopy was used to determine whether the cysteine mutants (with different structural features (Figure 11 A)) would demonstrate the same protective effect on endothelial cells treated with TNF-α as sGP-WT. To carry out analysis, confluent endothelial cells were cultured onto electrodes and treated with TNF-α with and without sGP (or the indicated cysteine mutant). As previously described (Wahl-Jensen et al., 2005b), simultaneous administration of sGP and TNF-α resulted in an accelerated recovery of the TER (Figure 22). In contrast, all mutants (C53G homodimer, C306G homodimer and C53/306G monomer) were impaired in their ability to reverse the TNF-α-mediated TER decrease of endothelial monolayers (Figure 22). This data clearly demonstrates that a correctly folded parallel homodimer is essential for this function of sGP.

The observation that a specific homodimeric structure is critical for the potential anti-inflammatory role of sGP is of considerable interest as it furthers the hypothesis that sGP specifically modulates endothelial barrier function with the possibility that sGP is

directly responsible for the lack of leukocyte infiltration into sites of virus replication. If this hypothesis is proven this could explain one of the major immunopathological mechanisms of disease and widespread virus replication. As shown previously, mutation of the four cysteine residues involved in intramolecular disulphide bond formation of EBOV sGP (cysteine residues 108, 121, 135, and 147) (Figure 17) resulted in protein aggregation and block of transport (Volchkova et al., 1998). Similarly, cysteine mutants of oligomeric viral glycoproteins, such as the non-structural protein NS1 of dengue virus, the hemagglutinin of influenza and the glycoprotein G of vesicular stomatitis virus resulted in misfolding, aggregation and eventual degradation (de Silva, Balch, and Helenius, 1990; Pryor and Wright, 1993; Segal et al., 1992). In contrast, mutations of the cysteine residues at position C53 and C306, which result in either monomeric or altered homodimeric sGP molecules, did not affect the biosynthesis and transport of these proteins. Instead, their function in the endothelial barrier function rescue assay was impaired (Falzarano et al., 2006). Impaired function due to the alteration of cysteines that participate in intermolecular bonds has also been demonstrated for the spike glycoprotein GP2b of Equine arteritis virus (Wieringa et al., 2003), the biological action of the pNR-2/pS2 single domain trefoil protein (Chadwick, Westley, and May, 1997), interaction between the lymphatic hyaluronan receptor Lyve-1 and hyaluronan (Banerji et al., 2009) and a naturally occurring SNP (C196R) that results in the inability of cysteine-rich secretory protein 2 (CRISP2) to bind to gametogenetin 1 (GGN1) (Jamsai et al., 2008).

The significance of the protective effect of sGP on the endothelium *in vivo* has yet to be determined and the mechanism by which it occurs is currently unknown. During EBOV infection, a lack of leukocyte infiltration into areas of focal tissue destruction has

been described, although neutrophil aggregation within the vascular system seems to be unaffected (Ryabchikova, Kolesnikova, and Luchko, 1999; Ryabchikova, Kolesnikova, and Netesov, 1999). This indicates proper activation of the endothelium, with subsequent recruitment of neutrophils; however, the transmigration process is impaired, a phenomenon that may be related to the action of sGP. Pro-inflammatory cytokines such as TNF-α, are important factors in establishing antiviral responses to infection. As a consequence, many viruses (in particular the large DNA viruses) have evolved mechanisms to counteract early host responses by encoding immunomodulating proteins that inhibit or modify antiviral activities of pro-inflammatory cytokines (Alcami and Koszinowski, 2000; Seet et al., 2003). It remains to be seen if this could also be the case for EBOV through expression of sGP, which may interfere either with TNF-α directly or with components of the TNF signalling pathway.

4.2.3 C-mannosylation of sGP is not essential for barrier function rescue

A role for C-mannosylation in protein function is currently unclear. It appears that for RNase2 as well as the six polypeptides from the complement system, the hydrophilic mannosyl residue fills a cavity formed by the main and side chain atoms of a loop on an exposed region of the protein thus playing a structural role (Loffler et al., 1996; Mosimann et al., 1996; Vliegenthart and Casset, 1998). The modified Trp residues are likely to occur on the surface of the protein, which is consistent with the position of Trp-7 in RNase 2 (Mosimann *et al.,* 1996). Earlier studies have identified that mutagenesis of either of the tryptophan residues in the WXXW motif abolishes binding of the ligand for the IL-2 receptor (Miyazaki et al., 1991); however, it is unclear whether the lack of binding is caused by a direct change at the ligand-binding site, or if fewer receptors are

transported to the cell surface (Hilton et al., 1996). C-mannosylation of MUC5AC and MUCB is necessary for proper domain folding, ER export (possibly related to proper folding) and interaction with lectins (Perez-Vilar, Randell, and Boucher, 2004). These findings allow for C-mannosylation to potentially play a role in either ligand binding, folding or directing transport of membrane proteins.

As C-mannosylation has been associated with proper protein folding, transport and function, this modification was eliminated from sGP to determine whether biosynthesis, transport, secretion, and function would be affected. The quantity of sGP-WXXA obtained from expression and purification was comparable to the wild-type protein, indicating that protein expression and secretion (and therefore transport) of sGP was not dependent on C-mannosylation. This is in contrast to bovine lens protein MP40 (and other C-mannosylated cellular proteins), which contains two C-mannosylation sites that appear to be necessary for efficient transport of this protein to the cell surface as well as its interaction with galactin-3 (Ervin et al., 2005).

The elimination of the C-mannosylation site appears to result in a change in structure, at least at the epitope, as monoclonal antibody Z42/3.7 did not detect sGP-WXXA. The sGP-induced rescue of the permeability increasing effect of TNF-α on endothelial cells (Wahl-Jensen et al., 2005b) was demonstrated to be dependent on sGP structure (Falzarano et al., 2006), thereby providing a functional assay that could be used to assess the effect of eliminating the C-mannosylation site. The sGP-WXXA mutant had a comparable ability to rescue barrier function and therefore did not affect its anti-inflammatory function. However, the potential anti-inflammatory effect of sGP (Wahl-Jensen et al., 2005b) may not be its sole function.

Others have suggested that sGP may play a role in immune evasion by acting as a decoy molecule for EBOV humoral immune responses (Dolnik et al., 2004; Feldmann et al., 2003; Ito et al., 2001). Alternatively, sGP may bind neutrophils, subsequently inhibiting their activation (Kindzelskii et al., 2000; Yang et al., 1998), a concept that has been challenged (Maruyama et al., 1998a; Sui and Marasco, 2002). Unfortunately, these proposed functions are difficult to prove. Moreover, the natural host of EBOV has still not been definitively identified and it is possible that sGP function and/or the requirement for C-mannosylation may differ in the reservoir species that presumably maintains the virus without the onset of disease. A clear role for C-mannosylation of sGP was not determined, which raises the question as to whether C-mannosylation of sGP has a functional role or if it is a fortuitous occurrence due to the parasitic nature of viruses in mammalian cells.

4.3 Potential for C-mannosylation of Other Viral Proteins

As this was this first identification of a viral protein containing a C-mannose moiety, a search for the other viral proteins with this motif was carried out. A large number (2323) of viral proteins contain a WXXW sequence; however, many of these proteins are unlikely to be modified as they are not processed through the ER. For the following analysis, only viral proteins that are predicted to cross the ER membrane were considered to have the potential to be modified. This resulted in 373 viral proteins with the potential to be C-mannosylated, the vast majority of which are surface glycoproteins (Table 3). Previous searches for mammalian proteins with the potential to be C-mannosylated identified 336 cellular proteins present in different organs and body fluids

and having many distinct functions (Krieg et al., 1998). Taken together, C-mannosylation may be a more common form of protein modification then suggested by the small number of confirmed proteins bearing this modification. EBOV $GP_{1,2}$ contains multiple potential C-mannosylation sites, with two located adjacent to the transmembrane region of GP_2 and one on W_{288} of GP_1 (the identical location as on sGP). With this in mind, the modification of sGP may be an anomaly resulting from the unique manner in which this protein is generated; as the product of unedited transcripts from the glycoprotein gene of EBOV (Feldmann et al., 2001). While a function of the C-mannose on sGP is not excluded, it is postulated that the function of the C-mannose may be seen in the EBOV transmembrane glycoprotein $GP_{1,2}$. The location of a C-mannose in close proximity to the membrane is not unprecedented, as bovine lens protein MP20 also contains this modification at a similar location (Perez-Vilar, Randell, and Boucher, 2004) despite the presumed requirement for a high level of hydrophobicity. The location of a C-mannosylation site just inside the transmembrane region of the Borna disease virus glycoprotein and on the extracellular portion of the VSV glycoprotein may further indicate that this modification is important for the orientation of membrane proteins or trafficking of viral membrane proteins to the cell surface as it has been suggested for other C-mannosylated mammalian proteins (Ervin et al., 2005; Hilton et al., 1996). C-mannosylation could also play a role in particle maturation or entry.

4.4 C-mannosylation of GP_1 and GP_2

The observation that C-mannosylation motifs in GP_1 and the presence of two adjacent C-mannosylation motifs in GP_2 were conserved among all species of EBOV suggested that either this sequence or the C-mannosylation modification itself could be

important for $GP_{1,2}$ structure or function. HPLC-MALDI MS analysis of $GP_{1,2}$ derived from purified heat-treated VLPs indicated that W_{288} of GP_1 was C-mannosylated (Figure 25 B). The unmodified peptide was also detected (Figure 25 A); however, they were obtained from different fractions so a comparison of the quantity of modified to unmodified peptides is not possible. The peptide from GP_2 (bearing the two adjacent motifs) was detected exclusively in its unmodified form (Figure 25 C) and both automated and manual searches of all fractions did not reveal any peaks with a +162 or +324 Da shift. This indicates that it is highly unlikely that either motif in GP_2 is C-mannosylated. The lack of C-mannosylation in GP_2 is not completely unexpected as this region (known as the MPER), is highly hydrophobic and is likely to be involved in interactions with the host and viral membranes. While other proteins (e.g. MP40) are C-mannosylated in close proximity to the membrane, this region of $GP_{1,2}$ is likely involved in membrane fusion, making the presence of one or even two hydrophilic moieties unlikely.

NetCGlyc 1.0 is a predictive model that evaluates the potential for C-mannosylation. It is based on data from 69 experimentally confirmed C-mannosylation sites on mammalian proteins. While the linear recognition sequence for C-mannosylation consists of W-x-x-W/F, in which the first tryptophan residue becomes mannosylated (Doucey et al., 1998), no other sequence specificity determinants had been identified. However, in the data analysis used to establish the NN model for NetCGlyc 1.0, it was observed that previously confirmed C-mannosylated proteins could contain a cysteine in the +3 position and there was a preference for small and/or polar residues (Ser, Ala, Gly, Thr) in the +1 position, with Phe and Leu being discriminated against (Julenius, 2007).

When EBOV sequences were analyzed, this model predicted that only W648 should be modified, while W288 and W645 should remain unaltered. Experimental analysis indicated that only W288 is modified, suggesting that this model works poorly in the case of EBOV proteins. The predictions are near the cut-off value; therefore, it is possible this model could be improved or its use in prediction of C-mannosylation of viral proteins may not be entirely accurate. Whether the model itself requires revision or an unconsidered factor unique to viral proteins plays a role, it is most certainly limited by the small number of proteins confirmed to be C-mannosylated and should be used with caution.

4.5 Functional Consequences of Altering Tryptophan Residues in GP_1 and GP_2

Prior to the availability of MS data on the C-mannosylation status of GP_1 and GP_2, the effect of altering the tryptophan residues potentially responsible for C-mannosylation was initiated. Alterations of tryptophans at positions 291, 648, 651, 648/651, 644/645/648/651 to alanine did not appear to significantly alter glycoprotein expression, as all constructs had similar intensities by western blot (Figure 26). To determine the functionality of these mutants, the iVLP assembly/entry assay was established for use with plasmids that express the glycoprotein with point-mutations. This assay had been previously used to assess the requirement of VP24 in RNP formation. It has also been optimized to allow infection of naïve target cells (i.e. cells that have not been transfected with plasmids encoding RNP proteins) (Hoenen et al., 2006b). The iVLP

assay allows glycoprotein incorporation (p0), particle assembly (p0), entry (p1) and initial transcription (p1) following entry to be studied in a BSL2 environment.

4.5.1 Functional importance of tryptophan residues in the GP_2 MPER

When plasmids encoding ZEBOV GP with tryptophan to alanine mutations were used, altered reporter activity was observed, which was significantly different from the wild-type (WT) glycoprotein (Figure 27). The reporter activity in p0 reflects initial minigenome replication and transcription, and would generally be expected to be equivalent between constructs. However, both W648/651A and W644/645/648/651A show statistically significant decreases in initial reporter activity. While the mechanism behind this decrease is unknown, it is suspected that a decrease in transcription occurs as result of accumulation of VP24 (Watanabe et al., 2007) and VP40, as a result of decreased particle assembly and egress. The total exclusion of GP (-GP and W644/645/648/651A) from iVLPs, leads to the largest decrease in initial reporter activity, which supports this hypothesis.

The reporter activity measured in p1 reflects assembly, binding, entry and initial transcription of iVLP minigenomes. Three mutants, W648A, W648/651A and W644/645/648/651A, significantly decreased reporter activity. The decrease in W648A was statistically significant; however, the decrease in W648/651A was more substantial. The largest decrease was in W644/645/648/651A, which was comparable to samples lacking GP altogether (-GP). All of these constructs were expressed at similar levels (Figure 26), transported to the cell surface (Figure 28) and thus should be available for iVLP formation. When GP incorporation into iVLPs was analyzed (Figure 29), it was apparent that W644/645/648/651A was not incorporated into iVLPs, a finding that is also

supported by the high level of $GP_{1,2}$ in the cell lysate for this mutant. This provides the basis for the absence of reporter activity (similar to -GP) in p1 of the iVLP assay, as iVLP particles will not bind/enter target cells and deliver the reporter in the absence of $GP_{1,2}$ on their surface. Furthermore, this mutant could not be rescued in the infectious clone system (data not shown), demonstrating the importance of incorporating the glycoprotein into virus particles. Surprisingly, W648A and W651A are incorporated into iVLPs at slightly higher levels than WT (which would be thought to result in enhanced iVLP reporter activity), while W648/651A shows slightly lower incorporation. Therefore, the observed decrease in p1 reporter activity suggests that these residues are important for the processes of virus assembly and/or entry.

Taken together, this data demonstrates an important role for the MPER tryptophan residues for glycoprotein incorporation as well as particle assembly or entry.

EBOV GP_2 appears to share a number of similarities to retroviral (e.g. HIV, avian sarcoma virus) transmembrane proteins, including the location of fusion peptides, an immunosuppressive motif, α-helical heptad repeats regions, a conserved amino acid loop defined by a disulphide bond, a hydrophobic transmembrane domain and a CX_6CC motif (Gallaher, 1996; Kuhn, 2008). In addition, both EBOV GP_2 and HIV gp41 posses a high number of tryptophan residues in the MPER; therefore, they may function in a similar manner.

Recently, the MPER of gp41 has received attention as a potential target for future therapies as it is targeted by three of the five identified broadly neutralizing antibodies. This region is required for HIV virus entry and fusion. Demonstrating the importance of these resides was the finding that, the deletion or alteration of 3 of the 5 tryptophan

residues in the MPER leads to a defect in cell-cell fusion as well as virus entry, while the alteration of a single tryptophan residue leads to decreased GP incorporation in virus particles (Salzwedel, West, and Hunter, 1999). The tryptophan content and the location of these residues appears to be important for these functions (Vishwanathan and Hunter, 2008). During HIV-host cell membrane fusion, the formation of the six helix bundle brings the viral and cell membranes into apposition and places the MPER in proximity to both of them (Vishwanathan and Hunter, 2008). Structural analysis of the HIV MPER in a lipid bi-layer suggests the amino acids form an L-shaped confirmation, which includes a flexible region allowing movement independent of the C-terminus. This flexibility is important for its ability to insert into the membrane (Sun et al., 2008). Furthermore, the three broadly neutralizing antibodies that target the MPER disrupt the fusogenic functions of the MPER by preventing either hinge motion or altering MPER orientation (depending of the antibody used) (Song et al., 2009). It is likely that the addition of alanines during mutagenesis studies act as α-helix stabilizers, preventing the flexibility required undergo this process (Chakrabartty, Kortemme, and Baldwin, 1994).

Given the similarities in location, the high tryptophan content and the findings presented above (i.e. alterations to GP incorporation and particle entry), it is plausible that the MPER of EBOV GP_2 may function in a similar manner and tryptophans in this region may play an important role similar to HIV gp41. Unfortunately, while crystal structures for GP_2 have been solved (Malashkevich et al., 1999; Weissenhorn et al., 1998a; Weissenhorn et al., 1998b) and a complete structure of $GP_{1,2}$ bound to an antibody has been proposed (Lee et al., 2008), these structures were generated with the MPER deleted (Lee et al., 2008; Malashkevich et al., 1999; Weissenhorn et al., 1998a) or were

only partially included and declared as an unstructured region (Weissenhorn et al., 1998b). As a result, additional structural data on the MPER of EBOV GP_2 would assist in determining the extent of structural similarity.

4.5.2 C-mannosylation of GP_1 is not critical for GP function

W291A showed significantly increased reporter activity in p1 suggesting enhanced iVLP assembly or entry. Recent data investigating the role of conserved residues in GP_1, supports the finding as it was noted that mutation of W291A/E292A resulted in little effect on GP incorporation into pseudotyped feline immunodeficiency virus (FIV) particles. Transduction efficiency was also slightly (20%) higher than wild-type (Brindley et al., 2007). Expression and transport of the mutant appeared to be identical to that of WT GP (Figure 26, 28); however, less $GP_{1,2}$ (approximately 50% of WT) appeared to be incorporated into iVLPs (Figure 29 A). This was corroborated by an increase in GP in the cell lysate (Figure 29 C), suggesting accumulation occurred due to less incorporation, given that overall expression was comparable. While W291A is not incorporated to the same extent as WT $GP_{1,2}$, the data suggest it is more efficient at gaining entry to target cells. The transport of W291A to the cell surface was similar to WT. This suggests that C-mannosylation of W288 is not critical for proper folding of $GP_{1,2}$ in contrast to other C-mannosylated proteins (Ervin et al., 2005; Miyazaki et al., 1991; Perez-Vilar, Randell, and Boucher, 2004; Wang et al., 2009), where elimination C-mannosylation decreases transport of the protein from the ER to the cell surface. It is assumed that improper folding results in the proteins being targeted to a degradation pathway.

Despite characterization of C-mannosylation on a number of mammalian proteins, other than a presumed structural role this post-translational modification is functionally undefined. Recently, the first well-defined function for C-mannosylation was described for the extracellular matrix protein mindin (spondin-2), a pattern recognition molecule. Mindin was observed to recognize lipopolysaccharide (LPS) through an interaction that was exclusively dependent on C-mannosylation (Li et al., 2009). Bacterially expressed mindin did not bind LPS, while mindin produced in HEK293 cells did. Detailed MS and computational analysis of the mindin sequence revealed that C-mannosylation was the only predicted post-translational modification. Furthermore, the C-mannosylation site was located on the proposed ligand-binding face (Tan et al., 2002). This demonstrates a potential importance of this small post-translational modification in protein-lipoglycan interactions, in this case when C-mannosylation is present on an exposed surface. As the C-mannosylation site on GP_1 is predicted to be exposed this could suggest that it has the potential to interact with sugar moieties.

In the case of GP_1, the W291A mutation would abolish the C-mannose on W288, causing an increase in the hydrophobicity of this region. According to the crystal structure data for GP_1, the region containing W288 and W291 is part of the glycan gap region and resides on an external loop characterized as being disordered (Lee et al., 2008). Given that this region is not known to be part of the receptor binding site (Kuhn et al., 2006) it is somewhat surprising that a potentially exposed region contains highly hydrophobic residues. However, the receptor(s) for EBOV remain unidentified; therefore, multiple interactions may drive viral attachment to the cell surface, which could involve this region. Conservation of Trp on protein surfaces suggests that a binding spot at this

region is highly likely. Trp/Met/Phe are conserved structurally only on protein-protein interaction interfaces and are not conserved structurally on exposed surfaces of the protein (Ma et al., 2003). Moreover, the conservation propensity for Trp on the binding sites is the highest of all amino acids (Ma and Nussinov, 2007). The large size of aromatic Trp allows it to simultaneously interact with a greater number of residues, thus making it a central node of a protein-protein interaction network (del Sol and O'Meara, 2005). Therefore, it is possible that elimination of the C-mannose creates a more reactive surface for interactions that could help initiate or stabilize interactions with target cells.

4.6 Summary

While there has been a recent increase in research associated with Ebola viruses, many aspects of basic virus biology (i.e. replication, assembly, budding, receptor binding, entry and fusion) are not well described. Numerous studies have suggested roles for sGP and to a more limited extent GP_1 and $GP_{1,2\Delta TM}$ (Δ-peptide and ssGP remain essentially unstudied); however, a widely accepted role for these soluble viral glycoproteins is absent. The data presented in this research advances the hypothesis that sGP exerts an effect on endothelial cells, providing the potential to modulate the host response to EBOV infection.

sGP was structurally characterized as a parallel-oriented homodimer (Barrientos et al., 2004; Falzarano et al., 2006) and its putative anti-inflammatory function was demonstrated to be dependent on this structure (Falzarano et al., 2006). The disruption of either C53-C53' or C306-C306' led to structural alterations that were sufficient to result in the complete loss of its rescue effect on TNF-α treated endothelial cells. Furthermore,

sGP-mediated rescue of endothelial barrier function was also observed under shear stress, which better simulates *in vivo* conditions. Structural characterization led to the identification of sGP as the first viral protein to be modified by the rarely described post-translational modification, C-mannosylation; however, the elimination of the C-mannose residue did not impact on its anti-inflammatory function (Falzarano et al., 2007). That the anti-inflammatory effect of sGP is structure-dependent and was also observed under shear stress conditions suggests that further characterization of its mechanism and significance should be pursued.

Multiple, highly conserved C-mannosylation motifs, were also noted in the spike glycoprotein $GP_{1,2}$. The motif in GP_1 was C-mannosylated on the identical location as in sGP and the elimination of this modification increased infectious virus-like particle (iVLP) entry into target cells. Therefore, this region of GP_1 may interact with the cell surface to enhance either binding or entry. While the two adjacent C-mannosylation motifs in the membrane proximal external region (MPER) of GP_2 were not modified, the tryptophans in this region were important for glycoprotein incorporation and particle entry. A similar function has been identified for tryptophans in the MPER of HIV gp41, where these residues are required for glycoprotein incorporation and membrane fusion. In HIV, this region contains binding sites for multiple broadly neutralizing antibodies and is currently under investigation as a possible therapeutic target; as such, this may also represent a future target for prevention or treatment of EBOV.

4.7 Future Directions

The link between sGP structure and its anti-inflammatory function provides evidence that the endothelial barrier function rescue effect is in fact valid. Moreover, the demonstration of this effect under shear stress conditions suggests that this function may also occur *in vivo*. Therefore, further investigations are warranted to define the mechanism as well as the role this anti-inflammatory effect plays in pathogenesis. Inflammation during EBOV infection is not the result of TNF-α alone; therefore, determining whether sGP can protect barrier function in the presence of other pro-inflammatory cytokines would be important for linking this *in vitro* function of sGP to the physiological conditions *in vivo*. While this could initially be performed under static conditions, this work should also be performed under shear stress conditions, as the endothelium undergoes significant alterations during flow. A number of inflammatory cytokines are known to be up-regulated during EBOV infection; therefore, a relevant starting point would be to determine the effect of plasma from infected animals on endothelial cells under shear stress. To eliminate sGP, this could be performed with the recombinant ZEBOV virus that lacks RNA editing capabilities in its glycoprotein gene and primarily expresses the spike glycoprotein. Recent improvements in technology and the availability of commercialized version of the rheometer permit these types of experiments, as shear stress impedance spectroscopy experiments can now be carried out in BSL4. If infected plasma alters barrier function, quantitative mass spectrometry analysis (i.e. using protein and/or peptide labelling) could be performed on the plasma to determine the protein composition, leading to the identification of inflammatory mediators and other proteins that are upregulated during EBOV infection.

While determining the breadth of protection offered by sGP could point to its relevance *in vivo*, determining how sGP exerts this effect would be important for the future development of therapeutic strategies if this effect plays a role in immunopathogenesis. So far, protein interaction experiments have failed to demonstrate an interaction between TNF-α and sGP; however, whether sGP interacts with cell surface receptors such as TNFR1, TNFR2, or another receptor remains unknown. Failure to identify an interaction between these targets would then require a more broad screening approach to identify whether sGP interacts with another receptor. The activation of signalling pathways could be also be monitored under different treatment conditions to determine how signalling is affected, which would then suggest possible targets of interaction.

Finally, it has been proposed that the anti-inflammatory function sGP may inhibit the extravisation of immune cells to sites of infection, leading to unchecked virus replication (Wahl-Jensen et al., 2005b). To test this hypothesis, lymphocytes could be added to endothelial cells. Following activation of the endothelium, transendothelial cell migration assays could be carried out in the presence and absence of sGP. Processes such as rolling, attachment and extravisation could be visualized directly and quantified by microscopy during shear stress conditions as described above.

Secreted glycoproteins do not appear to directly affect coagulation; however, the mechanism responsible for the initiation and disregulation of coagulation during EBOV infection remains to be determined. Previous evidence that inhibitors of coagulation improve survival (Geisbert et al., 2003a; Hensley et al., 2007), would suggest that a better

understanding of the mechanism behind the induction of coagulopathy and how this can be attenuated could lead to possible clinical interventions.

The MPER of GP_2, appears to play an important role in GP incorporation into virus particles and in virus entry. Based on data from other viruses (e.g. HIV-1 and HSV-1), the high tryptophan content in the MPER plays a significant role in glycoprotein incorporation, entry and fusion (Galdiero et al., 2007; Vishwanathan and Hunter, 2008). For HIV, the discovery of naturally occurring, broadly neutralizing antibodies that target this region are currently under investigation as a therapeutic. While such antibodies have not been described for EBOV, it is possible that antibodies designed to target the GP_2 MPER could be capable of neutralizing all species of EBOV. Further analysis of the importance of this region in the virus life cycle may result in similarities in function. To determine if this region is critical for glycoprotein function and virus infection, the effect of tryptophan substitutions in the MPER of mouse-adapted ZEBOV should be studied in the BALB/c mouse.

APPENDIX A – SEQUENCES OF PRIMERS

SITE-DIRECTED MUTAGENESIS PRIMERS

Primer	Sequence (5' – 3')
C53G (sGP)f	GATGTCGACAAACTAGTTGCGCGTGACAAACTGTCATCC
C53G (sGP)r	GGATGACAGTTTGTCACGCGCAACTAGTTTGTCGACATC
C306G (sGP)f	TTCGCAGTGAAGAGTGCGCTTTCACAGTTGTATCAAACGG
C306G (sGP)r	CCGTTTGATACAACTGTGAAAGCGCACTCTTCACTGCGAA
W288A(sGP)f	CGGGGAGTGGGCCTTCGCTGAAACTAAAAAAACCTCACTAG
W288A(sGP)r	CTAGTGAGGTTTTTTTAGTTTCGCAGAAGGCCCACTCCCCG
W288A(GP_1)f	CGGGGAGTGGGCCTTCGCTGAAACTAAAAAAAACCTCACTAG
W288A(GP_1)r	CTAGTGAGGTTTTTTTTAGTTTCGCAGAAGGCCCACTCCCCG
W644/645/648Af	GGGGACAATGACAATGCGGCGACAGGAGCGAGACAA
W644/645/648Ar	TTGTCTCGCTCCTGTCGCCGCATTGTCATTGTCCCC
W648Af	CAATTGGTGGACAGGAGCGAGACAATGGATACCGG
W648Ar	CCGGTATCCATTGTCTCGCTCCTGTCCACCAATTG
W651Af	GGACAGGATGGAGACAAGCGATACCGGCAGGTATTGG
W651Ar	CCAATACCTGCCGGTATCGCTTGTCTCCATCCTGTCC
W648/651Af	GGACAGGAGCGAGACAAGCGATACCGGCAGGTATTGG
W648/651Ar	CCAATACCTGCCGGTATCGCTTGTCTCGCTCCTGTCC

SEQUENCING PRIMERS

Primer	Sequence (5' – 3')
ZEBOV-GP-1F	ATGGGCGTTACAAGGAATATTG
ZEBOV-GP-501F	CACAGTTATCTACCGAGG
ZEBOV-GP-523R	GAAATGCAACGACACCTTCAG
ZEBOV-GP-750F	ACAGTTTCTGCTCCAGCTGAA
ZEBOV-GP-1001F	CAACAACTGAAGACCACAAAATC
ZEBOV-GP-1050R	CATTGCAGAGGAATTTTCTGAAG
ZEBOV-GP-1501F	AGAGAAGCAATTGTCAATG
ZEBOV-GP-1523R	TAATGTAAATTAGGGTTGC
ZEBOV-GP-1800F	ATGCCACATTCTGGGACC
ZEBOV-GP-2013R	CTAAAAGACAAATTTGAC

APPENDIX B – VECTOR MAP OF PCAGGS

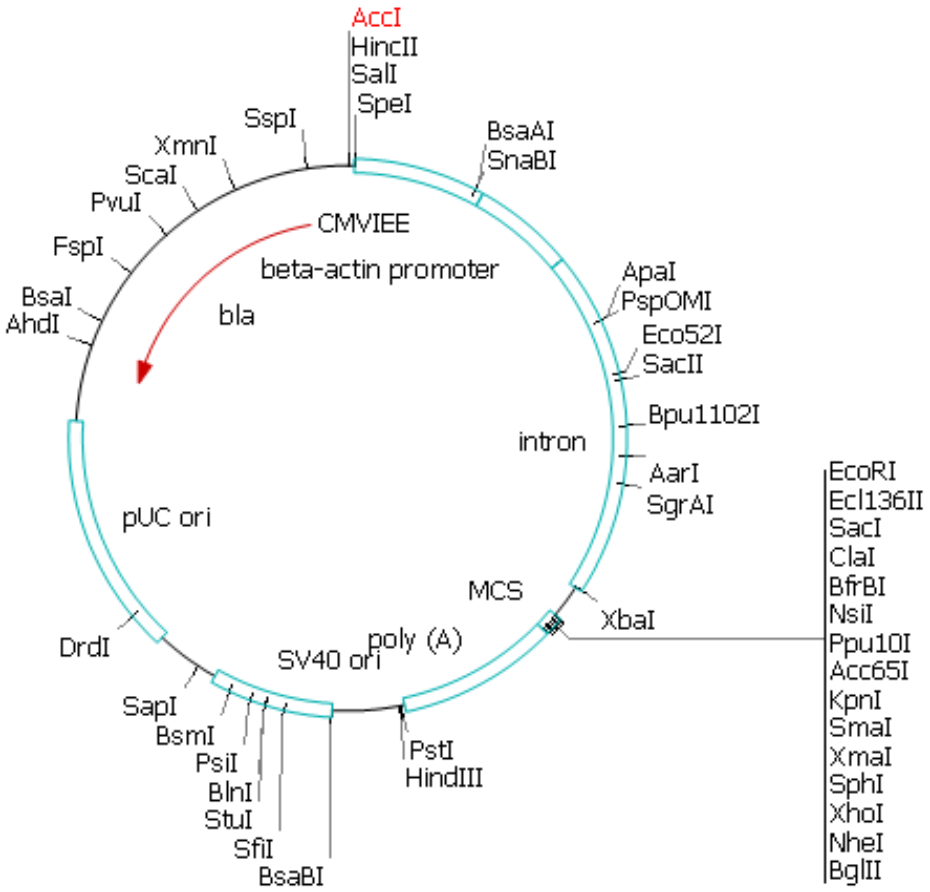

Figure 31. **Vector map of pCAGGS-MCS.** The locations of the chicken β-actin/rabbit β-globin hybrid promoter (beta-actin promoter), human cytomegalovirus immediate early promoter (CMVIEE) enhancer, pUC origin of replication (pUC ori), SV40 origin of replication (SV40 ori), poly (A) signal and the multiple cloning site (MCS) are indicated.

APPENDIX C – RECIPES

10% Resolving gel

4.4 ml	sterile dH_2O
3.0 ml	40% Acrylamide/Bis (BioRad)
2.5 ml	1.5M Tris-HCl (pH 8.8)
100 µl	10% SDS in dH_2O
50 µl	10% ammonium persulfate
8 µl	TEMED

4% Stacking gel

3.2 ml	sterile dH_2O
0.5 ml	40% Acrylamide/Bis (BioRad)
1.25 ml	0.5M Tris-HCl (pH 6.8)
50 µl	10% SDS in dH_2O
25 µl	10% ammonium persulfate
5 µl	TEMED

Anode buffer

75 ml	0.67M boric acid
200 ml	methanol
725 ml	sterile dH_2O

Cathode buffer

75 ml	0.67 boric acid
50 ml	methanol
875 ml	sterile dH_2O

Phosphate buffered saline (PBS)

TN/E buffer

8 ml	1M Tris HCl (pH 7.5)
8 ml	5M NaCl
80 µl	0.5M EDTA (Gibco) (omitted in TN buffer)
376 ml	sterile dH_2O

Wash buffer

50 ml	TNE buffer
25 µl	Tween20 (Fisher)

Regeneration buffer

50 ml	sterile dH_2O
0.375 g	glycine
pH 2.0	HCl

HA column storage buffer

9.55 ml	TNE buffer
445 µl	2% sodium azide

4x gel loading buffer (SDS-PAGE)

2 ml	1M Tris-HCl (pH 6.8)
0.8g	SDS
4 ml	10% glycerol
0.4 ml	14.7M β-mercaptoethanol
1 ml	0.5M EDTA
8 mg	bromophenol blue

6x gel loading buffer (agarose electrophoresis)

0.025 g	bromophenol blue
4 g	sucrose
10 ml	sterile RO water

Western stripping buffer

20 ml	10% SDS
12.5 ml	0.5M Tris-HCl pH 6.8
67.5 ml	sterile dH_20
0.8 ml	β-mercaptoethanol

Coomassie brilliant blue R-250 stain

1.25 g	Coomassie brilliant blue R250
50 ml	glacial acetic acid
225 ml	methanol
225 ml	distilled water

Coomassie destain

50 ml	glacial acetic acid
225 ml	methanol
225 ml	distilled water

APPENDIX D –

Table 6. Experimental masses for tryptic fragments of *Zaire ebolavirus* sGP containing N-glycans. *MS/MS analysis of labelled peptides showed a characteristic doublet (Krokhin et al., 2004) of fragment ions (non-modified peptide + 203 Da). We considered the identity of the glycopeptide confirmed if we observed the doublet and the mass of the non-modified peptide fragment corresponded to the calculated mass of non-modified peptide. ** MS/MS analysis of declycosylated peptide (M = 3287.526) unequivocally showed that only N228 was converted completely into D228, while N238 remained mostly intact. *** While peptides shown in this table were found with alternative cleavage patterns (extra missed cleavages, see Table 1 for PMF), only the most abundant species corresponding to each glycosylation site are shown here.

Calculated mass (Da)	Experimental mass (Da)	Error (ppm)	Residue number	Missed cleavages	Peptide sequence	Glycosylation site	Experimental mass (Da) of glycopeptides	Mass (Da) of sugar moiety	MS/MS confirmed (*)
2021.079	2022.061	-1	32-50	0	SIPLGVIHDSTLQV SDVDK	40	3465.636	1444.557	
							3479.553	1458.474	
							3627.681	1606.602	*
							3789.738	1768.659	*
							3830.766	1809.687	*
							3992.81	1971.731	*
							4080.823	2059.744	*
							4121.856	2100.777	
2085.949	2086.932	0	201-219	0	EPVDATEDPSSGY YSTTIR	204	3544.422	1458.473	
							3854.611	1768.662	*
							4145.706	2059.757	*
							4219.738	2133.789	*
							4510.838	2424.889	*
							4801.922	2715.973	*
							4876.008	2790.059	
							5167.06	3081.111	
3286.531	3287.526	3	220-247	0	YQATGFGTDETEY LFEVDNLTYVQLE SR	228**	4731.068	1444.537	*
							4893.117	1606.586	*
							5055.194	1768.663	*
							5096.166	1809.635	*
							5258.229	1971.698	
							5346.292	2059.761	
2099.094	2100.063	-7	248-265	0	FTPQFLLQLDETIY TSGK	257	4523.955	2424.861	*
							4815.068	2715.974	*
							4889.099	2790.005	*
							5180.199	3081.105	*
							5471.325	3372.231	*
							5762.338	3663.244	
762.398	763.388	7	266-272	1	RSDTTGK	268	2531.037	1768.639	*
							2822.144	2059.746	*
							3113.279	2350.881	*

APPENDIX E – VIRAL PROTEINS WITH THE POTENIAL TO BE C-MANNOSYLATED

NN-no/HMM-signal anchor

Herpesviridae (dsDNA)
gi|9629390|ref|NP_044611.1| virion glycoprotein M [Human herpesvirus 1]
gi|9629279|ref|NP_044479.1| virion glycoprotein M [Human herpesvirus 2]
gi|9625925|ref|NP_040172.1| envelope glycoprotein gM [Human herpesvirus 3 (strain Dumas)]
gi|9625696|ref|NP_039945.1| UL11 [Human herpesvirus 5 strain AD169]
gi|52139327|ref|YP_081602.1| US17 [Human herpesvirus 5 strain Merlin]
gi|9625853|ref|NP_040102.1| US17 [Human herpesvirus 5 strain AD169]
gi|9628326|ref|NP_042917.1| U24, glycoprotein [Human herpesvirus 6]
gi|9633094|ref|NP_050204.1| Hypothetical protein HhV6Bgp027 [Human herpesvirus 6B]
gi|14251024|ref|NP_116386.1| T37 [Tupaia herpesvirus]
gi|30984438|ref|NP_851869.1| virion glycoprotein M [Cercopithecine herpesvirus 1]
gi|13242444|ref|NP_077464.1| unknown [Cercopithecine herpesvirus 7]
gi|20026747|ref|NP_612789.1| US16 [Chimpanzee cytomegalovirus]
gi|20026710|ref|NP_612766.1| UL133 [Chimpanzee cytomegalovirus]
gi|38638247|ref|NP_944430.1| glycoprotein M [Psittacid herpesvirus 1]
gi|50313274|ref|YP_053078.1| membrane glycoprotein B [Equid herpesvirus 1]
gi|50313293|ref|YP_053096.1| membrane protein [Equid herpesvirus 1]
gi|9629759|ref|NP_045250.1| 33 [Equid herpesvirus 4]
gi|9629780|ref|NP_045269.1| 52 [Equid herpesvirus 4]
gi|61660145|ref|YP_214035.1| Hypothetical protein MuHV1gpm25.1 [Murid herpesvirus 1]
gi|9629555|ref|NP_044844.1| unknown [Murid herpesvirus 4]
gi|51557547|ref|YP_068381.1| putative ORF-3 protein [Suid herpesvirus 1]
gi|51557560|ref|YP_068394.1| putative ORF-3 protein [Suid herpesvirus 1]

Iridoviridae (dsDNA)
gi|49237340|ref|YP_031621.1| unknown [Frog virus 3]

Phycodnaviridae (dsDNA)
gi|73852862|ref|YP_294146.1| putative membrane protein [Emiliania huxleyi virus 86]
gi|73852835|ref|YP_294119.1| putative serine protease [Emiliania huxleyi virus 86]

Poxviridae (dsDNA)
gi|40556006|ref|NP_955091.1| CNPV068 GNS1/SUR4-like protein [Canarypox virus]
gi|9634718|ref|NP_039011.1| ORF FPV048 GNS1/SUR4 protein [Fowlpox virus]

Circoviridae (ssDNA)
gi|18875311|ref|NP_573443.1| capsid [Canary circovirus]

Parvoviridae (ssDNA)
gi|9627188|ref|NP_041400.1| polyprotein [canine parvovirus]

Caulimoviridae (RT)
gi|9627254|ref|NP_041738.1| polyprotein [Rice yellow mottle virus]

Retroviridae (RT)
gi|9629130|ref|NP_044281.1| env polyprotein [Human foamy virus]
gi|9629261|ref|NP_044451.1| envelope protein [Human spumaretrovirus]
gi|9626106|ref|NP_056804.1| envelope protein [Simian foamy virus]
gi|9629647|ref|NP_044930.1| envelope protein [Bovine foamy virus]
gi|9628094|ref|NP_042688.1| env precursor [Jembrana disease virus]
gi|9634980|ref|NP_054717.1| Env [equine foamy virus]
gi|9629927|ref|NP_056915.1| env [Feline foamy virus]
gi|9626202|ref|NP_040549.1| trans-acting factor [Avian leukosis virus - RSA]
gi|83722646|ref|YP_443923.1| envelope protein [Atlantic salmon swim bladder sarcoma virus]

Arteiviridae (+ssRNA)
gi|15426270|ref|NP_203542.1| ORF1a [Simian hemorrhagic fever virus]
gi|25777551|ref|NP_742092.1| ORF1ab [Simian hemorrhagic fever virus]

Coronaviridae (+ssRNA)
gi|38018029|ref|NP_937953.1| M protein [Human coronavirus OC43]
gi|15081552|ref|NP_150082.1| matrix protein [Bovine coronavirus]
gi|9629817|ref|NP_045301.1| E1 glycoprotein [Murine hepatitis virus strain A59]

Flaviviridae (+ssRNA)
gi|26251698|ref|NP_757356.1| putative NS2 protein [Hepatitis GB virus B]
gi|27735340|ref|NP_776039.1| putative matrix protein M [Cell fusing agent virus]
gi|37695581|ref|NP_937772.1| membrane protein [Kamiti River virus]
gi|27735362|ref|NP_776071.1| matrix protein M [Rio Bravo virus]
gi|27596785|ref|NP_775510.1| non-structural protein NS4b [Tick-borne encephalitis virus]

Potyviridae (+ssRNA)
gi|25013917|ref|NP_734354.1| 6K2 protein [Bean common mosaic necrosis virus]
gi|40254034|ref|NP_954624.1| 6K2 protein [Beet mosaic virus]
gi|32493283|ref|NP_871733.1| 6K2 [Papaya leaf-distortion mosaic potyvirus]
gi|25013837|ref|NP_734414.1| 6K2 protein [Peanut mottle virus]
gi|25013613|ref|NP_734197.1| 6K2 protein [Soybean mosaic virus]
gi|51949952|ref|YP_077273.1| 6K2 protein [Watermelon mosaic virus]
gi|25013664|ref|NP_734188.1| 6K2 protein [Zucchini yellow mosaic virus]

Togaviridae (+ssRNA)
gi|25121499|ref|NP_740685.1| 6K protein [Ross River virus]

NN-no/HMM-signal peptide

Herpesviridae (dsDNA)
gi|9629316|ref|NP_044516.1| tegument protein [Human herpesvirus 2]
gi|9625691|ref|NP_039940.1| UL6 [Human herpesvirus 5 strain AD169]
gi|52139193|ref|YP_081466.1| UL6 [Human herpesvirus 5 strain Merlin
gi|18845969|ref|NP_572055.1| ORF 7; transport protein homolog; EBV BALF3 homolog [Human herpesvirus 8]
gi|30984474|ref|NP_851906.1| tegument phosphoprotein [Cercopithecine herpesvirus 1]
gi|56694732|ref|YP_164452.1| virion glycoprotein M [Cercopithecine herpesvirus 2]
gi|83722578|ref|YP_443856.1| UL10 [Cercopithecine herpesvirus 16]
gi|9629829|ref|NP_045313.1| virion protein (tegument) [Bovine herpesvirus 1]
gi|9629847|ref|NP_045331.1| glycoprotein B [Bovine herpesvirus 1]
gi|13095632|ref|NP_076547.1| unknown [Bovine herpesvirus 4]
gi|40787899|ref|NP_954920.1| UL27 glycoprotein B [Bovine herpesvirus 5]
gi|40787881|ref|NP_954902.1| UL46 tegument protein [Bovine herpesvirus 5]
gi|61660158|ref|YP_214049.1| Glycoprotein present at IE times [Murid herpesvirus 1]
gi|9845364|ref|NP_064178.1| pR78 [Murid herpesvirus 2]
gi|83642892|ref|YP_438179.1| ORF55 [Ovine herpesvirus 2]
gi|51557495|ref|YP_068329.1| UL46 tegument protein [Suid herpesvirus 1]

Poxviridae (dsDNA)
gi|9633835|ref|NP_051914.1| gp025L [Rabbit fibroma virus]

Anellovirus (ssDNA)
gi|29502194|ref|NP_817122.1| VP1 [TT virus]

Retroviridae (RT)
gi|9630314|ref|NP_056791.1| env protein [Gibbon ape leukemia virus]

Alphaflexiviridae (+ssRNA)
gi|50428559|ref|YP_054406.1| coat protein [Zygocactus virus X]

Picornavirales - unclassified (+ssRNA)
gi|71480056|ref|NP_853560.2| polyprotein [Deformed wing virus]
gi|47177089|ref|YP_015696.1| polyprotein [Kakugo virus]
gi|56121876|ref|YP_145791.1| polyprotein [Varroa destructor virus 1]

Secoviridae (+ssRNA)
gi|20153412|ref|NP_619704.1| polyprotein [Grapevine chrome mosaic virus]
gi|25013712|ref|NP_734051.1| 84 kDa protein [grapevine chrome mosaic virus]

Closteroviridae (+ssRNA)
gi|21328573|ref|NP_041870.2| fusion protein of papin-like protease, methyltransferase, RNA helicase and RNA-dependent RNA polymerase [Beet yellows virus]
Flaviviridae (+ssRNA)
gi|20260782|ref|NP_620108.1| polyprotein [Langat virus]

gi|20260780|ref|NP_620099.1| putative [Powassan virus]
gi|11528014|ref|NP_041724.2| polyprotein precursor [West Nile virus]

Potyviridae (+ssRNA)
gi|9628430|ref|NP_056765.1| polyprotein [Pea seed-borne mosaic virus]

Togaviridae (+ssRNA)
gi|25121516|ref|NP_740664.1| glycoprotein E1 [Rubella virus]

Orthomyxoviridae (-ssRNA)
gi|9630644|ref|NP_047200.1| hypothetical protein [Aichi virus]

NN-yes/HMM-non-secretory protein
Adenoviridae (dsDNA)
gi|21450914|ref|NP_659537.1| RH2 (20.9kd) [Ovine adenovirus D]

Herpesviridae (dsDNA)
gi|9625838|ref|NP_040087.1| US2 [Human herpesvirus 5 strain AD169]
gi|52139314|ref|YP_081589.1| US2 [Human herpesvirus 5 strain Merlin]
gi|9625705|ref|NP_039954.1| UL20 [Human herpesvirus 5 strain AD169]
gi|52139206|ref|YP_081479.1| UL20 [Human herpesvirus 5 strain Merlin]
gi|9625722|ref|NP_039971.1| UL37 [Human herpesvirus 5 strain AD169]
gi|52139223|ref|YP_081496.1| UL37 [Human herpesvirus 5 strain Merlin]
gi|51874270|ref|YP_073788.1| envelope glycoprotein gH [Human herpesvirus 7]

Iridoviridae (dsDNA)
gi|15079130|ref|NP_149882.1| 419L [Invertebrate iridescent virus 6]
gi|15079142|ref|NP_149894.1| 431L [Invertebrate iridescent virus 6]

Poxviridae (dsDNA)
gi|9634784|ref|NP_039077.1| ORF FPV114 HAL3 domain [Fowlpox virus]
gi|62637413|ref|YP_227411.1| Palmitylated virion envelope protein [Mule deer poxvirus]
gi|9633966|ref|NP_051891.1| gp004.1L [Rabbit fibroma virus]
gi|9633965|ref|NP_052045.1| gp004.1R [Rabbit fibroma virus]

Nimaviridae (dsDNA)
gi|17158366|ref|NP_477785.1| wsv263 [Shrimp white spot syndrome virus]

Phycodnaviridae (dsDNA)
gi|9631581|ref|NP_048360.1| a12R [Paramecium bursaria Chlorella virus 1]

Coronaviridae (+ssRNA)
gi|12175752|ref|NP_073555.1| membrane protein [Human coronavirus 229E]

Picornaviridae (+ssRNA)
gi|21335365|ref|NP_653077.1| polyprotein [Equine rhinitis B virus 1]

NN-yes/HMM-signal anchor
Baculoviridae (dsDNA)
gi|9627840|ref|NP_054127.1| AcOrf-97 peptide [Autographa californica nucleopolyhedrovirus]
gi|14602295|ref|NP_148842.1| ORF58 LEF-11 [Cydia pomonella granulovirus]
gi|48843705|ref|YP_025277.1| per os infectivity factor [Neodiprion lecontei NPV]
gi|9634278|ref|NP_037817.1| ORF57 odv-e66 [Spodoptera exigua nucleopolyhedrovirus]

Herpesviridae (dsDNA)
gi|52139198|ref|YP_081471.1| UL11 [Human herpesvirus 5 strain Merlin]
gi|9628320|ref|NP_042911.1| U18, IE glycoprotein [Human herpesvirus 6]
gi|24943090|ref|NP_733852.1| C1 [Callitrichine herpesvirus 3]
gi|51556490|ref|YP_068124.1| rh30 [Cercopithecine herpesvirus 8]
gi|51518089|ref|YP_068017.1| LMP1 [Cercopithecine herpesvirus 15]
gi|20026639|ref|NP_612681.1| immediate-early glycoprotein UL37 [Chimpanzee cytomegalovirus]
gi|9626014|ref|NP_040260.1| unnamed protein product [Saimiriine herpesvirus 2]
gi|57790981|ref|YP_182385.1| glycoprotein M [Gallid herpesvirus 1]
gi|9629620|ref|NP_044896.1| unknown [Murid herpesvirus 4]
gi|51557531|ref|YP_068365.1| multiple membrane spanning glycoprotein gM precursor [Suid herpesvirus 1]
gi|14251066|ref|NP_116428.1| T78 [Tupaia herpesvirus]

Mimiviridae (dsDNA)
gi|55819291|ref|YP_142770.1| unknown [Acanthamoeba polyphaga mimivirus]
gi|55819675|ref|YP_143163.1| unknown [Acanthamoeba polyphaga mimivirus]
gi|55818949|ref|YP_142422.1| unknown [Acanthamoeba polyphaga mimivirus]
gi|55819750|ref|YP_143241.1| unknown [Acanthamoeba polyphaga mimivirus]

Nimaviridae (dsDNA)
gi|17158378|ref|NP_477797.1| wsv275 [Shrimp white spot syndrome virus]
gi|17158559|ref|NP_477980.1| wsv458 [Shrimp white spot syndrome virus]

Phycodnaviridae (dsDNA)
gi|73852851|ref|YP_294135.1| putative membrane protein [Emiliania huxleyi virus 86]
gi|73852889|ref|YP_294173.1| putative fatty acid desaturase [Emiliania huxleyi virus 86]
gi|9631729|ref|NP_048508.1| a160L [Paramecium bursaria Chlorella virus 1]
gi|9632047|ref|NP_048836.1| Gly-rich [Paramecium bursaria Chlorella virus 1]

Retroviridae (RT)
gi|9627208|ref|NP_054372.1| envelope protein [Simian immunodeficiency virus]

Reoviridae (dsRNA)
gi|77120610|ref|YP_338257.1| VP7 [Human rotavirus G3]

Corondaviridae (+ssRNA)
gi|9626542|ref|NP_040835.1| membrane protein [Avian infectious bronchitis virus]
gi|9626541|ref|NP_040834.1| small virion-associated protein [Avian infectious bronchitis virus]
gi|45655912|ref|YP_003770.1| membrane protein [Human coronavirus NL63]
gi|56807329|ref|YP_173241.1| membrane glycoprotein [Human coronavirus HKU1]
gi|60115399|ref|YP_209237.1| membrane protein (M) [Murine hepatitis virus strain JHM]
gi|29836504|ref|NP_828855.1| matrix protein [SARS coronavirus]
gi|30124073|ref|NP_828852.2| hypothetical protein sars3a [SARS coronavirus]

Flaviviridae (+ssRNA)
gi|27697399|ref|NP_775682.1| non-structural protein NS2a [Apoi virus]
gi|25014065|ref|NP_733809.1| nonstructural protein 2B [Dengue virus type 1]
gi|73671186|ref|YP_307188.1| nonstructural protein 2B [Dengue virus type 1]
gi|26053625|ref|NP_751923.1| NS2 protein [Hepatitis C virus]

NN-yes/HMM-signal peptide
Adenoviridae (dsDNA)
gi|52801678|ref|YP_094047.1| E3 ORFA [Bovine adenovirus A]
gi|9629489|ref|NP_044720.1| hypothetical protein DaV1gp23 [Duck adenovirus A]
gi|56158904|ref|AP_000100.1| ORF1 [Duck adenovirus 1]

Baculoviridae (dsDNA)
gi|29567203|ref|NP_818765.1| fusion protein [Adoxophyes honmai nucleopolyhedrovirus]
gi|46309422|ref|YP_006312.1| ORF32 [Agrotis segetum granulovirus]
gi|46309413|ref|YP_006303.1| ORF41 [Agrotis segetum granulovirus]
gi|9627869|ref|NP_054156.1| chitinase [Autographa californica nucleopolyhedrovirus]
gi|9630926|ref|NP_047523.1| CHITINASE=CHI-A=AcMNPV orf126 [Bombyx mori nucleopolyhedrovirus]
gi|37651339|ref|NP_932730.1| chitinase [Choristoneura fumiferana defective nucleopolyhedrovirus]
gi|68304201|ref|YP_249669.1| chitinase [Chrysodeixis chalcites nucleopolyhedrovirus]
gi|30387349|ref|NP_848428.1| chitinase [Choristoneura fumiferana MNPV]
gi|14602251|ref|NP_148794.1| ORF10 chitinase [Cydia pomonella granulovirus]
gi|14602283|ref|NP_148830.1| ORF46 metalloproteinase [Cydia pomonella granulovirus]
gi|15320767|ref|NP_203279.1| CHI [Epiphyas postvittana nucleopolyhedrovirus]
gi|22788757|ref|NP_690469.1| hypothetical protein HZV_50 [Heliothis zea virus 1]
gi|15426306|ref|NP_203597.1| chitinase [Helicoverpa armigera nuclear polyhedrosis virus]

gi|12597526|ref|NP_075110.1| chitinase [Heliocoverpa armigera nucleopolyhedrovirus G4]
gi|18138368|ref|NP_542664.1| chitinase [Helicoverpa zea single nucleocapsid nucleopolyhedrovirus]
gi|9631097|ref|NP_047767.1| envelope protein [Lymantria dispar nucleopolyhedrovirus]
gi|9631123|ref|NP_047793.1| fibroblast growth factor [Lymantria dispar nucleopolyhedrovirus]
gi|20069901|ref|NP_613105.1| chitinase [Mamestra configurata NPV-A]
gi|22549459|ref|NP_689232.1| hypothetical protein [Mamestra configurata nucleopolyhedrovirus B]
gi|22549421|ref|NP_689194.1| putative chitnase [Mamestra configurata nucleopolyhedrovirus B]
gi|9630062|ref|NP_046280.1| chitinase [Orgyia pseudotsugata multicapsid nucleopolyhedrovirus]
gi|23577834|ref|NP_703113.1| chitinase [Rachiplusia ou multiple nucleopolyhedrovirus]
gi|15617513|ref|NP_258310.1| chitinase [Spodoptera litura nucleopolyhedrovirus]
gi|9634240|ref|NP_037779.1| ORF19 chitinase [Spodoptera exigua nucleopolyhedrovirus]
gi|74229747|ref|YP_308951.1| chitinase [Trichoplusia ni SNPV]
gi|9635311|ref|NP_059209.1| ORF61 [Xestia c-nigrum granulovirus]

Herpesviridae (dsDNA)
gi|9629270|ref|NP_044470.1| virion glycoprotein L [Human herpesvirus 2]
gi|82503269|ref|YP_401713.1| BALF4 [Human herpesvirus 4]
gi|82503234|ref|YP_401678.1| BKRF2 [Human herpesvirus 4]
gi|82503262|ref|YP_401706.1| membrane glycoprotein [Human herpesvirus 4]
gi|9625694|ref|NP_039943.1| UL9 [Human herpesvirus 5 strain AD169]
gi|28373244|ref|NP_783773.1| UL14 [Human herpesvirus 5 strain AD169]
gi|28373218|ref|NP_783794.1| UL116 [Human herpesvirus 5 strain AD169]
gi|52139200|ref|YP_081473.1| UL14 [Human herpesvirus 5 strain Merlin]
gi|52139281|ref|YP_081556.1| UL116 [Human herpesvirus 5 strain Merlin]
gi|52139300|ref|YP_081575.1| UL141 [Human herpesvirus 5 strain Merlin]
gi|52139299|ref|YP_081574.1| UL142 [Human herpesvirus 5 strain Merlin]
gi|9633087|ref|NP_050198.1| immediate-early protein 6 [Human herpesvirus 6B]
gi|9633119|ref|NP_050229.1| glycoprotein H [Human herpesvirus 6B]
gi|51874240|ref|YP_073758.1| IE-B membrane glycoprotein [Human herpesvirus 7]
gi|18845967|ref|NP_572053.1| ORF 4; The HVS ORF 4 homolog has alternatively spliced messages encoding membrane bound and secreted proteins; complement binding protein vCBP homolog [Human herpesvirus 8]
gi|18845966|ref|NP_572052.1| ORF K1 [Human herpesvirus 8]
gi|18845974|ref|NP_572060.1| ORF K2; functional interleukin-6 vIL-6 homolog [Human herpesvirus 8]
gi|9631248|ref|NP_048029.1| orf 58 [Ateline herpesvirus 3]
gi|24943094|ref|NP_733856.1| ORF4 [Callitrichine herpesvirus 3]
gi|24943105|ref|NP_733867.1| ORF14 [Callitrichine herpesvirus 3]

gi|56694769|ref|YP_164489.1| tegument phosphoprotein VP11/12 [Cercopithecine herpesvirus 2]
gi|51556462|ref|YP_068095.1| rh01 [Cercopithecine herpesvirus 8]
gi|51556466|ref|YP_068099.1| rh05 [Cercopithecine herpesvirus 8]
gi|51556491|ref|YP_068125.1| rh31 [Cercopithecine herpesvirus 8]
gi|51556492|ref|YP_068126.1| rh32 [Cercopithecine herpesvirus 8]
gi|51556500|ref|YP_068134.1| rh40 [Cercopithecine herpesvirus 8]
gi|51556511|ref|YP_068145.1| rh51 [Cercopithecine herpesvirus 8]
gi|51556562|ref|YP_068196.1| rh103 [Cercopithecine herpesvirus 8]
gi|51556612|ref|YP_068246.1| rh157 [Cercopithecine herpesvirus 8]
gi|51518081|ref|YP_068009.1| BALF4 [Cercopithecine herpesvirus 15]
gi|51518074|ref|YP_068002.1| BILF2 [Cercopithecine herpesvirus 15]
gi|51518046|ref|YP_067974.1| BKRF2 [Cercopithecine herpesvirus 15]
gi|83722613|ref|YP_443891.1| UL44 [Cercopithecine herpesvirus 16]
gi|83722615|ref|YP_443893.1| UL46 [Cercopithecine herpesvirus 16]
gi|83722635|ref|YP_443913.1| US7 [Cercopithecine herpesvirus 16]
gi|19424752|ref|NP_598361.1| glycoprotein R8.1 [Cercopithecine herpesvirus 17]
gi|20026609|ref|NP_612651.1| glycoprotein UL6 [Chimpanzee cytomegalovirus]
gi|20026615|ref|NP_612657.1| UL13 [Chimpanzee cytomegalovirus]
gi|20026708|ref|NP_612750.1| UL131A [Chimpanzee cytomegalovirus]
gi|20026729|ref|NP_612771.1| UL150 [Chimpanzee cytomegalovirus]
gi|20026742|ref|NP_612784.1| glycoprotein US11 [Chimpanzee cytomegalovirus]
gi|66476636|ref|YP_238390.1| JM87 [Macaca fuscata rhadinovirus]
gi|66476693|ref|YP_238447.1| JM144 [Macaca fuscata rhadinovirus]
gi|66476718|ref|YP_238472.1| JM169 [Macaca fuscata rhadinovirus]
gi|10140934|ref|NP_065511.1| glycoprotein B [Alcelaphine herpesvirus 1]
gi|9629865|ref|NP_045349.1| glycoprotein M [Bovine herpesvirus 1]
gi|40787917|ref|NP_954938.1| UL10 glycoprotein M [Bovine herpesvirus 5]
gi|9628042|ref|NP_042636.1| glycoprotein M [Equid herpesvirus 2]
gi|57791002|ref|YP_182406.1| glycoprotein I [Gallid herpesvirus 1]
gi|9635078|ref|NP_057805.1| glycoprotein C [Gallid herpesvirus 2]
gi|12084828|ref|NP_073293.1| hypothetical protein [Meleagrid herpesvirus 1]
gi|61660176|ref|YP_214067.1| Glycoprotein B [Murid herpesvirus 1]
gi|61660246|ref|YP_214137.1| Putative glycoprotein [Murid herpesvirus 1]
gi|61660276|ref|YP_214167.1| Putative membrane glycoprotein [Murid herpesvirus 1]
gi|61660253|ref|YP_214144.1| MHC class I homolog [Murid herpesvirus 1]
gi|9845328|ref|NP_064142.1| pR37 [Murid herpesvirus 2]
gi|9845347|ref|NP_064161.1| pR55 [Murid herpesvirus 2]
gi|9845452|ref|NP_064266.1| pr152.4 [Murid herpesvirus 2]
gi|9845453|ref|NP_064267.1| pr152.5 [Murid herpesvirus 2]
gi|9845466|ref|NP_064280.1| pr171 [Murid herpesvirus 2]
gi|9845403|ref|NP_064217.1| pR115 [Murid herpesvirus 2]
gi|83642848|ref|YP_438135.1| ORF8 [Ovine herpesvirus 2]
gi|38638266|ref|NP_944449.1| glycoprotein I [Psittacid herpesvirus 1]
gi|51557552|ref|YP_068386.1| secreted glycoprotein gG precursor [Suid herpesvirus 1]
gi|14250984|ref|NP_116346.1| t16 [Tupaia herpesvirus]

gi|14250986|ref|NP_116348.1| t17 [Tupaia herpesvirus]
gi|14251029|ref|NP_116391.1| t42 [Tupaia herpesvirus]
gi|14251110|ref|NP_116472.1| t121 [Tupaia herpesvirus]

Iridoviridae (dsDNA)
gi|15078830|ref|NP_149580.1| 117L [Invertebrate iridescent virus 6]
gi|15079024|ref|NP_149775.1| 312R [Invertebrate iridescent virus 6]
gi|15079075|ref|NP_149827.1| 364L [Invertebrate iridescent virus 6]
gi|51870098|ref|YP_073651.1| Hypothetical protein LDVICp145 [Lymphocystis disease virus - isolate China]

Mimiviridae (dsDNA)
gi|55818999|ref|YP_142472.1| unknown [Acanthamoeba polyphaga mimivirus]

Nimaviridae (dsDNA)
gi|17158288|ref|NP_477706.1| wsv184 [Shrimp white spot syndrome virus]
gi|17158547|ref|NP_477968.1| wsv446 [Shrimp white spot syndrome virus]

Phycodnaviridae (dsDNA)
gi|73852897|ref|YP_294181.1| hypothetical protein EhV_423 [Emiliania huxleyi virus 86]
gi|73852836|ref|YP_294120.1| putative membrane protein [Emiliania huxleyi virus 86]
gi|73852587|ref|YP_293871.1| putative phosphate permease [Emiliania huxleyi virus 86]
gi|9632234|ref|NP_048997.1| a641L [Paramecium bursaria Chlorella virus 1]
gi|73852672|ref|YP_293956.1| hypothetical protein EhV_202 [Emiliania huxleyi virus 86]
gi|9631901|ref|NP_048689.1| PLPRNLLL (4X), SPPPSKP (3X) [Paramecium bursaria Chlorella virus 1]

Polydnaviridae (dsDNA)
gi|57753380|ref|YP_184838.1| hypothetical protein CcBVs18gp2 [Cotesia congregata virus]

Poxviridae (dsDNA)
gi|41057548|ref|NP_958021.1| ORF112 putative chemokine-binding protein [Bovine papular stomatitis virus]
gi|41057553|ref|NP_958026.1| ORF117 GM-CSF/IL-2 inhibition factor [Bovine papular stomatitis virus]
gi|9628943|ref|NP_043962.1| MC011L [Molluscum contagiosum virus]
gi|9633639|ref|NP_051875.1| M4.1 [Myxoma virus]
gi|9633798|ref|NP_051717.1| m4.1 [Myxoma virus]
gi|41057076|ref|NP_957790.1| ORF013 hypothetical protein [Orf virus]
gi|41057180|ref|NP_957894.1| ORF117 GM-CSF/IL-2 inhibition factor-like protein [Orf virus]

Hepadnaviridae (RT)
gi|21326586|ref|NP_647605.1| S protein [Hepatitis B virus]
gi|9630373|ref|NP_046801.1| surface protein [woolly monkey hepatitis B Virus]
gi|9628833|ref|NP_043867.1| small envelope protein [Arctic ground squirrel hepatitis B virus]
gi|40795676|ref|NP_955537.1| surface antigen [Ground squirrel hepatitis virus]
gi|38639786|ref|NP_944491.1| surface protein [Woodchuck hepatitis B virus]

Retroviridae (RT)
gi|19172954|ref|NP_579895.1| Envelope transmembrane glycoprotein gp41 [Human immunodeficiency virus 1]
gi|40317666|ref|NP_954656.1| Envelope transmembrane glycoprotein gp41 [Human immunodeficiency virus 1]
gi|9629363|ref|NP_057856.1| Envelope surface glycoprotein gp160, precursor [Human immunodeficiency virus 1]
gi|9628888|ref|NP_056844.1| env polyprotein [Human immunodeficiency virus 2]
gi|27311173|ref|NP_758892.1| env protein [Simian immunodeficiency virus 2]
gi|9629923|ref|NP_046130.1| env [Simian-Human immunodeficiency virus]
gi|45239019|ref|NP_777385.2| gp60 SU [Bovine leukemia virus]
gi|9626229|ref|NP_056899.1| gp60 SU [Bovine leukemia virus]
gi|9626960|ref|NP_057935.1| gPr80 [Murine leukemia virus]
gi|9626099|ref|NP_040334.1| envelope protein [Friend murine leukemia virus]
gi|9629517|ref|NP_044739.1| Env polyprotein [Rauscher murine leukemia virus]
gi|40018517|ref|NP_954554.1| env protein [Ovine lentivirus]

Coronaviridae (+ssRNA)
gi|12175749|ref|NP_073552.1| 4a protein [Human coronavirus 229E]
gi|12175748|ref|NP_073551.1| surface glycoprotein [Human coronavirus 229E]
gi|56807326|ref|YP_173238.1| spike glycoprotein [Human coronavirus HKU1]
gi|38018026|ref|NP_937950.1| S protein [Human coronavirus OC43]
gi|45655909|ref|YP_003767.1| spike protein [Human coronavirus NL63]
gi|9628706|ref|NP_043570.1| polyprotein precursor [GB virus C/Hepatitis G virus]
gi|9629719|ref|NP_045010.1| polyprotein precursor [Hepatitis GB virus A]
gi|28971396|ref|NP_803208.1| putative NS5A protein [GB virus C/Hepatitis G virus]
gi|29836496|ref|NP_828851.1| E2 glycoprotein precursor [SARS coronavirus]
gi|9626538|ref|NP_040831.1| spike protein [Avian infectious bronchitis virus]
gi|15081547|ref|NP_150077.1| spike structural protein [Bovine coronavirus]
gi|77118350|ref|YP_337907.1| spike glycoprotein [Breda virus]
gi|66391177|ref|YP_239357.1| M [Feline coronavirus]
gi|66391175|ref|YP_239355.1| S [Feline coronavirus]
gi|9629814|ref|NP_045300.1| E2 glycoprotein precursor [Murine hepatitis virus strain A59]
gi|60115395|ref|YP_209233.1| spike glycoprotein (S) [Murine hepatitis virus strain JHM]
gi|19387577|ref|NP_598310.1| spike protein [Porcine epidemic diarrhea virus]
gi|9635159|ref|NP_058424.1| spike protein [Transmissible gastroenteritis virus]
gi|13399294|ref|NP_058427.2| membrane protein [Transmissible gastroenteritis virus]

Flaviviridae (+ssRNA)
gi|27735339|ref|NP_776038.1| putative PreM protein [Cell fusing agent virus]
gi|25059133|ref|NP_739586.1| ns2b protein [Dengue virus type 2]
gi|73671174|ref|NP_740320.1| NS2B protein [Dengue virus type 4]
gi|24418985|ref|NP_722534.1| NS2B; nonstructural protein 2B; component of the virus-
gi|27696331|ref|NP_775669.1| non-structural protein NS2b [Japanese encephalitis virus]
encoded protease [Murray Valley encephalitis virus]
gi|56692449|ref|YP_164813.1| NS2b [Usutu virus]
gi|27735305|ref|NP_776017.1| non-structural protein NS2b [West Nile virus]

Luteoviridae (+ssRNA)
gi|20178353|ref|NP_620026.1| RNA-dependent RNA polymerase [Pea enation mosaic virus-1]
gi|20178351|ref|NP_619736.1| hypothetical protein [Pea enation mosaic virus-1]

Secoviridae (+ssRNA)
gi|19549044|ref|NP_599087.1| polyprotein [Strawberry mottle virus]

Sobemovirus (+ssRNA)
gi|38351800|ref|NP_941957.1| polyprotein [Cocksfoot mottle virus]
gi|10645643|ref|NP_066392.1| polyprotein [Sesbania mosaic virus]
gi|9627901|ref|NP_042301.1| polyprotein [Southern cowpea mosaic virus]
gi|21644718|ref|NP_660271.1| polyprotein [Southern bean mosaic virus]
gi|24323602|ref|NP_715627.1| polyprotein [Subterranean clover mottle virus]
gi|24323603|ref|NP_715628.1| polyprotein [Subterranean clover mottle virus]
gi|25013760|ref|NP_736579.1| serine protease [Subterranean clover mottle virus]

Tombusviridae (+ssRNA)
gi|9633808|ref|NP_051882.1| polymerase-associated protein [Carnation mottle virus]
gi|9633806|ref|NP_051883.1| polymerase-associated protein [Carnation mottle virus]
gi|9633805|ref|NP_051884.1| polymerase-associated protein [Carnation mottle virus]
gi|39163633|ref|NP_945124.1| p27 protein [Pelargonium flower break virus]
gi|39163632|ref|NP_945123.1| p86 protein [Pelargonium flower break virus]
gi|39163631|ref|NP_945122.1| p99 protein [Pelargonium flower break virus]
gi|9629191|ref|NP_044383.1| replication-related protein [Saguaro cactus virus]
gi|9629194|ref|NP_044382.1| SCVP86 [Saguaro cactus virus]
gi|19774243|ref|NP_608311.1| 82 kDa protein [Tobacco necrosis virus D]

Bunyaviridae (-ssRNA)
gi|39840946|ref|NP_950235.1| glycoprotein precursor [Crimean-Congo hemorrhagic fever virus]
gi|22788701|ref|NP_690575.1| glycoprotein precursor [Dugbe virus]
gi|20153372|ref|NP_619703.1| glycoprotein precursor [Groundnut bud necrosis virus]
gi|9632387|ref|NP_049359.1| G1 [Tomato spotted wilt virus]
gi|20564190|ref|NP_620767.1| glycoprotein precursor [Watermelon spotted wilt virus]

Bornaviridae (-ssRNA)
gi|9627497|ref|NP_042023.1| Glycoprotein [Borna disease virus]

Filoviridae (-ssRNA)
gi|22789226|ref|NP_690584.1| small/secreted non-structural glycoprotein [Reston ebolavirus]
gi|22789230|ref|NP_690583.1| structural glycoprotein [Reston ebolavirus]
gi|55770811|ref|YP_138524.1| nonstructural, soluble, secreted glycoprotein [Sudan ebolavirus]
gi|55770812|ref|YP_138523.1| structural glycoprotein [Sudan ebolavirus]
gi|10313994|ref|NP_066247.1| sGP [Zaire ebolavirus]
gi|10313996|ref|NP_066248.1| ssGP [Zaire ebolavirus
gi|10313995|ref|NP_066246.1| virion spike glycoprotein precursor [Zaire ebolavirus]

Paramyxoviridae (-ssRNA)
gi|34482043|ref|NP_899659.1| fusion protein F [Fer-de-lance virus]

Rhabdoviridae (-ssRNA)
gi|10086566|ref|NP_065402.1| virion transmembrane glycoprotein G [Bovine ephemeral fever virus]
gi|34610118|ref|NP_919033.1| glycoprotein [Hirame rhabdovirus]
gi|9628086|ref|NP_042679.1| glycoprotein [Infectious hematopoietic necrosis virus]
gi|50234103|ref|YP_052848.1| G [Maize fine streak virus]
gi|50234111|ref|YP_052854.1| G [Maize mosaic virus]
gi|55793421|ref|YP_142353.1| transmembrane glycoprotein G [Mokola virus]
gi|9633481|ref|NP_050583.1| transmembrane envelope protein [snakehead rhabdovirus]
gi|14336458|ref|NP_116747.1| glycoprotein [Spring viremia of carp virus]
gi|62327484|ref|YP_224082.1| G [Taro vein chlorosis virus]
gi|66508433|ref|YP_238533.1| glycoprotein [Tupaia rhabdovirus]
gi|9627233|ref|NP_041715.1| glycoprotein (G protein) precursor [Vesicular stomatitis Indiana virus]
gi|9632554|ref|NP_049548.1| glycoprotein [Viral hemorrhagic septicemia virus]

Orthomyxoviridae (-ssRNA)
gi|73919207|ref|YP_308839.1| hemagglutinin [Influenza A virus (A/New York/392/2004(H3N2))]
gi|52673231|ref|YP_089658.1| CM2 protein [Influenza C virus]
gi|56403995|ref|YP_145799.1| P5 [Infectious salmon anemia virus

REFERENCES CITED

Abeijon, C., and Hirschberg, C. B. (1992). Topography of glycosylation reactions in the endoplasmic reticulum. *Trends Biochem Sci* **17**(1)**,** 32-6.

Alazard-Dany, N., Volchkova, V., Reynard, O., Carbonnelle, C., Dolnik, O., Ottmann, M., Khromykh, A., and Volchkov, V. E. (2006). Ebola virus glycoprotein GP is not cytotoxic when expressed constitutively at a moderate level. *J Gen Virol* **87**(Pt 5)**,** 1247-57.

Alcami, A., and Koszinowski, U. H. (2000). Viral mechanisms of immune evasion. *Immunol Today* **21**(9)**,** 447-55.

Aleksandrowicz, P., Falzarano, D., Feldmann, H., and Schnittler, H. J. (2008). *ELSO Meeting – Frontiers of cellular, developmental and molecular biology, Nice, France*.

Alvarez, C. P., Lasala, F., Carrillo, J., Muniz, O., Corbi, A. L., and Delgado, R. (2002). C-type lectins DC-SIGN and L-SIGN mediate cellular entry by Ebola virus in cis and in trans. *J Virol* **76**(13)**,** 6841-4.

Aman, M. J., Bosio, C. M., Panchal, R. G., Burnett, J. C., Schmaljohn, A., and Bavari, S. (2003). Molecular mechanisms of filovirus cellular trafficking. *Microbes Infect* **5**(7)**,** 639-49.

Amblard, J., Obiang, P., Edzang, S., Prehaud, C., Bouloy, M., and Guenno, B. L. (1997). Identification of the Ebola virus in Gabon in 1994. *Lancet* **349**(9046)**,** 181-2.

Arrighi, J. F., Pion, M., Garcia, E., Escola, J. M., van Kooyk, Y., Geijtenbeek, T. B., and Piguet, V. (2004). DC-SIGN-mediated infectious synapse formation enhances X4 HIV-1 transmission from dendritic cells to T cells. *J Exp Med* **200**(10)**,** 1279-88.

Baize, S., Leroy, E. M., Georges-Courbot, M. C., Capron, M., Lansoud-Soukate, J., Debre, P., Fisher-Hoch, S. P., McCormick, J. B., and Georges, A. J. (1999). Defective humoral responses and extensive intravascular apoptosis are associated with fatal outcome in Ebola virus-infected patients. *Nat Med* **5**(4)**,** 423-6.

Baize, S., Leroy, E. M., Georges, A. J., Georges-Courbot, M. C., Capron, M., Bedjabaga, I., Lansoud-Soukate, J., and Mavoungou, E. (2002). Inflammatory responses in Ebola virus-infected patients. *Clin Exp Immunol* **128**(1)**,** 163-8.

Baize, S., Leroy, E. M., Mavoungou, E., and Fisher-Hoch, S. P. (2000). Apoptosis in fatal Ebola infection. Does the virus toll the bell for immune system? *Apoptosis* **5**(1)**,** 5-7.

Banerji, S., Hide, B. R., James, J. R., Noble, M. E., and Jackson, D. G. (2009). Distinctive properties of the hyaluronan binding domain in the lymphatic hyaluronan receptor Lyve-1 and their implications for receptor function. *J Biol Chem*.

Bar, S., Takada, A., Kawaoka, Y., and Alizon, M. (2006). Detection of cell-cell fusion mediated by Ebola virus glycoproteins. *J Virol* **80**(6)**,** 2815-22.

Baron, R. C., McCormick, J. B., and Zubeir, O. A. (1983). Ebola virus disease in southern Sudan: hospital dissemination and intrafamilial spread. *Bull World Health Organ* **61**(6)**,** 997-1003.

Barrette, R. W., Metwally, S. A., Rowland, J. M., Xu, L., Zaki, S. R., Nichol, S. T., Rollin, P. E., Towner, J. S., Shieh, W. J., Batten, B., Sealy, T. K., Carrillo, C., Moran, K. E., Bracht, A. J., Mayr, G. A., Sirios-Cruz, M., Catbagan, D. P.,

Lautner, E. A., Ksiazek, T. G., White, W. R., and McIntosh, M. T. (2009). Discovery of swine as a host for the Reston ebolavirus. *Science* **325**(5937)**,** 204-6.

Barrientos, L. G., Martin, A. M., Rollin, P. E., and Sanchez, A. (2004). Disulfide bond assignment of the Ebola virus secreted glycoprotein SGP. *Biochem Biophys Res Commun* **323**(2)**,** 696-702.

Barrientos, L. G., Martin, A. M., Wohlhueter, R. M., and Rollin, P. E. (2007). Secreted glycoprotein from Live Zaire ebolavirus-infected cultures: preparation, structural and biophysical characterization, and thermodynamic stability. *J Infect Dis* **196 Suppl 2,** S220-31.

Barstad, R. M., Hamers, M. J., Stephens, R. W., and Sakariassen, K. S. (1995). Retinoic acid reduces induction of monocyte tissue factor and tissue factor/factor VIIa-dependent arterial thrombus formation. *Blood* **86**(1)**,** 212-8.

Bashirova, A. A., Geijtenbeek, T. B., van Duijnhoven, G. C., van Vliet, S. J., Eilering, J. B., Martin, M. P., Wu, L., Martin, T. D., Viebig, N., Knolle, P. A., KewalRamani, V. N., van Kooyk, Y., and Carrington, M. (2001). A dendritic cell-specific intercellular adhesion molecule 3-grabbing nonintegrin (DC-SIGN)-related protein is highly expressed on human liver sinusoidal endothelial cells and promotes HIV-1 infection. *J Exp Med* **193**(6)**,** 671-8.

Baskerville, A., Bowen, E. T., Platt, G. S., McArdell, L. B., and Simpson, D. I. (1978). The pathology of experimental Ebola virus infection in monkeys. *J Pathol* **125**(3)**,** 131-8.

Baskerville, A., Fisher-Hoch, S. P., Neild, G. H., and Dowsett, A. B. (1985). Ultrastructural pathology of experimental Ebola haemorrhagic fever virus infection. *J Pathol* **147**(3)**,** 199-209.

Basler, C. F., and Amarasinghe, G. K. (2009). Evasion of interferon responses by Ebola and Marburg viruses. *J Interferon Cytokine Res* **29**(9)**,** 511-20.

Basler, C. F., Mikulasova, A., Martinez-Sobrido, L., Paragas, J., Muhlberger, E., Bray, M., Klenk, H. D., Palese, P., and Garcia-Sastre, A. (2003). The Ebola virus VP35 protein inhibits activation of interferon regulatory factor 3. *J Virol* **77**(14)**,** 7945-56.

Basler, C. F., Wang, X., Muhlberger, E., Volchkov, V., Paragas, J., Klenk, H. D., Garcia-Sastre, A., and Palese, P. (2000). The Ebola virus VP35 protein functions as a type I IFN antagonist. *Proc Natl Acad Sci U S A* **97**(22)**,** 12289-94.

Bausch, D. G., Towner, J. S., Dowell, S. F., Kaducu, F., Lukwiya, M., Sanchez, A., Nichol, S. T., Ksiazek, T. G., and Rollin, P. E. (2007). Assessment of the risk of Ebola virus transmission from bodily fluids and fomites. *J Infect Dis* **196 Suppl 2,** S142-7.

Bavari, S., Bosio, C. M., Wiegand, E., Ruthel, G., Will, A. B., Geisbert, T. W., Hevey, M., Schmaljohn, C., Schmaljohn, A., and Aman, M. J. (2002). Lipid raft microdomains: a gateway for compartmentalized trafficking of Ebola and Marburg viruses. *J Exp Med* **195**(5)**,** 593-602.

Becker, S., Klenk, H. D., and Muhlberger, E. (1996). Intracellular transport and processing of the Marburg virus surface protein in vertebrate and insect cells. *Virology* **225**(1)**,** 145-55.

Bergh, N., Ulfhammer, E., Glise, K., Jern, S., and Karlsson, L. (2009). Influence of TNF-alpha and biomechanical stress on endothelial anti- and prothrombotic genes. *Biochem Biophys Res Commun* **385**(3)**,** 314-8.

Boehmann, Y., Enterlein, S., Randolf, A., and Muhlberger, E. (2005). A reconstituted replication and transcription system for Ebola virus Reston and comparison with Ebola virus Zaire. *Virology* **332**(1)**,** 406-17.

Bowen, E. T., Lloyd, G., Harris, W. J., Platt, G. S., Baskerville, A., and Vella, E. E. (1977). Viral haemorrhagic fever in southern Sudan and northern Zaire. Preliminary studies on the aetiological agent. *Lancet* **1**(8011)**,** 571-3.

Bray, M., Davis, K., Geisbert, T., Schmaljohn, C., and Huggins, J. (1998). A mouse model for evaluation of prophylaxis and therapy of Ebola hemorrhagic fever. *J Infect Dis* **178**(3)**,** 651-61.

Bray, M., Hatfill, S., Hensley, L., and Huggins, J. W. (2001). Haematological, biochemical and coagulation changes in mice, guinea-pigs and monkeys infected with a mouse-adapted variant of Ebola Zaire virus. *J Comp Pathol* **125**(4)**,** 243-53.

Bray, M., and Mahanty, S. (2003). Ebola hemorrhagic fever and septic shock. *J Infect Dis* **188**(11)**,** 1613-7.

Breen, L. T., McHugh, P. E., and Murphy, B. P. (2009). Multi-axial mechanical stimulation of HUVECs demonstrates that combined loading is not equivalent to the superposition of individual wall shear stress and tensile hoop stress components. *J Biomech Eng* **131**(8)**,** 081001.

Brindley, M. A., Hughes, L., Ruiz, A., McCray, P. B., Jr., Sanchez, A., Sanders, D. A., and Maury, W. (2007). Ebola virus glycoprotein 1: identification of residues important for binding and postbinding events. *J Virol* **81**(14)**,** 7702-9.

Bwaka, M. A., Bonnet, M. J., Calain, P., Colebunders, R., De Roo, A., Guimard, Y., Katwiki, K. R., Kibadi, K., Kipasa, M. A., Kuvula, K. J., Mapanda, B. B., Massamba, M., Mupapa, K. D., Muyembe-Tamfum, J. J., Ndaberey, E., Peters, C. J., Rollin, P. E., Van den Enden, E., and Van den Enden, E. (1999). Ebola hemorrhagic fever in Kikwit, Democratic Republic of the Congo: clinical observations in 103 patients. *J Infect Dis* **179 Suppl 1,** S1-7.

Cambi, A., Koopman, M., and Figdor, C. G. (2005). How C-type lectins detect pathogens. *Cell Microbiol* **7**(4)**,** 481-8.

Camerer, E., Kolsto, A. B., and Prydz, H. (1996). Cell biology of tissue factor, the principal initiator of blood coagulation. *Thromb Res* **81**(1)**,** 1-41.

CDC (1976). Follow-up on Viral Hemorrhagic Fever - Zaire, United Kingdom. *MMWR Morb Mortal Wkly Rep* **25 (47),** 378, 383.

CDC (1979). Ebola Hemorrhagic Fever - Southern Sudan. *MMWR Morb Mortal Wkly Rep* **28(47)**(557-559).

CDC (1995a). Ebola haemorrhagic fever. *Wkly Epidemiol Rec* **70**(34)**,** 241-2.

CDC (1995b). Outbreak of Ebola viral hemorrhagic fever--Zaire, 1995. *MMWR Morb Mortal Wkly Rep* **44**(19)**,** 381-2.

CDC (1995c). Update: outbreak of Ebola viral hemorrhagic fever--Zaire, 1995. *MMWR Morb Mortal Wkly Rep* **44**(25)**,** 468-9, 475.

CDC (1995d). Update: outbreak of Ebola viral hemorrhagic fever--Zaire, 1995. *MMWR Morb Mortal Wkly Rep* **44**(20)**,** 399.

CDC (2001). Outbreak of Ebola hemorrhagic fever Uganda, August 2000-January 2001. *MMWR Morb Mortal Wkly Rep* **50**(5)**,** 73-7.

Chadwick, M. P., Westley, B. R., and May, F. E. (1997). Homodimerization and hetero-oligomerization of the single-domain trefoil protein pNR-2/pS2 through cysteine 58. *Biochem J* **327 (Pt 1),** 117-23.

Chakrabartty, A., Kortemme, T., and Baldwin, R. L. (1994). Helix propensities of the amino acids measured in alanine-based peptides without helix-stabilizing side-chain interactions. *Protein Sci* **3,** 843-852.

Chan, S. Y., Empig, C. J., Welte, F. J., Speck, R. F., Schmaljohn, A., Kreisberg, J. F., and Goldsmith, M. A. (2001). Folate receptor-alpha is a cofactor for cellular entry by Marburg and Ebola viruses. *Cell* **106**(1)**,** 117-26.

Chan, S. Y., Ma, M. C., and Goldsmith, M. A. (2000). Differential induction of cellular detachment by envelope glycoproteins of Marburg and Ebola (Zaire) viruses. *J Gen Virol* **81**(Pt 9)**,** 2155-9.

Chan, S. Y., Speck, R. F., Ma, M. C., and Goldsmith, M. A. (2000). Distinct mechanisms of entry by envelope glycoproteins of Marburg and Ebola (Zaire) viruses. *J Virol* **74**(10)**,** 4933-7.

Chandran, K., Sullivan, N. J., Felbor, U., Whelan, S. P., and Cunningham, J. M. (2005). Endosomal proteolysis of the Ebola virus glycoprotein is necessary for infection. *Science* **308**(5728)**,** 1643-5.

Chang, T. H., Kubota, T., Matsuoka, M., Jones, S., Bradfute, S. B., Bray, M., and Ozato, K. (2009). Ebola Zaire virus blocks type I interferon production by exploiting the host SUMO modification machinery. *PLoS Pathog* **5**(6)**,** e1000493.

Chepurnov, A. A., Tuzova, M. N., Ternovoy, V. A., and Chernukhin, I. V. (1999). Suppressive effect of Ebola virus on T cell proliferation in vitro is provided by a 125-kDa GP viral protein. *Immunol Lett* **68**(2-3)**,** 257-61.

Chung, C. T., Niemela, S. L., and Miller, R. H. (1989). One-step preparation of competent Escherichia coli: transformation and storage of bacterial cells in the same solution. *Proc Natl Acad Sci U S A* **86**(7)**,** 2172-5.

Cicha, I., Beronov, K., Ramirez, E. L., Osterode, K., Goppelt-Struebe, M., Raaz, D., Yilmaz, A., Daniel, W. G., and Garlichs, C. D. (2009). Shear stress preconditioning modulates endothelial susceptibility to circulating TNF-alpha and monocytic cell recruitment in a simplified model of arterial bifurcations. *Atherosclerosis* **207**(1)**,** 93-102.

Clarke, B. L., Naylor, C., and Lennarz, W. J. (1989). Comparative studies on mannosylphosphoryl dolichol and glucosylphosphoryl dolichol synthases. *Chem Phys Lipids* **51**(3-4)**,** 239-47.

Claude, P. (1978). Morphological factors influencing transepithelial permeability: a model for the resistance of the zonula occludens. *J Membr Biol* **39**(2-3)**,** 219-32.

Connolly, B. M., Steele, K. E., Davis, K. J., Geisbert, T. W., Kell, W. M., Jaax, N. K., and Jahrling, P. B. (1999). Pathogenesis of experimental Ebola virus infection in guinea pigs. *J Infect Dis* **179 Suppl 1,** S203-17.

Craig, R., Krokhin, O., Wilkins, J., and Beavis, R. C. (2003). Implementation of an algorithm for modeling disulfide bond patterns using mass spectrometry. *J Proteome Res* **2**(6)**,** 657-61.

Crary, S. M., Towner, J. S., Honig, J. E., Shoemaker, T. R., and Nichol, S. T. (2003). Analysis of the role of predicted RNA secondary structures in Ebola virus replication. *Virology* **306**(2)**,** 210-8.

Culotta, E., and Koshland, D. E., Jr. (1992). NO news is good news. *Science* **258**(5090)**,** 1862-5.

Cyranoski, D. (2009). Ebola outbreak has experts rooting for answers. *Nature* **457**(7228)**,** 364-5.

Dalgard, D. W., Hardy, R. J., Pearson, S. L., Pucak, G. J., Quander, R. V., Zack, P. M., Peters, C. J., and Jahrling, P. B. (1992). Combined simian hemorrhagic fever and Ebola virus infection in cynomolgus monkeys. *Lab Anim Sci* **42**(2)**,** 152-7.

Davis, K. J., Anderson, A. O., Geisbert, T. W., Steele, K. E., Geisbert, J. B., Vogel, P., Connolly, B. M., Huggins, J. W., Jahrling, P. B., and Jaax, N. K. (1997). Pathology of experimental Ebola virus infection in African green monkeys. Involvement of fibroblastic reticular cells. *Arch Pathol Lab Med* **121**(8)**,** 805-19.

de Beer, T., Vliegenthart, J. F., Loffler, A., and Hofsteenge, J. (1995). The hexopyranosyl residue that is C-glycosidically linked to the side chain of tryptophan-7 in human RNase US is α-mannopyranose. *Biochemistry* **34,** 11785-11789.

de Silva, A. M., Balch, W. E., and Helenius, A. (1990). Quality control in the endoplasmic reticulum: folding and misfolding of vesicular stomatitis virus G protein in cells and in vitro. *J Cell Biol* **111**(3)**,** 857-66.

Dejana, E., Spagnuolo, R., and Bazzoni, G. (2001). Interendothelial junctions and their role in the control of angiogenesis, vascular permeability and leukocyte transmigration. *Thromb Haemost* **86**(1)**,** 308-15.

del Sol, A., and O'Meara, P. (2005). Small-world network approach to identify key residues in protein-protein interaction. *Proteins* **58**(3)**,** 672-82.

DePaola, N., Phelps, J. E., Florez, L., Keese, C. R., Minnear, F. L., Giaever, I., and Vincent, P. (2001). Electrical impedance of cultured endothelium under fluid flow. *Ann Biomed Eng* **29**(8)**,** 648-56.

Dieterich, P., Odenthal-Schnittler, M., Mrowietz, C., Kramer, M., Sasse, L., Oberleithner, H., and Schnittler, H. J. (2000). Quantitative morphodynamics of endothelial cells within confluent cultures in response to fluid shear stress. *Biophys J* **79**(3)**,** 1285-97.

Dolnik, O., Kolesnikova, L., and Becker, S. (2008). Filoviruses: Interactions with the host cell. *Cell Mol Life Sci* **65**(5)**,** 756-76.

Dolnik, O., Volchkova, V., Garten, W., Carbonnelle, C., Becker, S., Kahnt, J., Stroher, U., Klenk, H. D., and Volchkov, V. (2004). Ectodomain shedding of the glycoprotein GP of Ebola virus. *Embo J* **23**(10)**,** 2175-84.

Doucey, M. A., Hess, D., Blommers, M. J., and Hofsteenge, J. (1999). Recombinant human interleukin-12 is the second example of a C-mannosylated protein. *Glycobiology* **9**(5)**,** 435-41.

Doucey, M. A., Hess, D., Cacan, R., and Hofsteenge, J. (1998). Protein C-mannosylation is enzyme-catalysed and uses dolichyl-phosphate-mannose as a precursor. *Mol Biol Cell* **9**(2)**,** 291-300.

Drake, T. A., Morrissey, J. H., and Edgington, T. S. (1989). Selective cellular expression of tissue factor in human tissues. Implications for disorders of hemostasis and thrombosis. *Am J Pathol* **134**(5)**,** 1087-97.

Ebihara, H., Takada, A., Kobasa, D., Jones, S., Neumann, G., Theriault, S., Bray, M., Feldmann, H., and Kawaoka, Y. (2006). Molecular determinants of Ebola virus virulence in mice. *PLoS Pathog* **2**(7)**,** e73.

Elliott, L. H., Kiley, M. P., and McCormick, J. B. (1985). Descriptive analysis of Ebola virus proteins. *Virology* **147**(1)**,** 169-76.

Elliott, L. H., Sanchez, A., Holloway, B. P., Kiley, M. P., and McCormick, J. B. (1993). Ebola protein analyses for the determination of genetic organization. *Arch Virol* **133**(3-4)**,** 423-36.

Emond, R. T., Evans, B., Bowen, E. T., and Lloyd, G. (1977). A case of Ebola virus infection. *Br Med J* **2**(6086)**,** 541-4.

Empig, C. J., and Goldsmith, M. A. (2002). Association of the caveola vesicular system with cellular entry by filoviruses. *J Virol* **76**(10)**,** 5266-70.

Engering, A., Geijtenbeek, T. B., van Vliet, S. J., Wijers, M., van Liempt, E., Demaurex, N., Lanzavecchia, A., Fransen, J., Figdor, C. G., Piguet, V., and van Kooyk, Y. (2002). The dendritic cell-specific adhesion receptor DC-SIGN internalizes antigen for presentation to T cells. *J Immunol* **168**(5)**,** 2118-26.

Ervin, L. A., Ball, L. E., Crouch, R. K., and Schey, K. L. (2005). Phosphorylation and glycosylation of bovine lens MP20. *Invest Ophthalmol Vis Sci* **46**(2)**,** 627-35.

Esmon, C. T. (2008). Crosstalk between inflammation and thrombosis. *Maturitas* **61**(1-2)**,** 122-31.

Esser, S., Wolburg, K., Wolburg, H., Breier, G., Kurzchalia, T., and Risau, W. (1998). Vascular endothelial growth factor induces endothelial fenestrations in vitro. *J Cell Biol* **140**(4)**,** 947-59.

Falzarano, D., Krokhin, O., Van Domselaar, G., Wolf, K., Seebach, J., Schnittler, H. J., and Feldmann, H. (2007). Ebola sGP--the first viral glycoprotein shown to be C-mannosylated. *Virology* **368**(1)**,** 83-90.

Falzarano, D., Krokhin, O., Wahl-Jensen, V., Seebach, J., Wolf, K., Schnittler, H. J., and Feldmann, H. (2006). Structure-function analysis of the soluble glycoprotein, sGP, of Ebola virus. *Chembiochem* **7**(10)**,** 1605-11.

Faulk, W. P., Labarrere, C. A., and Carson, S. D. (1990). Tissue factor: identification and characterization of cell types in human placentae. *Blood* **76**(1)**,** 86-96.

Faust, S. N., Heyderman, R. S., and Levin, M. (2001). Coagulation in severe sepsis: a central role for thrombomodulin and activated protein C. *Crit Care Med* **29**(7 Suppl)**,** S62-7; discussion S67-8.

Feldmann, H., Bugany, H., Mahner, F., Klenk, H. D., Drenckhahn, D., and Schnittler, H. J. (1996). Filovirus-induced endothelial leakage triggered by infected monocytes/macrophages. *J Virol* **70**(4)**,** 2208-14.

Feldmann, H., Geisbert, T., Jahrling, P., Klenk, H. D., Netesov, S. V., Peters, C. J., Sanchez, A., Swanepoel, R., and Volchkov, V., Eds. (2005). Virus Taxonomy, Eighth Report of the International Committee on the Taxonomy of Viruses. Edited by C. M. Fauquet, M. A. Mayo, J. Maniloff, U. Desselberger, and L. A. Ball. San Diego, CA: Elsevier.

Feldmann, H., Jones, S., Klenk, H. D., and Schnittler, H. J. (2003). Ebola virus: from discovery to vaccine. *Nat Rev Immunol* **3**(8)**,** 677-85.

Feldmann, H., Jones, S. M., Daddario-Dicaprio, K. M., Geisbert, J. B., Stroher, U., Grolla, A., Bray, M., Fritz, E. A., Fernando, L., Feldmann, F., Hensley, L. E., and

Geisbert, T. W. (2007). Effective Post-Exposure Treatment of Ebola Infection. *PLoS Pathog* **3**(1)**,** e2.

Feldmann, H., and Kiley, M. P. (1999). Classification, structure, and replication of filoviruses. *Curr Top Microbiol Immunol* **235,** 1-21.

Feldmann, H., Klenk, H. D., and Sanchez, A. (1993). Molecular biology and evolution of filoviruses. *Arch Virol Suppl* **7,** 81-100.

Feldmann, H., Nichol, S. T., Klenk, H. D., Peters, C. J., and Sanchez, A. (1994). Characterization of filoviruses based on differences in structure and antigenicity of the virion glycoprotein. *Virology* **199**(2)**,** 469-73.

Feldmann, H., Volchkov, V. E., Volchkova, V. A., and Klenk, H. D. (1999). The glycoproteins of Marburg and Ebola virus and their potential roles in pathogenesis. *Arch Virol Suppl* **15,** 159-69.

Feldmann, H., Volchkov, V. E., Volchkova, V. A., Stroher, U., and Klenk, H. D. (2001). Biosynthesis and role of filoviral glycoproteins. *J Gen Virol* **82**(Pt 12)**,** 2839-48.

Ferrero, E. (2004). Assessment of TNFa-induced endothelial damage through the loss of its barrier function. *In* "Tumor Necrosis Factor Methods and Protocols" (A. Corti, and P. Ghezzi, Eds.), pp. 127-136. Humana Press, Totowa, NJ.

Ferron, F., Longhi, S., Henrissat, B., and Canard, B. (2002). Viral RNA-polymerases -- a predicted 2'-O-ribose methyltransferase domain shared by all Mononegavirales. *Trends Biochem Sci* **27**(5)**,** 222-4.

Fisher-Hoch, S. P., Brammer, T. L., Trappier, S. G., Hutwagner, L. C., Farrar, B. B., Ruo, S. L., Brown, B. G., Hermann, L. M., Perez-Oronoz, G. I., Goldsmith, C. S., and et al. (1992). Pathogenic potential of filoviruses: role of geographic origin of primate host and virus strain. *J Infect Dis* **166**(4)**,** 753-63.

Fisher-Hoch, S. P., Platt, G. S., Lloyd, G., Simpson, D. I., Neild, G. H., and Barrett, A. J. (1983). Haematological and biochemical monitoring of Ebola infection in rhesus monkeys: implications for patient management. *Lancet* **2**(8358)**,** 1055-8.

Fisher-Hoch, S. P., Platt, G. S., Neild, G. H., Southee, T., Baskerville, A., Raymond, R. T., Lloyd, G., and Simpson, D. I. (1985). Pathophysiology of shock and hemorrhage in a fulminating viral infection (Ebola). *J Infect Dis* **152**(5)**,** 887-94.

Fleck, R. A., Rao, L. V., Rapaport, S. I., and Varki, N. (1990). Localization of human tissue factor antigen by immunostaining with monospecific, polyclonal anti-human tissue factor antibody. *Thromb Res* **59**(2)**,** 421-37.

Flossel, C., Luther, T., Muller, M., Albrecht, S., and Kasper, M. (1994). Immunohistochemical detection of tissue factor (TF) on paraffin sections of routinely fixed human tissue. *Histochemistry* **101**(6)**,** 449-53.

Formenty, P., Hatz, C., Le Guenno, B., Stoll, A., Rogenmoser, P., and Widmer, A. (1999). Human infection due to Ebola virus, subtype Cote d'Ivoire: clinical and biologic presentation. *J Infect Dis* **179 Suppl 1,** S48-53.

Freitas, M. S., Gaspar, L. P., Lorenzoni, M., Almeida, F. C., Tinoco, L. W., Almeida, M. S., Maia, L. F., Degreve, L., Valente, A. P., and Silva, J. L. (2007). Structure of the Ebola fusion peptide in a membrane-mimetic environment and the interaction with lipid rafts. *J Biol Chem* **282**(37)**,** 27306-14.

Furmanek, A., Hess, D., Rogniaux, H., and Hofsteenge, J. (2003). The WSAWS motif is C-hexosylated in a soluble form of the erythropoietin receptor. *Biochemistry* **42**(28)**,** 8452-8.

Furmanek, A., and Hofsteenge, J. (2000). Protein C-mannosylation: facts and questions. *Acta Biochim Pol* **47**(3)**,** 781-9.

Gade, G., Kellner, R., Rinehart, K. L., and Proefke, M. L. (1992). A tryptophan-substituted member of the AKH/RPCH family isolated from a stick insect corpus cardiacum. *Biochem Biophys Res Commun* **189**(3)**,** 1303-9.

Gallaher, W. R. (1996). Similar structural models of the transmembrane proteins of Ebola and avian sarcoma viruses. *Cell* **85**(4)**,** 477-8.

Geijtenbeek, T. B., Krooshoop, D. J., Bleijs, D. A., van Vliet, S. J., van Duijnhoven, G. C., Grabovsky, V., Alon, R., Figdor, C. G., and van Kooyk, Y. (2000). DC-SIGN-ICAM-2 interaction mediates dendritic cell trafficking. *Nat Immunol* **1**(4)**,** 353-7.

Geijtenbeek, T. B., and van Kooyk, Y. (2003). Pathogens target DC-SIGN to influence their fate DC-SIGN functions as a pathogen receptor with broad specificity. *Apmis* **111**(7-8)**,** 698-714.

Geisbert, T. W., Daddario-DiCaprio, K. M., Geisbert, J. B., Young, H. A., Formenty, P., Fritz, E. A., Larsen, T., and Hensley, L. E. (2007). Marburg virus Angola infection of rhesus macaques: pathogenesis and treatment with recombinant nematode anticoagulant protein c2. *J Infect Dis* **196 Suppl 2,** S372-81.

Geisbert, T. W., Hensley, L. E., Gibb, T. R., Steele, K. E., Jaax, N. K., and Jahrling, P. B. (2000). Apoptosis induced in vitro and in vivo during infection by Ebola and Marburg viruses. *Lab Invest* **80**(2)**,** 171-86.

Geisbert, T. W., Hensley, L. E., Jahrling, P. B., Larsen, T., Geisbert, J. B., Paragas, J., Young, H. A., Fredeking, T. M., Rote, W. E., and Vlasuk, G. P. (2003a). Treatment of Ebola virus infection with a recombinant inhibitor of factor VIIa/tissue factor: a study in rhesus monkeys. *Lancet* **362**(9400)**,** 1953-8.

Geisbert, T. W., Hensley, L. E., Larsen, T., Young, H. A., Reed, D. S., Geisbert, J. B., Scott, D. P., Kagan, E., Jahrling, P. B., and Davis, K. J. (2003b). Pathogenesis of Ebola hemorrhagic fever in cynomolgus macaques: evidence that dendritic cells are early and sustained targets of infection. *Am J Pathol* **163**(6)**,** 2347-70.

Geisbert, T. W., and Jahrling, P. B. (1995). Differentiation of filoviruses by electron microscopy. *Virus Res* **39**(2-3)**,** 129-50.

Geisbert, T. W., and Jahrling, P. B. (2004). Exotic emerging viral diseases: progress and challenges. *Nat Med* **10**(12 Suppl)**,** S110-21.

Geisbert, T. W., Jahrling, P. B., Hanes, M. A., and Zack, P. M. (1992). Association of Ebola-related Reston virus particles and antigen with tissue lesions of monkeys imported to the United States. *J Comp Pathol* **106**(2)**,** 137-52.

Geisbert, T. W., Young, H. A., Jahrling, P. B., Davis, K. J., Kagan, E., and Hensley, L. E. (2003c). Mechanisms underlying coagulation abnormalities in ebola hemorrhagic fever: overexpression of tissue factor in primate monocytes/macrophages is a key event. *J Infect Dis* **188**(11)**,** 1618-29.

Geisbert, T. W., Young, H. A., Jahrling, P. B., Davis, K. J., Larsen, T., Kagan, E., and Hensley, L. E. (2003d). Pathogenesis of Ebola hemorrhagic fever in primate models: evidence that hemorrhage is not a direct effect of virus-induced cytolysis of endothelial cells. *Am J Pathol* **163**(6)**,** 2371-82.

Georges, A. J., Leroy, E. M., Renaut, A. A., Benissan, C. T., Nabias, R. J., Ngoc, M. T., Obiang, P. I., Lepage, J. P., Bertherat, E. J., Benoni, D. D., Wickings, E. J., Amblard, J. P., Lansoud-Soukate, J. M., Milleliri, J. M., Baize, S., and Georges-

Courbot, M. C. (1999). Ebola hemorrhagic fever outbreaks in Gabon, 1994-1997: epidemiologic and health control issues. *J Infect Dis* **179 Suppl 1,** S65-75.

Gibb, T. R., Bray, M., Geisbert, T. W., Steele, K. E., Kell, W. M., Davis, K. J., and Jaax, N. K. (2001). Pathogenesis of experimental Ebola Zaire virus infection in BALB/c mice. *J Comp Pathol* **125**(4)**,** 233-42.

Gomis-Ruth, F. X., Dessen, A., Timmins, J., Bracher, A., Kolesnikowa, L., Becker, S., Klenk, H. D., and Weissenhorn, W. (2003). The matrix protein VP40 from Ebola virus octamerizes into pore-like structures with specific RNA binding properties. *Structure* **11**(4)**,** 423-33.

Gonzalez de Peredo, A., Klein, D., Macek, B., Hess, D., Peter-Katalinic, J., and Hofsteenge, J. (2002). C-mannosylation and o-fucosylation of thrombospondin type 1 repeats. *Mol Cell Proteomics* **1**(1)**,** 11-8.

Gorman, J. J., Wallis, T. P., and Pitt, J. J. (2002). Protein disulfide bond determination by mass spectrometry. *Mass Spectrom Rev* **21**(3)**,** 183-216.

Gramberg, T., Hofmann, H., Moller, P., Lalor, P. F., Marzi, A., Geier, M., Krumbiegel, M., Winkler, T., Kirchhoff, F., Adams, D. H., Becker, S., Munch, J., and Pohlmann, S. (2005). LSECtin interacts with filovirus glycoproteins and the spike protein of SARS coronavirus. *Virology* **340**(2)**,** 224-36.

Groseth, A., Feldmann, H., Theriault, S., Mehmetoglu, G., and Flick, R. (2005). RNA polymerase I-driven minigenome system for Ebola viruses. *J Virol* **79**(7)**,** 4425-33.

Halary, F., Amara, A., Lortat-Jacob, H., Messerle, M., Delaunay, T., Houles, C., Fieschi, F., Arenzana-Seisdedos, F., Moreau, J. F., and Dechanet-Merville, J. (2002). Human cytomegalovirus binding to DC-SIGN is required for dendritic cell infection and target cell trans-infection. *Immunity* **17**(5)**,** 653-64.

Han, Z., Boshra, H., Sunyer, J. O., Zwiers, S. H., Paragas, J., and Harty, R. N. (2003). Biochemical and functional characterization of the Ebola virus VP24 protein: implications for a role in virus assembly and budding. *J Virol* **77**(3)**,** 1793-800.

Harcourt, B. H., Sanchez, A., and Offermann, M. K. (1998). Ebola virus inhibits induction of genes by double-stranded RNA in endothelial cells. *Virology* **252**(1)**,** 179-88.

Hart, G. W. (1992). Glycosylation. *Curr Opin Cell Biol* **4**(6)**,** 1017-23.

Hartman, A. L., Towner, J. S., and Nichol, S. T. (2004). A C-terminal basic amino acid motif of Zaire ebolavirus VP35 is essential for type I interferon antagonism and displays high identity with the RNA-binding domain of another interferon antagonist, the NS1 protein of influenza A virus. *Virology* **328**(2)**,** 177-84.

Hartmann, S., and Hofsteenge, J. (2000). Properdin, the positive regulator of complement, is highly C-mannosylated. *J Biol Chem* **275**(37)**,** 28569-74.

Hayes, C. G., Burans, J. P., Ksiazek, T. G., Del Rosario, R. A., Miranda, M. E., Manaloto, C. R., Barrientos, A. B., Robles, C. G., Dayrit, M. M., and Peters, C. J. (1992). Outbreak of fatal illness among captive macaques in the Philippines caused by an Ebola-related filovirus. *Am J Trop Med Hyg* **46**(6)**,** 664-71.

Hensley, L. E., and Geisbert, T. W. (2005). The contribution of the endothelium to the development of coagulation disorders that characterize Ebola hemorrhagic fever in primates. *Thromb Haemost* **94**(2)**,** 254-61.

Hensley, L. E., Jones, S. M., Feldmann, H., Jahrling, P. B., and Geisbert, T. W. (2005). Ebola and Marburg viruses: pathogenesis and development of countermeasures. *Curr Mol Med* **5**(8)**,** 761-72.

Hensley, L. E., Stevens, E. L., Yan, S. B., Geisbert, J. B., Macias, W. L., Larsen, T., Daddario-DiCaprio, K. M., Cassell, G. H., Jahrling, P. B., and Geisbert, T. W. (2007). Recombinant human activated protein C for the postexposure treatment of Ebola hemorrhagic fever. *J Infect Dis* **196 Suppl 2,** S390-9.

Hensley, L. E., Young, H. A., Jahrling, P. B., and Geisbert, T. W. (2002). Proinflammatory response during Ebola virus infection of primate models: possible involvement of the tumor necrosis factor receptor superfamily. *Immunol Lett* **80**(3)**,** 169-79.

Herbert, J. M., Savi, P., Laplace, M. C., Lale, A., Dol, F., Dumas, A., Labit, C., and Minty, A. (1993). IL-4 and IL-13 exhibit comparable abilities to reduce pyrogen-induced expression of procoagulant activity in endothelial cells and monocytes. *FEBS Lett* **328**(3)**,** 268-70.

Herscovics, A., and Orlean, P. (1993). Glycoprotein biosynthesis in yeast. *Faseb J* **7**(6)**,** 540-50.

Heymann, D. L., Weisfeld, J. S., Webb, P. A., Johnson, K. M., Cairns, T., and Berquist, H. (1980). Ebola hemorrhagic fever: Tandala, Zaire, 1977-1978. *J Infect Dis* **142**(3)**,** 372-6.

Hilton, D. J., Watowich, S. S., Katz, L., and Lodish, H. F. (1996). Saturation mutagenesis of the WSXWS motif of the erythropoietin receptor. *J Biol Chem* **271**(9)**,** 4699-708.

Hoenen, T., Groseth, A., Falzarano, D., and Feldmann, H. (2006a). Ebola virus: unravelling pathogenesis to combat a deadly disease. *Trends Mol Med* **12**(5)**,** 206-15.

Hoenen, T., Groseth, A., Kolesnikova, L., Theriault, S., Ebihara, H., Hartlieb, B., Bamberg, S., Feldmann, H., Stroher, U., and Becker, S. (2006b). Infection of naive target cells with virus-like particles: implications for the function of ebola virus VP24. *J Virol* **80**(14)**,** 7260-4.

Hoenen, T., Volchkov, V., Kolesnikova, L., Mittler, E., Timmins, J., Ottmann, M., Reynard, O., Becker, S., and Weissenhorn, W. (2005). VP40 octamers are essential for Ebola virus replication. *J Virol* **79**(3)**,** 1898-905.

Hofsteenge, J., Blommers, M., Hess, D., Furmanek, A., and Miroshnichenko, O. (1999). The four terminal components of the complement system are C-mannosylated on multiple tryptophan residues. *J Biol Chem* **274**(46)**,** 32786-94.

Hofsteenge, J., Huwiler, K. G., Macek, B., Hess, D., Lawler, J., Mosher, D. F., and Peter-Katalinic, J. (2001). C-mannosylation and O-fucosylation of the thrombospondin type 1 module. *J Biol Chem* **276**(9)**,** 6485-98.

Hofsteenge, J., Muller, D. R., de Beer, T., Loffler, A., Richter, W. J., and Vliegenthart, J. F. (1994). New type of linkage between a carbohydrate and a protein: C-glycosylation of a specific tryptophan residue in human RNase Us. *Biochemistry* **33**(46)**,** 13524-30.

Hou, Y. C., Janczuk, A., and Wang, P. G. (1999). Current trends in the development of nitric oxide donors. *Curr Pharm Des* **5**(6)**,** 417-41.

Huang, Y., Xu, L., Sun, Y., and Nabel, G. J. (2002). The assembly of Ebola virus nucleocapsid requires virion-associated proteins 35 and 24 and posttranslational modification of nucleoprotein. *Mol Cell* **10**(2)**,** 307-16.

Hutchinson, K. L., and Rollin, P. E. (2007). Cytokine and chemokine expression in humans infected with Sudan Ebola virus. *J Infect Dis* **196 Suppl 2,** S357-63.

Hutchinson, K. L., Villinger, F., Miranda, M. E., Ksiazek, T. G., Peters, C. J., and Rollin, P. E. (2001). Multiplex analysis of cytokines in the blood of cynomolgus macaques naturally infected with Ebola virus (Reston serotype). *J Med Virol* **65**(3)**,** 561-6.

Ignatiev, G. M., Dadaeva, A. A., Luchko, S. V., and Chepurnov, A. A. (2000). Immune and pathophysiological processes in baboons experimentally infected with Ebola virus adapted to guinea pigs. *Immunol Lett* **71**(2)**,** 131-40.

IJID (2004). Fatal Ebola laboratory accident, Siberia. *IJID - International Journal of Infectious Disease* **8(4),** 199-200.

Isaacson, M., Sureau, P., Courteille, G., and Pattyn, S. R. (1978). *Proceedings of an International Colloquium on Ebola Virus Infection and Other Haemorrhagic Fevers, Antwerp, Belgium*.

Ishii, H., Horie, S., Kizaki, K., and Kazama, M. (1992). Retinoic acid counteracts both the downregulation of thrombomodulin and the induction of tissue factor in cultured human endothelial cells exposed to tumor necrosis factor. *Blood* **80**(10)**,** 2556-62.

Ito, H., Watanabe, S., Sanchez, A., Whitt, M. A., and Kawaoka, Y. (1999). Mutational analysis of the putative fusion domain of Ebola virus glycoprotein. *J Virol* **73**(10)**,** 8907-12.

Ito, H., Watanabe, S., Takada, A., and Kawaoka, Y. (2001). Ebola virus glycoprotein: proteolytic processing, acylation, cell tropism, and detection of neutralizing antibodies. *J Virol* **75**(3)**,** 1576-80.

Jaax, N., Jahrling, P., Geisbert, T., Geisbert, J., Steele, K., McKee, K., Nagley, D., Johnson, E., Jaax, G., and Peters, C. (1995). Transmission of Ebola virus (Zaire strain) to uninfected control monkeys in a biocontainment laboratory. *Lancet* **346**(8991-8992)**,** 1669-71.

Jaax, N. K., Davis, K. J., Geisbert, T. J., Vogel, P., Jaax, G. P., Topper, M., and Jahrling, P. B. (1996). Lethal experimental infection of rhesus monkeys with Ebola-Zaire (Mayinga) virus by the oral and conjunctival route of exposure. *Arch Pathol Lab Med* **120**(2)**,** 140-55.

Jahrling, P. B., Geisbert, T. W., Dalgard, D. W., Johnson, E. D., Ksiazek, T. G., Hall, W. C., and Peters, C. J. (1990). Preliminary report: isolation of Ebola virus from monkeys imported to USA. *Lancet* **335**(8688)**,** 502-5.

Jamsai, D., Reilly, A., Smith, S. J., Gibbs, G. M., Baker, H. W., McLachlan, R. I., de Kretser, D. M., and O'Bryan, M. K. (2008). Polymorphisms in the human cysteine-rich secretory protein 2 (CRISP2) gene in Australian men. *Hum Reprod* **23**(9)**,** 2151-9.

Janshoff, A., Wegener, J., Sieber, M., and Galla, H. J. (1996). Double-mode impedance analysis of epithelial cell monolayers cultured on shear wave resonators. *Eur Biophys J* **25**(2)**,** 93-103.

Jasenosky, L. D., and Kawaoka, Y. (2004). Filovirus budding. *Virus Res* **106**(2)**,** 181-8.

Jasenosky, L. D., Neumann, G., Lukashevich, I., and Kawaoka, Y. (2001). Ebola virus VP40-induced particle formation and association with the lipid bilayer. *J Virol* **75**(11)**,** 5205-14.

Jeffers, S. A., Sanders, D. A., and Sanchez, A. (2002). Covalent modifications of the ebola virus glycoprotein. *J Virol* **76**(24)**,** 12463-72.

Jiang, B. H., and Liu, L. Z. (2008). PI3K/PTEN signaling in tumorigenesis and angiogenesis. *Biochim Biophys Acta* **1784**(1)**,** 150-8.

Johnson, E., Jaax, N., White, J., and Jahrling, P. (1995). Lethal experimental infections of rhesus monkeys by aerosolized Ebola virus. *Int J Exp Pathol* **76**(4)**,** 227-36.

Johnson, K. M., Lange, J. V., Webb, P. A., and Murphy, F. A. (1977). Isolation and partial characterisation of a new virus causing acute haemorrhagic fever in Zaire. *Lancet* **1**(8011)**,** 569-71.

Jones, S. M., Feldmann, H., Stroher, U., Geisbert, J. B., Fernando, L., Grolla, A., Klenk, H. D., Sullivan, N. J., Volchkov, V. E., Fritz, E. A., Daddario, K. M., Hensley, L. E., Jahrling, P. B., and Geisbert, T. W. (2005). Live attenuated recombinant vaccine protects nonhuman primates against Ebola and Marburg viruses. *Nat Med* **11**(7)**,** 786-90.

Julenius, K. (2007). NetCGlyc 1.0: prediction of mammalian C-mannosylation sites. *Glycobiology* **17**(8)**,** 868-76.

Kash, J. C., Muhlberger, E., Carter, V., Grosch, M., Perwitasari, O., Proll, S. C., Thomas, M. J., Weber, F., Klenk, H. D., and Katze, M. G. (2006). Global suppression of the host antiviral response by Ebola- and Marburgviruses: increased antagonism of the type I interferon response is associated with enhanced virulence. *J Virol* **80**(6)**,** 3009-20.

Kibadi, K., Mupapa, K., Kuvula, K., Massamba, M., Ndaberey, D., Muyembe-Tamfum, J. J., Bwaka, M. A., De Roo, A., and Colebunders, R. (1999). Late ophthalmologic manifestations in survivors of the 1995 Ebola virus epidemic in Kikwit, Democratic Republic of the Congo. *J Infect Dis* **179 Suppl 1,** S13-4.

Kiley, M. P., Bowen, E. T., Eddy, G. A., Isaacson, M., Johnson, K. M., McCormick, J. B., Murphy, F. A., Pattyn, S. R., Peters, D., Prozesky, O. W., Regnery, R. L., Simpson, D. I., Slenczka, W., Sureau, P., van der Groen, G., Webb, P. A., and Wulff, H. (1982). Filoviridae: a taxonomic home for Marburg and Ebola viruses? *Intervirology* **18**(1-2)**,** 24-32.

Kindzelskii, A. L., Yang, Z., Nabel, G. J., Todd, R. F., 3rd, and Petty, H. R. (2000). Ebola virus secretory glycoprotein (sGP) diminishes Fc gamma RIIIB-to-CR3 proximity on neutrophils. *J Immunol* **164**(2)**,** 953-8.

Kornfeld, R., and Kornfeld, S. (1985). Assembly of asparagine-linked oligosaccharides. *Annu Rev Biochem* **54,** 631-64.

Kortepeter, M. G., Martin, J. W., Rusnak, J. M., Cieslak, T. J., Warfield, K. L., Anderson, E. L., and Ranadive, M. V. (2008). Managing potential laboratory exposure to ebola virus by using a patient biocontainment care unit. *Emerg Infect Dis* **14**(6)**,** 881-7.

Krieg, J., Glasner, W., Vicentini, A., Doucey, M. A., Loffler, A., Hess, D., and Hofsteenge, J. (1997). C-Mannosylation of human RNase 2 is an intracellular process performed by a variety of cultured cells. *J Biol Chem* **272**(42)**,** 26687-92.

Krieg, J., Hartmann, S., Vicentini, A., Glasner, W., Hess, D., and Hofsteenge, J. (1998). Recognition signal for C-mannosylation of Trp-7 in RNase 2 consists of sequence Trp-x-x-Trp. *Mol Biol Cell* **9**(2)**,** 301-9.

Krokhin, O., Ens, W., Standing, K. G., Wilkins, J., and Perreault, H. (2004). Site-specific N-glycosylation analysis: matrix-assisted laser desorption/ionization quadrupole-quadrupole time-of-flight tandem mass spectral signatures for recognition and identification of glycopeptides. *Rapid Commun Mass Spectrom* **18**(18)**,** 2020-30.

Krokhin, O. V., Cheng, K., Sousa, S. L., Ens, W., Standing, K. G., and Wilkins, J. A. (2003). Mass spectrometric based mapping of the disulfide bonding patterns of integrin alpha chains. *Biochemistry* **42**(44)**,** 12950-9.

Krokhin, O. V., Ens, W., and Standing, K. G. (2005). MALDI QqTOF MS combined with off-line HPLC for characterization of protein primary structure and post-translational modifications. *J Biomol Tech* **16**(4)**,** 429-40.

Ksiazek, T. G., Rollin, P. E., Williams, A. J., Bressler, D. S., Martin, M. L., Swanepoel, R., Burt, F. J., Leman, P. A., Khan, A. S., Rowe, A. K., Mukunu, R., Sanchez, A., and Peters, C. J. (1999). Clinical virology of Ebola hemorrhagic fever (EHF): virus, virus antigen, and IgG and IgM antibody findings among EHF patients in Kikwit, Democratic Republic of the Congo, 1995. *J Infect Dis* **179 Suppl 1,** S177-87.

Kuhn, J. H. (2008). "Filoviruses - A Compendium of 40 years of Epidemiological, Clinical, and Laboratory Studies." Archivies of Virology, Supplement 20 (C. H. Calisher, Ed.) Springer-Verlag/Wien, New York.

Kuhn, J. H., Radoshitzky, S. R., Guth, A. C., Warfield, K. L., Li, W., Vincent, M. J., Towner, J. S., Nichol, S. T., Bavari, S., Choe, H., Aman, M. J., and Farzan, M. (2006). Conserved receptor-binding domains of Lake Victoria marburgvirus and Zaire ebolavirus bind a common receptor. *J Biol Chem* **281**(23)**,** 15951-8.

Landry, D. W., and Oliver, J. A. (2001). The pathogenesis of vasodilatory shock. *N Engl J Med* **345**(8)**,** 588-95.

Le Guenno, B., Formenty, P., Wyers, M., Gounon, P., Walker, F., and Boesch, C. (1995). Isolation and partial characterisation of a new strain of Ebola virus. *Lancet* **345**(8960)**,** 1271-4.

Lee, J. E., Fusco, M. L., Hessell, A. J., Oswald, W. B., Burton, D. R., and Saphire, E. O. (2008). Structure of the Ebola virus glycoprotein bound to an antibody from a human survivor. *Nature* **454**(7201)**,** 177-82.

Leroy, E. M., Epelboin, A., Mondonge, V., Pourrut, X., Gonzalez, J. P., Muyembe-Tamfum, J. J., and Formenty, P. (2009). Human Ebola Outbreak Resulting from Direct Exposure to Fruit Bats in Luebo, Democratic Republic of Congo, 2007. *Vector Borne Zoonotic Dis*.

Leroy, E. M., Kumulungui, B., Pourrut, X., Rouquet, P., Hassanin, A., Yaba, P., Delicat, A., Paweska, J. T., Gonzalez, J. P., and Swanepoel, R. (2005). Fruit bats as reservoirs of Ebola virus. *Nature* **438**(7068)**,** 575-6.

Levi, M. (2004). Current understanding of disseminated intravascular coagulation. *Br J Haematol* **124**(5)**,** 567-76.

Li, Y., Cao, C., Jia, W., Yu, L., Mo, M., Wang, Q., Huang, Y., Lim, J. M., Ishihara, M., Wells, L., Azadi, P., Robinson, H., He, Y. W., Zhang, L., and Mariuzza, R. A.

(2009). Structure of the F-spondin domain of mindin, an integrin ligand and pattern recognition molecule. *Embo J* **28**(3)**,** 286-97.

Licata, J. M., Johnson, R. F., Han, Z., and Harty, R. N. (2004). Contribution of ebola virus glycoprotein, nucleoprotein, and VP24 to budding of VP40 virus-like particles. *J Virol* **78**(14)**,** 7344-51.

Lin, G., Simmons, G., Pohlmann, S., Baribaud, F., Ni, H., Leslie, G. J., Haggarty, B. S., Bates, P., Weissman, D., Hoxie, J. A., and Doms, R. W. (2003). Differential N-linked glycosylation of human immunodeficiency virus and Ebola virus envelope glycoproteins modulates interactions with DC-SIGN and DC-SIGNR. *J Virol* **77**(2)**,** 1337-46.

Lo, C. M., Keese, C. R., and Giaever, I. (1995). Impedance analysis of MDCK cells measured by electric cell-substrate impedance sensing. *Biophys J* **69**(6)**,** 2800-7.

Loboda, A. V., Krutchinsky, A. N., Bromirski, M., Ens, W., and Standing, K. G. (2000). A tandem quadrupole/time-of-flight mass spectrometer with a matrix-assisted laser desorption/ionization source: design and performance. *Rapid Commun Mass Spectrom* **14**(12)**,** 1047-57.

Loffler, A., Doucey, M. A., Jansson, A. M., Muller, D. R., de Beer, T., Hess, D., Meldal, M., Richter, W. J., Vliegenthart, J. F., and Hofsteenge, J. (1996). Spectroscopic and protein chemical analyses demonstrate the presence of C-mannosylated tryptophan in intact human RNase 2 and its isoforms. *Biochemistry* **35**(37)**,** 12005-14.

Luther, K. B., and Haltiwanger, R. S. (2009). Role of unusual O-glycans in intercellular signaling. *Int J Biochem Cell Biol* **41**(5)**,** 1011-24.

Lyberg, T. (1983). Effect of cyclic AMP and cyclic GMP on thromboplastin (factor III) synthesis in human monocytes in vitro. *Thromb Haemost* **50**(4)**,** 804-9.

Ma, B., Elkayam, T., Wolfson, H., and Nussinov, R. (2003). Protein-protein interactions: structurally conserved residues distinguish between binding sites and exposed protein surfaces. *Proc Natl Acad Sci U S A* **100**(10)**,** 5772-7.

Ma, B., and Nussinov, R. (2007). Trp/Met/Phe hot spots in protein-protein interactions: potential targets in drug design. *Curr Top Med Chem* **7**(10)**,** 999-1005.

Maeda, Y., and Kinoshita, T. (2008). Dolichol-phosphate mannose synthase: structure, function and regulation. *Biochim Biophys Acta* **1780**(6)**,** 861-8.

Mahanty, S., and Bray, M. (2004). Pathogenesis of filoviral haemorrhagic fevers. *Lancet Infect Dis* **4**(8)**,** 487-98.

Mahanty, S., Hutchinson, K., Agarwal, S., McRae, M., Rollin, P. E., and Pulendran, B. (2003). Cutting edge: impairment of dendritic cells and adaptive immunity by Ebola and Lassa viruses. *J Immunol* **170**(6)**,** 2797-801.

Malashkevich, V. N., Schneider, B. J., McNally, M. L., Milhollen, M. A., Pang, J. X., and Kim, P. S. (1999). Core structure of the envelope glycoprotein GP2 from Ebola virus at 1.9-A resolution. *Proc Natl Acad Sci U S A* **96**(6)**,** 2662-7.

Manicassamy, B., Wang, J., Jiang, H., and Rong, L. (2005). Comprehensive analysis of ebola virus GP1 in viral entry. *J Virol* **79**(8)**,** 4793-805.

Martin, N. B., Jamieson, A., and Tuffin, D. P. (1993). The effect of interleukin-4 on tumour necrosis factor-alpha induced expression of tissue factor and plasminogen activator inhibitor-1 in human umbilical vein endothelial cells. *Thromb Haemost* **70**(6)**,** 1037-42.

Maruyama, T., Buchmeier, M. J., Parren, P. W., and Burton, D. R. (1998a). *Science* **282,** 845a.

Maruyama, T., Buchmeier, M. J., Parren, P. W., and Burton, D. R. (1998b). Ebola virus, neutrophils, and antibody specificity. *Science* **282,** 843a.

Marzi, A., Akhavan, A., Simmons, G., Gramberg, T., Hofmann, H., Bates, P., Lingappa, V. R., and Pohlmann, S. (2006). The signal peptide of the ebolavirus glycoprotein influences interaction with the cellular lectins DC-SIGN and DC-SIGNR. *J Virol* **80**(13)**,** 6305-17.

Marzi, A., Moller, P., Hanna, S. L., Harrer, T., Eisemann, J., Steinkasserer, A., Becker, S., Baribaud, F., and Pohlmann, S. (2007). Analysis of the interaction of Ebola virus glycoprotein with DC-SIGN (dendritic cell-specific intercellular adhesion molecule 3-grabbing nonintegrin) and its homologue DC-SIGNR. *J Infect Dis* **196 Suppl 2,** S237-46.

McGee, M. P., Foster, S., and Wang, X. (1994). Simultaneous expression of tissue factor and tissue factor pathway inhibitor by human monocytes. A potential mechanism for localized control of blood coagulation. *J Exp Med* **179**(6)**,** 1847-54.

Mehedi, M., Falzarano, D., Carpenter, M. S., and Feldmann, H. (2008). *American Society for Virology Annual Meeting, Ithaca, New York.*

Miranda, M. E., Ksiazek, T. G., Retuya, T. J., Khan, A. S., Sanchez, A., Fulhorst, C. F., Rollin, P. E., Calaor, A. B., Manalo, D. L., Roces, M. C., Dayrit, M. M., and Peters, C. J. (1999). Epidemiology of Ebola (subtype Reston) virus in the Philippines, 1996. *J Infect Dis* **179 Suppl 1,** S115-9.

Miyazaki, T., Maruyama, M., Yamada, G., Hatakeyama, M., and Taniguchi, T. (1991). The integrity of the conserved 'WS motif' common to IL-2 and other cytokine receptors is essential for ligand binding and signal transduction. *Embo J* **10**(11)**,** 3191-7.

Mohamadzadeh, M. (2009). Potential factors induced by filoviruses that lead to immune supression. *Curr Mol Med* **9**(2)**,** 174-85.

Mohamadzadeh, M., Chen, L., Olinger, G. G., Pratt, W. D., and Schmaljohn, A. L. (2006). Filoviruses and the balance of innate, adaptive, and inflammatory responses. *Viral Immunol* **19**(4)**,** 602-12.

Mohamadzadeh, M., Chen, L., and Schmaljohn, A. L. (2007). How Ebola and Marburg viruses battle the immune system. *Nat Rev Immunol* **7**(7)**,** 556-67.

Morelle, W., Faid, V., Chirat, F., and Michalski, J. C. (2009). Analysis of N- and O-linked glycans from glycoproteins using MALDI-TOF mass spectrometry. *Methods Mol Biol* **534,** 5-21.

Mosimann, S. C., Newton, D. L., Youle, R. J., and James, M. N. (1996). X-ray crystallographic structure of recombinant eosinophil-derived neurotoxin at 1.83 A resolution. *J Mol Biol* **260**(4)**,** 540-52.

Mpanju, O. M., Towner, J. S., Dover, J. E., Nichol, S. T., and Wilson, C. A. (2006). Identification of two amino acid residues on Ebola virus glycoprotein 1 critical for cell entry. *Virus Res* **121**(2)**,** 205-14.

Muhlberger, E., Weik, M., Volchkov, V. E., Klenk, H. D., and Becker, S. (1999). Comparison of the transcription and replication strategies of marburg virus and Ebola virus by using artificial replication systems. *J Virol* **73**(3)**,** 2333-42.

Munte, C. E., Gade, G., Domogalla, B., Kremer, W., Kellner, R., and Kalbitzer, H. R. (2008). C-mannosylation in the hypertrehalosaemic hormone from the stick insect Carausius morosus. *Febs J* **275**(6)**,** 1163-73.

Murphy, F. A. (1978). Pathology of Ebola virus infection. *In* "Ebola Virus Haemorrhagic Fever" (S. R. Pattyn, Ed.), pp. 43-59. Elsevier/North Holland, Amsterdam.

Muyembe, T., and Kipasa, M. (1995). Ebola haemorrhagic fever in Kikwit, Zaire. International Scientific and Technical Committee and WHO Collaborating Centre for Haemorrhagic Fevers. *Lancet* **345**(8962)**,** 1448.

Ndambi, R., Akamituna, P., Bonnet, M. J., Tukadila, A. M., Muyembe-Tamfum, J. J., and Colebunders, R. (1999). Epidemiologic and clinical aspects of the Ebola virus epidemic in Mosango, Democratic Republic of the Congo, 1995. *J Infect Dis* **179 Suppl 1,** S8-10.

Neumann, G., Feldmann, H., Watanabe, S., Lukashevich, I., and Kawaoka, Y. (2002). Reverse genetics demonstrates that proteolytic processing of the Ebola virus glycoprotein is not essential for replication in cell culture. *J Virol* **76**(1)**,** 406-10.

Neumann, G., Geisbert, T. W., Ebihara, H., Geisbert, J. B., Daddario-Dicaprio, K. M., Feldmann, H., and Kawaoka, Y. (2007). Proteolytic Processing of the Ebola Virus Glycoprotein Is Not Critical for Ebola Virus Replication in Nonhuman Primates. *J Virol*.

Niwa, H., Yamamura, K., and Miyazaki, J. (1991). Efficient selection for high-expression transfectants with a novel eukaryotic vector. *Gene* **108**(2)**,** 193-9.

Noda, T., Ebihara, H., Muramoto, Y., Fujii, K., Takada, A., Sagara, H., Kim, J. H., Kida, H., Feldmann, H., and Kawaoka, Y. (2006). Assembly and budding of Ebolavirus. *PLoS Pathog* **2**(9)**,** e99.

Noda, T., Sagara, H., Suzuki, E., Takada, A., Kida, H., and Kawaoka, Y. (2002). Ebola virus VP40 drives the formation of virus-like filamentous particles along with GP. *J Virol* **76**(10)**,** 4855-65.

Normile, D. (2009). Emerging infectious diseases. Scientists puzzle over Ebola-Reston virus in pigs. *Science* **323**(5913)**,** 451.

Okware, S. I., Omaswa, F. G., Zaramba, S., Opio, A., Lutwama, J. J., Kamugisha, J., Rwaguma, E. B., Kagwa, P., and Lamunu, M. (2002). An outbreak of Ebola in Uganda. *Trop Med Int Health* **7**(12)**,** 1068-75.

Parton, R. G., and Richards, A. A. (2003). Lipid rafts and caveolae as portals for endocytosis: new insights and common mechanisms. *Traffic* **4**(11)**,** 724-38.

Perez-Vilar, J., Randell, S. H., and Boucher, R. C. (2004). C-Mannosylation of MUC5AC and MUC5B Cys subdomains. *Glycobiology* **14**(4)**,** 325-37.

Piot, P., Bureau, P., Breman, G., Heymann, D. L., Kintoki, V., Masamba, M., Mbuyi, M., Miatudila, M., Ruppol, F., Van Nieuwenhove, S., White, M. K., Van der Groen, G., Webb, P. A., Wulff, H., and Johnson, K. M. (1978). *Proceedings of an International Colloquium on Ebola Virus Infection and Other Haemorrhagic Fevers, Antwerp, Belgium*.

Pohlmann, S., Soilleux, E. J., Baribaud, F., Leslie, G. J., Morris, L. S., Trowsdale, J., Lee, B., Coleman, N., and Doms, R. W. (2001). DC-SIGNR, a DC-SIGN homologue expressed in endothelial cells, binds to human and simian immunodeficiency viruses and activates infection in trans. *Proc Natl Acad Sci U S A* **98**(5)**,** 2670-5.

Pourrut, X., Kumulungui, B., Wittmann, T., Moussavou, G., Delicat, A., Yaba, P., Nkoghe, D., Gonzalez, J. P., and Leroy, E. M. (2005). The natural history of Ebola virus in Africa. *Microbes Infect* **7**(7-8)**,** 1005-14.

Powell, D. W. (1981). Barrier function of epithelia. *Am J Physiol* **241**(4)**,** G275-88.

Prins, K. C., Cardenas, W. B., and Basler, C. F. (2009). Ebola virus protein VP35 impairs the function of interferon regulatory factor-activating kinases IKKepsilon and TBK-1. *J Virol* **83**(7)**,** 3069-77.

Pryor, M. J., and Wright, P. J. (1993). The effects of site-directed mutagenesis on the dimerization and secretion of the NS1 protein specified by dengue virus. *Virology* **194**(2)**,** 769-80.

Ramani, M., Khechai, F., Ollivier, V., Ternisien, C., Bridey, F., Hakim, J., and de Prost, D. (1994). Interleukin-10 and pentoxifylline inhibit C-reactive protein-induced tissue factor gene expression in peripheral human blood monocytes. *FEBS Lett* **356**(1)**,** 86-8.

Ramani, M., Ollivier, V., Khechai, F., Vu, T., Ternisien, C., Bridey, F., and de Prost, D. (1993a). Interleukin-10 inhibits endotoxin-induced tissue factor mRNA production by human monocytes. *FEBS Lett* **334**(1)**,** 114-6.

Ramani, M., Ollivier, V., Ternisien, C., Vu, T., Elbim, C., Hakim, J., and de Prost, D. (1993b). Interleukin 4 prevents the induction of tissue factor mRNA in human monocytes in response to LPS or PMA stimulation. *Br J Haematol* **85**(3)**,** 462-8.

Reed, D. S., Hensley, L. E., Geisbert, J. B., Jahrling, P. B., and Geisbert, T. W. (2004). Depletion of peripheral blood T lymphocytes and NK cells during the course of ebola hemorrhagic Fever in cynomolgus macaques. *Viral Immunol* **17**(3)**,** 390-400.

Regnery, R. L., Johnson, K. M., and Kiley, M. P. (1980). Virion nucleic acid of Ebola virus. *J Virol* **36**(2)**,** 465-9.

Reid, S. P., Leung, L. W., Hartman, A. L., Martinez, O., Shaw, M. L., Carbonnelle, C., Volchkov, V. E., Nichol, S. T., and Basler, C. F. (2006). Ebola virus VP24 binds karyopherin alpha1 and blocks STAT1 nuclear accumulation. *J Virol* **80**(11)**,** 5156-67.

Reid, S. P., Valmas, C., Martinez, O., Sanchez, F. M., and Basler, C. F. (2007). Ebola virus VP24 proteins inhibit the interaction of NPI-1 subfamily karyopherin alpha proteins with activated STAT1. *J Virol* **81**(24)**,** 13469-77.

Roels, T. H., Bloom, A. S., Buffington, J., Muhungu, G. L., Mac Kenzie, W. R., Khan, A. S., Ndambi, R., Noah, D. L., Rolka, H. R., Peters, C. J., and Ksiazek, T. G. (1999). Ebola hemorrhagic fever, Kikwit, Democratic Republic of the Congo, 1995: risk factors for patients without a reported exposure. *J Infect Dis* **179 Suppl 1,** S92-7.

Rollin, P. E., Bausch, D. G., and Sanchez, A. (2007). Blood chemistry measurements and D-Dimer levels associated with fatal and nonfatal outcomes in humans infected with Sudan Ebola virus. *J Infect Dis* **196 Suppl 2,** S364-71.

Rollin, P. E., Williams, R. J., Bressler, D. S., Pearson, S., Cottingham, M., Pucak, G., Sanchez, A., Trappier, S. G., Peters, R. L., Greer, P. W., Zaki, S., Demarcus, T., Hendricks, K., Kelley, M., Simpson, D., Geisbert, T. W., Jahrling, P. B., Peters, C. J., and Ksiazek, T. G. (1999). Ebola (subtype Reston) virus among quarantined

nonhuman primates recently imported from the Philippines to the United States. *J Infect Dis* **179 Suppl 1,** S108-14.

Roth, J., Wang, Y., Eckhardt, A. E., and Hill, R. L. (1994). Subcellular localization of the UDP-N-acetyl-D-galactosamine: polypeptide N-acetylgalactosaminyltransferase-mediated O-glycosylation reaction in the submaxillary gland. *Proc Natl Acad Sci U S A* **91**(19)**,** 8935-9.

Rubins, K. H., Hensley, L. E., Wahl-Jensen, V., Daddario DiCaprio, K. M., Young, H. A., Reed, D. S., Jahrling, P. B., Brown, P. O., Relman, D. A., and Geisbert, T. W. (2007). The temporal program of peripheral blood gene expression in the response of nonhuman primates to Ebola hemorrhagic fever. *Genome Biol* **8**(8)**,** R174.

Ryabchikova, E. I., Kolesnikova, L. V., and Luchko, S. V. (1999). An analysis of features of pathogenesis in two animal models of Ebola virus infection. *J Infect Dis* **179 Suppl 1,** S199-202.

Ryabchikova, E. I., Kolesnikova, L. V., and Netesov, S. V. (1999). Animal pathology of filoviral infections. *Curr Top Microbiol Immunol* **235,** 145-73.

Saeed, M. F., Kolokoltsov, A. A., Freiberg, A. N., Holbrook, M. R., and Davey, R. A. (2008). Phosphoinositide-3 kinase-Akt pathway controls cellular entry of Ebola virus. *PLoS Pathog* **4**(8)**,** e1000141.

Salzwedel, K., West, J. T., and Hunter, E. (1999). A conserved tryptophan-rich motif in the membrane-proximal region of the human immunodeficiency virus type 1 gp41 ectodomain is important for Env-mediated fusion and virus infectivity. *J Virol* **73**(3)**,** 2469-80.

Sanchez, A. (2007). Analysis of filovirus entry into vero e6 cells, using inhibitors of endocytosis, endosomal acidification, structural integrity, and cathepsin (B and L) activity. *J Infect Dis* **196 Suppl 2,** S251-8.

Sanchez, A., Geisbert, T., and Feldmann, H., Eds. (2007). Filoviridae: Ebola and Marburg Viruses. 5th ed. Field's Virology. Edited by D. M. Knipe, P. M. Howley, D. E. Griffin, R. A. Lamb, M. A. Martin, B. Roizman, and S. E. Straus. Philadelphia, PA: Lippincott Williams & Wilkins.

Sanchez, A., Khan, A. S., Zaki, S. R., Nabel, G. J., Ksiazek, T. G., and Peters, C. J., Eds. (2001). Filoviridae. Field's Virology. Edited by D. M. Knipe, P. M. Howley, D. E. Griffin, R. A. Lamb, M. A. Martin, B. Roizman, and S. E. Straus. Philadelphia, PA: Lippincott Williams and Wilkins.

Sanchez, A., and Kiley, M. P. (1987). Identification and analysis of Ebola virus messenger RNA. *Virology* **157**(2)**,** 414-20.

Sanchez, A., Kiley, M. P., Holloway, B. P., and Auperin, D. D. (1993). Sequence analysis of the Ebola virus genome: organization, genetic elements, and comparison with the genome of Marburg virus. *Virus Res* **29**(3)**,** 215-40.

Sanchez, A., Lukwiya, M., Bausch, D., Mahanty, S., Sanchez, A. J., Wagoner, K. D., and Rollin, P. E. (2004). Analysis of human peripheral blood samples from fatal and nonfatal cases of Ebola (Sudan) hemorrhagic fever: cellular responses, virus load, and nitric oxide levels. *J Virol* **78**(19)**,** 10370-7.

Sanchez, A., and Rollin, P. E. (2005). Complete genome sequence of an Ebola virus (Sudan species) responsible for a 2000 outbreak of human disease in Uganda. *Virus Res* **113**(1)**,** 16-25.

Sanchez, A., Trappier, S. G., Mahy, B. W., Peters, C. J., and Nichol, S. T. (1996). The virion glycoproteins of Ebola viruses are encoded in two reading frames and are expressed through transcriptional editing. *Proc Natl Acad Sci U S A* **93**(8)**,** 3602-7.

Sanchez, A., Yang, Z. Y., Xu, L., Nabel, G. J., Crews, T., and Peters, C. J. (1998). Biochemical analysis of the secreted and virion glycoproteins of Ebola virus. *J Virol* **72**(8)**,** 6442-7.

Schnittler, H. J., and Feldmann, H. (1999). Molecular pathogenesis of filovirus infections: role of macrophages and endothelial cells. *Curr Top Microbiol Immunol* **235,** 175-204.

Schnittler, H. J., and Feldmann, H. (2003). Viral hemorrhagic fever--a vascular disease? *Thromb Haemost* **89**(6)**,** 967-72.

Schnittler, H. J., Franke, R. P., Akbay, U., Mrowietz, C., and Drenckhahn, D. (1993). Improved in vitro rheological system for studying the effect of fluid shear stress on cultured cells. *Am J Physiol* **265**(1 Pt 1)**,** C289-98.

Schnittler, H. J., Stroeher, U., Seebach, J., and Feldmann, H. (2004). The role of endothelial cells in filovirus hemorrhagic fever. *In* "Ebola and Marburg Viruses" (H. D. Klenk, and H. Feldmann, Eds.), pp. 179-303. Horizon Biosciences, Norfolk, U.K.

Schnittler, H. J., Wilke, A., Gress, T., Suttorp, N., and Drenckhahn, D. (1990). Role of actin and myosin in the control of paracellular permeability in pig, rat and human vascular endothelium. *J Physiol* **431,** 379-401.

Schornberg, K., Matsuyama, S., Kabsch, K., Delos, S., Bouton, A., and White, J. (2006). Role of endosomal cathepsins in entry mediated by the Ebola virus glycoprotein. *J Virol* **80**(8)**,** 4174-8.

Seebach, J., Dieterich, P., Luo, F., Schillers, H., Vestweber, D., Oberleithner, H., Galla, H. J., and Schnittler, H. J. (2000). Endothelial barrier function under laminar fluid shear stress. *Lab Invest* **80**(12)**,** 1819-31.

Seebach, J., Madler, H. J., Wojciak-Stothard, B., and Schnittler, H. J. (2005). Tyrosine phosphorylation and the small GTPase rac cross-talk in regulation of endothelial barrier function. *Thromb Haemost* **94**(3)**,** 620-9.

Seet, B. T., Johnston, J. B., Brunetti, C. R., Barrett, J. W., Everett, H., Cameron, C., Sypula, J., Nazarian, S. H., Lucas, A., and McFadden, G. (2003). Poxviruses and immune evasion. *Annu Rev Immunol* **21,** 377-423.

Segal, M. S., Bye, J. M., Sambrook, J. F., and Gething, M. J. (1992). Disulfide bond formation during the folding of influenza virus hemagglutinin. *J Cell Biol* **118**(2)**,** 227-44.

Shimojima, M., Ikeda, Y., and Kawaoka, Y. (2007). The mechanism of Axl-mediated Ebola virus infection. *J Infect Dis* **196 Suppl 2,** S259-63.

Shimojima, M., Takada, A., Ebihara, H., Neumann, G., Fujioka, K., Irimura, T., Jones, S., Feldmann, H., and Kawaoka, Y. (2006). Tyro3 family-mediated cell entry of Ebola and Marburg viruses. *J Virol* **80**(20)**,** 10109-16.

Simmons, G., Rennekamp, A. J., Chai, N., Vandenberghe, L. H., Riley, J. L., and Bates, P. (2003). Folate receptor alpha and caveolae are not required for Ebola virus glycoprotein-mediated viral infection. *J Virol* **77**(24)**,** 13433-8.

Simmons, G., Wool-Lewis, R. J., Baribaud, F., Netter, R. C., and Bates, P. (2002). Ebola virus glycoproteins induce global surface protein down-modulation and loss of cell adherence. *J Virol* **76**(5)**,** 2518-28.

Simons, K., and Ikonen, E. (1997). Functional rafts in cell membranes. *Nature* **387**(6633)**,** 569-72.

Sinn, P. L., Hickey, M. A., Staber, P. D., Dylla, D. E., Jeffers, S. A., Davidson, B. L., Sanders, D. A., and McCray, P. B., Jr. (2003). Lentivirus vectors pseudotyped with filoviral envelope glycoproteins transduce airway epithelia from the apical surface independently of folate receptor alpha. *J Virol* **77**(10)**,** 5902-10.

Smith, D. H., Francis, D. P., and Simpson, D. I. H. (1978). *Proceedings of an International Colloquium on Ebola Virus Infection and Other Haemorrhagic Fevers, Antwerp, Belgium*.

Snyder, G. A., Ford, J., Torabi-Parizi, P., Arthos, J. A., Schuck, P., Colonna, M., and Sun, P. D. (2005). Characterization of DC-SIGN/R interaction with human immunodeficiency virus type 1 gp120 and ICAM molecules favors the receptor's role as an antigen-capturing rather than an adhesion receptor. *J Virol* **79**(8)**,** 4589-98.

Song, L., Sun, Z. Y., Coleman, K. E., Zwick, M. B., Gach, J. S., Wang, J. H., Reinherz, E. L., Wagner, G., and Kim, M. (2009). Broadly neutralizing anti-HIV-1 antibodies disrupt a hinge-related function of gp41 at the membrane interface. *Proc Natl Acad Sci U S A*.

Stroher, U., West, E., Bugany, H., Klenk, H. D., Schnittler, H. J., and Feldmann, H. (2001). Infection and activation of monocytes by Marburg and Ebola viruses. *J Virol* **75**(22)**,** 11025-33.

Sugrue, R. J. (2007). Viruses and glycosylation: an overview. *Methods Mol Biol* **379,** 1-13.

Sui, J., and Marasco, W. A. (2002). Evidence against Ebola virus sGP binding to human neutrophils by a specific receptor. *Virology* **303**(1)**,** 9-14.

Sullivan, N. J., Peterson, M., Yang, Z. Y., Kong, W. P., Duckers, H., Nabel, E., and Nabel, G. J. (2005). Ebola virus glycoprotein toxicity is mediated by a dynamin-dependent protein-trafficking pathway. *J Virol* **79**(1)**,** 547-53.

Sumner, L. W., Wolf-Sumner, B., White, S. P., and Asirvatham, V. S. (2002). Silver stain removal using H2O2 for enhanced peptide mass mapping by matrix-assisted laser desorption/ionization time-of-flight mass spectrometry. *Rapid Commun Mass Spectrom* **16**(3)**,** 160-8.

Sun, Z. Y., Oh, K. J., Kim, M., Yu, J., Brusic, V., Song, L., Qiao, Z., Wang, J. H., Wagner, G., and Reinherz, E. L. (2008). HIV-1 broadly neutralizing antibody extracts its epitope from a kinked gp41 ectodomain region on the viral membrane. *Immunity* **28**(1)**,** 52-63.

Sureau, P. H. (1989). Firsthand clinical observations of hemorrhagic manifestations in Ebola hemorrhagic fever in Zaire. *Rev Infect Dis* **11 Suppl 4,** S790-3.

Szotowski, B., Antoniak, S., Poller, W., Schultheiss, H. P., and Rauch, U. (2005). Procoagulant soluble tissue factor is released from endothelial cells in response to inflammatory cytokines. *Circ Res* **96**(12)**,** 1233-9.

Takada, A., Fujioka, K., Tsuiji, M., Morikawa, A., Higashi, N., Ebihara, H., Kobasa, D., Feldmann, H., Irimura, T., and Kawaoka, Y. (2004). Human macrophage C-type

lectin specific for galactose and N-acetylgalactosamine promotes filovirus entry. *J Virol* **78**(6)**,** 2943-7.

Takada, A., Robison, C., Goto, H., Sanchez, A., Murti, K. G., Whitt, M. A., and Kawaoka, Y. (1997). A system for functional analysis of Ebola virus glycoprotein. *Proc Natl Acad Sci U S A* **94**(26)**,** 14764-9.

Takada, A., Watanabe, S., Ito, H., Okazaki, K., Kida, H., and Kawaoka, Y. (2000). Downregulation of beta1 integrins by Ebola virus glycoprotein: implication for virus entry. *Virology* **278**(1)**,** 20-6.

Tan, K., Duquette, M., Liu, J. H., Dong, Y., Zhang, R., Joachimiak, A., Lawler, J., and Wang, J. H. (2002). Crystal structure of the TSP-1 type 1 repeats: a novel layered fold and its biological implication. *J Cell Biol* **159**(2)**,** 373-82.

Thomas, S. M., Lamb, R. A., and Paterson, R. G. (1988). Two mRNAs that differ by two nontemplated nucleotides encode the amino coterminal proteins P and V of the paramyxovirus SV5. *Cell* **54**(6)**,** 891-902.

Timmins, J., Schoehn, G., Ricard-Blum, S., Scianimanico, S., Vernet, T., Ruigrok, R. W., and Weissenhorn, W. (2003). Ebola virus matrix protein VP40 interaction with human cellular factors Tsg101 and Nedd4. *J Mol Biol* **326**(2)**,** 493-502.

Timmins, J., Scianimanico, S., Schoehn, G., and Weissenhorn, W. (2001). Vesicular release of ebola virus matrix protein VP40. *Virology* **283**(1)**,** 1-6.

Towner, J. S., Sealy, T. K., Khristova, M. L., Albarino, C. G., Conlan, S., Reeder, S. A., Quan, P. L., Lipkin, W. I., Downing, R., Tappero, J. W., Okware, S., Lutwama, J., Bakamutumaho, B., Kayiwa, J., Comer, J. A., Rollin, P. E., Ksiazek, T. G., and Nichol, S. T. (2008). Newly discovered ebola virus associated with hemorrhagic fever outbreak in Uganda. *PLoS Pathog* **4**(11)**,** e1000212.

Tuffs, A. (2009). Experimental vaccine may have saved Hamburg scientist from Ebola fever. *Bmj* **338,** b1223.

Vigerust, D. J., and Shepherd, V. L. (2007). Virus glycosylation: role in virulence and immune interactions. *Trends Microbiol* **15**(5)**,** 211-8.

Villinger, F., Rollin, P. E., Brar, S. S., Chikkala, N. F., Winter, J., Sundstrom, J. B., Zaki, S. R., Swanepoel, R., Ansari, A. A., and Peters, C. J. (1999). Markedly elevated levels of interferon (IFN)-gamma, IFN-alpha, interleukin (IL)-2, IL-10, and tumor necrosis factor-alpha associated with fatal Ebola virus infection. *J Infect Dis* **179 Suppl 1,** S188-91.

Vincent, J. L., and De Backer, D. (2005). Does disseminated intravascular coagulation lead to multiple organ failure? *Crit Care Clin* **21**(3)**,** 469-77.

Vishwanathan, S. A., and Hunter, E. (2008). Importance of the membrane-perturbing properties of the membrane-proximal external region of human immunodeficiency virus type 1 gp41 to viral fusion. *J Virol* **82**(11)**,** 5118-26.

Vliegenthart, J. F., and Casset, F. (1998). Novel forms of protein glycosylation. *Curr Opin Struct Biol* **8**(5)**,** 565-71.

Volchkov, V. E., Becker, S., Volchkova, V. A., Ternovoj, V. A., Kotov, A. N., Netesov, S. V., and Klenk, H. D. (1995). GP mRNA of Ebola virus is edited by the Ebola virus polymerase and by T7 and vaccinia virus polymerases. *Virology* **214**(2)**,** 421-30.

Volchkov, V. E., Blinov, V. M., and Netesov, S. V. (1992). The envelope glycoprotein of Ebola virus contains an immunosuppressive-like domain similar to oncogenic retroviruses. *FEBS Lett* **305**(3)**,** 181-4.

Volchkov, V. E., Chepurnov, A. A., Volchkova, V. A., Ternovoj, V. A., and Klenk, H. D. (2000). Molecular characterization of guinea pig-adapted variants of Ebola virus. *Virology* **277**(1)**,** 147-55.

Volchkov, V. E., Feldmann, H., Volchkova, V. A., and Klenk, H. D. (1998a). Processing of the Ebola virus glycoprotein by the proprotein convertase furin. *Proc Natl Acad Sci U S A* **95**(10)**,** 5762-7.

Volchkov, V. E., Volchkova, V. A., Muhlberger, E., Kolesnikova, L. V., Weik, M., Dolnik, O., and Klenk, H. D. (2001). Recovery of infectious Ebola virus from complementary DNA: RNA editing of the GP gene and viral cytotoxicity. *Science* **291**(5510)**,** 1965-9.

Volchkov, V. E., Volchkova, V. A., Slenczka, W., Klenk, H. D., and Feldmann, H. (1998b). Release of viral glycoproteins during Ebola virus infection. *Virology* **245**(1)**,** 110-9.

Volchkova, V., Dolnik, O., Reynard, O., Carbonnelle, C., Martinez, M. J., Alazard-Dany, N., and Volchkov, V. (2008). *International Congress of Virology, Istanbul, Turkey*.

Volchkova, V., Feldmann, H., Klenk, H. D., and Volchkov, V. (1999). *11th International Congress of Virology, Sydney, Australia*.

Volchkova, V. A., Feldmann, H., Klenk, H. D., and Volchkov, V. E. (1998). The nonstructural small glycoprotein sGP of Ebola virus is secreted as an antiparallel-orientated homodimer. *Virology* **250**(2)**,** 408-14.

Volchkova, V. A., Klenk, H. D., and Volchkov, V. E. (1999). Delta-peptide is the carboxy-terminal cleavage fragment of the nonstructural small glycoprotein sGP of Ebola virus. *Virology* **265**(1)**,** 164-71.

Wahl-Jensen, V., Kurz, S. K., Hazelton, P. R., Schnittler, H. J., Stroher, U., Burton, D. R., and Feldmann, H. (2005a). Role of Ebola virus secreted glycoproteins and virus-like particles in activation of human macrophages. *J Virol* **79**(4)**,** 2413-9.

Wahl-Jensen, V. M., Afanasieva, T. A., Seebach, J., Stroher, U., Feldmann, H., and Schnittler, H. J. (2005b). Effects of Ebola virus glycoproteins on endothelial cell activation and barrier function. *J Virol* **79**(16)**,** 10442-50.

Wang, L. W., Leonhard-Melief, C., Haltiwanger, R. S., and Apte, S. S. (2009). Post-translational modification of thrombospondin type-1 repeats in ADAMTS-like 1/punctin-1 by C-mannosylation of tryptophan. *J Biol Chem* **284**(44)**,** 30004-15.

Watanabe, S., Noda, T., Halfmann, P., Jasenosky, L., and Kawaoka, Y. (2007). Ebola virus (EBOV) VP24 inhibits transcription and replication of the EBOV genome. *J Infect Dis* **196 Suppl 2,** S284-90.

Watanabe, S., Takada, A., Watanabe, T., Ito, H., Kida, H., and Kawaoka, Y. (2000). Functional importance of the coiled-coil of the Ebola virus glycoprotein. *J Virol* **74**(21)**,** 10194-201.

Watanabe, S., Watanabe, T., Noda, T., Takada, A., Feldmann, H., Jasenosky, L. D., and Kawaoka, Y. (2004). Production of novel ebola virus-like particles from cDNAs: an alternative to ebola virus generation by reverse genetics. *J Virol* **78**(2)**,** 999-1005.

Wegener, J., Zink, S., Rosen, P., and Galla, H. (1999). Use of electrochemical impedance measurements to monitor beta-adrenergic stimulation of bovine aortic endothelial cells. *Pflugers Arch* **437**(6)**,** 925-34.

Weik, M., Enterlein, S., Schlenz, K., and Muhlberger, E. (2005). The Ebola virus genomic replication promoter is bipartite and follows the rule of six. *J Virol* **79**(16)**,** 10660-71.

Weik, M., Modrof, J., Klenk, H. D., Becker, S., and Muhlberger, E. (2002). Ebola virus VP30-mediated transcription is regulated by RNA secondary structure formation. *J Virol* **76**(17)**,** 8532-9.

Weissenhorn, W., Calder, L. J., Wharton, S. A., Skehel, J. J., and Wiley, D. C. (1998a). The central structural feature of the membrane fusion protein subunit from the Ebola virus glycoprotein is a long triple-stranded coiled coil. *Proc Natl Acad Sci U S A* **95**(11)**,** 6032-6.

Weissenhorn, W., Carfi, A., Lee, K. H., Skehel, J. J., and Wiley, D. C. (1998b). Crystal structure of the Ebola virus membrane fusion subunit, GP2, from the envelope glycoprotein ectodomain. *Mol Cell* **2**(5)**,** 605-16.

Whelan, S. P., Barr, J. N., and Wertz, G. W. (2004). Transcription and replication of nonsegmented negative-strand RNA viruses. *Curr Top Microbiol Immunol* **283,** 61-119.

WHO (1977). Viral haemorrhagic fever. *Wkly Epidemiol Rec* **52(21),** 177-180.

WHO (1978a). Ebola hemorrhagic fever in Sudan, 1976. *Bull World Health Organ* **56,** 247–270.

WHO (1978b). Ebola hemorrhagic fever in Zaire, 1976. *Bull World Health Organ* **56,** 271-293.

WHO (1979). Viral hemorrhagic fever surveillance. *Wkly Epidemiol Rec* **54,** 342–343.

WHO (1992). Viral haemorrhagic fever in imported monkeys. *Wkly Epidemiol Rec* **67**(19)**,** 142-3.

WHO (1995a). Ebola haemorrhagic fever in Cote d'Ivoire. *Wkly Epidemiol Rec* **70 (51-52),** 367.

WHO (1995b). Ebola haemorrhagic fever: Zaire. *Wkly Epidemiol Rec* **70(34),** 241-242.

WHO (1997). Ebola haemorrhagic fever. A summary of the outbreak in Gabon. *Wkly Epidemiol Rec* **72**(1-2)**,** 7-8.

WHO (2000). Ebola, Uganda. *Wkly Epidemiol Rec* **75**(42)**,** 337-8.

WHO (2001). Outbreak of Ebola haemorrhagic fever, Uganda, August 2000-January 2001. *Wkly Epidemiol Rec* **76**(6)**,** 41-6.

WHO (2005). Outbreak of Ebola haemorrhagic fever in Yambio, south Sudan, April - June 2004. *Wkly Epidemiol Rec* **80**(43)**,** 370-5.

WHO (2008). Outbreak news. Ebola haemorrhagic fever, Uganda--end of the outbreak. *Wkly Epidemiol Rec* **83**(10)**,** 89-90.

WHO (2009). Outbreak news. Ebola Reston in pigs and humans, Philippines. *Wkly Epidemiol Rec* **84**(7)**,** 49-50.

Wieringa, R., De Vries, A. A., Post, S. M., and Rottier, P. J. (2003). Intra- and intermolecular disulfide bonds of the GP2b glycoprotein of equine arteritis virus: relevance for virus assembly and infectivity. *J Virol* **77**(24)**,** 12996-3004.

Wool-Lewis, R. J., and Bates, P. (1998). Characterization of Ebola virus entry by using pseudotyped viruses: identification of receptor-deficient cell lines. *J Virol* **72**(4)**,** 3155-60.

Worrall, N. K., Chang, K., LeJeune, W. S., Misko, T. P., Sullivan, P. M., Ferguson, T. B., Jr., and Williamson, J. R. (1997). TNF-alpha causes reversible in vivo systemic vascular barrier dysfunction via NO-dependent and -independent mechanisms. *Am J Physiol* **273**(6 Pt 2)**,** H2565-74.

Yaddanapudi, K., Palacios, G., Towner, J. S., Chen, I., Sariol, C. A., Nichol, S. T., and Lipkin, W. I. (2006). Implication of a retrovirus-like glycoprotein peptide in the immunopathogenesis of Ebola and Marburg viruses. *Faseb J* **20**(14)**,** 2519-30.

Yang, Z., Delgado, R., Xu, L., Todd, R. F., Nabel, E. G., Sanchez, A., and Nabel, G. J. (1998). Distinct cellular interactions of secreted and transmembrane Ebola virus glycoproteins. *Science* **279**(5353)**,** 1034-7.

Yang, Z. Y., Duckers, H. J., Sullivan, N. J., Sanchez, A., Nabel, E. G., and Nabel, G. J. (2000). Identification of the Ebola virus glycoprotein as the main viral determinant of vascular cell cytotoxicity and injury. *Nat Med* **6**(8)**,** 886-9.

Yasuda, J., Nakao, M., Kawaoka, Y., and Shida, H. (2003). Nedd4 regulates egress of Ebola virus-like particles from host cells. *J Virol* **77**(18)**,** 9987-92.

Yonezawa, A., Cavrois, M., and Greene, W. C. (2005). Studies of ebola virus glycoprotein-mediated entry and fusion by using pseudotyped human immunodeficiency virus type 1 virions: involvement of cytoskeletal proteins and enhancement by tumor necrosis factor alpha. *J Virol* **79**(2)**,** 918-26.

Zaki, S. R., and Goldsmith, C. S. (1999). Pathologic features of filovirus infections in humans. *Curr Top Microbiol Immunol* **235,** 97-116.

Zaki, S. R., Shieh, W. J., Greer, P. W., Goldsmith, C. S., Ferebee, T., Katshitshi, J., Tshioko, F. K., Bwaka, M. A., Swanepoel, R., Calain, P., Khan, A. S., Lloyd, E., Rollin, P. E., Ksiazek, T. G., and Peters, C. J. (1999). A novel immunohistochemical assay for the detection of Ebola virus in skin: implications for diagnosis, spread, and surveillance of Ebola hemorrhagic fever. Commission de Lutte contre les Epidemies a Kikwit. *J Infect Dis* **179 Suppl 1,** S36-47.

Zampieri, C. A., Fortin, J. F., Nolan, G. P., and Nabel, G. J. (2007). The ERK mitogen-activated protein kinase pathway contributes to Ebola virus glycoprotein-induced cytotoxicity. *J Virol* **81**(3)**,** 1230-40.